UNIVERSIDADE DE LISBOA

INSTITUTO SUPERIOR TÉCNICO

Development and evaluation of orthopedic bioabsorbable implant products based on chitosan

Lígia Margarida Jorge de Figueiredo

Supervisor: Doctor Maria Alexandra Sousa Rodrigues

Co-supervisor: Doctor Frederico Castelo Alves Ferreira

Doctor Luís Filipe Verga Vieira Pinto

Thesis approved in public session to obtain the PhD Degree in
Leaders for Technical Industries

Jury final classification: **Pass with Distinction**

2018

UNIVERSIDADE DE LISBOA
INSTITUTO SUPERIOR TÉCNICO

Development and evaluation of orthopedic bioabsorbable implant products based on chitosan

Lígia Margarida Jorge de Figueiredo

Supervisor: Doctor Maria Alexandra Sousa Rodrigues

Co-supervisor: Doctor Frederico Castelo Alves Ferreira

Doctor Luís Filipe Verga Vieira Pinto

Thesis approved in public session to obtain the PhD Degree in
Leaders for Technical Industries

Jury final classification: Pass with Distinction

Jury

Chairperson: Doctor Rogério Anacleto Cordeiro Colaço, Instituto Superior Técnico da Universidade de Lisboa

Members of Committee:
Doctor Maria Helena Mendes Gil, Faculdade de Ciências e Tecnologia da Universidade de Coimbra.

Doctor Paulo Rui Alves Fernandes, Instituto Superior Técnico da Universidade de Lisboa.

Doctor Maria de Fátima Reis Vaz, Instituto Superior Técnico da Universidade de Lisboa.

Doctor Stan Neil Finkelstein, Institute for Data, Systems, and Society, Massachusetts Institute of Technology, USA.

Doctor Ana Paula Valagão Amadeu do Serro, Instituto Superior Técnico da Universidade de Lisboa.

Doctor Maria Alexandra Sousa Rodrigues, Instituto Superior de Engenharia de Lisboa - Instituto Politécnico de Lisboa.

Funding Institution: Fundação para a Ciência e Tecnologia

2018

To my mom, dad and brother; family and friends.

To Ricardo, for his patience, love and support throughout this long journey.

Abstract

Bioabsorbable implants play a very important role in orthopedics, due to their capability to degrade over time, avoiding the need for its removal after tissue repair and healing. However, there are still problems to solve such as the biocompatibility of the degradation products which can be addressed using chitosan. This natural occurring polymer has many advantages, such as its biodegradability and biocompatibility properties, and the promotion of tissue regeneration without causing inflammatory reactions. However, for orthopedic applications, chitosan has limited strength, an issue addressed in this thesis by blending chitosan with different groups of materials: plasticizers and ceramics. Hence, different concentrations of these materials were blended with chitosan to produce 3D dense products for orthopedic applications. The plasticizer (10% w/v glycerol) and ceramic (10% w/v glycerol + 10% w/w biphasic mixture of calcium phosphates) blends selected were based on their mechanical properties and ease of machining without breaking, thus allowing different geometries to the final application design. The selected blends were also compared based on the results of biological and sterilization tests; the degradation over 24 weeks and the osteoinduction behaviors were studied and the mechanical, physical, microstructural, chemical and cytotoxic properties were analyzed before and after the use of different sterilization methods.

These two compositions were used in the production of bioabsorbable screws, replicating the geometry of currently commercially available implants used in the Anterior Cruciate Ligament Reconstruction (ACLR). This application was selected based on the need and impact of bioabsorbable implants for the different orthopedic applications. An economic model was developed to study the impact of having a new ACLR bioabsorbable implant in the market. The economic effects in different scenarios, according to multiple levels of improvement provided by a new bioasborbable implant, were assessed for the incidence of complications after this surgery. This economic model, based on Monte Carlo simulations, indicated that a new bioabsorbable implant potentiate cost savings if the incidence of the complications is reduced by, at least, 14%.

The results obtained in this thesis confirm the need for the development of new bioabsorbable implants and show the potentialities of the two chitosan blends in such development. The plasticizer composition revealed better properties considering biodegradation, osteoinduction and cytotoxic studies, whereas the ceramic composition revealed higher mechanical strength and versatility necessary for the successful machining of screw prototypes for the selected orthopedic application. The two compositions can be tested *in vivo*, for commercial applications, in future orthopedic bioabsorbable implants.

Keywords: chitosan, plasticizers, ceramics, mechanical strength, bioabsorbable orthopedic implants, economic model

Resumo

Os implantes bioabsorvíveis possuem um papel muito importante na área ortopédica, graças à sua capacidade de degradar ao longo do tempo, eliminando a necessidade da sua remoção após a reparação tecidular. Contudo, existem ainda diversos problemas para resolver, em particular a biocompatibilidade dos produtos de degradação, que podem ser resolvidos através da utilização de quitosano. Este polímero natural oferece diversas vantagens, tais como a sua biodegradabilidade e biocompatibilidade, bem como a promoção da regeneração de tecidos sem causar reações inflamatórias. Porém, para aplicações ortopédicas, o quitosano possui uma limitação na resistência mecânica, uma questão abordada nesta tese através da mistura de quitosano com outros materiais, tais como cerâmicos e plastificantes. Assim, misturaram-se diferentes concentrações destes materiais com o quitosano para a obtenção de amostras tridimensionais densas para aplicações ortopédicas. As misturas de plastificante (10% m/v glicerol) e de cerâmico (10% m/v glicerol + 10% m/m mistura bifásica de fosfatos de cálcio) foram selecionadas para testes subsequentes, atendendo às suas propriedades mecânicas e à facilidade de maquinagem sem partir, possibilitando a obtenção de diferentes geometrias no desenho final da aplicação desejada. Estas duas composições selecionadas foram comparadas com base nos resultados de testes biológicos e de esterilização: analisaram-se as suas degradações ao longo de 24 semanas e os seus comportamentos osteoindutores, tendo-se analisado também as suas propriedades mecânicas, físicas, microestruturais, químicas e citotóxicas antes e depois da aplicação dos vários métodos de esterilização.

Estas duas composições foram utilizadas na produção de parafusos bioabsorvíveis, replicando a geometria de implantes já disponíveis no mercado e utilizados na reconstrução do ligamento cruzado anterior (LCA). Esta aplicação foi escolhida com base na necessidade e no impacto de implantes bioabsorvíveis em diferentes aplicações ortopédicas. Desenvolveu-se um modelo económico para estudar o impacto de ter um novo implante no mercado destinado ao LCA. Os efeitos económicos dos vários cenários, de acordo com diferentes níveis de melhoramento potenciados por um novo implante, foram avaliados com base na redução do nível de complicações após a cirurgia de reconstrução. Este modelo económico, baseado em simulações de Monte Carlo, indicou que um novo implante pode gerar uma redução de custos, se a incidência das complicações for reduzida em, pelo menos, 14%.

Os resultados obtidos nesta tese confirmam a necessidade do desenvolvimento de novos implantes bioabsorvíveis e demonstram as potencialidades das duas misturas de quitosano nesse desenvolvimento. A composição só com o plastificante revelou melhores propriedades após estudos de biodegradação, de osteoindução e de citotoxicidade, enquanto que a composição contendo componentes cerâmicas revelou ter maior resistência e versatilidade mecânicas, o que facilitou o fabrico de protótipos de um parafuso a partir das amostras tridimensionais densas, para a aplicação escolhida. As duas composições podem ser testadas em condições *in vivo*, para serem aplicadas, comercialmente, em futuros implantes ortopédicos bioabsorvíveis.

Palavras-chave: quitosano, plastificantes, cerâmicos, resistência mecânica, implantes ortopédicos bioabsorvíveis, modelo económico

Acknowledgements

This thesis is a multidisciplinary work, fruit of several discussions with many colleagues and professors, as well as partnerships with multiple research groups. I would like to thank:

- my supervisors Prof. Alexandra Rodrigues, Prof. Frederico Ferreira and Dr. Luís Pinto who guided me throughout this work. Dealing with chitosan was extremely difficult, and Dr. Luís Pinto gave a fundamental help;
- Prof. Stan Finkelstein, who welcomed me and closely followed my work at MIT;
- Prof. Rogério Colaço for all the hints, contacts, financial support and his knowledge, which was of extreme importance in the later stages of this thesis;
- M.D. Nuno Ribeiro who was always available to welcome me at Hospital dos Lusíadas and answered all the emails concerning the issues related with the orthopedic areas, including the identification of the currently available bioasbsorbable implants on the market and the screw design specifications;
- all my colleagues and former colleagues at Altakitin S.A. (Ana, Andreia, Alex, Bruna, Carlos, João, José, Lara, Liliana, Luís, Mário, Pedro, Sara, Sofia, Telma, Thierry, Sara and Vânia), for their friendship and support. Thank you also to Dr. Eduardo Pires, CEO of Altakitin S.A., for the help and financial support;
- all the professors in the Department of Mechanical Engineering, who helped me to clarify doubts and to solve some problems: Prof. Fátima Vaz, Prof. Luís Reis, Prof. Pedro Amaral, Prof. Augusto Dias de Deus, Prof. Relógio Ribeiro, Prof. Marco Leite, Prof. Luís Sousa, Prof. Vírginia Infante, Prof. Paulo Fernandes, Prof. Alberto Ferro, Prof. Manuel Freitas and Prof. Elsa Rodrigues. A special thank you to professors Fátima Vaz and Luís Reis, also for all the friendly words;
- Prof. Pedro Rosa, also from the Department of Mechanical Engineering, who gave me a huge support in the last experiments of this thesis, especially for the development of the screw;
- colleagues from the MIT-Portugal group, especially those who took the year of classes with me and were with me at MIT. A special thank you to Bruna and Elçin for being so good friends and work buddies (we did it!);
- Dr. Nuno Guitian, for helping to clarify all the initial doubts;
- Prof. Ana Paula Serro, for her support in the contact angle and DSC tests. Also, thank you to Prof. Anabela Fernandes for answering all the questions regarding the DSC;
- Eng. Diana Silva, for her help and patience in explaining the functioning of the equipments and all the necessary fundaments;
- Prof. Amélia Almeida, for her help in the nanoindentation tests;
- Dr. Luísa Carvalho, who helped carry out the ^{1}H-NMR tests and all other chemical tests performed at FCT-UNL;
- Prof. Luísa Ferreira (FCT-UNL) for making the ATR-FTIR tests available;
- Prof. Ana Paula Soares Dias, Dr. Marisa Santos and Prof. Teresa Cidade (FCT-UNL), for their help in the identification of the viscosity of the different chitosan batches;
- the technical staff Pedro Teixeira, João Vicente, Ricardo Pereira and Daniel Jesus;
- Eng. Isabel Nogueira, for her help in SEM analysis;
- Dr. Fernando Oliveira from Laboratório Nacional de Engenharia e Geologia, LNEG;

- Dr. Rita Fonseca and Dr. Margarida Franco, for their help in the microCT tests at CDRSP/IPL;
- all my fellow research colleagues from the Mechanical Department, especially those who were involved the most in my work: Catarina Vale, Joanna Kuszczak, Vítor Anes, Elçin Calado, Samuel Furtado and Bruno Soares.
- Taguspark colleagues, especially those who were directly involved in the biological study: Carla Moura, João Silva, Marta Carvalho, Marta Costa and Cátia Bandeiras.
- M.D. Meghan Dierks and M.D. Eric Makhani, who directly contributed to the work started at MIT;
- Dr. Abigail Horn from MIT, who helped me to understand the Monte Carlo simulation and the colleagues from Prof. Richard Larson's group;
- M.D. João Gamelas (Coordinator of the Orthopedics Unit, Hospital dos Lusíadas) and M.D. Jacinto Monteiro (Director of Orthopedic Service, Hospital de Santa Maria);
- M.D. Shawn Ferrullo (MIT Medical), M.D. Anthony Schena (MIT Medical), physical therapist Peter Solis-Cohen (Joint Ventures), researcher Ali Hosseini (MGH) and M.D. Carlos Maia (Hospital da Luz), for their help in the development of the early health technology assessment study;
- Eng. João Durão de Carvalho from Hospital de Santa Maria;
- Mrs Marina Branco from M.J. Branco, Lda.
- Estereobato Lda, specially to Eng. Ana Silveira and Eng. Glória Matos;
- Dr. Eduardo Alves and Eng. Paula Matos, from CTN;
- Dr. Raquel Galante and Ozônio Brasil, for making possible the sterelizations performed in Brazil;
- Eng. Afonso Gregório and technician Flávio Mocho, who helped in the final experimental setups and machinings.

To all, thank you very much!

Table of Contents

Abbreviations

AA	Antibiotic-antymicotic
AB	Alamar Blue
ACL	Anterior Cruciate Ligament
ALP	Alkaline Phosphatase
ATR-FTIR	Attenuated Total Reflectance – Fourier Transform Infrared Spectrocopy
BMPs	Bone morphogenetic proteins
BPTB	Bone-patellar tendon-bone
CAGR	Compounded annual growth rate
cDNA	complementary DNA
CEA	Cost effectiveness analysis
CFU	Colony forming units
Ch+Gly	Blend of chitosan with 10% (w/v) glycerol
Ch+Gly+HA-TCP	Blend of chitosan with 10% (w/v) glycerol and 10% (w/w) biphasic mixture HA and β-TCP
CNC	Computer numerical control machine
COL1A1	Alpha-1 type I collagen
CT	Computerized tomography
D.D.	Degree of deacetylation
DMEM	Dulbecco's Modified Eagle Medium
DMTA	Dynamic Mechanical Thermal Analysis
DSC	Differential Scanning Calorimetry
ECM	Extracellular matrix
EGF	Epidermal growth factors
EtO	Ethylene oxide
FBS	Fetal bovine serum
FDA	Food and Drug Administration
GAG	Glycosaminoglycans
GAPDH	Glyceraldehyde-3-phosphate dehydrogenase
HA	Hydroxyapatite
hBMSC	Human bone marrow mesenchymal stem cells
HDPE	High density polyethylene
HSS	High speed steel
HST	Quadrupled hamstring tendons
HTA	Health technology assessment
ICER	Incremental cost-effectiveness ratio
IF	Infrared
MARS	Multicenter ACL Revision Group Study
MCDA	Multi-criteria decision analysis
M_n	Average molecular weights
MRI	Magnetic Resonance Imaging
mRNA	messenger RNA
MSCs	Mesenchymal stem cells

MTT	3-(4,5-dimethylthiazol-2-yl)-2,5-diphenyl-tetrazolium bromid
M_W	Molecular weight
NHS	UK National Health Service
NMR	Nuclear magnetic resonance spectroscopy
NICE	UK National Institute for Health and Clinical Excellence
OCD	Osteochondritis dissecans
P4HB	Poly-4-hydroxybutyrate
PBS	Phosphate-buffered saline
PCL	Polycaprolactone
PDS	Polydioxanone
PE	Polyethylene
PEEK	Polyether etherketone
PEG	Polyethylene glycol
PET	Polyethylene terephthalate
PGA	Polyglycolic acid
PHAs	Polyhydroxyalkanoates
PHB	Poly 3-hydroxybutyrate
PHBV	3-hydroxyvalerate
PLGA	Poly(lactic acid-co-glycolic) Acid
PMA	Premarket approval
PP	Polypropylene
PPF	Polypropylene fumarate
PTFE	Polytetrafluoroethylene
PU	Polyurethanes
PVC	Polyvinyl chloride
QALY	Quality-Adjusted Life-Years
QT	Quadriceps tendons
qPCR	Real time Polymerase Chain Reaction
R&D	Research and development
RCT	Randomized controlled trials
RGD	Arginine-glycine-aspartic acid
ROA	Real options analysis
Runx2	Runt-related transcription factor 2
SAL	Security assurance level
SEM	Scanning Electron Microscopy
SD	Standard deviation
SR	Self-reinforcement manufacturing technique
Tg	Glass transition temperature
TGA	Thermogravimetric Analysis
TMC	Trimethylene carbonate
VOI	Value-of-information
UV	Ultraviolet radiation
XRD	X-ray powder diffraction
YLDs	Years lived with disability
β-TCP	β-tricalcium phosphate

List of Figures

List of Tables

SECTION A: Contextualization

1. Introduction

The number of people affected worldwide by or dying from non-communicable diseases (NCDs) or chronic diseases has grown 30% since 1990, according to The Global Burden of Disease Study 2010 [1]. This is happening since many people are living longer and the population is growing older [1]. As the body ages, the bone and muscle tissues start degenerating, giving rise to various indications manifested by pain, for example, in joints or in the back. These aging-related problems are especially relevant in developed countries, where the percentage of the elderly is increasing. Within the NCDs, musculoskeletal disorders such as rheumatoid arthritis, osteoporosis, osteoarthritis, injuries caused by sports and workplace accidents, spine and back disorders, have been growing and their social and economic burden is expected to grow due to the aging of the population and changes in lifestyle.

Musculoskeletal diseases combined with fractures and soft tissue injuries reached a total of 20.8% of global years lived with disability (YLDs) in 2013 [2]. These problems represent an elevated cost for the individuals and the society through the associated disability and the healthcare needs. Most costs are associated with their impact on activities of daily living, in particular on productive work along with the need for support by the family, caregivers or the society [3]. In fact, musculoskeletal disorders cause loss of productivity and economic capacity through absenteeism (time off work for those in paid work), presenteeism (lost productivity because of diminished capacity while at work) and work disability (permanent, partial or complete inaptitude for work purposes) [3,4].

Biomaterials have been used extensively for the development of different types of orthopedic fixation devices for the treatment of the musculoskeletal disorders. In this area, attention has been given to the bioabsorbable implants of synthetic origin in the last couple of years, which became clinically available in the 1970s [5]. Bioabsorbable implants are devices made from biopolymers that are able to be eliminated from the body once healing has occurred. Ideally, they should provide a temporary function for as long as they are needed and the biodegradability should occur at the same rate the patient's own tissue is regenerated, into harmless, non-toxic, by-products [6]. The resulting by-products are then eliminated from the body via natural pathways, thus avoiding the need for a second surgical event for implant removal [5,6]. However, since these implants are fabricated from biopolymers of synthetic origin, in practice several drawbacks are associated with bioabsorbable implants currently available in the market. Among the problems reported in the literature it stands out the adverse tissue reactions caused by the release of degradation products of acidic nature. If the degradation products exceed the body's local ability to eliminate them, they have an effect on the microenvironment pH, which may cause local inflammation [7,8]. Therefore, there is continuous interest in searching for new and improved solutions for the development of new bioabsorbable implants. In this area, natural polymers such as chitosan can have an important role.

Chitosan is a linear polysaccharide derived from chitin, which is composed of glucosamine and *N*-acetyl glucosamine linked in a β(1–4) bond [9]. Chitosan is distinguished from chitin by its degree of deacetylation (D.D.), being equal or higher than 50%. If the D.D. is lower than 50% the polysaccharide is denominated chitin [9].

Chitosan reported properties include good biocompatibility and biodegradability, as well as analgesic, hemostatic, antimicrobian and antioxidant properties [10,11]. Moreover, it was also

reported that chitosan promote bone formation since it can be shaped into several scaffold structures, suitable for cell ingrowth and osteoconduction [12], depending on the chitosan characteristics. Therefore, these remarkable properties have been recognized as being of high potential, offering unique opportunities to the development of biomedical and pharmaceutical applications.

Despite being a promising material for orthopedic applications, practical applications involving 3D dense geometries have been severely limited due to the inherent difficulties of the development process; chitosan has stronger intramolecular and intermolecular hydrogen bonds, its melting temperature is higher than its decomposing temperature [13]. As a consequence, it is not possible to produce 3D chitosan-based products using conventional plastics processing techniques. This occurs due to chitosan's high extent capacity of water absorption [14]. For all these reasons, the traditional forms of chitosan include membranes, films, powders and fibers in research areas such as artificial skin, sutures, tissue engineering, drug delivery and cell encapsulation [15–17].

To overcome the limitations associated to the development of 3D dense constructs based on chitosan, this research work proposes to produce and characterize 3D dense chitosan-based compositions to be used as bioabsorbable fixation devices for orthopedic applications. Therefore, this research aims to contribute to the development and implementation of new treatment strategies in orthopedics that rely on the good biological properties of chitosan.

1.1. Motivation and research goals

The main aim of this research is to produce and characterize 3D dense chitosan-based compositions to be used as bioabsorbable fixation devices for orthopedic applications. To obtain these bioabsorbable implants is necessary to produce dense chitosan-based products with the following key-properties (target product performance):

1 - A processable product that can be machined in different shapes without breaking under machining;
2 - A product with suitable strength and stiffness, to comply with bone tissue requirements. At least, these properties should attain the values of current bioabsorbable implants;
3 - A product with a biodegradation rate that allows holding the mechanical properties at least for 6 months;
4 - A product that can be sterilized with minimal change of its properties;
5 - A product that is not cytotoxic;
6 - A product that interplays with surrounding tissues, promoting bone formation;
7 - A product that does not induce chronic inflammation.

To improve the control over the produced specimens and their final mechanical and biological properties, the following objectives are addressed:

a) Identify in which orthopedic area a new bioabsorbable implant will have a higher positive impact based on the users' needs and expert opinion;

b) Identify and optimize process parameters to systematize the production of 3D dense chitosan-based products with adequate mechanical properties and biological behavior, able to fulfill the first 6 key-properties described above;
c) Study different blends of chitosan with other materials in order to improve the properties of 3D dense chitosan-based products, able to fulfill the first 6-key properties described above;
d) Study the effect of different sterilization methods on the properties of the chitosan blends;
e) Machine an implant that from the chitosan based products, considering its impact in the orthopedic medical field and the characteristics of the produced chitosan based specimens.

1.2. Research questions

Aligned with the step objectives, these were the questions pursued in this work:

1) Which orthopedic application will benefit the most from the development of a new bioabsorbable implant based on chitosan and how much the clinical outcome has to improve to economically justify its production?

2) Which process parameters are critical for an optimized production process in order to obtain chitosan-based products for orthopedic applications with adequate and systematize mechanical properties and biological behavior?

3) Which chitosan blends should be used to produce chitosan-based products for orthopedic applications with adequate mechanical properties and biologic behavior?

4) Which mechanical, biological and chemical effects are produced on the properties of the chitosan blends when they are sterilized?

5) Considering the selected orthopedic application, is it possible to construct an implant based on the 3D dense chitosan-based products developed, with adequate design and according to the mechanical and biological properties that were attained?

1.3. Structure of the thesis

In addition to this introductory chapter, this thesis is composed of fourteen chapters in which are presented the strategies and results obtained during the development of chitosan-based products for the constitution of new bioabsorbable implants for orthopedic applications. The chapters are divided in five main sections, as represented in the schematization in Table 1.1.

Table 1.1. Thesis structure.

Section A: **Contextualization**
Chapter 1: Introduction **Chapter 2:** Bioabsorbable orthopedic implants: review **Chapter 3:** Chitosan as a natural polymer for biomedical applications
SECTION B: **Early HTA of a new bioabsorbable orthopedic implant**
Chapter 4: Early health technology assessment in medical devices **Chapter 5:** Economic analysis model for a new bioabsorbable orthopedic implant candidate
SECTION C: **Methodologies for the development and evaluation of 3D dense chitosan-based compositions for orthopedic applications**
Chapter 6: Experimental tests to define the physicochemical properties of chitosan **Chapter 7:** Experimental tests and methods for the evaluation of 3D dense chitosan-based product compositions **Chapter 8:** Sterilization methods on 3D dense chitosan-based product compositions
SECTION D: **Development and experimental evaluation of 3D dense chitosan-based compositions for orthopedic applications**
Chapter 9: Preliminary studies: production process optimization and materials selection **Chapter 10:** Mechanical behavior of different chitosan blends in the development of bioabsorbable implant products **Chapter 11:** Biological behavior of the chitosan-based compositions selected for the development of bioabsorbable implant products **Chapter 12:** Sterilization of the chitosan-based compositions selected for the development of bioabsorbable implant products **Chapter 13:** Development of bioabsorbable screws based on the chitosan-based compositions selected
SECTION E: **Final conclusion and future directions**
Chapter 14: Conclusion and future directions

Section A explains the motivations and research goals of this thesis (chapter 1) and reviews the current bioabsorbable implants (chapter 2) and chitosan materials in biomedicine (chapter 3), in order to identify the problems and challenges that still exist and which require further research.

Section B gives insight information about the importance of early health technology assessment (HTA) studies in the medical area (chapter 4) and presents a model that assesses the application that will benefit the most from the development of a new bioabsorbable implant, as well as the economic impact of developing such implant (chapter 5).

Section C presents several methodologies used to characterize the properties of chitosan (chapter 6) and to evaluate the mechanical, microstructural, physical, chemical and biological properties of the chitosan-based compositions (chapter 7) that will be used as candidates to the production of the new bioabsorbable implants of natural origin. Additionally, the different sterilization methodologies used in this study are also explained (chapter 8).

Section D resumes the main results obtained during the development of the candidate implant materials. First, the production process was optimized, the strategy was defined and the

materials were selected (chapter 9). In the next step, different specimens were produced by blending chitosan with different types of plasticizers and ceramics, and the compositions that showed better mechanical properties, such as strength, hardness and stiffness were selected for the following studies (chapter 10). Among the tested blends, two compositions, from each material group, were selected to study the *in vitro* degradation and the *in vitro* differentiation behavior (chapter 11). The effect of different sterilization methods was determined by assessing the mechanical, cytotoxic, microstructural, chemical and the wettability properties before and after the sterilizations of the specimens (chapter 12). This section ends with the development of a screw for an ACL reconstruction (chapter 13).

The last section (Section E) establishes guidelines for the use of chitosan in the industry of orthopedic devices, namely for the production of bioabsorbable implants. Additionally, it presents the final remarks and conclusions of this work as well as the future directions in this area (chapter 14).

2. Bioabsorbable orthopedic implants: review

Orthopedic fixation implants have a significant role in modern medicine, such as in the treatment of musculoskeletal disorders. Among these, bioabsorbable implants have attracted special attention for internal fixation of fractures, osteotomies, arthrodesis and ligament injuries, since they are capable of degrading and dissolving inside the human body [18]. This promotes a better biological interaction with damaged tissues since the mechanical stresses are transferred gradually from the implant to the healing tissue over material degradation [19,20]. Additionally, the bioabsorbable orthopedic implants eliminate the problems that are associated with the metal fixation devices, such as growth disturbances and hypersensitivity reactions, avoiding additional surgery for the removal of the implant after the biological consolidation [21]. These improved characteristics may result in social and financial benefits as well as physical and psychological advantages [22].

Despite several advantages, continuous research is still needed in order to develop new bioabsorbable implants that effectively eliminate clinical episodes of implant loosening, fibrous encapsulation and inflammation. In addition, current research aims to develop bioabsorbable implants that promote osteointegration, osteoinduction, vascularization and with improved mechanical stability [23].

In the next chapters, properties and characteristics of the existing bioabsorbable orthopedic implants are revised, their composition and current market are analyzed and a literature review about the clinical drawbacks of such implants is presented. To complete this review, the current research strategies regarding the development of new bioabsorbable fixation implants are discussed, and future directions for such development are outlined.

2.1. Orthopedic implants: evolution and main features

Since their implementation in Medicine, orthopedic implants have either replaced function or provided temporary or permanent bone support, thus facilitating healing. The main goal of fracture fixation is to stabilize the fractured bone, to enable fast healing, to restore full mobility and function and to remove pain [24,25]. Additionally, bone fixation implants are also used in the treatment of various types of deformities of the skeleton as well as to maintain the relative position of bone grafts [25]. Some of the diseases associated with the musculoskeletal system and their correspondent treatments are briefly described in the table of Appendix A.1.

Historically, metal has been the most popular material used in orthopedic and reconstructive surgery of skeletal injuries. The two most commonly used metals in orthopedic devices are stainless steel and titanium special alloys, in hardware such as pins, screws, anchors and plates [26]. These materials are stiffer than bone, providing stability during the healing process. However, there are several complications associated with the metallic-based implants, such as stress shielding which results in bone weakening and resorption and long term physiological response due to the presence of the implant, leading to its surgical removal [5,26].

Table 2.1 shows a qualitative comparison between the performance of metallic and bioabsorbable polymeric implants on different criteria.

Table 2.1. Qualitative comparison between the performances of metallic and bioabsorbable implants. The material that has the better characteristics is selected, for each criterion.

	Higher strength	Lower stress shielding	Lower growth restriction	Lower need of removal	Higher biological interaction	No sterilization effects	Lower cost
Metallic fixation implants	×					×	×
Bioabsorbable fixation implants		×	×	×	×		

The listed disadvantages of metal based implants have created an opportunity to improve the performance and safety of orthopedic implants. As an obvious consequence, biostable and bioabsorbable polymers have started to be tested and used in the orthopedic field [26]. Biostable (or bioinert) polymers are inert towards biological tissue, causing minimal response in the surrounding tissue, and retain their properties for years. The primary goal for using such polymers in orthopedic surgery is to minimize and adjust material-tissue interactions, such that the material remains chemically and physically unchanged during its application time [27]. Examples of biostable (or bioinert) polymers are polyethylene (PE), polypropylene (PP) and polyether etherketone (PEEK). However, some relevant problems are found in these types of implant, namely poor osteointegration (similar problem while using metals) and severe wear problems, which release wear debris, causing foreign body reactions and eventual osteolysis [20,26].

The shift of focus on bone repair evolution, from a purely mechanical stable fixation to a more biologically orientated approach. For this reason, researchers began studying bioabsorbable materials in order to obtain better results, while limiting adverse outcomes from metallic and biostable implants [28]. These polymers can either be obtained from natural or synthetic origin [22]. Natural polymers can closely mimic the biological environment (e.g. extracellular matrix, ECM) and present some biofunctionalities. However the natural polymers have some disadvantages, which includes structural complexity, immunogenicity risks and inferior biomechanical properties [29]. In opposition, synthetic polymers are the most widely used materials in bioabsorbable implants production due to their more predictable properties and batch-to-batch uniformity [22].

The main attraction of bioabsorbable polymers, both to surgeons and patients, is their capacity to decompose gradually over time, while the load is safely transferred to the healed bone, joint or muscle. Therefore, there is no need for additional surgery to remove the orthopedic implant, which reduces the total cost of the treatment and the rehabilitation time of the patient [8]. Besides the enormous benefit for the patient there is also an obvious cost advantage for the health care system (less medical staff involvement, hospitalization time, drugs, etc.). In a perfect example, as soon as the implant loses all its strength, the healing union should be strong enough to maintain stability. Both hard and soft tissue are considered healed after 6-8 weeks, despite the rate of healing being dependent on the site of implantation, the age of the patient and comorbidities [30].

Nonetheless, not all the orthopedic applications are considered suitable for the current implants composed by bioabsorbable polymers. These implants are particularly advantageous

in low-weight bearing orthopedic applications (e.g. metacarpal fractures) and in applications that require only a transient existence of the implant as in specific fracture fixations in the foot, where removal of the hardware is often mandatory (e.g Lisfranc's dislocations) [31,32].

The use of bioabsorbable polymers in orthopedics has been severely limited due to the intrinsic load bearing limitations of the materials. However, with recent technological advancements (see section 2.4), significant improvements in material properties have been achieved and this is reflected in the increasing number of bioabsorbable fixation devices available commercially for orthopedics [33]. Currently, these implants are commonplace in the treatment of fractures and osteotomies in extremities, in craniomaxillofacial surgery and in sports medicine surgeries, especially in the reattachment of ligaments, tendons, meniscal tears and other soft tissue structures. For example, it is common practice to use bioabsorbable implants in shoulder and knee ligamentous reconstruction in sports medicine [34]. Figure 2.1 shows two examples of bioabsorbable screws used in the treatment of ligamentous injuries in the knee. The next chapter shows further examples of bioabsorbable implants on the market.

Figure 2.1. Examples of bioabsorbable polymeric interference screws currently available in the market. Right screw: Lactosorb®, Biomet. Left screw: ComposiTCP60®, Biomet.

2.2. Market of bioabsorbable orthopedic implants

The global market for orthopedic implants is projected to reach USD 46.5 billion this year, growing by a Compounded Annual Growth Rate (CAGR) of 8.2% in the last decade. The U.S. alone represents about 51% of the global orthopedic market whereas emerging economies, such as India and China, offer immense growth opportunities due a huge untapped patient population [35,36].

Currently the largest segment of the orthopedic implant market is the reconstructive joint segment, followed by spinal products and trauma products [35]. Reconstructive joint implants will remain the largest segment in the orthopedic field as the direct result of an increasingly aging population, suffering from diseases such as osteoarthritis. Thus, a higher demand for this medical procedure is most certain for the following years and decades. Considering the entire orthopedic reconstructive joint replacement market, knee reconstruction is the largest segment, followed by hip and shoulder reconstruction, respectively [35].

Orthopedic areas where bioabsorbable polymeric implants are used include sports medicine, trauma and spine surgery. The global market of sports medicine was valued at USD 5.6 billion in 2015 (8% of total market) and it is expected to grow at a CAGR of 8% until 2020, reaching the total of USD 8.3 billion [37]. Additionally, the trauma orthopedic implants market was valued

at USD 5.7 billion in 2013 and it is expected to reach an estimated value of USD 9.4 billion in 2020, growing at a CAGR of 7% from 2014 to 2020 [38]. In the latter case, internal fixators are the largest market segment and North America holds the largest share of the market worldwide [38]. In the US, the total trauma fixation sales market in 2012 was USD 3.1 billion and it is projected to reach USD 5 billion by 2020 [39]. Moreover, the spine fusion market is expected to reach USD 4.4 billion [40].

Bioabsorbable polymeric implant products presented in the portfolio of some major orthopedic players are shown in table below.

Table 2.2. Examples of bioabsorbable polymeric fixation implants available in the market.

Company	Product	Type of Application	Composition
Stryker	BioZip	Suture anchor	PLLA
	XCEL	Suture anchor	PLLA
	Biosteon	Interference screw	HA/PLLA
	Wedge	Interference screw	PLLA
DePuy Synthes	Absolute	Interference screw	PLLA
	Milagro Advance	Interference screw	70% PLGA/ 30% β-TCP
	Biocryl	Interference screw	70% PLLA/ 30% β-TCP
	RigidFix Family	ACL Fixation Pins	70% PLLA/ 30% β-TCP
	Biointrafix	Tibial fixation system	70% PLLA/ 30% β-TCP
	Healix Advance BR Family	Suture anchor	70% PLGA/ 30% β-TCP
	Lupine BR	Suture anchor	70% PLGA/ 30% β-TCP
	Gryphon BR	Suture anchor	70% PLGA/ 30% β-TCP
	Microfix	Suture anchor	PLLA
	Minilok anchor	Suture anchor	PLLA
	Bioknotless BR	Suture anchor	70% PLGA/ 30% β-TCP
	Panalok anchor	Suture anchor	PLLA
	RapidLoc	Meniscal repair	PDS/PLA
	RapidSorb Cranial Clamp	Fixation of cranial bone flaps	85% PLA/ 15% PGA
	RapidSorb System	Plates, screws and tacks for cranium facial bone	85% PLA/ 15% PGA
	ASLS – Angular Stable Locking System	Screw locking system for intramedullary nails	70:30 Poly-L-co-D/L-lactic acid
Smith & Nephew	Biorci	Interference screw	HA/PLLA
	Biosure HA	Interference screw	HA/PLLA
	Raptormite 3.7	Suture anchor	PLLA
	Twinfix Ultra HA	Suture anchor	HA/PLLA
	Osteoraptor 2.3	Suture anchor	HA/PLLA
	Healicoil Regenesorb	Suture anchor	β-TCP/PLGA/Calcium Sulfate
Biomet	Ratler	Interference screw	82% PLLA/18% PGA

Company	Product	Type of Application	Composition
	ReUnite	Screw system, pin	82% PLLA/18% PGA
	GentleThreads	Interference screw	82% PLLA/18% PGA
	ComposiTCP60	Interference screw	60% β-TCP/ 40% PLDLA
	ComposiTCP30	Interference screw	30% β-TCP/ 70% PLDLA
	Lactosorb	Interference screw	82% PLLA/18% PGA
	LactoNail	Nail	82% PLLA/18% PGA
	ALLthread	Suture anchor	85% PLLA/15% PGA
	Hitch	Suture anchor	85% PLLA/15% PGA
Arthrex	Bio-PushLock	Suture anchor	PLLA
	Biocomposite PushLock	Suture anchor	β-TCP/ PLDLA
	Bio-SwiveLock	Suture anchor	PLLA
	Biocomposite SwiveLock	Suture anchor	β-TCP/ PLDLA
	Bio-FASTak	Suture anchor	PLDLA
	Trim-IT Pins	Pins	PLLA
	Bio-Corckscrew	Suture anchor	PLDLA
	Biocomposite Corckscrew FT	Suture anchor	β-TCP/ PLLA
	Bio-Tenodesis	Screw	PLLA
	Biocomposite Tenodesis	Screw	β-TCP/ PLLA

2.3. Properties and characteristics of the bioabsorbable polymers in orthopedics

2.3.1. Most common bioabsorbable polymers

The first bioabsorbable polymer used in medical applications was polyglycolic acid (PGA), specifically in the development of the first synthetic degradable suture line. This historic event occurred in 1969 [41]. Several developments and innovations have been accomplished in the area of bioabsorbable polymers since then, allowing bioabsorbable polymers to become very interesting materials for tissue engineering applications and bone repair implants [42].

The majority of the bioabsorbable polymers used as orthopedic implants are aliphatic polyesters derivatives of α-hydroxy acids monomers with the general formula HO-CHR-COOH [5]. Due to the difficulty of achieving both high molecular weight (M_W) and molecular control, bioabsorbable polyesters are synthesized in a two-step procedure. In the first step, the hydroxy acids are transformed into intramolecular lactones, which are then used in the second step, as monomers in ring-opening polymerizations [41].

The dimers of the most common bioabsorbable polymeric implants are shown in Figure 2.2. From left to right: PGA, Polylactic Acid (PLA) and Polydioxanone (PDS).

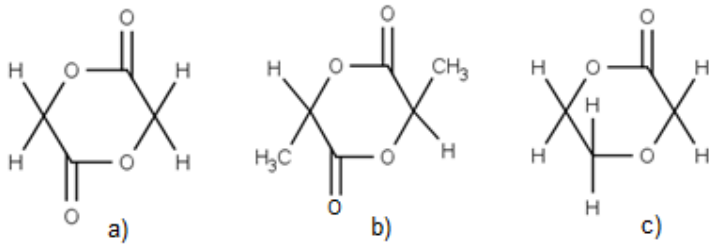

Figure 2.2. Cyclic dimers of a) PGA, b) PLA, and c) PDS.

Nowadays, PLA is made from 100% renewable resources such as cornstarch and sugarcane. As a result of Lactid Acid chirality, it is possible to have two stereoregular polymers of PLA: the D-PLA (PLDA) and the L-PLA (PLLA). Additionally, it is possible to have the racemic polymer D,L-PLA, which is obtained from a mixture of L- and D-Lactic Acid (PLDLA). Important properties of these implants include the semi-crystalline property of PLLA and PLDLA, with a glass transition temperature (Tg) of approximately 60°C, and the amorphous property of PLDLA, with a Tg of 55°C [41]. Both semi-crystalline PLLA and amorphous PLDLA polymers are rigid materials, however the semi-crystalline polymer is preferred in applications where high mechanical strength and toughness are required (e.g. sutures and orthopedic implant devices) [41].

On the other hand, PGA has a simpler structure and is more hydrophilic than PLAs. Further properties of PGA are its high crystallinity, low solubility in organic solvents and its high melting point [43]. Due to its hydrophilic nature as well as its quick water uptake, PGA has a high degradation rate and loses its mechanical strength faster than the other degradable polymers. To increase the range of clinical applications for these polymers, it was necessary to modify some of the properties of PGA. Hence, the development of copolymers of PGA with PLA or PLGA have been extensively researched [43,44]. The hydrophobicity provided by PLA limits the water uptake and results in a rate of backbone hydrolysis lower than that of PGA. Despite these improvements, the crystallinity is lost in the PLGA copolymers, which lead to changes in the rates of hydration and hydrolysis. Therefore, copolymers tend to degrade more rapidly than either PGA or PLA [41].

The main advantage of PDS is the less acidic nature of the by-products released during the degradation process, comparing to the previous bioabsorbable polymers [43]. This intrinsic chemical property allows PDS to have low-toxicity *in vivo* and thus practically no inflammation is observed in the studies [45]. However, PDS has severe limitations, which include a rapid degradation profile. Moreover, the relative weakness and lack of stiffness and strength required for most orthopedic applications drastically limits the range of applications of PDS in the area of orthopedic implants [41].

The polymers PGA, PLA and their copolymers Poly(lactic acid-co-glycolic) Acid (PLGA), are the most widely used synthetic degradable polymers in medicine [46]. The main mechanical properties and the degradation profile of some bioabsorbable polymer materials used in orthopedic surgery are shown in Table 2.3.

Table 2.3. Properties of some metallic and no reinforced polymeric materials, used in orthopedic surgery (High density polyethylene – HDPE) [28,44,46–51].

Materials	Young's Modulus (GPa)	Tensile Strength (MPa)	Elongation at break (%)	Loss of total strength (months)	Degradation time (months)
Bioabsorbable polymers					
PGA	6,5 - 7	60 - 100	15 - 20	1	6 to 12
PLLA	2,7 - 4	75 - 83	5 - 10	3	> 24
PLDLA	1,9 - 3,2	27,6 - 50	3 - 10	1 - 2	12 to 16
PLGA	2	40 - 55	3 - 10	1	1 to 12
PDS	1,5	48,3	>500	1 - 2	6 to 12
Biostable polymers					
HDPE	1	39	500	n/a	n/a
PEEK	4	100	32	n/a	n/a
Metals					
Titanium alloy	110 - 127	900	10 - 15	n/a	n/a
Stainless Steel	180 - 205	500 - 1.000	10 - 40	n/a	n/a
Bone					
Cortical Bone	7 - 30	50 - 150			
Trabecular Bone	0,05 – 0,5	10 - 20			

2.3.2. Biodegradation

Bioabsorbable polymers are eliminated from the body in a two-stage biological procedure. In the first stage enzymatic hydrolysis of the bonds occurs. In the second stage the monomers will be broken down through further enzymatic activity [43,52]. Four steps characterize the resorption profile of the material: 1) water sorption, 2) reduction of physical and mechanical properties, 3) reduction of molar mass and 4) loss of weight [53]. In the end, the implant loses its form and breaks into particles that can be phagocytized by macrophages. The by-products that result are excreted through the lungs and kidneys [19,54]. For this reason, giant cells and macrophages are considered responsible for the final elimination of polymer debris, contributing to the local tissue reaction that takes place around the biabsorbable implants [55].

The process of bioabsorption can also be classified in two erosion mechanisms: bulk erosion and surface erosion [53]. In the first case, hydrolysis occurs from the inside out while in the other case the resorption of the implant occurs from its outer surface toward its center, maintaining the bulk integrity [53].

A scheme of the degradation process of PLA, PGA and PDS is shown in Figure 2.3. Several factors can influence the degradation profile of the polymers and, consequently, the resulting biological response and mechanical properties of the implants. These factors include the polymer composition, density, M_W distribution, porosity, site of implantation, method of manufacture and sterilization, amorphous-crystalline ratio and implant geometry [56]. For example, the greater the density and the more hydrophobic the polymer, the slower will be the rate of hydrolysis [57]. The healing rate of the patient will also depend on the type of tissue

involved, the extent of injury, age and metabolic status of the patient, as well as diet and lifestyle [56].

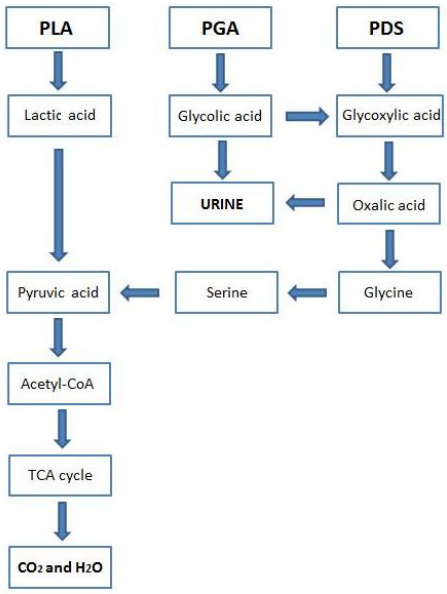

Figure 2.3. Degradation process of the bioabsorbable implants, according to the constituent polymer.

2.3.3. Production, storage, sterilization and testing

The production process of biopolymer-based orthopedic implants is of high relevance for their mechanical and biological performance. Since this type of polymers (α-hydroxy acids) are typically hygroscopic and hydrolytically labile, the presence of moisture may degrade them during processing, after fabrication and in storage [44,58]. During the fabrication process, it is important to avoid the hydrolytic degradation, in order to preserve the M_W of the polymer and, consequently, the final properties of the orthopedic implant. To do so, precautions should be taken to allow the polymer to dry before processing and to prevent it coming into contact with moisture while processing [44,58]. After manufacture, the polymers are quickly packaged in an inert atmosphere or vacuum. The packaged polymer should be handled as little as possible at room temperature when opened, in order to minimize condensation. Final packaging consists of placing the device in an airtight moisture-proof container. In certain situations the device may be stored at sub-ambient temperatures as an added precaution against degradation [44,58].

The sterilization method may influence the degradation profile of the polymer. Two of the most typical sterilization methods - autoclaving and dry heating - can significantly modify the device properties and specifications [5,59]. Typically the polymeric orthopedic devices are sterilized by γ-radiation, exposure to ethylene oxide (EtO) or, to a lesser extent, plasma etching[5,59]. However, these methods are not problem-free: gamma irradiation doses >20 kGy can degrade the bioabsorbable polymeric implant, reducing its M_W and influencing its final properties. In the case of EtO, it is necessary to ensure that the gas is totally removed from the device before packaging [5,59]. For example, for medical device applications PLA, PGA and PDS polymers are usually sterilized by exposure to EtO. Therefore, great care is needed to extract all the gas from the device before it is finally packaged, which may result in long vacuum aeration times [44].

Temperature and humidity conditions should also be considered during sterilization. Regarding temperature, this must be kept below the glass transition temperature to avoid changes in the polymer geometry and to preserve its shelf-life [5,44].

Before new fixation implants are approved and used in the clinical setting, they need to be properly tested for safety and performance for certification purposes. The same principle is applied in case of bioabsorbable polymer implants. The main goal of these tests is to determine and evaluate the implant's properties, clinical adequacy and design efficiency (materials and shape included). The array of tests includes *in vitro* and *in vivo* testing of the implants according to strict guidelines and specific requirements. For more information about the tests required by the FDA for the approval of the bioabsorbable implants, consult Appendix A.2.

2.4. Strategies developed to improve the properties of bioabsorbable polymeric fixation implants

Despite the clinical advantages of using bioabsorbable polymers in orthopedic fixation applications, the first generation of these implants presented adverse tissue reactions [55,57,60]. The reported problems are related with complications such as sterile sinus tract formation, synovitis, local osteolysis, hypertrophic fibrous encapsulation, intraosseous cyst formation, intra-articular inflammatory reactions and systemic allergic response [55,57,60]. The factors that can cause these problems are, for instance, the type of polymer, the site of implantation and its placement in a poor vascular area, the size of the implant and a fast degradation profile [55,57,60]. For instance, if the degradation rate exceeds the local clearance ability of the tissue, acidic by-products may accumulate in the medium and cause inflammatory reaction, hence interfering with bone formation. In addition, the initial mechanical properties of bioabsorbable fixation implants based on polymers are not ideal. Examples [61]:

a) Weakness of bioabsorbable implants after cannulation;

b) Bioabsorbable pins are unable to resist as much bending force as their metallic equivalents.

The initial production methods of bioabsorbable polymeric fixation implants were based on their thermoplastic properties, i.e. they were heated past their Tg temperature, softened, shaped and then cooled to retain their shape, through processes such as compression molding, injection molding and solving casting [5]. However, since the first generation of these implants presented a rapid degradation profile and unfavorable mechanical properties, new fabrication strategies were devised, including the development of copolymers and the self-reinforcement (SR) manufacturing technique [55]. In the first case, it is possible to combine two materials, optimizing the copolymer properties by changing the enantiomeric polymer rate - for example, PLDLA in the ratio 70:30. The development of the SR technique allowed for the production of smaller bioabsorbable polymeric implants, with higher strength, durability, ductility and biocompatibility [46]**.** This approach consists of reinforcing the polymer matrix with oriented fibers or fibrils of the same material, which have the same chemical composition as the matrix [20,46]. The non-reinforced bioabsorbable polymer can be transformed into a SR structure by solid state deformation techniques such as zone annealing, ram extrusion, hydrostatic extrusion and rolling such as die drawing, oven drawing and zone drawing [62]. In the case of

partially crystalline polymers, the reinforcement elements are normally groups of oriented polymeric chains that can form morphological structures (microfibrils, fibres, extended chain crystals, among others) [46]. Since there is a higher degree of molecular orientation, the polymers become stronger and more rigid in the direction of their long axis, which make them more comparable with cortical bone and even with metallic implants [55]. Therefore, these reinforced materials present appropriate mechanical properties for the construction of orthopedic implants. These properties include adequate initial strength, appropriate initial Young's modulus and ductile fracture mechanism, which prevent inflammatory reactions due to detachment of fragments [55]. The introduction of the SR technique has also enabled the manufacturing of devices that can be molded (in the operating room) with pliers and without the need for additional heating appliances [60]. For example, from the reported bending strength of 113-142 MPa [46], Törmalä *et al*.[63] were able to attain the value of 300 MPa with the construction of a SR-PLLA sample.

To improve both the biocompatibility and the mechanical properties of bioabsorbable polymers, biocomposites were also investigated. A composite consists of two different materials and normally a bioactive ceramic is used to mimic normal bone thus stimulating bone formation. In fact, bone is a composite material itself, comprising a mix of inorganic bone mineral and organic collagen fibers [64].

Bioactive ceramics include hydroxyapatite (HA), β-tricalcium phosphate (β-TCP), biphasic calcium phosphate, calcium carbonate and calcium sulfate. Both HA and β-TCP are composed of calcium and phosphate, the primary inorganic components of bone [26,28]. More specifically, synthetic HAp is a highly crystalline form of calcium phosphate, which presents the same chemical and crystalochemical properties of the bone. The crystallinity and chemical composition of β-TCP are also similar to those of the mineral phase of bone. These materials are excellent osteoconductive materials, capable of stimulating the formation, precipitation, and deposition of calcium phosphate from simulated body fluid resulting in enhanced bone-matrix interface strength [64].

The combination of a bioabsorbable polymer and ceramic creates allows a faster resorption of the calcium phosphate components during polymer degradation and therefore a better bone ingrowth [26]. Thus, less inflammatory responses were registered when ceramics were added, for example, to PLLA and PLGA. Additionally, ceramic degradation releases basic salts that buffer the acidic breakdown products of the polymers [26]. Cells responsible for the degradation/resorption of ceramics act through two main mechanisms: phagocytosis and extracellular acidification (resorption). These processes are modulated by various parameters, such as the implantation site and the presence of various proteins [65]. The cells implicated in this degradation process (mesenchymal cells, monocytes/macrophages, osteoclasts) will intervene directly or indirectly through their cytokines/growth factor secretions and their sensitivity to the same substances which modulate cellular activities [65].

The design of the bioabsorbable polymeric implants also influences its properties [58]. With reference to screws, there are several studies that indicate that design characteristics such as thread diameter, screw length, gap size and drive mechanism influence the fixation strength and, consequently, bone stability [66,67]. Therefore, several geometries and/or dimensions of bioabsorbable pins, screws and plates are currently available in the market.

Although bioabsorbable polymeric fixation implants have been used extensively over the last years, their use has not overtaken metals in the majority of orthopedic applications areas. This

may be explained by the fact that most physicians are not familiar with this technology and/or their long term experience-based confidence with the use of metals; concerns regarding limitations of polymer implants in terms of mechanical properties, the clinical efficacy and the physiological response of the tissues to the degrading products; and higher commercial costs of bioabsorbable implants [5,30]. Despite such limitations, bioabsorbable fixation implants do not lose popularity since they avoid removal and do not affect bone remodeling due to the lack of stress shielding effect [61].

2.5. Reported drawbacks of the clinical use of bioabsorbable polymeric fixation implants

The successes and drawbacks resulting from the use of bioabsorbable implants in clinical practice can be assessed by reviewing the literature. Gawęda *et al*.[68] compared the clinical results of 20 patients who had been treated with bioabsorbable screws made of PLLA with 22 patients treated with metal screws, in an ACL reconstruction. The results showed that there was no difference between the two groups in terms of easy-to-use and knee stability. However, 14 of the 20 patients in the study group had severe pain, which was not relieved after regular doses of non-steroidal anti-inflammatory medication. Of these patients, 6 had developed a large cyst. In the case of the control group, none of the patients developed clinical symptoms despite mild pain during palpation over the screw head area.

Parsons *et al.*[69] evaluated the degradation profile of a 85% PLLA/15% PGA cross-pins in four patients who underwent ACL reconstruction using hamstring autograft (in femoral fixation). The results showed that the cross-pins remain unchanged 4 months after surgery, which means that this pin ensured the structural integrity time during the critical period of biologic graft healing. After one year, the pins had degraded by a mean of 49.1% and two of them had fractured; after two years they had degraded by a mean of 75%, and all of them had fractured but no signs of osteolysis or other signs of aggressive inflammation were registered.

In another study, Shen *et al.*[70] collected the clinical outcomes of a set of studies comprising 790 patients who were treated with bioabsorbable and metallic screw fixation in ACL reconstruction. The results, for a follow-up period of 1-2 years, suggested that there is no obvious advantage of one type of screw over the other regarding the clinical functional outcome (e.g. knee joint stability and knee joint function). However, the results indicated that PLLA implants caused more local osteolysis than metal implants and a prolonged effusion in the knee joint was more likely to happen after ACL reconstruction surgery with bioabsorbable screw fixation.

Using another approach, Pereira *et al.*[71] did a PubMed review search looking for complications related with bioabsorbable screws used in ACL reconstruction, with the goal of understanding whether migration was a possible complication. The authors concluded that migration could happen, although only 10 articles referred to this complication among the 102 studies selected by the authors. Based on these 10 articles, the authors concluded that the migration problem was mostly reported in studies involving PLLA screws, which could also be related to the fact that this polymer is the most frequently used in ACL reconstructions. However, given the low evidence level of the studies and the lack of prevalence control of such

complications when metallic screws were used, the authors were not able to made statistical calculations.

In the shoulder, Dhawan *et al.*[72] performed a literature review on complications related with the use of bioabsorbable suture anchors in the shoulder. The authors reported literature evidences of foreign body reactions, osteolysis, chondrolysis and implant failure. Nho *et al.*[73] explained that bioabsorbable suture anchors are gradually being replaced by metallic anchors due to migration, implant loosening and breakage and articular cartilage injury concerns. These authors analyzed the literature and reported a series of problems, concluding that there is evidence that complete PLLA degradation can take several years and complete osseous replacement was not registered. On the other hand, they found that composite implants (example: TCP and PLLA) induce minimal tissue reaction with complete absorption followed by bone ingrowth. Park *et al.*[74] analyzed a cohort of 348 patients who underwent arthroscopic superior labrum repair and followed them in the same institution over a 10-year period. The authors observed a significantly higher repair failures when bioabsorbable PLDLA anchor material was used compared with nonabsorbable suture anchors. PLDLA 96L/4D anchors were used in 62 patients and in 15 of these patients a second operation was required due to recurrent or persistent symptoms of pain and disability. The authors suggested that the mechanical properties and the material composition of the suture anchors may contribute to the difference of reoperation rates between bioabsorbable and non-bioabsorbable suture materials. As a consequence, loss of fixation, premature anchor breakdown and osteolysis may occur. McCarty III *et al.*[75] analyzed a cohort of 44 patients who had undergone an arthroscopic debridement procedure to treat loss of motion and pain following a primary labral or rotator cuff repair with PLLA implants. Macroscopic anchor debris was observed and biopsy samples were obtained, concluding that most patients had chondral damage within the glenohumeral joint, and the majority of the synovial biopsies revealed giant cell reaction, papillary synovitis and crystalline breakdown products.

Givissis *et al.*[76] assessed the outcome of treating metacarpal fractures with bioabsorbable plates and screws composed of the following copolymers: trimethylene carbonate (TMC), PLLA and PLDA. Foreign-body reactions were observed in 3/10 patients during the second post-operative year. These patients presented pain that interfered with daily life and required new surgery to perform debridement of the implant remnants. Two other patients reported transient local swelling. The authors concluded that modern implants, with slow degradation rates, do not avoid foreign body reactions but simply postpone their occurrence during the post-operative time. They also suggested that the anatomic location of the fractures can influence the adverse reactions since the relative paucity of subcutaneous fat and insufficient muscle vascularity can hinder the dissipation of degradation products. Clinical problems resulting from bioabsorbable polymer implants use in the treatment of fractures in distal radius are also mentioned in the literature. For instance, Yang, *et al.*[77] reported a case of a fracture that was reduced anatomically and fixed with a bioabsorbable plate and six screws composed of TMC, PLLA and PLDA. However, one year after the primary surgery, a painful nodule developed over the volar aspect of the right wrist and the patient had to undergo further surgery. The nodule was excised and histology confirmed the diagnosis of foreign body reactions.

Several studies have also been published taking into account applications of bioabsorbable implants in young patients. The group Camathias, *et al.*[78] assessed the results of using

bioabsorbable screws in the treatment of osteochondritis dissecans (OCD) in skeletally immature patients. The authors followed 24 patients (30 knees) for a minimum period of 2 years. These patients were treated with a total of 61 screws composed of PLDA (96L/4D copolymer). After 6 months, edema was present in 17 out of 30 knees (34 out of 61 screws). However, of the 24 patients only 4 presented pain or locking sensations at the last follow-up. The authors observed 4 patients with completely implant failure and 5 patients with additional 7 broken screws. All implant failures led to revision surgery, the majority occurring in the eighth month. In conclusion, the authors hypothesized the differential decomposition, between screw head and body, as the major factor that lead to screw failure**.** In another pediatric area, An, *et al.*[79] treated different mandibular fractures in 39 young patients using bioabsorbable plates . Follow up by computed tomography revealed osteolysis, evident just one month after surgery and within one year after surgery. However, the authors concluded that the use of bioabsorbable fixation in pediatric mandibular fractures is safe and effective, and the osteolysis detected did not affect the fracture healing process.

2.6. Current Research for Bioabsorbable Polymer Fixation Implants in Orthopedics

The shortcomings associated with the use of bioabsorbable polymer fixation implants have encouraged scientists and surgeons to look for alternatives. Current strategies to design new bioabsorbable polymeric fixation implants are dependent in the research and development of bioactive implant materials [80]. These must be able to support bone growth and encourage the ingrowth of surrounding bone (osteoconductive property) as well as promote the differentiation of progenitor cells into osteoblastic cells (osteoinductive property). They must be also capable of integrating into the surrounding tissue (osteointegration property) and able to promote vascularization and mechanical stability [23,81].

The area of tissue engineering plays a crucial role in the development of new treatment strategies for a wide array of orthopedic tissues**.** The goal of tissue engineering is to assemble functional constructs able to restore, maintain or repair damaged tissues [64,82]. These constructs involve scaffolds, which are three-dimensional degradable structures produced, for example, by freeze-drying.

Scaffolds have two parallel roles in the tissue healing process: 1) to provide support and 2) to allow new bone formation and growth inside the porous structure, which degrades over time, leaving a new regenerated bone tissue [20,28]. In fact, orthopedic implants with an interconnected pore structure are of particular interest for orthopedic applications due to their ability to enable cell nutrition, cell migration and cell attachment [80,83]. For this reason, scaffold architecture and morphology are important factors in the development of these structures. Further important properties of scaffolds are their biodegradability and the physical stability required to meet the functionalities possessed by the different tissues [80,83].

The application of scaffolds includes [84–87]:

a) Bone tissue engineering, for bone augmentation in the treatment of bone defects and large bone fractures;

b) Cartilage tissue engineering, to promote proper chrondrogenesis and ECM development;

c) Ligament tissue engineering, in the development of tissue grafts;

d) Tendon tissue engineering, in the regeneration of tendon tissues and nerves.

A broad number of natural and synthetic bioabsorbable polymers are currently used in the tissue engineering field. The synthetic polymers list includes the previously referenced, PLA, PGA and PDS, but also polymers such as polycaprolactone (PCL), polypropylene fumarate (PPF), polyurethanes (PU), among others. Natural polymers includes polyhydroxyalkanoates (PHAs), gelatin, elastin, albumin, collagen, chitosan, alginic acid, chitin, cellulose, silk and hyaluronic acid [64,83].

Research findings include the evidence that scaffolds loaded with mesenchymal stem cells (MSCs) are an efficient technique, capable of healing large bone defects [88–90]. MSCs are multipotent cells able to differentiate into several cell lineages, including osteogenic precursors [91]. Bone marrow is the major source of these cells, although they are present in other tissues including the placenta, the umbilical cord blood and adipose tissue [91,92].

To construct biologically oriented implants, studies have been made incorporating antibiotics, anti-inflammatory agents and growth factors [56]. Antibiotics help to reduce infections**,** anti-inflammatory agents (e.g. dexamethasone and prednisolone) control the foreign body reactions upon implantation, whereas growth factors, namely bone morphogenetic proteins (BMPs), stimulate the bone formation thus enhancing the healing process [93,94]. Among the family of BMPs, the BMP-2, -4 and -7 possesses a strong ability to induce bone formation [95]**.** To be effective and exert their biological effect, BMPs need to be combined with carriers for a controlled release, mainly due to their pharmokinetics, short half-life and lack of form [93,96]. Various materials and formulations of delivery system may be applied, according to the type of tissue to be regenerated and the local mechanical solicitation [93,96]. However, further research in this area is still needed for the creation of an optimal delivery system that can decrease the dose of BMP, maintaining a more sustained release pattern [96].

Bioactive glass is another type of material that promotes the bioactivity of the implant. The first bioactive glass investigated for biomedical applications was Bioglass 45S5, but currently several other different types of bioactive silicate glasses, in a variety of compositions, are being investigated for potential use in the orthopedic field [97,98]. The common characteristic of these materials is their high surface reactivity, which enables the effective interaction of the material with the host tissue [97]. Recent research has been focused on bioactive glass/bioabsorbable polymer composite materials, where conventional (micron-sized) bioactive glass particles are used as fillers or coatings [99]. However, it is expected that nano-sized bioactive glass particles and nanofibers, which have only become available in the last few years, will be employed in the future. These nanostructured materials are expected to improve both the mechanical and biological properties of such composites [99].

Altering the surface of the implants is a current research strategy aiming to reduce or even eliminate the foreign body reactions associated to the implant [100]. The surface wettability of the implants plays an important role in biological host responses. For implants with hydrophilic surfaces, there is a higher functionality of the absorbed proteins. Cell functions are impaired by hydrophobic surfaces since these promote conformational changes of the adsorbed proteins, which limit cellular adhesion and function [100–102]. Various strategies can be then employed to increase the hydrophilicity of the biomaterials, such as plasma treatments to induce polarized groups, by using reaction gases, and photo-oxidation to introduce peroxide groups by immersing the polymers in hydrogen peroxide under UV radiation [7,100–104].

Further strategies employed to stimulate osteointegration and promote bone ingrowth include nano-texturing the implant surface as well as coating the implant surface with hydroxyapatite (HA) and attaching arginine-glycine-aspartic acid (RGD) sequences to a modified implant surface. RGD sequences can be used because cells use them to attach to the ECM [7,105]. Implant morphology influences bone metabolism: rougher surfaces stimulate differentiation, growth and attachment of bone cells and increase mineralization. Therefore, the degree of roughness is important [7,105]. The most reported methods in the literature for creating implant roughness are acid etching, sandblasting, titanium and HA plasma spray coating [100]. A current tendency is the manufacturing of implants with micro and nano topography [100].
To stimulate blood vessel ingrowth around implants, their surfaces could also be coated with a polymer coating containing the angiogenic growth factor VEGF. Recent studies have also revealed that the addition of exogenous Wnt-3a protein (Wnt family member) to an injury site stimulates bone regeneration, stimulating the differentiation of pluripotent stem cells towards an osteoblast cell fate [105]. This relates with the role of Wnt signaling in bone formation [105].
To promote the osteintegration of bioabsorbable implants Hur, *et al.*[106] coated a commercial bone plate with alendronate. They showed that this drug can have an active role in preventing the failure of the fixation systems since it promoted a higher volume of newly formed bone, in an animal model, when compared with plate samples without the drug. However, the authors suggested further studies to assess all the clinical advantages of using such constructs in the treatment of fractures or bone loss due to osteoporosis. Another alternative is to promote osteointegration throught new surgical techniques. In this sense, based on the clinical experience with metal implants, Augat *et al.*[107] liquefied bioabsorbable pins by ultrasonic energy. In this case, the pins were used for the fixation of hallux valgus corrections. The implant material has flowed into the trabecular bone porosities, forming a more stable fixation. According to the authors, this technique allowed adequate and consistent mechanical fixation with high reproducibility and revealed good short-term resorption and biocompatibility. This surgical technique was also used sucessfuly by Schneider *et al*.[108] in the treatment of mandibular fractures of the condylar neck.

Other research topic in the area of bioabsorbable polymer fixation is the improvement of the mechanical properties of the implants, in relation to the bone's intrinsic mechanical properties. Efforts have been made towards the creation of better composites by joining bioabsorbable polymers with ceramics (chapter 2.4). However, the potential of using other bioabsorbable polymers as raw-materials for the development of new orthopedic implants is also being studied. In this field, chitosan is being used to produce dense bioabsorbable specimens using the solution casting process. This processing method is necessary to overcome the relevant limitations of chitosan when being processed using conventional plastics processing techniques [109]. These limitations include its sensitivity to heat, since chitosan's decomposing temperature is lower than its glass transition temperature (Tg) [13,109]. Despite such limitations, chitosan has other excellent properties (e.g. availability, biocompatibility and biodegradability), which make it an excellent candidate for temporary orthopedic applications [110]. Chapter 3 further explores the properties and applications of chitosan materials.
Bioabsorbable polymers belonging to the PHAs family are also under study for the production of new bioabsorbable implants, with improved mechanical properties. These polymers are

derived from microorganisms and are produced commercially by biotechnology, hence they are renewable by nature [111,112]. The biocompatibility, rate of degradation and mechanical properties can be controlled by changing the composition of PHA polymers, since they are influenced by the functionalized groups in the side chain of monomers (e.g. carboxyl, hydroxyl, etc.) [112]. In this class of polymers, studies on poly-4-hydroxybutyrate (P4HB) polymer revealed that it is well tolerable by the body and it is more flexible than PGA and PLLA, with a slow degradation rate and a higher tensile modulus [112–114]. The use of this material for the construction of bioabsorbable fixation implants is still under development. However, orthopedic products based on this polymer are already on the market, for example, in the form of Phasix® mesh for hernia repair and BioFiber® orthopedic soft tissue scaffold for sports medicine [114]. Other polymers belonging to the PHAs class, studied for the treatment of orthopedic conditions with , include poly 3-hydroxybutyrate (PHB) and 3-hydroxyvalerate (PHBV) [115].

Biostable polymers such as polyethylene terephthalate (PET), nylon and PEEK have recently been studied in order to transform them into bioabsorbable polymers through changing of the backbone chain of the biostable polymer. The goal is to combine attributes of biostable and bioabsorbable polymers in new orthopedic implant creation, which will allow for improved stability and a better degradation profile [116].

Outside the scope of polymeric materials, magnesium (Mg) has also started to be studied as bioabsorbable implant material [117–119]. Studies have revealed that Mg is a suitable material for orthopedic applications, since its direct degradation product (by oxidation), Mg^{2+}, is safely absorbed under physiological conditions, being one of the essential elements of the human body [120]. It also provides mechanical properties superior to bioabsorbable polymeric materials but inferior to permanent metallic implants, avoiding the stress shielding effect [119]. Mg alloys are an attractive material since they are easily manufactured and have properties close to the bone [42,121]. With the advances in corrosion prevention, processing techniques, novel structure designs and surface modification methods, Mg-based alloys have become a feasible candidates for bioabsorbable implants [119,122]. Examples include alloys with elements that also exist in the human body or have a beneficial effect during the regeneration and healing of the tissue, such as Mg-Zn, Mg-Sr, Mg-Zn-Sr and Mg-Ca-Zn alloys [123]. However, there are still difficulties in assessing and controlling the *in vivo* corrosion and biocompatibility of Mg-based materials for orthopedic applications [118], which motivates continuos research in this field. In the future, it is also expected that other materials, namely Ca-based, Sr-based and Zn-based bulk metallic glasses, could also be considered an option for orthopedic applications [124,125].

Silk-based implants are also being developed as a strategy to solve the limitations presented by the current implant materials [126]. However, Perrone *et al.*[126] showed that the mechanical strength of such materials decrease considerably when hydrated, which represents a limitation in *in vivo* conditions. Once again, further research is still necessary in this field.

The new developments in the area of bioabsorbable polymeric fixation implants in orthopedics can be assessed not only through literature, but also through the knowledge of currently ongoing clinical trials. A few searches on the Clinical Trials database [127] for the terms “bioabsorbable”, “bone fixation”, “bone fracture”, “scaffolds”, “screw” and “plates”, demonstrate that clinical trials are focusing on the tissue engineering field. Completed clinical trials include the study of antibiotic releasing bioabsorbable screws or CPC/rhBMP-2

microffolds for bone regeneration, for the treatment of tibial plateau fractures, proximal humeral fractures and calcaneal fractures.

2.7. Conclusion and future directions

The use of bioabsorbable polymeric fixation implants in orthopedic surgery has enormous potential and has evolved considerably over the past few years. Currently, the commercial bioabsorbable implants are mainly based on synthetic polymers or on composites of ceramics and synthetic polymers. However, since these materials present some drawbacks, several methodologies are currently being studied to improve their performance. Points of improvement include the creation of a tunable degradation profile of the materials, to more closely match the bone healing process, and the improvement of implant biocompatibility, in order to reduce or even eliminate the cases of inflammation or other reactions resulting from the interaction between implant and biological tissue.

The ideal orthopedic composite material implant should combine osteogenic, osteoinductive and osteconductive properties. Therefore, the main function of an optimal bioabsorbable implant should be the following:

a) Support the injured area, providing adequate initial mechanical strength and stiffness;
b) Stimulate new bone formation;
c) Degrade over time, without causing any tissue reaction;
d) Allow the remodeling of the new bone while assuming the mechanical support function.

In this order, the area of tissue engineering is considered promising for the development of implants that promote bone tissue repair, due to either a normal fracture or some bone pathology. In this field, a wide range of strategies are being studied, including the construction of scaffolds loaded with cells (for example, MSCs) and growth factors, thereby stimulating the formation of new bone. However, scaffolds can only be successfully applied to the treatment of musculoskeletal disorders, namely in trauma fixation, if they present an adequate anatomic geometry, mechanical strength and regenerative capacity. Mainly due to the weak mechanical properties associated with scaffolds, the immediate future applications may rely on the improvement of current bioabsorbable polymeric implants using the composite approach, eventually coated by substances that improve the osteointegration and agents that promote bone healing without inflammation.

The expected developments in the area of bioabsorbable implants will also allow for the exploitation of manufacturing techniques of individual and personalized bioabsorbable polymeric implants. Therefore, CAD-/CAM-based manufacturing techniques could help to design and manufacture an implant structure based on a previous scan of the bone defect. The benefit for the patient is obvious: a more correct and precise fit of the implant to the bone. In this field, additive manufacturing techniques could have the potential to manufacture scaffolds/implants of any desired shape with a defined and interconnected porous structure. Furthermore, these techniques (e.g. laser sintering and fused deposition modeling) have the potential to generate structures with gradients of cells and with mechanical properties that are able to support implant integration and osteoconduction.

With the advances of the additive manufacturing technology, the future of orthopedic personalized surgery could also include bioprinting bone directly into the patient's body.

Nanotechnology will also have an important role in the development of new bioabsorbable polymer orthopedic implants. As explained previously, bone is a natural nanostructured composite material composed of inorganic material (calcium and phosphates) and an organic matrix (collagen type I). Thus, the advantage of nanotechnology is to create materials that mimic the natural nanostructure of the bone. Additionally, bone presents different levels of structure: the nanostructure (e.g. the small crystals of calcium and phosphates), the microstructure (e.g. Haversian systems) and the macrostructure (cortical and trabecular bone), which shows that to design better bioabsorbable polymeric fixation implants it is also necessary to take into account these heterogeneous and anisotropic characteristics of the bone.

It is also anticipated that in the future there will be an increased consciousness and concern about the source of the raw materials used for the construction of bioabsorbable fixation implants. Since the current sources of material are finite, sustainable and environmental friendly material resources are recognized being fundamental for the growth of a green economy and a productive industry. Therefore, natural polymers such as PHAs, cellulose and chitosan, among others, have great potential due to their availability and properties.

As a main conclusion, there is currently no optimal bioabsorbable polymeric fixation implant on the market. For the development of new successful bioabsorbable polymeric fixation implants, the mechanical properties, the degradation/resorption profiles and the interfacing between the material and the surrounding bone tissue need to be better studied and controlled in order to construct bioactive fixation implants.

3. Chitosan as a natural polymer for biomedical applications

A large proportion of by-products generated by the seafood industry are considered as waste. The pollution caused by these by-products can have a negative impact in the environment and society if their disposal is not done properly. For example, the management of waste from the seafood processing industries (e.g. heads, tails, shells and backbones) is simply to throw them back at sea, burn them or landfill them [128].

To reduce risks and optimize the value of the production chain, the resulted waste of the seafood industry began to be considered an excellent source of substances of high value, with notable biological properties: proteins, pigments, polymers and lipids [128]. Due to this vision, chitin and its water soluble derivative - chitosan - started to be commercially produced and applications based on these materials were promoted, studied and developed.

Besides the environmental motivation, other factors promote the industrial production of chitin and chitosan. These factors rely on their distinctive structures, with vast possibilities for structural modifications due to the presence of reactive functional groups [17]. This capacity allows multidimensional properties, functions and, consequently, applications. The positive attributes of these natural polymers include their excellent biocompatibility and biodegradability, their low toxicity and immunogenicity as well as their antimicrobian and antioxidant capacity [129].

The research around chitin and chitosan is quite large, and involves areas such as biomedicine, chemistry, biotechnology, veterinary medicine, dentistry, agriculture, food processing, environmental protection and textile production[130]. A recent search on Pubmed (search executed on October 2016) for “chitin” revealed over 20.000 results and for “chitosan” revealed over 18.000 results. This observation proves the importance of these two materials in the previously described areas.

In this chapter, the source and production methods of chitin and chitosan will be explored. Focus will be given to chitosan properties, since it has more commercial applicability. A brief summary about the several industrial applications of chitosan will be presented, and attention will be given to its biomedical applications. Current trends of chitosan in the biomedical field are explored, and the issues that regulate the approval of chitosan-based products in this area are explained. Finally, the challenges for the development and manufacturing of new products based on chitosan are discussed, which are strongly related with the stability of chitosan materials.

3.1. Source and production

Chitin is the second most available polysaccharide worldwide, after cellulose, and it is also considered the most abundant biopolymer in the marine environment, since it is produced by many marine organisms [131]. Annually, the chitin production by living organisms is approximately 10^{10} tons [131]. However, the commercial production of chitin results from its extraction from the crustaceans´ shells, due to its high content and ready availability [132]. According to Merzendorfer [133], more than 10.000 tons of chitin could be available every year

from the waste of the seafood industry. The majority of companies who produce large amounts of chitin and chitosan are localized in Japan and the U.S. [130].

The availability of chitin in crustaceans' shells waste vary, but normally the exoskeletons contain 15%-40% chitin along other compounds (pigments and lipids), 30%-50% proteins and 30%-50% minerals (mainly calcium carbonate) [128,130]. The variation of these components is depends on the species, body parts and harvesting season [128]. For example, the content of mineral salts is influenced by the hardness and permeability of the crustaceans' shells, which in turn depend on the age and the reproductive cycle of the animals [130]. Another example: reporting the distribution of fatty acids in crustacean lipids is difficult, since it is hard to assess the influence of these data by the type of ecosystem (marine water vs fresh water), species and its maturation, harvesting season, feeding conditions, storage and processing history [130].

Among crustaceans, shrimp is the most processed species in the seafood industry. The waste of shrimp consists of its exoskeleton and the cephalothorax, which represent 50%-70% of its weight [132]. The approximate composition of shells waste from certain shrimp species are shown in Table 3.1.

Table 3.1. Approximate composition of shrimp shell wastes - dry basis [130].

Shrimp species	Chitin content (%)	Protein content (%)	Lipid content (%)	Ash content (%)
Pandalus borealis	17	41,9	5,2	34,2
Crangon crangon	17,8	40,6	9,9	27,5
Penaeus monodon	40,4	47,4	1,3	23,0

Chitin extraction consists of three main steps: demineralization, deproteinization and discoloration/bleaching. The common chemical method used to accomplish these steps is outlined in Figure 3.1.

Besides the chemical process, chitin can also be obtained by biotechnological methods. In this case, the demineralization process is accomplished by organic acids, such as lactic acid produced by bacteria. In turn, the deproteinization process is promoted by proteases (e.g pepsin, trypsin and pronase) secreted into the fermentation medium or by adding exo-proteases and/or proteolytic bacteria [134].

Chitosan is obtained from chitin, as illustrated in Figure 3.2. The chemical process is performed at elevated temperatures (80 to 140°C) at prolonged exposures, using concentrated alkaline solutions (30% to 60% w/v) [130]. The alkali concentration, time and temperature of the process should be controlled rigorously, because these parameters strongly influence the intrinsic properties of the chitosan (e.g. deacetylation degree, D.D., and M_w) [130,135].

An alternative to the chemical deacetylation of chitin is the enzymatic process by deacetylases produced by bacteria. The enzymatic deacetylation produces chitosan with well-defined content of N-acetylated residues and range of M_W, contrary to what happens in the chemical production process of chitosan.

Comparing the two processes of chitin extraction and chitosan production, several advantages and disadvantages can be identified. The chemical process has the main advantage of having short processing times, however several negative implications result from the use of strong acids and bases, as reported in Table 3.2 [134,136]. For these reasons, the interest in the biological processes is increasing, being considered a safer a less expensive method. Nevertheless, to be used in large scale, some difficulties should be overcome in order to

achieve an optimization of the biological process. The goal is to bring the impurities down and to minimize chitin degradation [136].

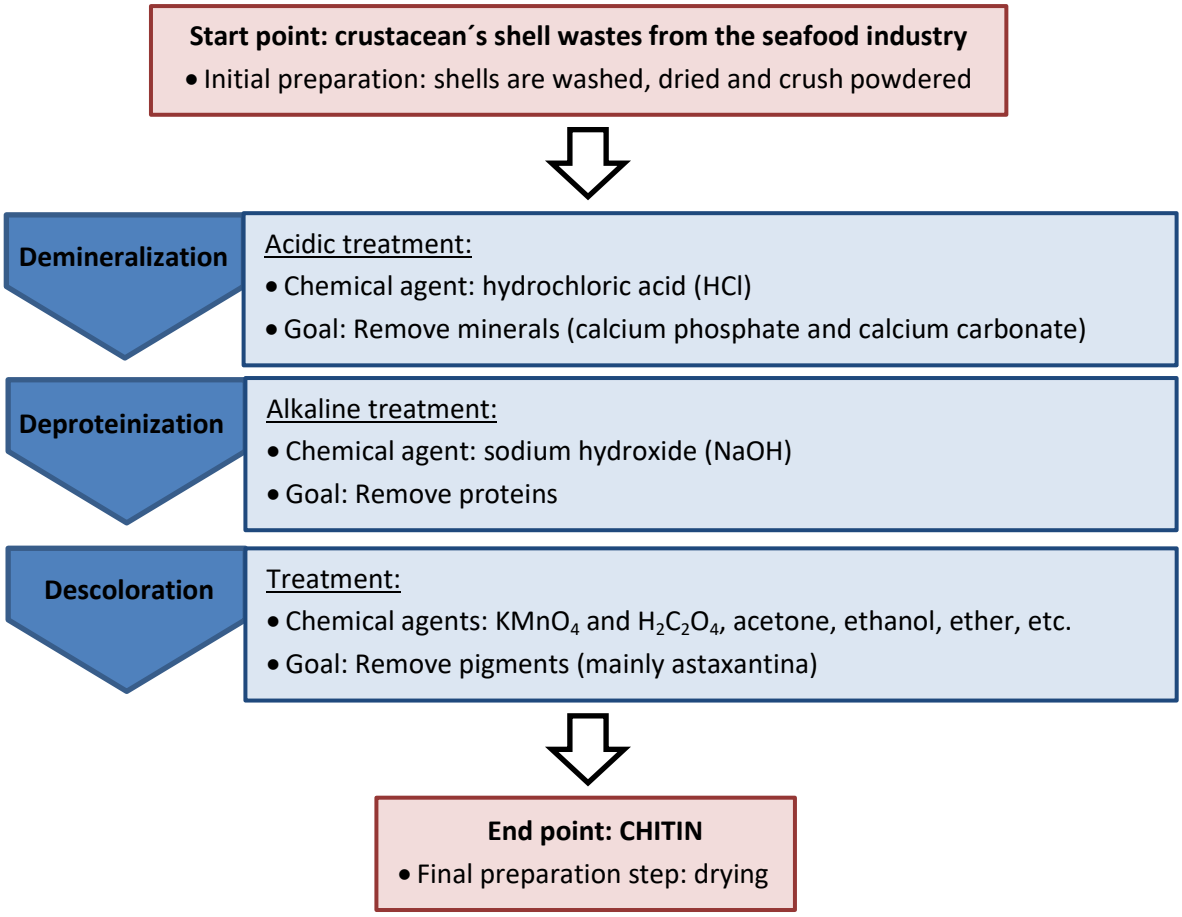

Figure 3.1. Chemical extraction of chitin.

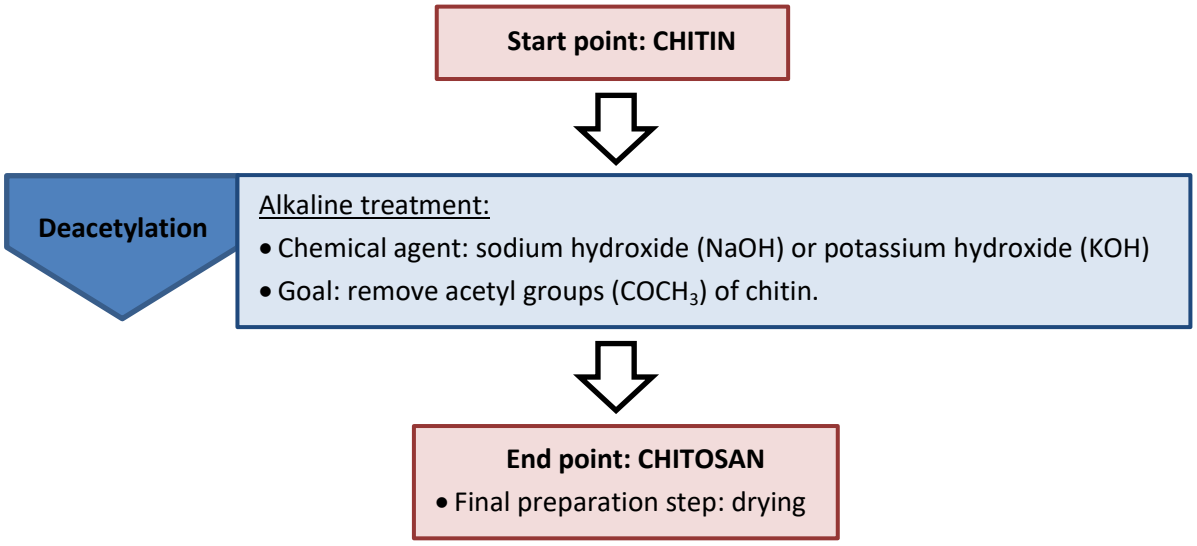

Figure 3.2. Chemical production of chitosan.

Table 3.2. Comparison between chemical and biological production methods [134,136].

	Chemical production method	Biological production method
Advantages	• Used at the industrial scale. • Well established process and short processing times at large scales.	• Environmentally safe due to the absence of effluents. • Lower cost. • Removed proteins and minerals may be used as human and animal nutrients source.
Disadvantages	• Environmentally unsafe – effluent wastewater contains highly concentrated chemicals. • Increases the cost of purification. • Removed proteins and minerals cannot be used in human and animal food supplements. • High cost.	• Current technology is limited to laboratory scale studies. • Biological contamination caused by microorganisms.
Product Quality	• Inconsistent levels of D.D. which affect the intrinsic properties of the products. • The organic salts are completely removed; however, at the same time, deacetylation and depolymerization reactions may occur.	• Homogeneous and high quality of the final product.

3.2. Structure and properties

Chitin is a linear polysaccharide, composed of D-glucosamine and *N*-acetyl glucosamine linked by β(1–4) glycosidic bonds. In turn, chitosan is a linear polysaccharide that contains copolymers of D-glucosamine (deacetylated units) and *N*-acetyl-D-glucosamine (acetylated units) linked, as well, by β(1–4) glycosidic bonds. The chemical structure of both biopolymers is shown in Figure 3.3.

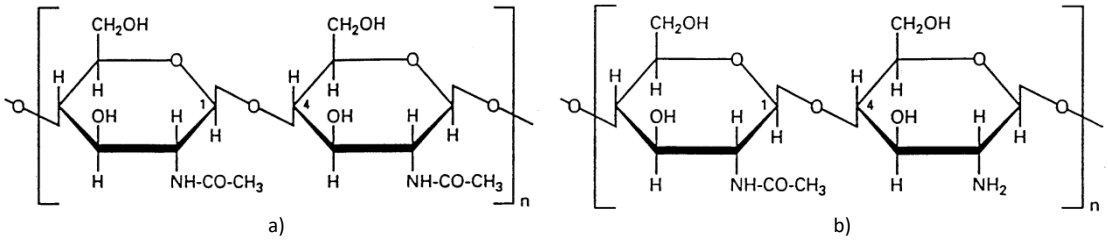

Figure 3.3. Chemical structure of (a) chitin and (b) chitosan repeat units.

Chitin occurs in nature in three different structural forms, according to the arrangement of the carbohydrate chains: α-chitin, β-chitin and γ-chitin [128,137]. The first configuration is much more abundant and has higher stability comparing to the others. The stability of α-chitin comes from the hydrogen interactions between chains [137].

Chitin is highly hydrophobic, thus it is insoluble in water and in common solvents. This characteristic of chitin is related to its rigid chain structure caused by existent strong intermolecular hydrogen bonding [128]. In turn, chitosan is insoluble either in water and organic solvents, but it can be dissolved in weak acidic aqueous solutions (pH<6) which makes chitosan

a more versatile polymer than chitin [135,138]. The solubilization of chitosan is due to the presence of amino groups and occurs by protonation of the amino group on the C-2 position of the D-glucosamine repeat unit [16,138].

The ratio between glucosamine/*N*-acetyl glucosamine, referred as the D.D., can vary from 30%-100% [110]. Commonly, if the D.D. is lower than 50% the biopolymer is named chitin, otherwise it is named chitosan [110].

Crystallinity may reach a maximum for a D.D. equal to 0% or 100% (chitin or fully deacetylated chitosan, respectively - homopolymers) and decreases for intermediate D.D. [139]. Therefore, chitin and chitosan are considered semi-crystalline polymers [17,138].

Chitosan become the focus of more attention since it is more reactive than chitin, which allows higher range of applications [17,140]. The polycationic nature of chitosan promotes the formation of ionic complexes with several different natural and synthetic anionic materials such as DNA, lipids, proteins, glycosaminoglycans (GAG), proteoglycans and poly (acrylic acid) [16,139]. The amino and hydroxyl functions allow the formation of stable bonds with other materials along the chitosan backbone [139]. Reactions such as quaternization, alkylation, grafting, O-acetylation, H-bonding with polar atoms, among others, enable a variety of products and applications [17,139,141]. This polyvalent capacity of chitosan allows the development of products with advanced properties and functions such as antibacterial, anti-fungal, anti-viral, muchoadhesive, analgesic, non-toxic, hemostatic, biocompatible, biodegradable, etc. [17,139].

So far, the information available indicates that any allergic and inflammatory reactions after implantation, topical application, injection and ingestion of chitosan have been reported in the human body by clinical trials [129]. The biocompatibility of chitosan is explained by the glucosamine and its derivative *N*-acetylglucosamine that are natural components of mammalian tissues [129]. Additionally, *in vitro* cytocompatibility of chitosan has been proved with fibroblasts, hepatocytes, condrocytes, keratinocytes and myocardial, endothelial and epithelial cells [142,143].

The hemostatic property refers to the coagulation of the blood in order to stop its flow through the injured vessel wall [144]. The hemostatic activity of chitosan is related to its positive charge that causes agglutination of red blood cells, which have negatively charged membranes [143]. Besides its capacity to control bleeding, the antimicrobial activity of chitosan helps in controlling infection at a bleeding site [145].

The antimicrobial activity is one of the most studied properties of chitosan [146]. The studies suggest two main mechanisms of action against bacteria, yeast or fungi. One of these mechanisms is the interaction of chitosan with anionic groups on the cell surface, causing the formation of an impermeable layer around the cell of the microorganism [143,147]. This impermeable layer changes the permeability and avoids the transport of fundamental solutes into the cells and/or lead to the leaking of solutes out of the cells [139]. The other mechanism involves the penetration of chitosan into the cell structure, the binding with DNA and the inhibition of the RNA and protein synthesis [143,147].

The analgesic effect of chitosan comes from its polycationic nature. In this case, the amino groups of the D-glucosamine residues can protonate in the presence of the proton ions released in the inflammatory area [10,143]. As a consequence, the pH of the inflammation area decreases, promoting the analgesic effect [143].

The antitumor activities of chitosan were detected by a direct effect on tumor cells, since it inhibits their proliferation by inducing apoptosis [147,148]. Further studies observed an immune

stimulation effect of chitosan, due to an increase in secretion of interleukin-1 and interleukin-2 which caused maturation and proliferation of cytolytic T-lymphocytes (type of white blood cells that kills tumor cells) [149].

The mucoadhesion of chitosan is promoted by the sialic acid present in the mucin, which is the glycoprotein that composes the mucus [139]. In the stomach, chitosan is positively charged due to the acid environment, thus it can interact with mucin by electrostatic forces [143]. Therefore, not only the intrinsic properties of chitosan influence this union, but also the amount of sialic acid present on the mucin.

The permeation effect of chitosan is based on the interaction between its positive charges with the negative part of the cells membrane [139,143]. This interaction leads to a reorganization and opening of the tight junction-associated proteins, which explains this permeation enhancing effect of chitosan [139,143].

The antioxidant property of chitosan results from its capacity of scavenging oxygen radicals such as hydroxyl, superoxide and alkyl [147]. Therefore, chitosan and its derivatives act as hydrogen donors to prevent the oxidative sequence [147]. Additionally, chitosan can also prevent oxidative damage of human body by interrupting the radical chain reaction of oxidation [144].

The majority of the biological properties of chitosan come from the presence of the amino groups that confers its positive charge. However, the biodegradability characteristic of chitosan results from its polysaccharide structure which contains breakable glycosidic bonds.

Chitosan is enzymatically degraded *in vitro* by chitinase, chitosanase, lysozyme and pectinase [150]. Some proteolytic enzymes can also degrade chitosan, however they have a lower-level effect than the others [150]. The action of lysozyme through the hydrolysis of acetylated residues causes *in vivo* degradation of chitosan [139]. This degradation leads to the formation of non-toxic and non-immunogenic oligosaccharides of variable length, which can be incorporated in metabolic pathways or can be further excreted [139,146]. The degradation rate of chitosan is influenced by the D.D., the crystallinity and the structure of the biopolymer [139,146]. The degradation of chitosan decreases by increasing the D.D. and, consequently, the degree of crystallinity [146,151]. The homogenous distribution of acetyl groups along the polymer chain (random pattern) and long chains will also promote lower rate of enzymatic degradation [146,151].

Like the biodegradability, further physicochemical and biological properties of chitosan (and chitin) preparations are influenced by its intrinsic properties such as the D.D., M_W and the polydispersity of the polymer, which in turn depend on the source of chitin and the preparation conditions [140]. These intrinsic properties can influence the final performance of the biopolymer in many of its applications, as shown in Table 3.3.

Different methods can be employed to assess the intrinsic properties of chitosan, as indicated in Table 3.4. It is important to note that different results are obtained when different methods are used, thus the characterization method should always be specified [143]. The ash, proteins and the endotoxin content as well as the moisture and content of heavy metals should be also determined in case of medical applications or applications related to human consumption [143].

Table 3.3. Relationship between DD and M_W on the physicochemical and biological properties of chitosan preparations [143,147,152].

↑ Physicochemical Properties		
Solubility	DD ↑	
Crystallinity	DD ↑	
Viscosity	DD ↑	
↑ Biological Properties		
Biodegradability	DD ↓	M_W ↓
Biocompatibility	DD ↑	
Antimicrobial	DD ↑	M_W ↓
Analgesic	DD ↑	
Antioxidant	DD ↑	M_W ↓
Haemostatic	DD ↑	
Mucoadhesion	DD ↑	M_W ↑
Permeation enhancing effect	DD ↑	M_W ↑
Antitumor		M_W ↓

Table 3.4. Methods to determine some physicochemical properties of chitosan [11,143,149].

Chitosan properties	Determination methods
Average M_W and/or M_W distribution	Gel permeation chromatography Viscosimetry Light scattering analysis High performance liquid chromatography Matrix assisted laser desorption/ionization-mass spectrometer
D.D.	Nuclear magnetic resonance spectroscopy: ^{1}H-NMR and ^{13}C-NMR Infrared spectroscopy First derivative UV-spectrophotometry Colloidal titration Conductometric titration Potentiometric titration Differential scanning calorimetry
Crystallinity	X-ray diffraction
Protein	Bradford analysis Micro-Biuret method
Ash content	Gravimetric analysis
Moisture content	Gravimetric analysis

3.3. Industrial applications

Due to the enormous structural possibilities of chitosan, able to produce a vast range of products and applications with appealing biological, physical and chemical properties, it became a high valuable biomaterial for several industries. The versatility of chitosan enables its use in industries ranging from pharmaceutical and biomedical to agriculture and water treatment.

Table 3.5 summarizes the various industries and applications that use chitosan. It is important to note that different applications require different properties of chitosan.

Table 3.5. Some applications and potential uses of chitosan [128,153].

Application	Examples
Pharmaceutical	Pharmaceutical ingredient's carriers/drug delivery system; non-viral vectors for gene delivery; gene and active constituents' encapsulation and protection;
Biomedical	Scaffolds fabrication for tissue engineering; preparation of artificial skin; surgical sutures; wounds, ulcers and burns treatment; contact lenses; blood anticoagulant; dental therapy; hypocholesterolemic and antithrombogenic agent; antigastritis; blood dialysis membranes and artificial blood vessels; dental therapy.
Cosmetic and dermatological	Skin, hair and oral care products; moisturizer and anti-aging agents.
Agriculture	Seeds germination acceleration; coating agent to enhance plant and seeds defenses and protection; chemical pesticides replacement/fertilizer and fungicide.
Foods	Color stabilization; reduction of lipid adsorption; food preservative additive; antioxidant agent; thickening and stabilizing agent; prebiotics/dietary fibers ingredients; natural flavor extender; emulsifying; protective barrier against food spoilage.
Textiles	Antimicrobial and non-allergic fibers.
Water treatment	Recovery of metal ions and pesticides; removal of phenol, proteins, radioisotopes and dyes; recovery of solid materials from food-processing; removal of petroleum and petroleum products from waste water; color removal from textile mill effluents;
Analytical and bioanalytical chemistry	Immobilization of enzymes (e.g. matrix in affinity of gel permeation chromatography); biosensors manufacturing for metabolite control.
Paper	Moisture protection; biodegradable packaging for food wrapping.

The market price of chitosan depends on the quality of the product. The price ranges from U.S.$ 5/kg for use as low-grade product in agriculture to U.S. $2000/kg for ultra-pure and high quality product to be used in pharmaceutical and biomedical industry [154,155].

Focusing on the applications for human consumption and health, chitosan has been approved as a natural food additive for general use in Japan and Korea and it is allowed for dietary use in several countries such as the U.S., Italy, Finland, Portugal and England [154,156].

The European Food Safety Authority (EFSA) Panel on Dietetic Products, Nutrition and Allergies has permitted the use of a health claim of chitosan (maintenance of normal blood LDL-cholesterol concentrations) for chitosan [156] and a derivative of chitosan (chitosan hydrochloride) has been included in European Pharmacopeia in 2002 [143,157]. However, this European directive does not include the requirement for a detailed characterization in terms of chitosan's purity (e.g. bioburden, proteins, etc.), which is essential for the production of high value products in medicine [143].

The U.S. Food and Drug Administration (FDA) have only regulated chitosan as a dietary supplement and wound dressing, but not as a drug for biomedical applications [143,158]. So far, few chitosan products have been registered as GRAS (acronym for "generally recognized as safe.") by FDA, which is needed for approval as a food ingredient or food additive [159]. Examples include KitoZyme® (Kitozyme S.A.) and ChitoClear® (Primex EHF) [156,160].

International standards are fundamental for the development of new biomedical products based on chitosan. In the European Union, the regulatory approval for chitosan products requires compliance with ISO 22442 [159]. Furthermore, ASTM International conducted efforts to develop guidelines in the area of tissue engineering products, and the safety and functionality of chitosan is also under their scrutiny [143,159]. The F2103 guide covers the evaluation of chitosan salts suitable for use in biomedical and tissue-engineered product applications [143,159].

3.3.1. Biomedical applications of chitosan

Due to the its easy processability, controllable properties, availability of reactive functional groups and biocompatibility, chitosan is used in several biomedical applications, as referred in Table 3.5. However, the major drawbacks of chitosan are its low mechanical strength and insolubility in neutral pH solutions, which could be balanced by blending chitosan with other natural and synthetic polymers, with the desired properties [83]. Additionally, chitosan's decomposing temperature is lower than its glass transition temperature (Tg), which makes it sensitive to processing techniques involving heat [13,109].

The chitosan-based products offered in the biomedical area are available or have been studied in different applied forms, according to the intended application and function: hydrogels, membranes, nanofibers, beads, micro/nanoparticles, sponges, scaffolds, tablets, capsules, films, powders, solutions or shaped objects [128,140,147]. Figure 3.4 presents some these forms in the biomedical field.

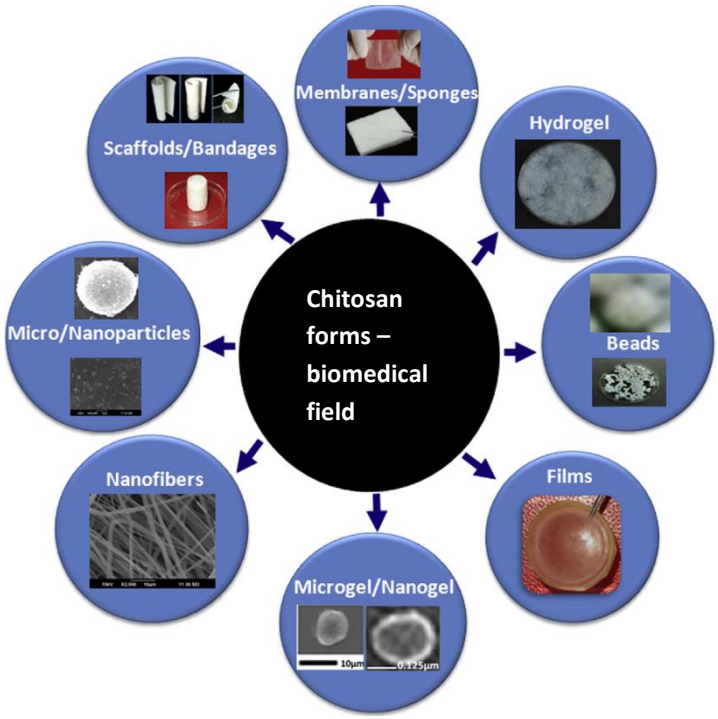

Figure 3.4. Examples of different chitosan presentations used in biomedical applications [152].

The majority of current commercial chitosan-based products for biomedical applications are intended for wound treatment. For example, Chitodine ®, Vulnsorb ® and AbsorKi ® are

commercial wound dressings for dermis regeneration; HemCon® bandage, ChitoFleX®, Syvek® Patch, ChitoSeal® and HemoKi ® are commercial dressing agents with hemostatic properties.
Tissue engineering and regenerative medicine plays an important role in current biomedical research, as explained in chapter 2.5. Focusing in the orthopedic area, chitosan is used for the regeneration of tissues such as cartilage, bone, muscle, tendon and ligament. Some examples:

- Chitosan scaffolds are used in bone regeneration, for example in the treatment of bone defects [161]. In this context, several studies have been made, combining chitosan with ceramics, with promising results in terms of cell attachment, morphology, mineralization and expression of marker proteins of osteogenesis [12,162–164]. This composite strategy has been used because even though chitosan is able to support the attachment and proliferation of bone-forming osteoblast cells, it is not able to promote osteoconduction by itself [129]. Thus, the addition of ceramic-based materials to chitosan improves this property as well as the mechanical strength of the scaffold [12]. Methods for the fabrication of these scaffolds include freeze-drying technique, phase separation and rapid prototyping technology [12,161].
- Chitosan hydrogels are another useful application in bone tissue engineering [161]. Hydrogels are composed of networks with a high content of hydrophilic groups that promotes the polymer hydration and its high water content [149]. The hydrogel dissolution is prevented by the crosslinked networks that are achieved, for example, by physical entanglements or by ionic bonding [165]. These formulations are normally used in bone tissue engineering for sustained delivery of cells and/or growth factors [161]. In this context, Park *et al.*[166] revealed the capacity of chitosan–alginate hydrogels loaded with BMP-2 and MSCs in inducing bone formation. Other studies also identified bone regeneration when growth factors and/or stem cells were seeded in polymeric hydrogels combined with chitosan-based nano- and microparticles [167,168]. In addition, Dhivya *et al.*[169] revealed accelerated bone formation when nano-hydroxyapatite was added to the chitosan-based hydrogels preparation
- Functional constructs based on chitosan are also used to repair and regenerate articular cartilage, since it has structural similarity with GAGs [152]. GAGs are a cartilage-specific ECM component that play a critical role in regulating expression of the chondrocytic phenotype and in supporting chondrogenesis both *in vitro* and *in vivo* [170]. Yan *et al*.[171] revealed that genipin-cross-linked collagen/chitosan biodegradable porous scaffolds seeded with chondrocytes are suitable scaffold materials in cartilage tissue engineering. In another study, Silva *et al.*[172] studied preparations of chitosan/ chondroitin-4-sulphate, build-up by a layer-by-layer methodology. The biological performance of these scaffolds was evaluated and the authors concluded that chondrogenic phenotype was maintained and the differentiation was successfully induced. Other examples of chitosan for cartilage regeneration include hydrogel formulations [85,173,174].

3.3.1.1. Bioabsorbable chitosan implants for orthopedic applications

Currently, it is still a challenge to have orthopedic implant applications that involve 3D dense chitosan geometries, due to the difficulties in the production and shaping of such specimens. One of the difficulties in having such applications is chitosan's lack of mechanical strength, which needs to be addressed.

In this area, Oliveira *et al*.[109] described a new methodology for the production of 3D dense specimens based on chitosan, which allows the production of implants with low porosity and promising mechanical properties. The production process developed by these authors includes the following stages:

1) Dissolve 3% (w/v) of chitosan in 2% (v/v) acetic acid solution at room temperature;
2) After the complete dissolution of chitosan, pour the solution in molds and left it at rest for until all air bubbles disappear;
3) Froze the molds at -20°C for 24 hours, so that chitosan solutions obtain a 3D structure;
4) Remove the frozen solutions from the molds and immerse them into a 10% (v/v) NaOH solution for 48 hours;
5) Wash the specimens intensively until the pH is approximately 7;
6) Dry the specimens at 40°C;
7) Shape the specimens.

The main conclusions and knowledge gained from the work of these authors can be summarized in the following points [109,175]:

- the production process of 3D dense chitosan specimens involves seven main steps, allowing the production of 3D dense chitosan-based specimens capable of being machined;
- higher mechanical properties were obtained by dissolving 3% of a chitosan with high M_W, DD and viscosity (800 kDa, 90% DD and 1.200 cP), and when chitosan was blended with glycerol. Not considering the use of a plasticizer, the mechanical properties of the specimens (flexural modulus and flexural strength) were improved when two types of chitosan, with different molecular weights (high and medium), were mixed;
- better mechanical properties were obtained when 10% (w/v) NaOH was used for 48h, and the drying temperature was 40°C;
- the specimens were easily machined when glycerol was blended with chitosan;
- preliminary experiments revealed no cytotoxic effect of the produced specimens when they were placed in contact with cells.

The experiments performed by these authors, through the developed production process, have revealed great potential of 3D dense chitosan specimens for implant applications in orthopedic area.

3.4. Regulation of chitosan in biomedical applications

The major regulatory issues required for the chitosan-based products approval must include the following information [159]:

a) Material source: biological source or synthetic source;

b) Characterization: physicochemical (e.g. D.D. and M_W), biological (biocompatibility), and absence of immunological effects;

c) Purity: heavy metals, protein content, microbiological bioburden, endotoxins, and residual chemicals from the manufacturing process;

d) Type of biomedical application (e.g. wound dressing);

e) Previous regulatory history (approved devices or approved combination products);

f) Compliance to pharmacopoeia monographs and international standards, as described in chapter 3.3.

It is important to note that the review and approval processes for biologic and drug products in the European Union are different from those required by FDA. However, both applications require material characterization, production consistency and the establishment of the material and product safety profile [159].

3.5. Stability of chitosan in biomedical applications

As previously reported, there are no chitosan-based tissue-engineering scaffolds, gene delivery products, and drug products approved by the FDA so far. Despite the intense research in biomedical and pharmaceutical field, it is difficult to obtain regulatory approval for chitosan-based products that go beyond the current applications (wound dressing and dietary products). This occurs mainly due to the chitosan's susceptibility to several external and internal factors, as explained in Table 3.6. This might be a result of the strong hygroscopic nature of chitosan [129] and also the fact that its properties strongly depend on the source of the material and manufacturing process.

Table 3.6. Factors that affect chitosan stability [176].

Internal Factors	**External Factors**	
▪ Purity Level ▪ M_W ▪ Polydispersity index ▪ D.D. ▪ Pattern of deacetylation ▪ Moisture content	<u>Environmental</u> ▪ Humidity ▪ Temperature	<u>Processing</u> ▪ Acidic dissolution ▪ Sterilization ▪ Thermal processing ▪ Physical methods

The purity level of chitosan is a factor that affects not only its biological properties, but also its solubility and stability [176]. Therefore, chitosan should be of high purity and free of contaminants, according to the pharmacopeia recommendations [159], and this information should be clearly provided by the chitosan suppliers.

The M_w of chitosan can range between 10 kDa and 100.000 kDa and it is defined as the weight average molar mass. Furthermore, the polydispersity index is the ratio of M_W to the average molecular weights (M_N). A ratio between 0,85 and 1,15 is considered as having good polymer homogeneity [176]. It is known that M_w is affected by several factors including high temperatures, irradiation and physical methods like compression force and centrifugation [176–178]. These factors could be present during the product preparation, contributing to the reduction of the M_w distribution on the final product.

Both the M_w and the D.D. can be estimated experimentally by different techniques and the results may differ depending on the applied technique [11,143,149]. This difficult the direct comparison of these two properties between chitosan materials obtained from different manufacturers.

According to the pharmacopeia specifications, the D.D. of chitosan must vary from 70% to 95% [157,179]. Studies revealed that a higher D.D. promotes a slower rate of acidic hydrolysis

observed during storage, however a higher D.D. is also more susceptible to photodegradation [176]. The pattern of deacetylation (random vs block) also has an impact on the charge density, which affects the solubility of chitosan with the same M_w and D.D [146,180].

Another important internal factor that affects chitosan based-constructs stability is its moisture content. Chitosan is an hygroscopic material, able to form hydrogen bonds with water [129]. The amount of absorbed water depends on the initial moisture content as well as on the storage conditions [176]. Studies revealed that physicochemical and mechanical properties of chitosan-based systems are influenced by fluctuations in moisture levels, and the higher the water content in the chitosan structure, the faster the damage to the polymer [181,182]. Therefore, it is essential to measure the initial water content of the chitosan material, and the moisture level should be carefully controlled upon storage.

The external factors that also influence the stability of chitosan include environmental factors and processing factors [176].

The ambient relative humidity strongly influences the moisture level in the chitosan material, being responsible for a plasticizing or swelling effect of polymer constructs [181]. In addition, the physicochemical and biological properties may be damaged by long-term storage at high levels of relative humidity [181]. Temperature also affects long term storage of chitosan solutions, resulting in faster degradation rates of chitosan chains [176]. Additionally, exposure to high temperatures during product processing might change the polymer properties, including aqueous solubility, viscosity, and appearance [183].

One important external factor affecting chitosan properties and the final performance of chitosan- based products is sterilization. Common sterilization methods include exposure to dry heat and ethylene oxide (EtO), saturated steam or gamma irradiation [184]. Sterilization by dry heat reduces tensile strength and affects the solubility of chitosan, which may be related to interchain crosslinking involving the amino groups [176]. The same phenomenon is found when saturated steam is used [176]. On the other hand, studies revealed that exposure to EtO caused minor changes in the physicochemical properties and structure of chitosan dried powder or membranes. However, in solid chitosan structures, there are studies reporting structural alterations in the polymer, especially on the polymer surface [184,185]. Lastly, gamma irradiation was found to cause significant chain scissions to chitosan. The studies revealed that the decreasing of $M_{W,}$ followed by an increasing of D.D., depend on the γ-irradiation dose, with more pronounced effects starting at doses of 25 kGy [176,184].

Due to the irreversible effects caused by the various sterilization methods, it is essential to study the effects of these processes on the properties and performance of the chitosan materials in order to determine optimal sterilization conditions.

3.5.1. Strategies for stability improvement

In order to improve the stability of chitosan, several strategies are being employed to avoid chain damage of the polymer, thus preserving its properties. Storage conditions should be optimized to provide optimum stability to the material. Temperatures below 5°C and relative humidity below 60% are good starting points for this optimization [176]. Stabilizing agents are being added to chitosan solutions to protect chitosan during thermal processing and/or sterilization treatment. Some examples of stabilizing agents are: glycerol, sorbitol, and disaccharides such as mannitol and sucrose [176]. Glycerol and the other polyols, have a

protective effect attributed to the creation of a protective layer around the chitosan chains through interchain hydrogen bonds [186]. In addition, studies revealed that the addition of polyols decreased the water uptake and improved mechanical properties of the chitosan formulations [187].

Chitosan blends with nonionic polymers are alternatives to improve its physicochemical properties [176]. These interactions may involve ionic bonds, hydrogen or dipole interference, and depend on the miscibility of the binary mixtures [188].

An alternative method consists on the preparation of chitosan-based material through crosslinking agents. Covalent crosslinking guarantees the stability of chitosan, but also by other interactions such as hydrogen or hydrophobic bonds [176,189]. It leads to a permanent network structure, since irreversible chemical bonds are formed [189]. Some common covalent crosslinking agents are genipin, silk, fibroin, polyethylene glycol (PEG) and dialdehydes such as glutaraldehyde and glyoxal [176,189]. However, due to the lack of information, it is essential to study the biological effects of these agents in the human body. For example, it is known that glutaraldehyde is neurotoxic, but its elimination in the human body is not fully understood yet [189].

On the other hand, ionic crosslinking occurs due to the reactions with negatively charged components, either ions or molecules, leading to the creation of a network of ionic bridges which enhances the stability of the chitosan complexes [189]. One of the main advantages of this process is avoiding the toxicity present in most of the crosslinkers used to perform covalent crosslinking [189]. When compared to the covalent crosslinking, this is a simpler process which does not require either the presence of catalysts or the purification of the final product method [176]. Additionally, it favors drug delivery applications: an increase in crosslinking density improves the stability of the network, inducing a decrease in swelling and pH-sensitivity thus decreasing the drug release [189,190]. Different types of ionic crosslinkers form complexes with chitosan [176]: metallic ions (e.g. Fe(III) and Mo(VI)), small-size anions or anionic molecules (e.g. sodium succinate and inorganic phosphate salts), natural anionic polymers (e.g. gelatin, hyaluronic acid sodium salt, sodium alginate and xanthan gum) and synthetic anionic polymers (e.g. poly(acrylic acid) and poly(methacrylate)).

Despite all the previously described methods, it is important to note that the selection of the most proper storage conditions is still necessary in order to ensure maximal stability of chitosan based-products.

3.6. Conclusion

Chitosan has generated great interest in the medical community due to its availability, biocompatibility, biodegradability, capacity in promoting bone formation, among other properties, all of whom make it an excellent candidate for biomedical applications. Despite the inherent limitations of working with this material, several biomedical products and forms can be achieved, including 3D dense specimens able to be transformed into bioabsorbable implants with low porosity and promising mechanical properties. However, new studies and investigations are still necessary to translate these results, with great potential, into commercial applications in regenerative medicine in the near future.

SECTION B: Early health technology assessment of a new bioabsorbable orthopedic implant

4. Early health technology assessment in medical devices

Normally, medical devices companies have a strong engineering culture towards their product development (e.g. customer requirements, prototyping and marketing authorization) [191]. However, in order to develop medical devices that can have a great impact in the society and easily penetrate in the market, it is necessary to concentrate on the healthcare milestones (e.g. clinical indications, product profile and reimbursement) in order to increase the value of their research and development (R&D) [191].

Billions of dollars are invested in medical product development worldwide. To maximize the revenues of these investments, companies need to manage their product development in order to maximize both profits and societal benefits, and governments need to be informed - about these benefits before spending public resources [192]. Therefore, it is crucial to apply the health technology assessment (HTA) in the early stages of medical technology development and implementation. The main goal of early HTA is to reduce the failure rate at each stage of the development process, thus prioritizing the innovations most likely to succeed and more likely to be approved by regulatory and reimbursement agencies [193].

The main propose of HTA is to support decisions on coverage and adoption of new medical products from a variety of perspectives [192]. In healthcare, the adoption of new technologies is mainly related to the ability to produce cost-effective solutions [192]. Hence, the cost effectiveness analysis (CEA) is used to compare the relative value of different interventions in creating better and/or longer life [194]. For example, the UK National Institute for Health and Clinical Excellence (NICE) is the organism responsible for making recommendations such as implementation of treatments or medical devices within the UK National Health Service (NHS) [195]. This organism uses CEA to appraisal two or more alternatives in terms of their costs and benefits [195]. The comparison is then summarized using the expected incremental cost-effectiveness ratio (ICER), which represents the additional cost of obtaining a unit health effect from a given health intervention when this intervention is compared with an alternative [194,195]. NICE uses preferably the Quality-Adjusted Life-Years (QALY) gained to describe the health outcome of each intervention [195]. Therefore, ICER is the cost per QALY gained. The QALY assigns a weight to each period of time, ranging from 0 to 1, corresponding to the quality of life during that period (1 for perfect health and 0 is equivalent to death). The number of QALYs then represents the number of healthy years of life that are valued equivalently to the actual health status [196].

According to the NICE evaluation process, the ICER for each technology is compared with a threshold value to establish whether the technology represents an efficient use of limited NHS resources [195].

However, new medical devices are more easily defined as cost-effective if its potential impact was previously anticipated. Therefore, early HTA has been introduced as an emerging form of HTA and currently there is a growing interest in assessment methods that allow making decisions in early stages of product development [192,197]. These decisions may go through specific features in new medical devices or decisions on minimal clinical performance to be able to complete with existing products [192]. To do so, several issues must be determined:

market size, product specifications, patient needs, market acceptance, potential barriers for the product implementation, etc.[192,197].

The concept of early HTA is then related with early examination of the medical, social, economic, ethical, and regulatory implications of medical technologies, to determine the potential for incremental value in healthcare [192,193]. As shown in Figure 4.1, the early HTA starts from initial basic research to stage I of clinical trials. At each of these stages, different qualitative and quantitative assessment methods can be used to provide the best available information to feed the decision making process and, consequently, the stakeholders responsible for such decisions [193]. Different levels of stakeholders' involvement are seen in the different development stages, and different information needs are required by them in each one of these stages [192].

Cosh *et al.* [198] proposed the following algorithm for the decision process:

1) The organization needs to start with strategic considerations by asking questions like: Does this new technology fit with our capacity and strategy? Who are the competitors? Similar technologies exist in the market or are they about to be launched?

2) The clinical need should be clearly identified and all the conditions of the new medical technology should be examined. Therefore, the statement of the new technology, the disease context, the prevalence and incidence of the disease, the current treatment and the cost-effectiveness of such treatments should be clearly defined. The identification of the strengths and weaknesses of current treatments is then essential to the uptake of the new medical technology.

3) The incremental benefit (Δ QALY) of the new technology, when compared the existing one, should be estimated based on optimistic but plausible estimates of effectiveness of the technology being assessed.

4) If the new technology shows benefit to society, it is also necessary to assess whether or not the technology has the potential to succeed once its commercialization. The factors implied in this evaluation are more related with internal factors to the organization rather than the technology itself.

Several management tools can be employed for the different phases of the decision process. For example, PEST (Political, Economic, Social and Technological) and SWOT (Strengths, Weaknesses, Opportunities and Threats) analysis can be used to structure the strategic considerations described by Cosh *et al.*[198]. Multi-criteria decision analysis (MCDA) is a tool to support decisions in case of multiple competing attributes [192]. Health economic modelling (Bayesian methods) may be used to gather evidence on the benefits of the new medical technologies [199]. Bayesian methods combine empiric data with an explicit use of subjective probability [199]. This meta-analysis technique allows for existing evidence, knowledge or beliefs about a parameter, formally expressed as a probability distribution, to be updated by new information as it becomes available, making explicit and quantitative use of all the information available at certain point [200].

Final examples of decision tools are the value-of-information (VOI) analysis and real options analysis (ROA) [192].

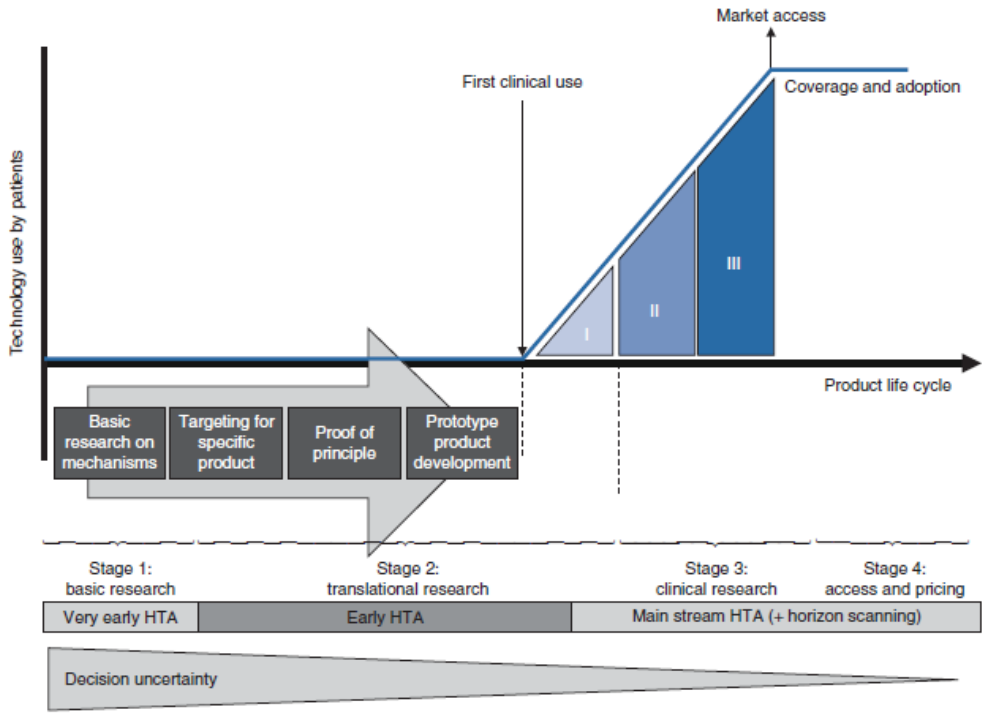

Figure 4.1. Representative model of the different stages of medical product development, from basic research (very early HTA), product development (early HTA), clinical research and market access (main stream HTA) [192].

Since several quantitative methods can be employed in early HTA, it becomes clear that there is no agreed-upon theoretical framework for early assessment. The lack of uniformity is related with the dynamic nature of the development process, which requires flexibility for the assessment process.

As a final remark, it is important to note that there are several challenges when early HTA is performed. These challenges go through how to handle uncertainty in interpreting the results and how to involve patients directly in the decision making process [192,193].

4.1. Early HTA studies in the development of orthopedic bioabsorbable implants

There are not many studies published in the early evaluation of bioabsorbable orthopedic implants. However, Vallejo-Torres *et al.*[201] demonstrated the power of early HTA during the product development process by applying an early assessment methodology to a product already in the market, which was the case study of the proposed methodology. The selected case study was the development of new bioabsorbable pins for Hallux Valgus osteotomy by Johnson & Johnson. The authors applied an iterative Bayesian approach to the early assessment of cost-effectiveness of the pins at four different stages of the development process, using the information available at that time. Based on the assumptions taken into account in this study, including the elicit impact of the new device on quality of life that were made by experts (group of manufacturers with experience with standard and innovative devices) the bioabsorbable pins appeared to be cost-effective. The authors also constructed a decision model using information available in 1987, 1990, and 1995. They found that bioabsorbable pins were the most cost-effective strategy in Hallux Valgus osteotomy for a

cost-effectiveness threshold of £20.000, and showed a high probability (higher than 70%) of this implant being cost-effective, in all of these stages, by probabilistic sensitivity analyses and after accounting for all the parameter uncertainty. As the last analysis, data used in the decision model were updated with evidence from RCT. Bioabsorbable pins remained the most-effective option, although the probability after addressing uncertainty fell to 55%. The reason for this reduction, pointed out by the authors, was the reduced effect on quality of life of bioabsorbable pins over other methods used in Hallux Valgus osteotomies in the RCT. Based on several assumptions, including experts' opinions, the bioabsorbable pins appeared to be cost-effective. However, such methodology may not truly represent the challenges posed by uncertainty since this product was already in the market and therefore the available data and knowledge may have introduced biased beliefs and assumptions in the results obtained in the initial stages of the analysis.

5. Economic analysis model for a new bioabsorbable orthopedic implant candidate

To reduce the impact of musculoskeletal disorders, it is crucial to research and implement effective and affordable strategies for the prevention, treatment and management of such diseases. For example, prevention programs can target the individuals in order to modify their lifestyle behaviors and choices. These programs can involve both strategies to reduce the incidence of musculoskeletal disorders and strategies to reduce the extent of disability.

Regarding the treatment of musculoskeletal disorders, bioabsorbable implants have a huge impact since they are able to reduce the problems associated with the rigid fixation implants (e.g stress shielding effect) and avoid the need for a second surgery after the biological consolidation. However, problems such as lack of mechanical strength and inflammatory reactions motivate the continuous research in this field, in order to achieve a bioabsorbable implant with optimal mechanical and biological features.

In order to evaluate the impact of new R&D in the area of bioabsorbable orthopedic implants, an economic tool was developed as an early HTA method for this area. The main output of this economic analysis is to assess the eventual cost reduction capable of being generated if a new implant, with improved properties, is used instead of the current implants. Therefore, this chapter explains the methodology used to select the orthopedic application that will benefit the most from the construction of a new bioabsorbable implant and explains how this model was constructed, using a decision tree which was solved using the Monte Carlo simulation. Different scenarios and assumptions were integrated in this study, and several sensitivity analysis were performed to identify which are the prevalence of health outcomes and, consequently, the costs, necessary to be reduced in order to classify a new bioabsorbable implant as beneficial for all the society and, in particular, for the healthcare system.

5.1. Proposed methodology to identify an orthopedic application for the R&D of new bioabsorbable orthopedic implants

To select an orthopedic application for the construction of a new bioabsorbable orthopedic implant, it was assumed that the potential applications are limited to those that already exist (see section 5.1.1). This study is based on the assumption that the new bioabsorbable implant will continue to not bear heavy loads, which are necessary for applications such as hip arthroplasty.

The orthopedic surgical intervention will be selected according to the defined selection criteria as well as the information collected after the analysis of the current market of bioabsorbable implants and the analysis of the features required for such implants, which are not yet satisfied.

5.1.1. Analysis of the current market of bioabsorbable implants

Bioabsorbable implants are especially advantageous in low-weight bearing orthopedic applications (e.g. fractures on the extremities) and in applications that require only a transient existence of the implant. Therefore, not all the orthopedic areas are considered suitable for the use of bioabsorbable implants. Currently, these implants are used in the orthopedic surgery in the treatment of fractures and osteotomies in the lower and upper extremities; in craniomaxillofacial surgery reconstruction; in spine surgeries; and in sports medicine surgeries, in the reattachment of ligaments, tendons, meniscal tears and other soft tissue structures.

Bioabsorbable implants vary from interference screws, staples, needles, sutures, tacks and suture anchors (see Table 2.2). In the past, these implants were mainly used in trauma surgery, however the advancement of sports medicine greatly boosted the development and diffusion of bioabsorbable implants, and nowadays the market offers a multitude of implants with different geometries, sizes and materials [202]. The explanation lies in the need for higher mechanical strength in applications where the implant is exposed to high load solicitations, contrary to what happens in applications in sports medicine. For example, in sports medicine, it is common practice to use bioabsorbable polymeric fixation implants in shoulder and knee ligamentous reconstruction.

Some examples of commercial bioabsorbable implants available in the market are shown in Figure 5.1 to Figure 5.3.

Figure 5.1. RapidSorb plate® (DePuy Synthes).

Figure 5.2. ComposiTCP® (Biomet).

Figure 5.3. BioZip® (Styker).

5.1.2. Critical features for the development of new bioabsorbable implants

Currently, there is no ideal bioabsorbable orthopedic implant, since all the available commercial implants present some disadvantages. However, this type of implant material is not the only one that requires improvements. Table 5.1 summarizes the disadvantages of all the orthopedic implants currently used in the orthopedic areas that were described in the previous chapter.

Table 5.1. Disadvantages of the different types of orthopedic implants currently used in craniomaxillofacial and spine surgeries, sports medicine surgeries and in the treatment of fractures in the extremities [5,26].

Type of Fixation	Disadvantages
Bioabsorbable implants	▪ Byproducts released during implant degradation are acidic; ▪ Possible foreign body reactions of the implant which interfere with bone and soft tissue healing; ▪ Possible implant failure during insertion; ▪ Possible implant migration; ▪ Lower material strength and, consequently, lower stabilization of the injured zone; ▪ Possible interference of sterilization on the stability of the materials; ▪ Higher cost.
Metal implants	▪ Stress shielding effect (bone weakening and resorption); ▪ Tissue growth restrictions; ▪ Interference of the implant with magnetic resonance imaging and in subsequent revision surgeries; ▪ Possible implant migration; ▪ Possible graft laceration; ▪ Poor biological interactions and osteointegration of the implant; ▪ Need of surgical removal of the implant.
Biostable implants	▪ Poor biological interactions and osteointegration of the implant; ▪ Inertness and hydrophobicity of the material; ▪ Possible material wear debris to cause foreign body reactions.

Based on the information in the previous table, it is possible to infer which are the critical features required for the orthopedic applications that also must be considered in the development of a new bioabsorbable implant. In general, the ideal material should: 1) provide adequate mechanical fixation and 2) degrade completely after finishing its function, being replaced by bone causing no harm [26]. Therefore, the three important factors that must be taken into account are [44,46,203] :

1) *mechanical properties*

Bioabsorbable implants should have high initial strength and appropriate initial modulus, to withstand the mechanical stresses imposed by the surgical procedure and to support the injured area. Bioresorption rates should be compatible with the healing rates of the tissues, leading to graded load transfer; controlled strength and modulus over time until the surrounding tissue is healed.

2) *biological response*

Bioabsorbable implants should not invoke inflammatory and immunogenic responses. They should be biocompatible both in the local and the systemic response.

3) *osteointegration*

Bioabsorbable implants should form direct bone-implant contact, allowing an effective transmission of loading forces, which is essential for long-term stabilization. They should positively promote bone formation.

Table 5.2 shows a qualitative evaluation of the existing orthopedic implants according to the three factors mentioned previously. In this table, the performance of the orthopedic implants is compared considering the different types of fixation (bioabsorbable, metal and biostable) and the information present in Table 5.1. This qualitative comparison allows the identification of the research opportunities for the development of new bioabsorbable implants. As a proposal, a "better" bioabsorbable implant may be designed to improve the biological response of the body to the presence of the implant, especially during the biodegradation process. On the other hand, an "ideal" bioabsorbable implant may be designed to improve both the biological response and the mechanical properties of the current implants. These proposed improvements are described in Table 5.3 and Figure 5.4.

Table 5.2. Qualitative comparison between different types of fixations currently used in craniomaxillofacial and spine surgeries, sports medicine surgeries and in the treatment of fractures in the extremities. Green circle denotes a good performance in the assessed feature and the orange circle denotes a bad performance in the assessed feature.

Type of Fixation	Mechanical properties	Biological response	Osteointegration
Bioabsorbable (e.g. PLLA)			
Metallic alloy (e.g. titanium)			
Biostable (e.g. PEEK)			

Table 5.3. Proposed improvements for the construction of new bioabsorbable orthopedic fixation implants. Green circle denotes a good performance in the assessed feature and the orange circle denotes a bad performance in the assessed feature.

New Fixation	Mechanical properties	Biological response	Osteointegration
Better bioabsorbable implant			
Ideal bioabsorbable implant			

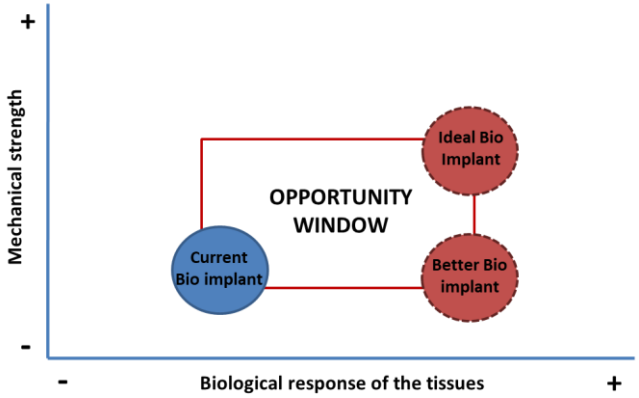

Figure 5.4. Opportunity window for the research of new bioabsorbable implants, in terms of mechanical and biological improvements.

5.1.3. Criteria for the selection of the orthopedic application

The criteria defined for the selection of the case study are shown in Figure 5.5.

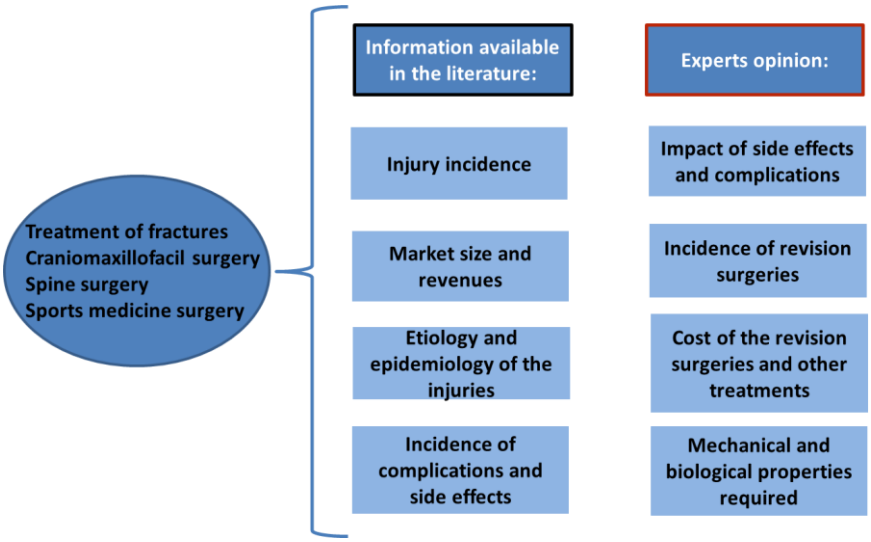

Figure 5.5. Criteria for the selection of the orthopedic intervention (case study).

In a first stage, it was selected the intervention(s) within each different orthopedic area under study that have higher incidence, market size and associated complications. Therefore, giving greater importance to these criteria, the following interventions were selected:

- Anterior cruciate ligament (ACL) reconstruction and rotator cuff repair (sports medicine);
- Hand and distal radius fractures (treatment of fractures in extremities);
- Mandibular fractures (craniomaxillofacial surgery reconstruction);
- Spine fusions (spine surgeries).

Among the selected interventions, the implants used either in the treatment of mandibular fractures and in spine fusions are those who will be subjected to higher local stresses. Additionally, there is less information available in the literature regarding the problems and side effects caused by the bioabsorbable implants used in these two interventions.

The second stage of the selection process was performed based in the opinions of three orthopedic surgeons and one orthopedic researcher, who advised on the preferable option among the six previously described interventions. The experts gave greater importance to the incidence and costs of complications' treatment, as well as incidence and costs of revision surgeries, in cases where bioabsorbable implants are used. Based on the opinions, the ACL reconstruction was chosen as object of the case study.

5.1.4. Final selection: ACL reconstruction

ACL reconstruction surgery is the case study selected for the analysis of the economic impact of a new bioabsorbable implant in the market. The goals of this surgery are 1) to stabilize the knee joint, 2) to restore normal kinematics and 3) to prevent the onset of arthrosis [204].

ACL rupture is one of the most common knee injuries in athletes, and occurs when the player is cutting, pivoting, jumping or abruptly stopping [205,206]. The exact mechanism includes poor knee positioning and a strong, unopposed quadriceps contraction. It is estimated that 200.000 ACL ruptures occur each year in the U.S., and ACL reconstruction is performed in 175.000 of the cases [207].

The current gold standard of treatment (adult patients) is an ACL reconstruction with a tendon graft, placed through tunnels in the distal femur and proximal tibia and anchored at both sides [208] – Figure 5.6. Different surgical choices can be made for each patient: graft type (autograft or allograft), type and material fixation (intratunnel or extra-articular; metal or bioabsorbable) and the surgical technique (double-bundle or single-bundle) [204]. The treatment protocols are not rigid and surgical choices depend not only on the patient status, but also on the surgeon's preference and experience – see Table 5.4. The complications after an ACL reconstruction include infection, stiffness, inability to regain pre-injury function, recurrent functional instability, residual laxity, chronic pain, loss of range of motion and development of osteoarthritis [209–211]. The costs of treating the complications logically depend on how serious the complications are.

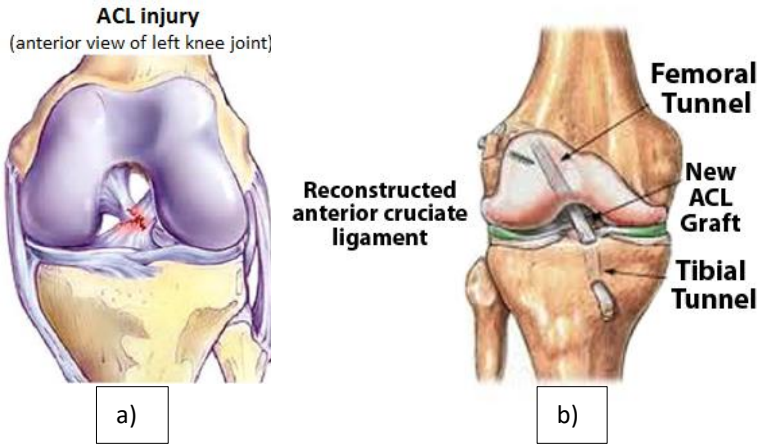

Figure 5.6. a) Rupture of the ACL and b) fixation of the injury by an ACL reconstruction surgery [212].

Table 5.4. Surgical choices for the ACL reconstruction [213–217].

Graft Type	
Autograft	**Bone-patellar tendon-bone (BPTB)** Most secure fixation and lower failure rate. However, it is associated with increased anterior knee pain, numbness, extension loss, long term osteoarthritis of the knee and possible fracture of the patella. **Quadrupled hamstring tendons (HST)** Consisting of either doubled semitendinosus/ gracilis or quadrupled semitendinosus tendons. Associated with less harvesting morbidity than BPTB, however they exhibit a slighter degree of laxity, especially in females. **Quadriceps tendons (QT)** Low incidence of anterior knee pain and almost no residual numbness. However it is technically more difficult to harvest the graft from the patient.
Allograft	Avoids complications related with tendon harvesting. Currently fresh frozen allografts are the most widely used (tibialis anterior or posterior tendons, Achilles' tendon with bone plug and BPTB). They have a longer incorporation time and are associated with an increased risk of ACL graft rupture.
Type of graft fixation	
Intratunnel or aperture fixation	**Interference screws and cross pins** Interference screws (metal or bioabsorbable) are mainly used in bone-tendon-bone graft fixation once high fixation strength is necessary. In these cases, healing occur between 4 and 12 weeks after surgery.
Extra-articular fixation	**Cortical fixation devices, femoral loops and tibial cortical fixation.** Cortical fixation is commonly used in soft tissue graft fixation. In these situations, healing normally occur between 6 and 12 weeks after surgery.
Surgical Technique	
Single-bundle	The most common technique in ACL reconstruction. It creates one single femoral tunnel and one single tibial tunnel.
Double-bundle	Reconstructs the two functional bundles of the ACL (anteromedial bundle and posterolateral bundle), which improves knee kinematics and rotational stability. It increases the costs of the surgery.

In the U.S., there are approximately 3.000 to 10.000 revision ACL reconstructions performed annually [211]. If a revision is needed, additional costs should be expected. The surgeon must develop a careful management algorithm to optimize surgical outcome including consideration of skin incision placement, tunnel widening, implanted hardware, graft selection, tunnel placement, and graft fixation [218].

Despite extensive research in this topic, leading to constant improvements over the last 30 years, controversy remains regarding the natural history of ACL injuries, surgical technique, graft choice and long-term outcomes [204,219].

5.2. Proposed economic model for early HTA of new bioabsorbable orthopedic implants for the ACL Reconstruction

In ACL reconstruction, there are several publications performing HTA considering different aspects of this surgery. Economic methodologies such as cost-effectiveness analysis and cost-utility analysis were used to compare variables such as surgery with non-operative treatment

[220–222], single-bundle with double-bundle technique [223] and different type of grafts [224]. Further literature reported different types of cost-models, for example, the analysis of the economic benefit of double-bundle technique vs single-bundle technique [217] and autograft vs allograft [225]. In 2016, Saltzman *et al.*[226] published a systematic review of the economic studies published on ACL reconstruction. The authors found that the majority of studies were cost identification studies.

Regarding the type of implants used in ACL reconstruction, there are no economic studies done yet to establish which type of fixation is most effective. However, several publications compare the outcomes of this surgery when metal and bioabsorbable implants are used (statistical comparison) [70,227–230]. These studies are mostly prospective randomized controlled trials (RCT).

There are no published studies on early HTA in the development of bioabsorbable implants for the ACL reconstruction, or in the development of any other type of fixation implants for this orthopedic application.

With the goal of developing an early economic model to anticipate the societal benefits of having a new bioabsorbable implant for the treatment of the ACL ruptures, the complications and the failure rates of the current implants were determined and the reasons for their origin were identified. The health events after an ACL reconstruction were represented by a decision tree, and scenarios were established according to the type of complications and the features presented by the new implant. The advantage for the patients in having a new bioabsorbable implant for ACL reconstruction was measured in terms of reduction of complications and the correspondent benefit to the society was measured by the reduction of the extra costs that are incurred by the treatment of such complications after an ACL reconstruction.

It was not possible to perform this evaluation based on clinical trials that would collect information regarding the patients' health events of a specific bioabsorbable implant when placed in the human body. Therefore, several sensitivity analyses were executed to identify the threshold that allows characterizing the new bioabsorbable implant as beneficial, when compared to the current fixation strategies.

5.2.1. Framing the study

Table 5.5 describes the characteristics of this study, namely the type of intervention, the comparison programs and the perspective of the study.

Table 5.5. Framing the economic study by defining its characteristics.

Intervention	Use a new bioabsorbable implant in the ACL reconstruction surgery
Audience	Society, R&D companies, universities and policy makers.
Target Population	Individuals from all ages (children and adults) that may suffer an ACL rupture.
Comparison Programs	Current metal implants (screws) used in ACL reconstruction surgery. Current bioabsorbable implants (screws) used in ACL reconstruction surgery
Perspective	Societal
Time Horizon	2 years

One important aspect of economic evaluations is the definition of the perspective of the study, since it has implications in the study design. The "societal" perspective was incorporated in this study since it allows to assess the impact of the intervention on the society's welfare [231]. This perspective intends to incorporate all costs and all health events regardless of whom pays and who obtains the effects [232] .

The comparator programs selected for this study are the ACL reconstruction surgeries that use the current implants (screws) for the graft fixation in femur and tibia. Since metal and bioabsorbable implants are the most commonly used implants in ACL reconstruction, thus two comparison programs were established.

The selected time horizon of the study was 2 years. This is the shortest follow-up time that is most commonly used in studies that follow groups of patients who have performed ACL reconstructions.

5.2.2. The conceptual model and assumptions

A conceptual model was developed to outline the health events that may occur after an ACL reconstruction and further treatments that are still needed.

The conceptual model was constructed using a decision tree. Decision trees are composed of a set of nodes (represented by circles or squares) interconnected by branches (represented by lines). A decision node is represented by a square and an uncertain node is represented by circular nodes. In this study, the intervention and each comparison program were represented by main branches in the tree, after a decision node. The subsequent events (uncertain events) were depicted by further branches.

Table 5.6 describes the possible events after an ACL reconstruction, identified through an extensive literature review.

Table 5.6. Complications after an ACL reconstruction [210,211,233].

Complications		
Symptom	**Causes**	**Treatment options**
Pain	▪ Chondral injuries ▪ Meniscal injuries ▪ Neuroma pain from the harvest site ▪ Arthritis ▪ Synovitis ▪ Patellofemoral pain ▪ Chronic inflammation	▪ Proper treatment exists according to the specific pathology. Examples: anti-inflammatory medication for pain and swelling and treatment of chondral injuries with arthroscopic debridement (chondroplasty).
Stiffness	▪ Poor positioning of the graft ▪ Prolonged period of immobilization ▪ Arthrofibrosis ▪ Excessive tension of the graft ▪ Cyclops lesion ▪ Persistent pain ▪ Time from injury to surgery	▪ Treatments are directed towards improvement of the range of motion and limb function. The range of motion can be achieved through rehabilitation exercises and/or open or arthroscopic debridement of the knee.
Instability/Laxity	▪ Early return to sport - new trauma ▪ Technical errors ▪ Biological factors ▪ Failure of initial diagnosis ▪ Inadequate postoperative rehabilitation	▪ Revision surgery ▪ Physical rehabilitation, when a new surgery is not advised

To reduce the complexity of the model, these complications were divided into three main groups of symptoms: a) persistent pain, b) stiffness (loss of motion), and c) recurrent instability/laxity, causing the patient's sensation of giving-way. Infection was not considered in this model, since it is a rare event [234].

The literature is not unanimous regarding the definition of failure after an ACL reconstruction [235] . The surgical procedure may be considered to have failed when the patient has a perception of instability or objective laxity develops in an ACL-reconstructed knee, or when postoperative pain and/or stiffness occurs in a stable ACL-reconstructed knee [236]. However, some authors prefer the definition of Johnson and Coen, who define failure as the presence of recurrent instability when performing daily sports activities or as a stable, but painful knee, with more than 10° motion loss after the surgery [211]. In cases of objective evaluation of failure, measurements include motion deficits, the Lachman test, the anterior drawer test, the pivot shift test or KT arthrometer [237].

Despite the inexistence of a universally accepted definition of ACL reconstruction failure, it is generally accepted that the Revision Surgery is only performed in cases of recurrent instability/laxity, i.e., when the reconstructed ligament cannot provide adequate anterior and/or rotatory stability of the knee [236,238]. The ACL reconstruction failures can occur for different reasons: a) early failures (less than 3 months after the surgery) are typically related to loss of fixation, sepsis, and failure of graft incorporation due to aseptic biological reaction, b) midterm failures (3-12 months after the surgery) are most common and are often due to surgical technique errors, aggressive physical therapy, and graft failures secondary to unrecognized loss of secondary stabilizing structures and c) late failures (more than 12 months after the surgery) are mainly related with trauma [239].

Figure 5.7 shows the decision tree constructed from the Tree Plan sofware, to outline the health events after an ACL reconstruction. This decision tree includes the comparison programs and the proposed intervention. The first node represents the decision that the sports medicine surgeon will make regarding which type of fixation should be used: metal fixation, current bioabsorbable or new implant (bioabsorbable) fixation. Despite all the fixation alternatives, this model focused on interference screws, since this is the most reported fixation method in the literature [240]. To simplify the model, the surgical technique and type of graft were neglected. However, the use of an autograft was assumed. For the remaining decision tree construction, the following assumptions were also taken into consideration:

- the complications caused by instability/laxity of the graft are addressed in the branch "Failure". In this case, it was assumed that the patient necessarily requires an ACL Revision, thus the option of "no Revision" was not included.
- if patients require an ACL Revision, there is a chance of doing it in two stages. In addition, it was considered that the implant used in the Revision Surgery was the same used in the primary surgery.
- the branch "Other complications" encompasses the complications that cause pain and stiffness. These complications have essentially an inflammatory origin and can be treated by surgery (arthroscopic release/debridement or manipulation under anesthesia) or by a more conservative treatment (physical rehabilitation and steroid injections).

- to reduce the complexity of the problem, it was assumed that the patient's symptoms improve after the treatment of the complications, and therefore the patient does not suffer from further problems during the remaining follow-up period.
- the health events after an ACL reconstruction occur regardless of the type of interference screw that was used. The difference between the fixation methods lies on the probability of such outcomes.

5.2.3. Scenarios and assumptions

To assess the economic benefit of having a new implant in the market, two potential implants were studied, according to the improvements proposed in Table 5.3**.** Therefore, two types of implants were studied:

a) the new (bioabsorbable) implant improves only the biological interactions, maintaining the same mechanical performance of the current bioabsorbable implants - "better implant".
b) the new (bioabsorbable) implant improves both the biological interactions and the mechanical properties of the current bioabsorbable implants – "ideal implant".

In addition, the economic evaluation was executed by studying separately the occurrence of complications that cause pain and the complications that cause stiffness. These scenarios have been chosen to understand in which situation it will be more beneficial to launch a new implant in the market. This benefit will be measured in terms of reduction of the rate of complications and their treatment costs and, consequently, the expected cost of the primary ACL reconstruction.
In total, two symptom scenarios and two implant improvement levels were considered for this economic model, as described in Table 5.7.

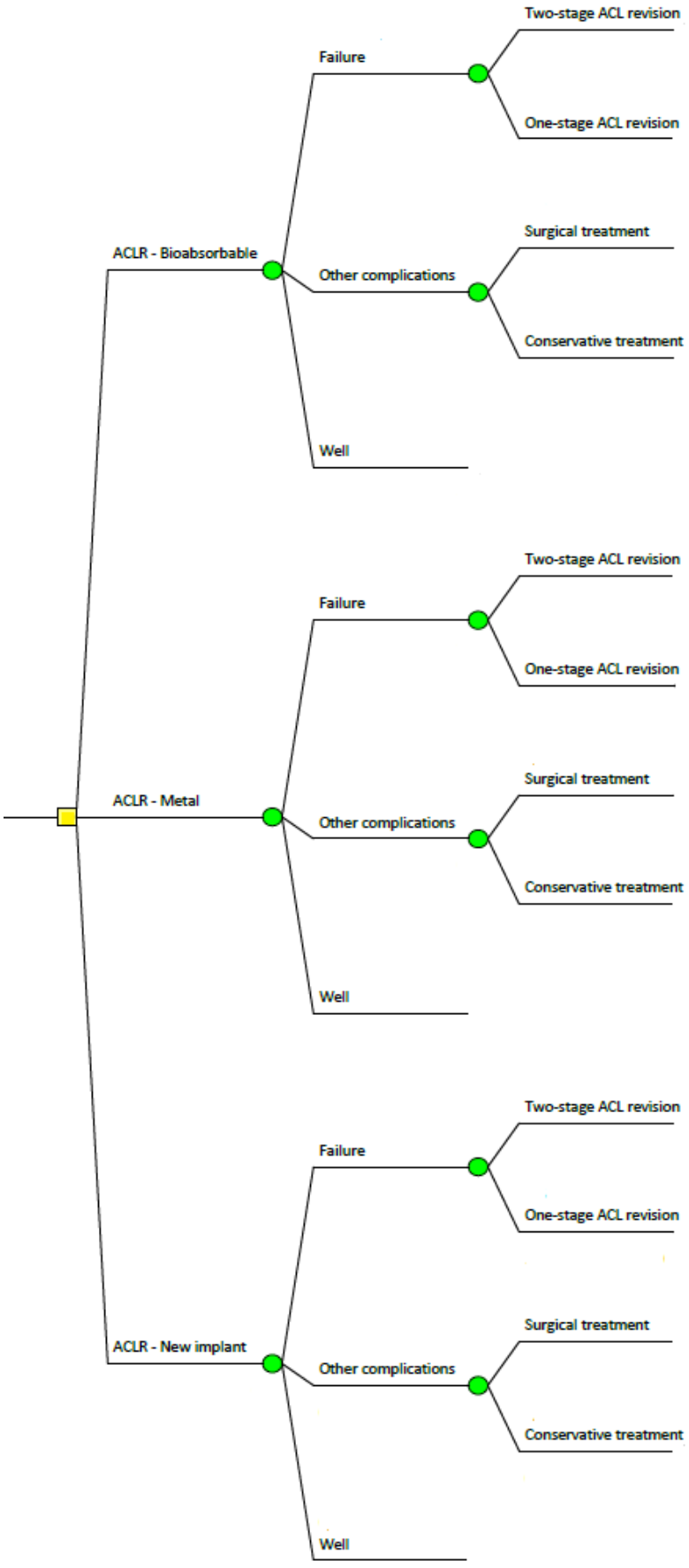

Figure 5.7. Schematic representation of the decision tree.

Table 5.7. Symptom scenarios and implant improvement levels included in the study.

Scenario		Description
Pain Scenario	**Pain 1**	The new implant under study only improves the biological properties of the current bioabsorbable implants **(Better implant)**.
	Pain 2	The new implant under study improves the biological and the mechanical properties of the current bioasborbable implants **(Ideal implant)**.
Stiffness Scenario	**Stiffness 1**	The new implant under study only improves the biological properties of the current bioabsorbable implants **(Better implant)**.
	Stiffness 2	The new implant under study improves the biological and the mechanical properties of the current bioasborbable implants **(Ideal implant)**.

5.2.4. Probabilities and assumptions

To identify the probabilities of the health events depicted in Figure 5.7 an in-depth literature review was carried out to determine the incidence of the complications and their associated treatments (Table 5.8). Attention was given to the studies that followed the patients over a mean period of 2 years or up to 2 years.

Table 5.8. Literature review on the incidence of the health events and treatments after an ACL reconstruction.

Events/Treatments		Data from Literature
Failure		-1,82% [241]; 5,3% [242]; 1,7% [240]; 4,9% [224]
Two-Stage ACL Revision (Failure)		-5,4% to 8,3% [243]
Other complications	Pain scenario	-Anterior knee pain: 22% [224] -Meniscal and cartilage injuries: 37% [244]
	Stiffness scenario	-Loss >5º extension: 9% [224] -Loss of extension: 25,3% [245] -Cyclops Lesion: 3,61% [246]
Surgical treatment (Other complications)	Pain scenario	-6% (4/68) of the patients subjected to an ACL reconstruction, undergo another arthroscopy to treat pain related complications [247]
	Stiffness scenario	-Arthroscopy for loss of extension: 12,2% [245] -Anterior debridement: 3,3% [242] -3% (2/68) of the patients subjected to an ACL reconstruction undergo another arthroscopy to treat stiffness related complications [247]

The small number of published data difficults the identification of well-defined complications' rates. Additionally, from the studies that followed the patients during a mean period of 2 years/up to 2 years, only one related the complications that arose with the type of implant used [248]. However, this study followed patients who received a type of bioabsorbable implant that is no longer in the market.

Table 5.9 and 5.10 detail the probabilities of health events delineated in the decision tree, according to the different scenarios that were defined in this model. The probabilities were chosen based on the information collected after the literature review – Table 5.8.

Table 5.9. Probabilities for the scenario Pain.

SCENARIO PAIN	Current implants		New implant	
	Bioabsorbable	Metal	Pain 1 (Better)	Pain 2 (Ideal)
Probability of Failure	0% - 5%	0% - 5%	**-5% Bioabsorbable** 0% - 4.8%	**-20% Bioabsorbable** 0% - 4%
Probability of Two-stage ACL revision (due to Failure)	0% - 8%	0% - 5%	**-50% Bioabsorbable** 0% - 4%	**-60% Bioabsorbable** 0% - 3.2%
Probability of Other complications	0% - 40%	0% - 35%	**-15% Bioabsorbable** (0% - 34 %)	**-20% Bioabsorbable** (0% - 32%)
Probability of Surgical treatment (due to Other complications)	0% - 15%	0% - 10%	**-15% Bioabsorbable** 0% - 12.8%	**-20% Bioabsorbable** 0% - 12%

Table 5.10. Probabilities for the scenario Stiffness.

SCENARIO STIFFNESS	Current implants		New implant	
	Bioabsorbable	Metal	Stiffness 1 (Better)	Stiffness 2 (Ideal)
Probability of Failure	0% - 5%	0% - 5%	**-5% Bioabsorbable** (0% - 4.8%)	**-20% Bioabsorbable** (0% - 4%)
Probability of Two-stage ACL Revision (due do Failure)	0% - 8%	0% - 5%	**-50% Bioabsorbable** (0% - 4%)	**-60% Bioabsorbable** (0% - 3.2%)
Probability of Other complications	0% - 25%	0% - 20%	**-25% Bioabsorbable** (0% - 18.8%)	**-30% Bioabsorbable** (0% - 17.5%)
Probability of Surgical treatment (due to Other complications)	0% - 12%	0% - 7%	**-25% Bioabsorbable** (0% - 9%)	**-30% Bioabsorbable** (0% - 8.4%)

The following assumptions were taken into consideration, for the definition of the probabilities of the previous tables:

a) Branch: Failure

The maximum probability of Failure was established at 5%, as indicated in Table 5.8**.** The probabilities of this branch are the same, regardless of the type of scenario under study.
The failure incidence is reduced by 5% when a new implant with improved biological properties is used. In this case, the new implant only eliminates the causes of failure related with inflammatory reactions caused by graft/hardware interface, which are a consequence of the patient's immune response. According to the Multicenter ACL Revision Group Study (MARS), the reasons that lead to an ACL revision are trauma (32%), technical errors (24%), biologic failure (7%), or a combination of factors (37%) [249]. Therefore, the biological factors do not strongly contribute for the reduction of this event, especially when inflammation is the only source of the biological failure of the graft. These assumptions are considered both in the pain and the stiffness scenarios.

Technical errors include malpositioned tunnels, improper graft choice and technique, failure to diagnose conditions associated with the ACL rupture (e.g. other ligamentous injuries), improper fixation sizing and graft tensioning [218]. Therefore, even if there is a new implant in the market, with better biological and mechanical properties, the ACL failures continue to occur if the surgeon is unable to avoid these technical errors. However, it is considered that mechanical properties of the implants contribute both for the fixation and the biomechanics of the graft, which are factors that can foster a new trauma [215]. Thus, it was assumed that improving both the biological and mechanical properties of a new implant can reduce the need for an ACL revision by 20%.

b) Branch: Other complications

The pain situations mostly reported in the literature are related with anterior knee pain. The prevalence of this complication is often related with the donor site morbidity, resulting from the harvest of the graft. However, the authors suggest that it might be associated with loss of motion, which could be related to the inadequate rehabilitation techniques rather than the graft choices [235,250]. Therefore, anterior knee pain symptoms will be associated with loss of motion, and the occurrence of this complication will be studied in the stiffness scenario.

Considering that the complications that cause pain are mainly due to the chondral and meniscal injuries, loose bodies and chronic inflammation (e.g arthritis and synovitis) then the pain scenario complication's probability will be fixed at 40% maximum, which is related to the number found by Røtterud *et al.*[244], indicated in Table 5.8. In this study, the authors found more prevalence of meniscal injuries than cartilage injuries.

Regarding the stiffness scenario, the maximum probability of complications related with loss of motion will be set at 25%, as indicated in Table 5.10.

The information available in the literature only indicates a greater bone tunnel widening, knee effusion, pain and swelling when bioabsorbable implants are used instead of metal implants [251]. However, this statement is only justified by statistical significance [70,227,252,253] and the prevalence and origin of complications among a cohort of patients who were treated with bioabsorbable implants are not studied. However, to integrate this finding in the model, it was established a difference of 5% between the maximum probability rate of complications of the metal and bioabsorbable implants.

In the pain scenario, it was assumed a reduction of the complications by 15% if a new implant becomes available in the market, able to improve only the biological interactions of the current bioabsorbable implants. This reduction was established in 20% if this new implant is able to improve both the biological and mechanical properties. In the latter case, the new implant will be able to avoid slippage of the graft and migration of the screw, which happens less often when compared to the foreign body reactions. These numbers were assumed considering that even if the inflammation caused by the fixation method is avoided, the episodes of persistent pain do not disappear completely since it comes mostly from the meniscal and cartilage injuries.

In the stiffness scenario, it was assumed a slightly higher reduction of the incidence of complications since the inflammation has higher impact in the problems related with loss of motion. The new implant which provides only better biological properties will reduce

complications by 25% whereas the new implant that is able to reduce both the biological and mechanical properties will reduce complications by 30%.

c) Branch: Two-stage ACL revision

A two-stage revision surgery in required in situations that: a) there is a widening of the tunnel, b) there is bone loss, c) it is necessary to treat other complications, for example arthrofibrosis or inflammation due to the foreign body reactions [254] .

Although the data collected in the literature do not relate the incidence of this event with the type of implant material that was used, it was also assumed, in this health event, a different rate between metal and bioabsorbable. The highest probability found in the literature (8%) was assigned to the current bioabsorbable implants, and the lowest probability found in the literature (5%) was assigned to the current metal implants. However, it is important to note that these numbers were collected from studies that include patients who took more than 4 years to perform the ACL Revision. The same rate values were established regardless of the type of complication scenario being studied, since these scenarios do not influence the occurrence of the graft failure (instability/laxity) and, consequently, the need of an ACL revision surgery.

It was assumed that the new implant with improved biological properties greatly reduces the need of a staged surgery, because it will avoid the widening of the tunnels and other complications of inflammatory origin. Based on the information present in the literature, the widening of the tunnels is a common complication when the current bioabsorbable implants are used. The factors that may contribute for this complication are pitfalls in the graft fixation, causing micromotion and residual laxity, as well as osteolysis around the implant due to acidic degradation products [255,256]. Therefore, this event can be drastically reduced if the biological properties of the current implants are improved. It was then assumed that a new implant with better biological properties reduces the need of a stage surgery by 50%. On the other hand, improving both the biological and mechanical properties of the current bioabsorbable implants reduces the need to perform a two-stage surgery by 60%. In addition to the enlargement of the tunnels and other complications of inflammatory origin, there are further reasons that contribute to a staged ACL revision: a) tunnel defect which limits fixation or anatomic graft placement, b) conflict with previous tunnels and/or hardware, which requires the removal of all material, c) bone voids [254]. It was then assumed that the improvement of the mechanical properties of the current implants prevent the occurrence of these complications, although to the lesser extent.

d) Branch: Surgical treatment

The range of values attributed to the chance of this event depends on the scenario that is being studied. Based on the study of Heijne and Werner [247], among the 8 patients who underwent another surgical arthroscopy for the treatment of complications after an ACL reconstruction, 4 patients were treated mainly due to pain symptoms and 2 patients were treated mainly due to lack of mobility. Considering the total number of patients followed in that study, and the probabilities defined for the two complication scenarios, the chance interval of the branch “Surgical treatment” was set at 15% and 12% maximums for the pain

and stiffness scenarios, respectively. Once again, a 5% difference is assumed between metal and bioabsorbable implants.
It was assumed the same reduction of the incidence of this event, like in the event of "Other complications", when the effect of a new implant was studied. According to the scenario, the reduction of the event "Surgical treatment" was established at 15% or 20% maximum in the pain scenario, and at 25% or 30% maximum in the scenario stiffness.

5.2.5. Costs and assumptions

In total, there are eight aggregate costs associated with each node: 1) ACL reconstruction (ACLR - branches bioabsorbable, metal or new implant), 2) Failure, 3) Other complications (pain or stiffness), 4) Well, 5) Two-stage ACL revision, 6) One-stage ACL revision, 7) Surgical treatment and 8) Conservative treatment. These aggregate costs were calculated after defining the cost items responsible for each one of them, as shown in Table 5.11. This definition was made with the help of doctors, physical therapists and also the information collected in the literature [220,225,257,258]. In some cases, the cost items are multiplied by the number of times that are present in a certain aggregate cost. For example, the cost item "Manual Rehabilitation" is multiplied by the average number of sessions necessary in each different situation. It is important to note that the sessions of physical rehabilitation are billed in periods of 15 minutes. The surgical treatments assumed the occurrence of pre- and post-operative rehabilitation sessions, which last for different periods of time. As an example: the post-ACL Reconstruction rehabilitation lasted for 6 months, whereas the post-ACL revision rehabilitation lasted for 12 months.
Regarding the cost of the anesthesia, the anesthesiologist fee depends on the surgery time (in periods of 15 minutes) of the different procedures. To cover all possibilities, the surgery time was not fixed in an average time but in a probable interval.
The "Conservative treatment" node refers to a less aggressive treatment of complications, wherein a surgery is not necessary. In this case, as an assumption, the treatment lasts for 6 months, which include 2 steroid injections (spaced by 3 months) and continuous physical rehabilitation during the entire period.
Not all the cost items were integrated in each different aggregate cost, but at least the most relevant direct costs were included. The range of values for each cost item was obtained from a U.S. health insurance database, by searching the Medical Billing Code corresponding to each cost item – see Table 5.12. For each cost item, the existing data was used to fit a MATLAB probability distribution object using the *fitdist* function. Given the knowledge of the probability function associated to the data, it was possible to obtain a set of random data with that distribution, which was used afterwards in the calculation of random values associated to each cost item, for each iteration of the simulation.

Table 5.11. Cost items responsible for each different aggregate cost.

Node/Aggregate Cost	Cost Item	Units	
		Pain Scenario	Stiffness Scenario
ACL Reconstruction	XRay	1	
	MRI	1	
	Surgeon Fee	1	
	Facility Fee	1	
	Anesthesiologist Fee	1	
	Anesthesia time	5 – 8.3 (75 min – 125 min)	
	Implant	2	
	Physical Evaluation	2	
	Strength Therapy	42	
	Neuromuscular Therapy	42	
	Manual Therapy	22	
	Brace	1	
	CPM	14	
Failure	XRay	1	
Other complications	XRay	1	
Well	-	-	
One-stage ACL Revision	MRI	1	
	Surgeon Fee	1	
	Facility Fee	1	
	Anesthesiologist Fee	1	
	Anesthesia units of 15 min	6 – 10 (90 min – 150 min)	
	Implant	2	
	Physical Evaluation	2	
	Strength Therapy	60	
	Neuromuscular Therapy	60	
	Manual Therapy	34	
	CPM	14	
Two-Stage ACL revision	CT	1	
	Surgeon Fee*	1	
	Facility Fee*	1	
	Anesthesiologist Fee	1	
	Anesthesia units of 15 min.	6 – 10 (90 min – 150 min)	
	Physical Evaluation	2	
	Strength Therapy	26	
	Neuromuscular Therapy	26	
	Manual Therapy	14	
	CPM	14	
	+ One-stage ACL Revision		
Surgical treatment	MRI	1	
	Surgeon Fee	1	1
	Facility Fee	1	1
	Anesthesiologist Fee	1	
	Anesthesia units of 15 min.	2 – 4 (30 min – 60 min)	

Surgical treatment	Physical Evaluation	2
	Strength Therapy	26
	Neuromuscular Therapy	26
	Manual Therapy	14
	CPM	14
Conservative treatment	Injection Drug	2
	Injection Fee	2
	Physical Evaluation	2
	Strength Therapy	32
	Neuromuscular Therapy	32
	Manual Therapy	24

* average cost between two different procedures

Table 5.12. Medical billing codes included in the economic model.

Code	Category	Description	Item of the model
73722	**Imaging studies**	MRI Knee Arthrogram	MRI
73562		Standard Imaging Knee - 3 views	XRay
73700		CT Extremity Lower without contrast	CT
01400	**Anesthesia**	Anesthesia - Professional Component (per 15 minutes)	Anesthesiologist Fee
29888	**Surgical Procedure – Professional and Facility Component**	Professional Component – Arthroscopically ACL Reconstruction	Surgeon Fee
29888		Facility Component – Arthroscopically ACL Reconstruction	Facility Fee
29874		Professional Component – Arthroscopy Knee Removal Loose/Foreign Body	Surgeon Fee (Pain)
29874		Facility Component – Arthroscopy Knee Removal Loose/Foreign Body	Facility Fee (Pain)
29884		Professional Component – Arthroscopy Knee W/Lysis of Adhesions	Surgeon Fee (Stiffness)
29884		Facility Component – Arthroscopy Knee W/Lysis of Adhesions	Facility Fee (Stiffness)
J1040	**Conservative treatment**	Methylprednisolone 80 mg - injection	Injection Drug
20610		Arthrocentesis*, aspiration and /or injection, major joint or bursa (e.g., shoulder, hip, knee, subacromial bursa)	Injection Fee
97001	**Rehabilitation**	Physical Evaluation	Physical Evaluation
97110		Therapeutic exercise to develop strength, endurance, range of motion, and flexibility, each 15 minutes	Strength Therapy
97112		Therapeutic procedure to re-educate brain-to-nerve-to-muscle function , each 15 minutes	Neuromuscular Therapy
97140		Manual therapy techniques to 1 or more regions, each 15 minutes	Manual Therapy
L1845	**Medical Equipment and Implant**	Knee Orthosis, Double Upright, Thigh And Calf, With Adjustable Flexion And Extension Joint	Brace
E0935		Continuous Passive Motion Exercise Device	CPM
C1713		Anchor/screw for opposing bone-to-bone or soft tissue-to-bone (implantable)	Implant

* synovial fluid aspiration

Although different types of surgeries can be performed for the treatment of complications, for simplicity it was assumed that the surgeries for the treatment of pain complications have, in average, the same cost of the arthroscopy for the removal of loose/foreign body. The same assumption was made for the stiffness scenario: the average cost of all the surgeries needed in this case is represented by the cost of the arthroscopy for the lysis of adhesions.
Regarding the two-stage revision surgery, it occurs due to several reasons and in this model its probability is defined regardless of the type of complication that is being study. To cover the different types of surgical procedures, it was assumed that the surgeon fee used in the calculation of this aggregate cost would be the average cost of the surgeon fee when an arthroscopy is performed for the removal of loose/foreign body, plus the surgeon fee of an arthroscopy for the lysis of adhesions. The same was assumed for the facility fee.

5.2.6. Monte Carlo simulation

A Monte Carlo simulation was executed in MATLAB to study how the model responds to randomly generated inputs. This technique helps to assess the risk in quantitative analysis and decision making by building models of possible results by replacing a range of values (probability distribution) for any factor that has uncertainty [259]. It then calculates results over and over (iterations), using different sets of random values from the probability distributions. Therefore, a Monte Carlo simulation uses probability distributions as the realistic way of describing uncertainty in variables of a risk analysis [259].
The Monte Carlo simulation was then used to solve the decision tree represented in Figure 5.7. The probabilities values for each scenario were chosen uniformly from the respective established ranges (Table 5.9 and Table 5.10), whereas, for each iteration, all the cost variables were selected according to their calculated distribution. For all the simulations performed in this study, it was run 150.000 iterations.
The decision tree solutions were obtained by calculating the terminal values of each branch, i.e. summing up all the aggregate costs along the path leading to a given terminal node. The tree was then “rolled back” by computing the expected value at each event node and, in the end, the result was obtained by minimizing the expected value obtained in each of the three branches. The option obtained in the decision node indicates then the alternative/branch that has the lower average cost.
In each iteration the program selects different values for the cost items as well as for the probabilities, according to the corresponding distributions. The same value of a given cost item is used in each iteration to calculate the aggregate costs. This rule applies except for the implant cost. In each iteration, values for the cost of the bioabsorbable, metal and new implants are randomly selected based on the same cost distribution function since the database does not distinguish between the costs of bioabsorbable and metal implants. Additionally, as an initial assumption, it was considered the same cost distribution function of the current implants for the new implant.
Table 5.13 indicates the mean cost of the eight aggregate costs included in this model, assuming the same cost for the three implants. These costs are compared with the costs available in the literature. Additionally, Table 5.13 also indicates the mean cost of the current implants.

Table 5.13. Comparison between the costs calculated in this model and the costs presented in the literature.

Aggregate costs	Cost from the economic model (average cost - USD$)	Cost from the literature (USD$)
ACL reconstruction	15.556	17.160 [220]
Failure	56	
Other complications		
Well	0	-
One-stage ACL revision (due to Failure)	16.966	20.000 [223,224]
Two- stage Revision Surgery (due to Failure)	24.563 (additional surgery: 7.597)	-
Surgical Treatment (due to Other complications)	Pain scenario: 7.194 Stiffness scenario: 8.816	5.644 [220]
Conservative Treatment (due to Other complications)	4.416	Physical rehabilitation after ACL injury: 4.993 [220] Physical rehabilitation due to stiffness symptoms: 3.000 [224]
Other costs	**Costs from the economic model (average cost, USD$)**	**Costs from the literature (USD$)**
Implant	686	200 – 300 [260]

5.2.7. Results

In this chapter, more attention was given to the Pain 1 and Stiffness 1 scenarios, since they have the lowest probabilities' reductions on the various health events.

- *Scenario PAIN 1*

Figure 5.8 shows the distribution results of a Monte Carlo simulation. For this scenario, the probability ranges for the different variables in the simulation are indicated in Table 5.9. The bioabsorbable option had the lowest expected cost in 30,0 % of the iterations, the metal option 34,2% and the new implant option 35,8% of all iterations.

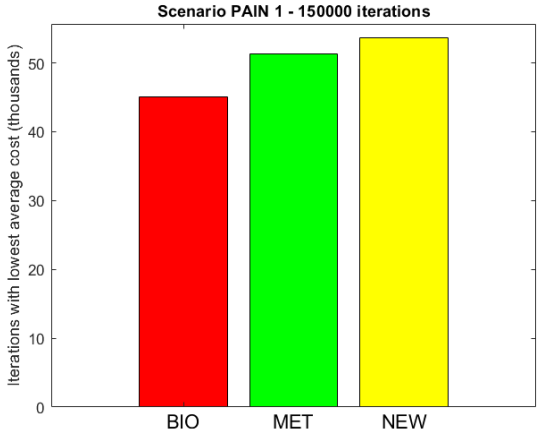

Figure 5.8. Number of times each implant had the lowest expected cost after 150.0000 iterations of the Monte Carlo simulation in the scenario Pain 1.

To assess the impact of the different events' probabilities in the average expected value of the new implant option, a series of two-variable sensitivity analyses were performed.

In Figure 5.9, the reductions promoted by the new implant on the incidence of the Failure and Other complications were studied, respectively, from 0% to 20% (2% of discretization) and 0% to 50% (2% of discretization), keeping fixed the other probabilities' reduction at 0%**.**

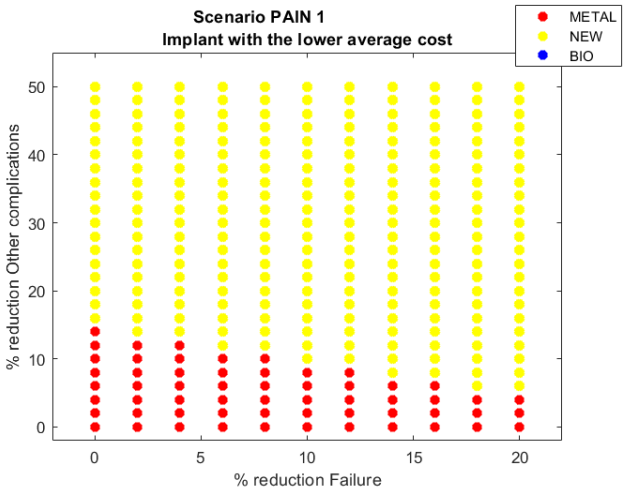

Figure 5.9. Two-variable sensitivity analysis in Pain 1 scenario, where the branches Other complications and Failure vary from 0% to 50% and 0% to 20%, respectively, while the other probabilities' reductions are maintained at 0%.

The results in Figure 5.9 indicate that the new implant option starts to have an average expected cost lower than the metal option when the incidence of Other complications is reduced by 16%, even if the remaining events are not reduced. This value becomes 14% if the incidence of Failure is reduced by 2%. However, it would be necessary to reduce the incidence of Failure by more than 20% to eventually obtain a lower expected value for the new implant option, if the incidence of the remaining events does not alter.

To study if the treatments Two-stage ACL revision and Surgical treatment have any impact on the output of the model, new two-variable sensitivity analyses were performed. In this case, it was assumed a) a default reduction values for these two events, attributed to the scenario Pain 1 (Table 5.9) and b) an extreme reduction: 80% reduction for Two-stage ACL revision and 50% reduction for the Surgical treatment of other complications. These new simulations are represented, respectively, in Figure 5.10 a) and Figure 5.10 b).

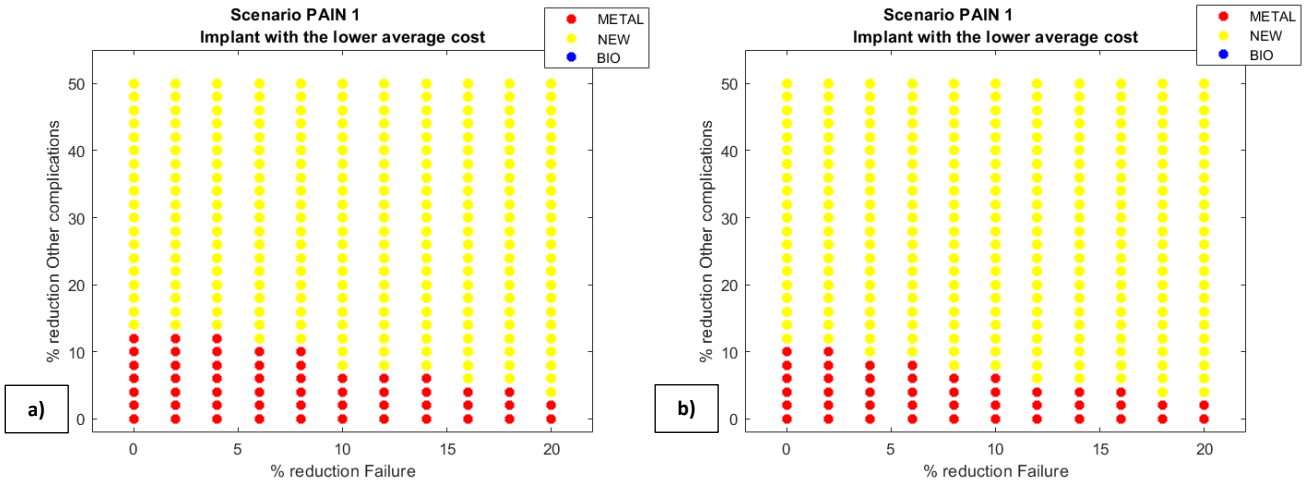

Figure 5.10. Two-variable sensitivity analysis in scenario Pain 1, where the branches Other complications and Failure vary from 0% to 50% and 0% to 20%, respectively, while the other probabilities' reductions are maintained at: a) default values (Table 5.9), b) 80% for Two-stage ACL revision and 50% for the Surgical treatment.

The results shown in Figure 5.10 indicate a similar trend, i.e. the probability' reductions of the Two-stage ACL revision and Surgical treatment do not significantly affect the output of the model. In both analyses, if the probability of Failure is not reduced, then it is enough to reduce the probability of Other complications by 14% in a) situation or by 12% in b) situation for the new implant option to have a lower average expected cost. Additionally, it is not enough to reduce the probability of Failure by 20% for the new implant option to have a lower expected cost. In this case, it is also necessary to reduce the incidence of Other complications. Therefore, these differences do not alter the preference of the model for the new implant option, especially in the ranges defined for this scenario (Table 5.9).

Figure 5.11 shows the importance of the event Other complications in the scenario Pain 1. This study compares the average expected cost of the three options, in which all the probabilities reductions were fixed at the default values (Table 5.9), except for this event. In this case, the reduction of Other complications varies from 0% to 50%.

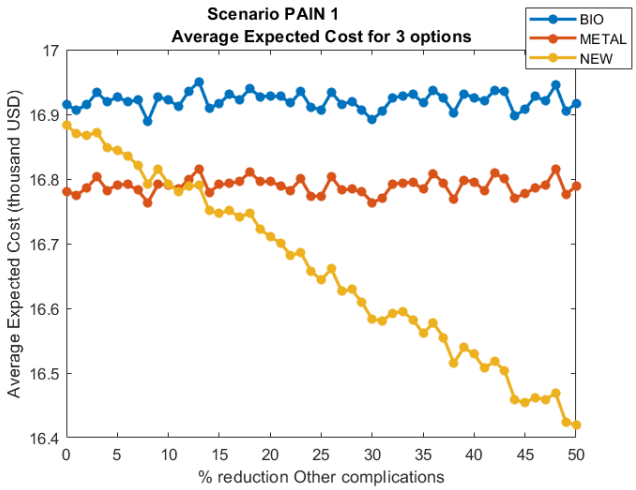

Figure 5.11. Average expected cost of the three options, obtained when the reduction of Other complications varies from 0% to 50%. The probabilities used in the remaining events were the default assigned for the scenario Pain 1.

Based on the results of the previous figure, the average expected cost is lower for the new implant when the event Other complications is reduced by 12%. This expected average cost falls more rapidly for reductions above 14%. When the reduction is 15% (Pain 1 scenario) the average expected costs are USD$ 16.917, USD$ 16.791 and USD$ 16.747 for the option bioabsorbable, metal and new implant, respectively.

Returning to the initial inputs of the model, described in Table 5.9, a new study was performed to assess whether the new implant remains the most attractive option even if it has a higher cost than the current implants. In this study, shown in Figure 5.12, the cost increase of the new implant varied between 0% and 20% (1% discretization).

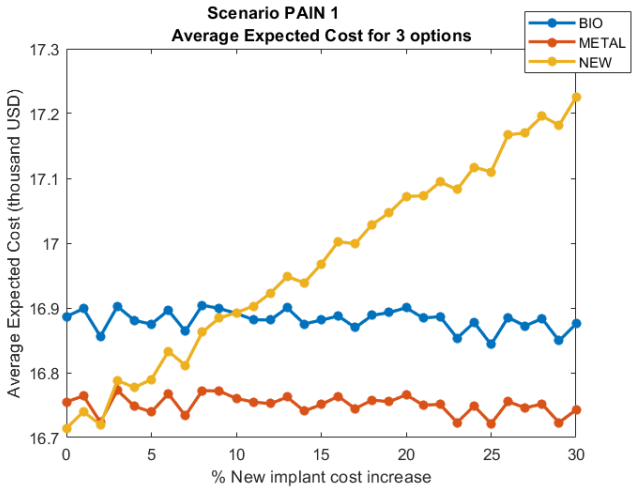

Figure 5.12. Average expected cost of the three options, obtained when the cost of the new implant increases (0 to 20%) comparing to the costs of the current implants. The probabilities used for the events were the default assigned for the scenario Pain 1.

According to the previous figure, there is a minimum margin for increasing the cost of the new implant. The average expected cost of the new implant option is lower than the other options only if the increase is up to 2%. Above 2%, the new implant is no longer the most attractive option, performing even worse than the bioabsorbable option if the cost increase is greater than 10%.

Next, a three-variable sensitivity analysis was performed to study the variation of the cost increase of the new implant alongside the reduction of the two most important events for the model. Therefore, in this study, the cost increase varied from 0% to 30% (increments of 5%), and the reduction of Failure and Other complications varied from 0% to 20% and 0% to 30%, respectively (increment of 2%). Figure 5.13 shows the implant with the lowest average cost for each situation.

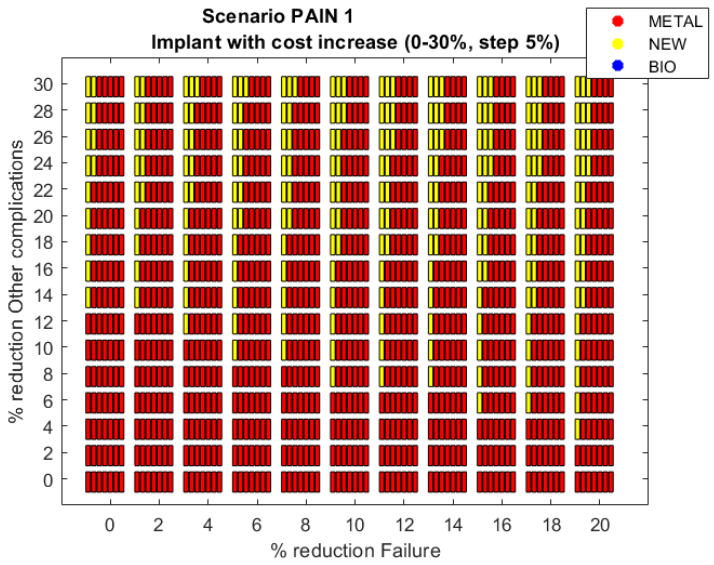

Figure 5.13. Three-variable sensitivity analyses in the scenarios Pain 1. The reduction of Other complications (0% to 30%, increment of 2%) was compared with the reduction of Failure (0% to 20%, increment of 2%) and the increase of the cost of the new implant (0% to 30%, 5% of increment). For each group of bars, the leftmost bar corresponds to a cost increase of 0% and the rightmost bar to a cost increase of 30%.

Based on the results of the previous figure, for a 10% cost increase it would be necessary to reduce at least the probability of Failure by 4% and Other complications by 30% for the new implant to still have a lower cost compared to the other implant choices. Another possibility is to reduce at least the probability of Failure by 16% and Other complications by 24%. In this figure, the cost increase of the new implant is represented by each bar, from left to right (increase of 5%).

Another study was executed to determine the annual cost savings that are generated from replacing the current treatment options by the new option, which uses a new implant for the ACL Reconstruction. This study used the default reduction values described in Table 5.9.

According to the information detailed in chapter 5.1.4, it is estimated that 175.000 ACL reconstructions are performed in the U.S., per year. Assuming that half of these surgeries (87.500) are performed using the bioabsorbable implant and the remaining using the metal implant, an additional simulation was performed to determine the yearly cost savings generated by replacing the current treatment options by the new implant option. The yearly cost savings were determined assuming the default probabilities assigned to Pain 1 (Table 5.9) and they were compared by increasing cost of the new implant, from 0% to 14%.

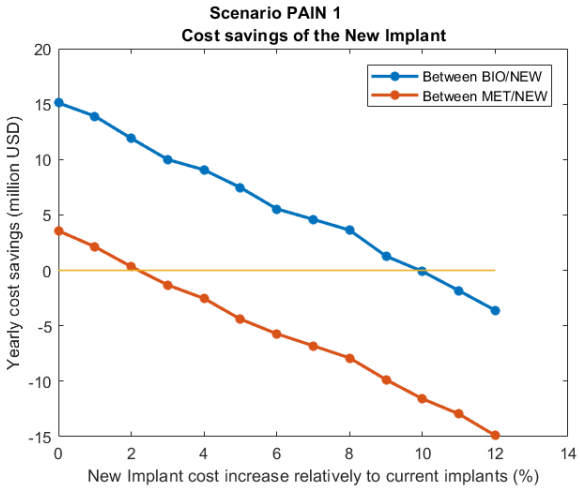

Figure 5.14. Yearly cost savings generated on the scenario Pain 1 by replacing the current treatment options by the new option, and according to the percentage of cost increase (0% to 14%).

The social advantages of a new commercially available implant, with better biological properties, is always positive when the treatments with the current bioabsorbable implants are replaced by a new treatment option, and assuming only a maximum cost increase of 10% for the new implant. The same is not valid for the metal option; in this case, the new implant is advantageous if the cost does not increase more than 2%. Assuming the same cost for all the implants, the estimated savings are USD$ 15,1M, comparing with the Bioabsorbable option, and USD$ 3,6M, comparing with the Metal option.

- *Scenario PAIN 2*

The scenario Pain 2 has three different assumptions when compared to the scenario Pain 1. They are summarized as follows: a) a 20% reduction both in the probability of Other complications and the probability of Surgical treatment of complications; b) a 20% reduction in maximum probability of failure, and c) a 60% reduction in maximum probability of the Two-stage ACL revision.

Figure 5.15 shows the distribution results of a Monte Carlo simulation, using the default values assigned to the scenario Pain 2. The bioabsorbable option had the lowest expected cost in 28,5 % of the iterations, the metal option 32,8% and the new implant option was chosen in 38,6% of the iterations.

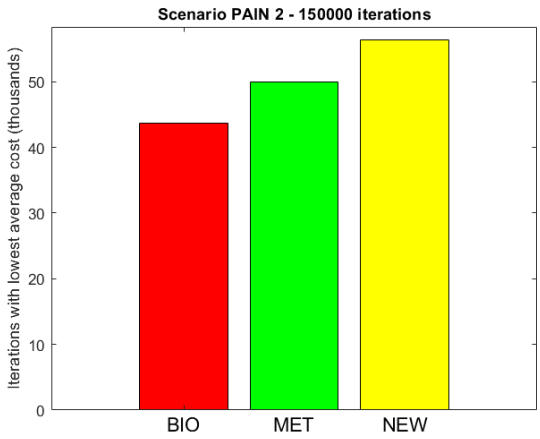

Figure 5.15. Number of times each implant had the lowest expected cost after running 150.000 iterations of the Monte Carlo simulation in the scenario Pain 2.

Next, it is presented an impact analysis of the branch Other complications in this scenario. The average expected value of the three treatment options are compared to each other, when the reduction of the event Other complications varies from 0% to 50% (increments of 1%), while the other reductions are kept at the values defined for this scenario (Table 5.9).

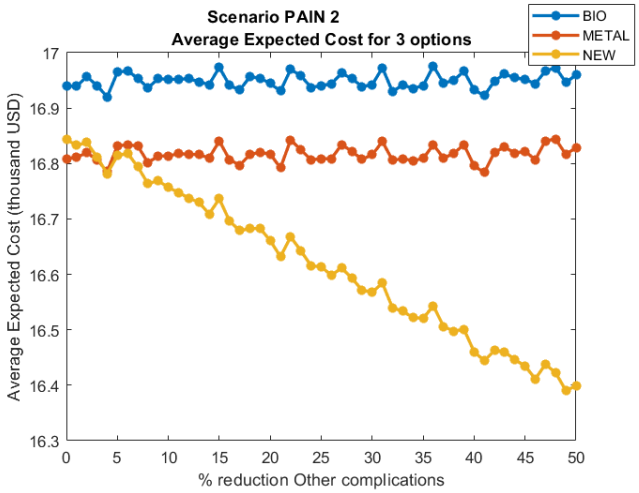

Figure 5.16. Average expected cost of the three options, obtained when the reduction of Other complications varies from 0% to 50%. The probabilities used in the remaining events were the default assigned for the scenario Pain 2.

The results indicated in Figure 5.16 reveal that if the event Other complications decreases by 20% (scenario Pain 2) the average expected cost of the bioabsorbable, metal and new implant options are, respectively, USD$16.944, USD$16.817and USD$16.661. In this case, the new implant has a lower expected cost for a reduction of more than 5% in this event.

Figure 5.17 compares the average expected cost of the three options when the cost of the new implant increases relatively to the cost of the current implant strategies. It is verified that the new implant remains the most attractive option if its cost does not increase more than 6%. When the cost increases by 14%, the new implant option is more unfavorable than the bioabsorbable option. Therefore, there is more room to increase the cost of the new implant in the scenario Pain 2 than in the scenario Pain 1.

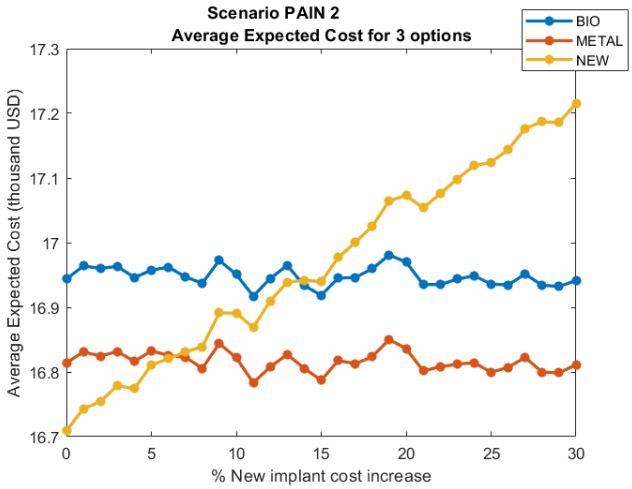

Figure 5.17. Average expected cost of the three options, obtained when the cost of the new implant increases (0 to 30%) comparing to the costs of the current implants. The probabilities used for the events were the default assigned for the scenario Pain 2.

Assuming that 87.500 ACL reconstructions are performed in U.S., per year, using metal implants and the same number or surgeries are performed using bioabsorbable implants, the yearly cost savings (Figure 5.18) resulting from replacing the current treatment options by the new implant option correspond to USD$ 20,5M and USD$ 9,2M, respectively, if all the implants have the same cost. However, if the cost of the new implant increases by more than 6%, there are no positive savings by replacing the metal option by the new implant option.

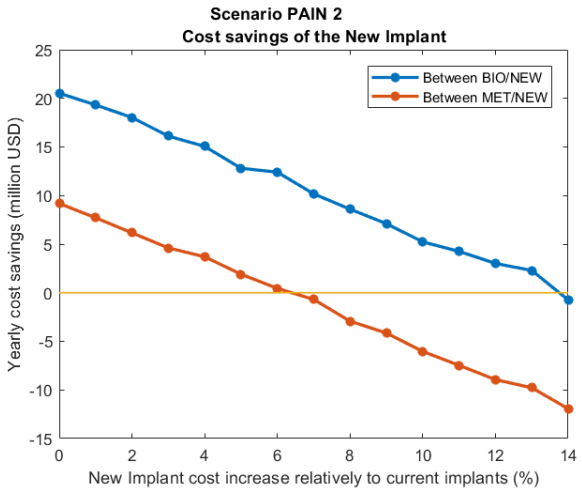

Figure 5.18. Yearly cost savings generated on the scenario Pain 2 by replacing the current treatment options by the new option and according to the percentage of cost increase (0% to 15%, increment of 1%).

- *Scenario STIFFNESS 1*

Figure 5.19 shows the distribution results of a Monte Carlo simulation, when the default values assigned to the scenario Stiffness 1 are used (Table 5.10). The results show that the bioabsorbable option had the lowest expected cost in 29,2% of the iterations, the metal option in 34,3% and the option New Implant in 36,5% of the iterations.

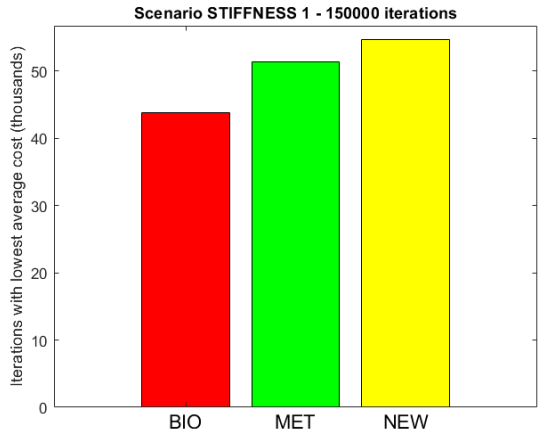

Figure 5.19. Number of times each implant had the lowest expected cost after running 150.000 iterations of the Monte Carlo simulation in the scenario Stiffness 1.

New simulations were run to study the impact of the reduction of the different events on the average expected cost of the three options. The goal was to evaluate in which conditions the new implant option is selected, i.e., it has a lower average expected cost. Therefore, as performed in scenario Pain 1, the reductions promoted by the new implant on the incidence of Failure and Other complications were studied from 0% to 20% (2% of discretization) and 0% to 50% (2% of discretization), respectively, keeping fixed the other probabilities' reduction at 0%**.** Figure 5.20 shows the results of this two-variable sensitivity analyses study.

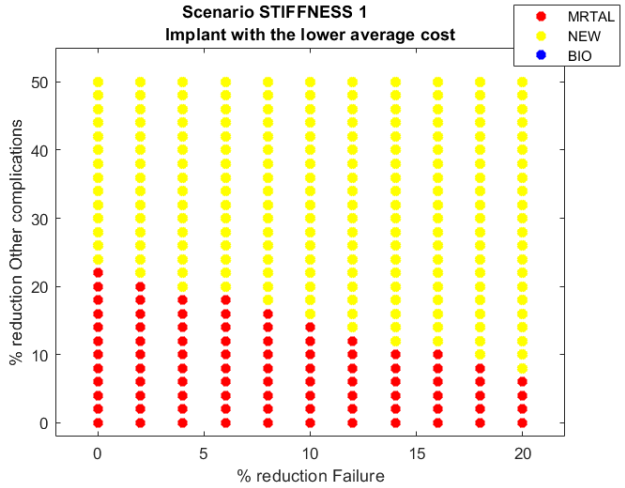

Figure 5.20. Two-variable sensitivity analysis in Stiffness 1 scenario, where the branches Other complications and Failure vary from 0% to 50% and 0% to 20%, respectively, while the other probabilities the other probabilities' reductions are kept at 0%.

The results in the previous figure show that the new implant needs to reduce the event Other complications by 24% to become the selected option, even if the other health events are not reduced. However, this reduction drops to 20% if the incidence of Failure is also reduced by 4%. For a 20% reduction in the incidence of Failure, it is still necessary to reduce the incidence of Other complications by 8%. As a comparison, for the scenario Pain 1, it was only necessary to reduce this event by 6%.

New two-variable sensitivity analyses were performed to study the impact of the events Two-stage ACL revision and Surgical treatment on the average expected cost of the three options.

Once again, the reduction of the events Other complications and Failure varied, respectively, from 0% to 50% and from 0% to 20%, with an increment of 2%. The reduction of the probabilities of the events Two-stage ACL revision and Surgical treatment were kept either a) on the default values defined in Table 5.10 or b) in 80% and 50%, respectively. Figure 5.21 a) and Figure 5.21 b) show the results of the simulations.

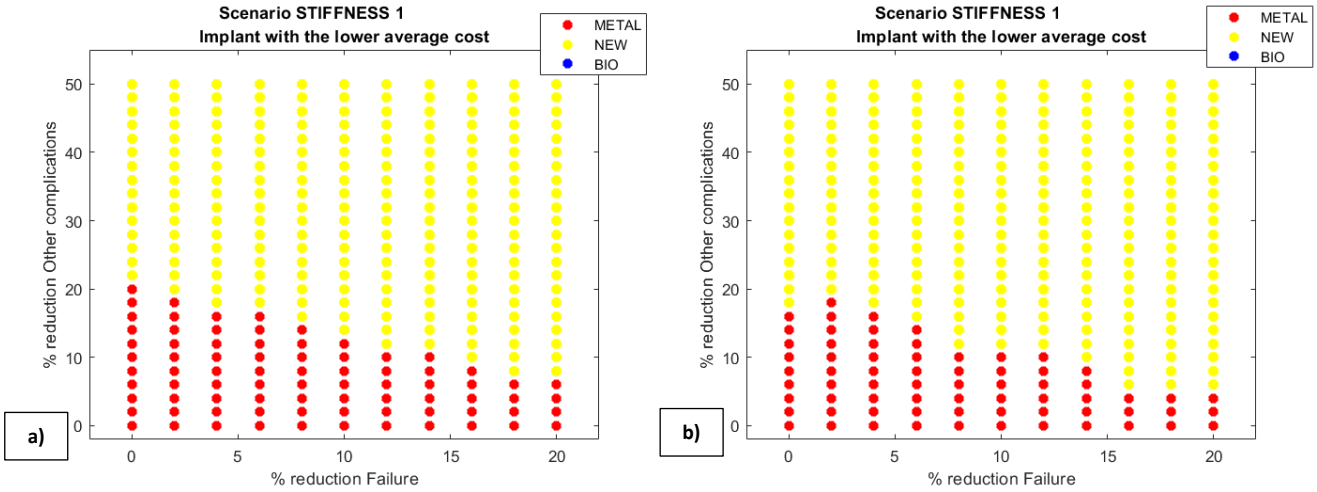

Figure 5.21. Two-variable sensitivity analysis in scenario Stiffness 1, where the branches Other complications and Failure vary from 0% to 50% and 0% to 20%, respectively, while the other probabilities' reductions are maintained at: a) default values (Table 5.10), b) 80% for Two-stage ACL revision and 50% for the Surgical treatment.

Analyzing the results in previous figure, no relevant differences are found in the output of the model when the incidence of the events Two-stage ACL revision and Surgical treatment is also reduced. For example, in both situations, to reduce incidence of Other complications by 18%, it is also necessary to reduce the incidence of Failure by 4%. Even though the simulation b) further reduces the incidence of Other complications when the incidence of Failure is 20%, these differences do not significantly alter the model response. Additionally, the results obtained in Figure 5.20 are similar to those on Figure 5.21 a).

Figure 5.22 shows the impact of the event Other complications in the scenario Stiffness 1. In this simulation, the average expected cost of the three options is compared when the reduction of Other complications varies between 0% and 50%, fixing the other reductions at the default values (Table 5.10). In this case, the results reveal that it is necessary to reduce the incidence of this event by more than 18% to obtain a smaller expected cost in the new implant option. This reduction level was also obtained in the study shown in Figure 5.20, when the incidence of Failure was reduced by 4%.

For a 25% reduction in the event Other complications (scenario Stiffness 1), the average expected cost of the bioabsorbable, metal and new implant options are, respectively, USD$16.598, USD$16.469 and USD$16.322.

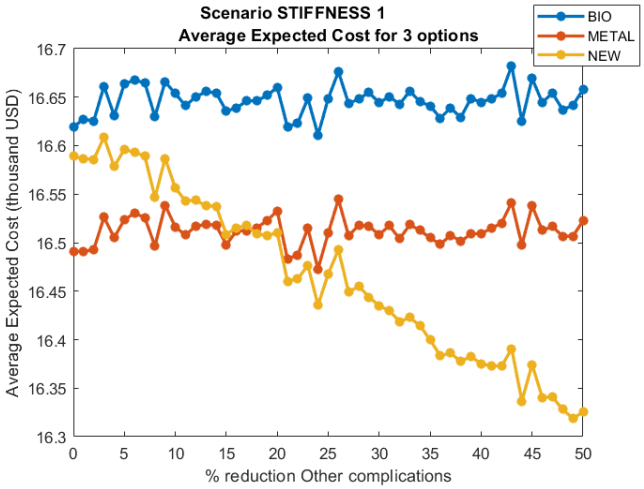

Figure 5.22. Average expected cost of the three options, obtained when the reduction of Other complications varies from 0% to 50%. The probabilities used in the remaining events were the default assigned for the scenario Stiffness 1.

Returning to the inputs assigned to the scenario Stiffness 1 (Table 5.10) a new simulation was performed to assess whether the new implant remains the most attractive option even if it has a higher cost comparing to the cost of the current implants. The results in Figure 5.23 reveal that if the cost of the new implant increases by more than 3%, then this option is no longer the most attractive, performing even worse than the bioabsorbable option if the cost increases by 10%. The cost boundary defined in this scenario for the new implant is in accordance with the boundary defined in the scenario Pain 1.

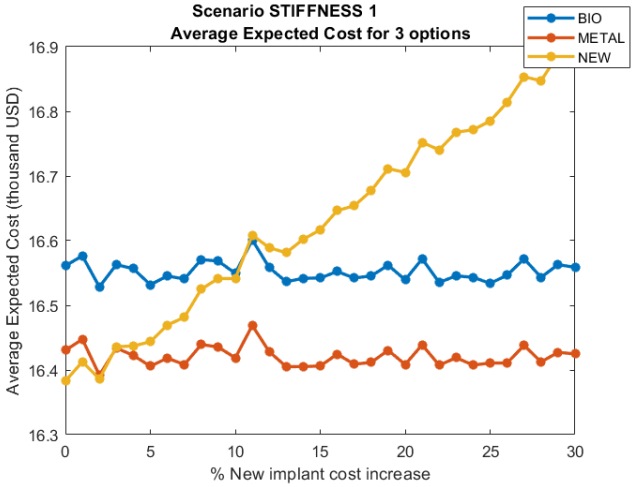

Figure 5.23. Average expected cost of the three options, obtained when the cost of the new implant increases (0 to 20%) comparing to the costs of the current implants. The probabilities used for the events were the default assigned for the scenario Stiffness 1.

The next simulation, summarized in Figure 5.24, is a three-variable sensitivity analysis used to study the variation of the cost increase of the new implant alongside with the variation of the probability of the events Other complications and Failure. In this case, the cost increase varies from 0% to 30%, with an increment of 5%, the reduction of the events Other complications and Failure varied from 0% to 50% and 0% to 20%, respectively, with an increment of 2% in both cases.

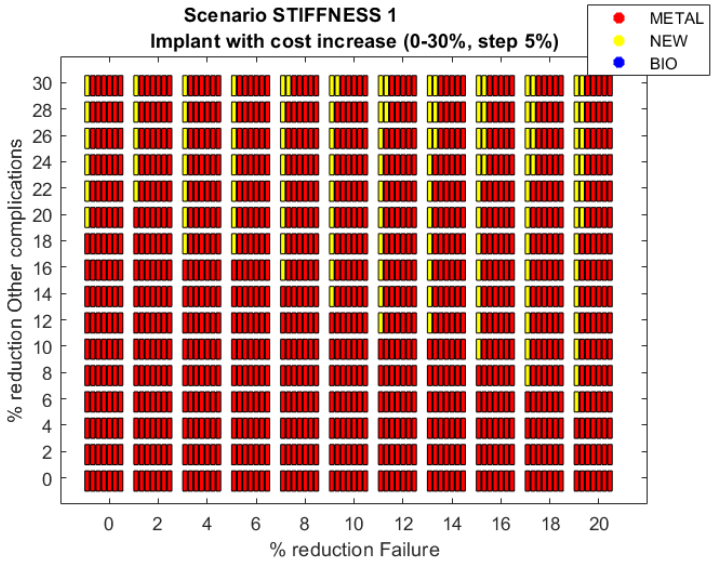

Figure 5.24. Three-variable sensitivity analyses in the scenario Stiffness 1. The reduction of Other complications (0% to 30%, increment of 2%) was compared with the reduction of Failure (0% to 20%, increment of 2%) and the increase of the cost of the new implant (0% to 30%, 5% of increment). For each group of bars, the leftmost bar corresponds to a cost increase of 0% and the rightmost bar to a cost increase of 30%.

As shown in the previous figure, to compensate the increase of the cost of the new implant by 10%, it is necessary to reduce the incidence of Other complications by more than 30% and the incidence of Failure by more than 20%. To compensate an increase of the cost of the New Implant by 10%, it is then necessary to reduce the incidence of Other complications at least by 45% (this result is not shown in Figure 5.24). Therefore, there is less room to increase the cost of the new implant in scenario Stiffness 1 than in scenario Pain 1.

Next, a study was executed to determine the cost savings obtained from replacing the current treatment options by the new option, which uses a new implant with better biological properties. This study assumed the reductions assigned to the scenario Stiffness 1 (Table 5.10). However, the cost savings were computed according to the cost increase of the new implant, which varied from 0% to 14%. Additionally, the cost savings were extrapolated considering the yearly number of ACL reconstruction surgeries performed in the U.S., using bioabsorbable and metal implants. According to the results indicated in Figure 5.25, if all the implants have the same cost, the estimated yearly cost savings are USD$ 16,6M and USD$ 4,2M if the new implant option replaces, respectively, the bioabsorbable and metal options. The cost of the new implant can increase only by 3% or by 10% to be the option with a lower expected cost, if compared with the metal and the bioabsorbable options, respectively.

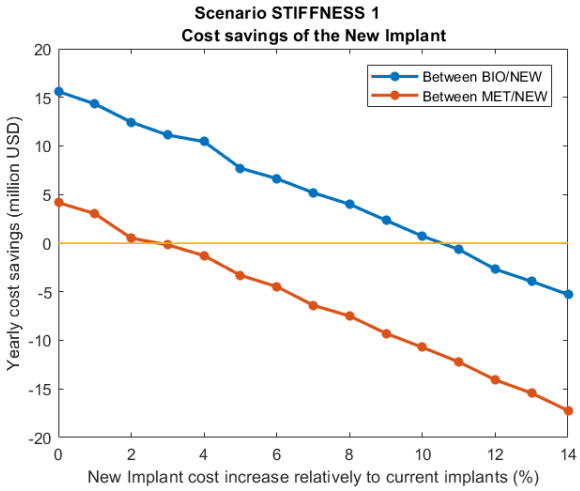

Figure 5.25. Yearly cost savings generated on the scenarios Pain 2 by replacing the current treatment options by the new option, and according to the percentage of cost increase (0% to 14%, increment of 1%).

- *Scenario STIFFNESS 2*

According to the information presented in Table 5.10, the scenario Stiffness 2 has the following assumptions: a) a 30% reduction in both maximum probability of Other complications and maximum probability of Surgical treatment, b) a 20% reduction in maximum probability of Failure and c) a 60% reduction in maximum probability of the Two-stage ACL revision.
Figure 5.26 shows the distribution results of a Monte Carlo simulation after running the 150.000 iterations, using the values assigned to the scenario Stiffness 2. In this case, the bioabsorbable option had the lowest expected cost in 28,0% of the iterations, the metal option in 32,8% and the new implant option in 39,2% of the iterations.

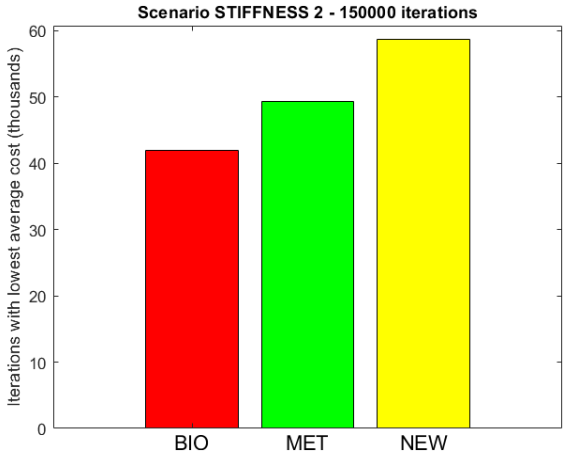

Figure 5.26. Number of times each implant had the lowest expected cost after running 150.000 iterations of the Monte Carlo simulation in the scenario Stiffness 2.

Figure 5.27 shows a study that simulates the cost savings obtained when the current treatment options are replaced by a new option, which uses an ideal bioabsorbable implant for the ACL Reconstruction. Under the conditions of the scenario Stiffness 2, the average expected cost of the three options were computed when the probability of Other complications varied between 0% and 50%. The other probability reductions were fixed at the values assigned to this scenario.

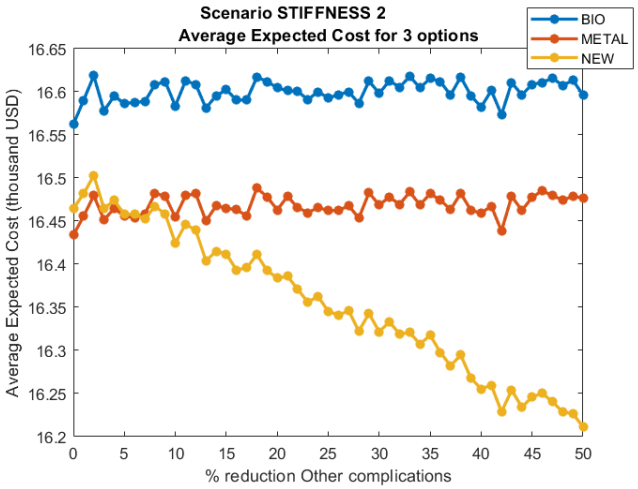

Figure 5.27. Average expected cost of the three options, obtained when the reduction of Other complications varies from 0% to 50%. The probabilities of the remaining events were the default assigned for the scenario Stiffness 2.

According to these results, if the probability of the event Other complications is reduced by 7%, or more, the new implant option becomes the option with the lowest expected cost. The average expected costs of the bioabsorbable, metal and new implant options are, respectively, USD$16.598, USD$16.469 and USD$16.322 if this event is reduced by 30%, as assigned for the scenario Stiffness 2.

Figure 5.28 shows the average expected cost of the three options when the cost of the new implant increases between 0% and 20% relatively to the cost of the current implants. Assuming the reductions attributed to the scenario Stiffness 2, for all the events (Table 5.10), the results in Figure 5.28 reveal that it is possible to increase the cost of the new implant by at least 8%, ensuring at the same time a lower expected cost in this scenario. The same boundary value was obtained when this simulation was performed in the scenario Pain 2. Comparing with the bioabsorbable option, it is only possible to increase the cost of the new implant by 16%.

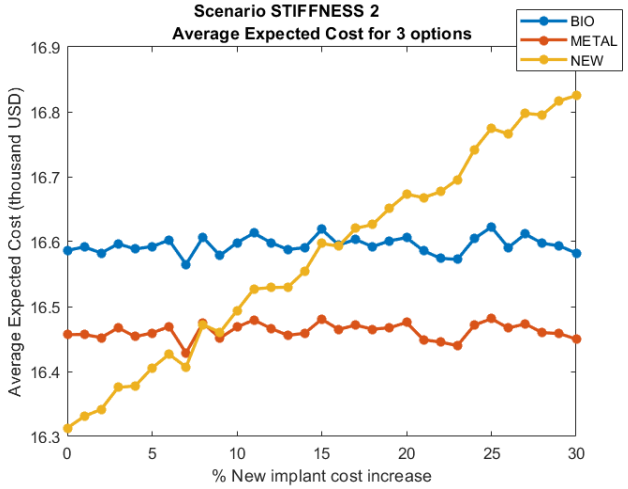

Figure 5.28. Average expected cost of the three options, obtained when the cost of the New Implant increases (0 to 20%) comparing to the costs of the current implants. The probabilities used for the health events were the default assigned for the scenario Stiffness 2.

Figure 5.29 shows the last study that involved the computation of the savings generated if the current treatment options are replaced by a new option. This new option uses a new implant with improved biological and mechanical properties. Considering the yearly ACL reconstructions performed using bioabsorbable and metal implants, and assuming that all the implants have the same cost, the generated savings correspond to USD$ 47M and USD$ 25M if the new implant replaces the bioabsorbable and the metal options, respectively. However, if the cost of the new implant increases more than 8%, there are no positive savings when the new implant option replaces the metal option.

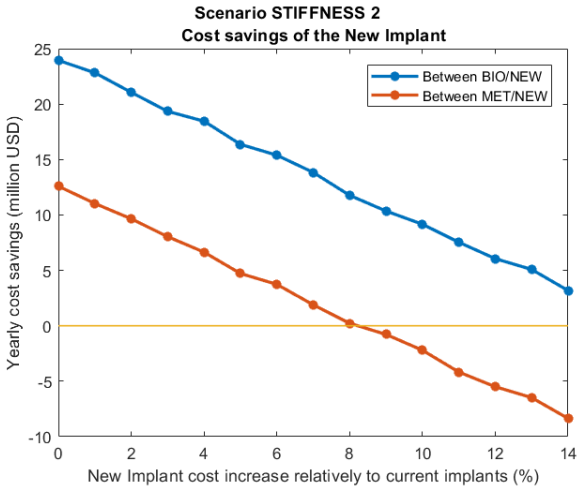

Figure 5.29. Yearly cost savings generated on the scenarios Stiffness 2 by replacing the current treatment options by the new option, and according to the percentage of cost increase (0% to 14%, increment of 1%).

5.3. Discussion of the Results

To construct this economic model, it was necessary to determine the health events after an ACL Reconstruction. The time period chosen for this evaluation was two years of follow-up after the primary surgery. Therefore, a patient who performed an ACL reconstruction, after two years of follow-up he can be placed in one of the following categories:

1) the patient recovered well;
2) the patient needed an ACL Revision;
3) the patient did not need an ACL Revision, but needed to treat other complications.

The literature is not clear regarding the prevalence of complications and the exact nature of the complications associated to the ACL Reconstruction. Several authors report results for "satisfactory outcomes" or "good results" after an ACL reconstruction, without defining which criteria were used for such reference. Additionally, many studies that follow the patients after an ACL Reconstruction only record problems as those requiring a revision procedure, not including the patients who declined a new surgery or have complications other than instability. Therefore this study was divided in two main symptom scenarios:

- pain, in which the complications are mainly from inflammatory origin and cause pain symptoms;
- stiffness, in which the complications arise from loss of mobility and stiffness symptoms.

Although the instability symptoms are also considered as complications, these cases were mostly studied in the Failure branch. Dividing the complications only in stiffness and in pain reduces the complexity of the model, because it does not include the cases of the patients who suffer from both types of complications. Additionally, it allows to infer which group of patients benefits the most from the use a new bioabsorbable implant, with improved biological and/or mechanical properties.

Two additional levels were created in each main scenario:

- Pain 1 and Stiffness 1 studied the use of a better bioabsorbable implant, which has better biological properties;
- Pain 2 and Stiffness 2 studied the use of an ideal bioabsorbable implant, which improves both the biological and the mechanical properties.

After defining which would be the expected reduction on the probability of the health events, resulting from the use of a new implant in the ACL Reconstruction, several simulations were performed to assess the potential economic impact of such implant. The reductions promoted by the new implant are related to the probabilities of the health outcomes that come from using the current bioabsorbable implants.

Table 5.14 summarizes the annual cost savings for the different scenarios if the current treatment strategies (bioabsorbable and metal) are replaced by the new strategy, which uses the new implant for the ACL Reconstruction.

Table 5.14. Expected yearly cost savings generated when the current treatment options are replaced by a new option that uses a new implant.

Scenario	Pain 1 (Better implant)	Pain 2 (Ideal implant)	Stiffness 1 (Better implant)	Stiffness 2 (Ideal implant)
Cost Savings – Replacing Bioabsorbable Option	USD$ 15,1M (-1,0%)	USD$ 20,5M (-1,7%)	USD$ 15,6M (-1,1%)	USD$ 23,9M (-1,7%)
Cost Savings –Replacing Metal Option	USD$ 3,6M (- 0,3%)	USD$ 9,2M (-0,9%)	USD$ 4,2M (-0,3%)	USD$ 12,6M (-0,9%)

According to the results in last table, it is clear that the use of a new implant promotes similar cost savings, regardless of the type of scenario under study. However, the most evident cost savings are generated when the new implant option replaces the bioabsorbable option and if the new implant can improve both the biological and the mechanical properties of the current bioabsorbable implants (ideal implant). Nevertheless, cost savings are generated in any situation, even if the new Implant is only able to improve the biological properties of the current implants (better implant).

Further attention was given to the scenarios Pain 1 and Stiffness 1, since are these scenarios that present smaller reductions on the probability of complications when a new implant is used.

Based on the several simulations performed, it becomes clear that the probability of the event Other complications has higher impact on the average expected cost of the ACL Reconstruction. Assuming that the new implant necessarily reduces the probability of this event, even if the reductions of the other reductions are kept at 0% and its cost of does not increase, the following values are then defined as the minimum probability reduction:

- Pain 1 scenario: 16% reduction in the probability of Other complications;
- Stiffness 1 scenario: 24% reduction in the probability of Other complications.

On the other hand, assuming the default reductions assigned to the Pain 1 and Stiffness 1 scenarios, for the events Failure, Two-stage ACL revision and Surgical Treatment of other complications, it becomes only necessary to reduce the incidence of Other complications by 12% and 18%, respectively for each scenario. These results show the impact of this event in the model, which greatly depends on the cost of the new implant.

This study also shows several limitations. One important limitation is due to the uncertainty regarding the real prevalence of the health events after an ACL Reconstruction, when the current implants are used. This occurs as a direct consequence of poor reporting as health outcomes are rarely associated with the type of implant that was used by the studies reported in the literature.

As an assumption, this model considered a different prevalence on the following health outcomes, between the bioabsorbable and metal options: Other complications (5% difference), Surgical treatment of complications (5% difference) and Two-stage ACL revision (3% difference). The introduction of these differences is consistent with the largest number of the cases reported in the literature when the primary surgery is performed using a bioabsorbable implant. The exception is the incidence of Failure. In this case, the literature only associates the prevalence of Failure to the type of graft or technique. In many occasions, studies do not even indicate which type of implant was used. For this reason, the average expected cost of the new implant option is often compared with the metal option.

To simplify the model, interest rates were not applied to the costs. However, it is important to point out that the cost items used to calculate the aggregate costs of this model were obtained from a U.S. health insurance database in April 2016.

Although this study assumed a societal perspective, unfortunately it was not possible to integrate indirect costs in this economic model. These costs are associated with disease morbidity and include, for example, costs associated with work loss (cessation or reduction), whose consequences are lost taxes, lost contributions to the economy from decreased spending (e.g. in leisure activities) and an increased burden on the social and healthcare systems. Eventually, if this study had included indirect costs, it is estimated that the usage of a new implant would also promote a reduction of such costs. One of the advantages of the new implant could be a faster and more effective treatment, which saves patients' time on dislocations, increasing work hours and productivity, among others. Greater efficacy in the treatment could also be accounted by reducing the number of physical rehabilitation sessions.

In the model, it was assumed that if certain health events occur, then the same treatment protocols are used. However, this model integrated the direct costs that could have higher impact in its outcomes. This explains why certain cost items were not included, such as the medication cost for pain or swelling relief.

Through the database consultation, it was not possible to distinguish differences between the costs of implants. According to Prodomos *et al*.[260] the cost differential between metal and bioabsorbable implants is reducing (U.S. healthcare system). Thus, the model assumes the same cost for these two implants. Nonetheless, had the model considered that the bioabsorbable implant has a higher cost, greater yearly cost savings would be obtained if the new treatment option replaces the current bioabsorbable option.

Table 5.13 compares the costs calculated in this model with the costs in the literature. The model assumed lower costs for the ACL reconstruction surgery and One-stage ACL revision, but the cost of the implant was higher when compared with the range values found in the

literature. After simulating the cost impact of the new implant, it became clear that it is only possible to increase its costs by 2% or by 3%, respectively, in Pain 1 and Stiffness 1 scenarios. If the percentage of cost increases more than those values, the new implant option will have an average expected cost higher than the metal option.

5.4. Conclusion and future work

The results indicate that the health event that most influences the response of the model is Other complications, being either associated to pain or to stiffness symptoms. Therefore, the new implant can only be the option with the lowest average expected cost if it can reduce the probability of this event, especially when compared with current bioabsorbable implants. If the new implant reduces the probability of complications by 15%, without reducing the prevalence of the other health events, it is already introducing benefits to the patients that suffer from pain after an ACL Reconstruction.

Since this economical study started from the premise that the new implant improves at least the biological properties of the current bioabsorbable implants, then it is concluded that the development of a new implant has benefits to society, since the expectation is that it will reduce the probability of complications by 15%, in the scenario Pain 1, or by 25%, in the scenario Stiffness 1. This expectation is supported by the information presented in the chapter 2.5. (Current Research for Bioabsorbable Polymer Fixation Implants in Orthopedics), where several strategies were presented for the development of new bioabsorbable implants, with improved biological properties. This thesis focuses in the development of new bioabsorbable implants based on chitosan (see the next chapters).

To be the option with the lowest expected cost, the commercial cost of the new implant should be similar to the current implants used in the ACL Reconstruction. To introduce a more expensive implant in the market, it is necessary to guarantee that it will introduce a greater reduction in the probability of Other complications. However, such higher reduction may not be achieved, since the complications that arise after an ACL Reconstruction can be influenced by other factors, such as other concomitant injuries associated with the ACL rupture and technical errors.

As future work, the following points are proposed:

- A new bioabsorbable implant should be developed, since the introduce improvements will have a positive impact in the society;
- This model intended to study the economic potential of a new bioabsorbable implant, for the treatment of ACL ruptures. However, the decision tree that supports the model was constructed as general as possible, thus allowing its application in further studies, for different orthopedic areas. As an example, this model can be applied to study the potential development of a new bioabsorbable implant for the treatment of the shoulder's ligaments (e.g. rotator cuff injury);
- Given the difficulties to obtain data for the probabilities of the health events and for the costs of the several items, it is recommended that the hospitals and orthopedic surgeons report, in an accessible way, all the important information regarding the ACL Reconstruction surgeries, as well as all the short- and long-term outcomes of such procedures. The information can be accessible through scientific articles and/or hospital databases. The success of early HTA models is only possible if information on

the outcomes of the surgeries and treatments is easily obtainable. In this case, it would be important, for example, to know the prevalence and origin of certain complications. This is important not only to conciliate medical practice with scientific research, but also to give orthopedic surgeons more information for better decision making, thus helping to reduce the future clinical errors.

- The data introduced in the model should be constantly updated, especially after eventual clinical trials.

SECTION C: Methodologies for the development and evaluation of 3D dense chitosan-based compositions for orthopedic applications

6. Experimental tests to define the physicochemical properties of chitosan

The different functions of chitosan depend both on its chemical structure and molecular size. Therefore, the characterization of a chitosan sample requires the determination of its D.D., viscosity and M_w, being the M_w the feature that companies generally prefer to use as the representative feature of their commercial products.
This chapter introduces and explains the methodologies that were used to characterize the D.D. and the viscosity of the chitosan samples tested in this study.

6.1. Viscosity

Viscosity is a property of all liquids that measures their resistance to flow or shear as a function of the temperature and pressure [261]. With η representing the dynamic viscosity, the relation between the shear stress, σ, and the strain rate, *ė*, is given by equation 1. The most common unit of measurement for viscosity is the poise (P) [261].

$$\sigma = \eta \times \dot{e} \tag{1}$$

The flow characteristics of liquids are divided into three categories: Newtonian, time-dependent Non-Newtonian and time-independent Non-Newtonian [261]. In the first case, the viscosity of the liquid does not depend on the shear stress [261]. However, for Non-Newtonian liquids, the viscosity depends on the applied shear force and time [261]. For time-dependent fluids, there is a change in viscosity with time under same conditions of constant shear rate (thixotropic and rheopectic fluid), whereas for time-independent fluids, the shear stress does not vary proportionally with the shear rate [261]. Figure 6.1 represents different types of time-dependent Non-Newtonian fluids.

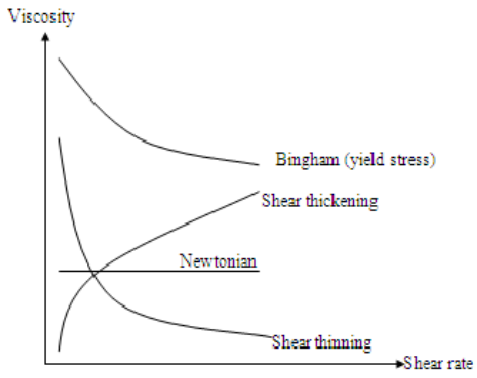

Figure 6.1. Different types of time-independent Non-Newtonian fluids [262].

There are different types of rheometers and viscometers that are able to measure a fluid's viscosity [263]. The Brookfield viscometer is a type of rotational viscometer that commonly uses a rotating disk in a fluid at a known speed, and the torque force required to rotate the disk is related to the viscosity of such liquid [263].

Several published studies report the rheological behavior of chitosan. Kienzle-Sterze *et al*.[264] showed that the viscosity of chitosan increases with its concentration. The authors also showed that at higher concentrations of chitosan solutions revealed a shear thinning behavior. Wang and Xu [265] reported that the non-Newtonian behavior of chitosan solutions increased for higher D.D., which is explained by the increase of entanglements. Other studies showed that the chitosan's M_w affects the viscosity of its dispersions [266,267]. In fact, the viscosity of chitosan solutions can be related to its Mw according to the Mark-Houwink-Sakurada equations [268].

6.1.1. Experimental Procedure

Chitosan viscosity procedure used followed the protocol defined by Altakitin S.A. A 1% (w/v) of chitosan was dissolved in a 1% (v/v) acetic acid solution. After the total dissolution of chitosan, the solution was left to rest for 1 hour, for air bubbles to collapse.
The viscosity of the solution was measured at room temperature (21°C) and at 50 RPM using a Brookfield viscometer. The spindle of the measurement (R2 or R3) was chosen accordingly with the samples behavior (torque of about 50% on the viscometer display). Registration of the viscosity was performed after the values stabilized.

6.2. Molecular Weight

Gel permeation chromatography (GPC) is an analytical technique that separates dissolved macromolecules according to their size throughout a specific stationary phase [269,270]. The main use of GPC is identifying the molar mass averages (M_n, M_w, M_z) or molar mass distributions (MMD) of natural and synthetic polymers, which is normally accomplished through the application of calibration curves [269]. In addition to the molar mass determination, the GPC also allows to prepare molecular fractions for characterization or further use, to serve as a method for desalting or buffer exchange and to estimate molecular association constants (e.g. macromolecular aggregation) [269].
GPC employs a stagnant liquid present in a porous-particle column packing (stationary phase) and a flowing liquid (mobile phase) [269,270]. The mobile phase can flow between and in and out of the pores of the packing. The separation phenomena occurs by repeated exchange of the solute molecules between the bulk solvent of the mobile phase and the stagnant liquid phase within the pores of the packing [269,270]. The pore size of the packing particles determines the molecular size range within which separation occurs [269,270].
Briefly, a GPC instrumentation includes: a pump (to push the solvent through the instrument), an injection port (to introduce the test sample onto the column), a column (to hold the stationary phase), one or more detectors (to detect the components as they leave the column) and a software(to control the different parts of the instrument and calculate and display the results [270].

6.2.1. Experimental procedure

The M_w of chitosan samples were determined by GPC at room temperature. A sodium acetate/acetic acid buffer solution was prepared as eluent, and 2 mg of each different chitosan

powder was dissolved in 1 ml of such solution. To prevent insoluble particles from compromising the proper functioning of the column, all the dissolutions were filtered through a cellulose acetate syringe filter (pore size 0,45 µm).
The GPC equipment included a Smartline RI Detector 2300 (refraction index detector) and a Smartline Pump 1000 from Knauer. The column was a PL aquagel-OH Mixed-H 8, from Aligent Technologies. The flow rate used was 1 mL/min and the sample injection volume was 100 µL per run.
Calibration curve was previously obtained by using Pullulan polysaccharides calibration kit from Varian (same chromatography parameters). Acquisition and data processing was done using Clarity ® software from DataApex.

6.3. Degree of Deacetylation

There are multiple methods available to determine the D.D. of chitosan samples (see chapter 3.2.). One of this methods, the nuclear magnetic resonance (NMR) studies the molecules by assessing the interaction of radiofrequency electromagnetic radiations with their nuclei when placed in a strong magnetic field [271].
The atomic nuclei of certain isotopes, such as ^{1}H, ^{2}H, ^{13}C, ^{15}N, and ^{19}F, possess a spin angular momentum and a corresponding magnetic moment. Considering the ^{1}H nucleus, it has a spin quantum number (I) of 1/2, which generates two quantized orientations in the presence of a magnetic field: parallel to the applied field (lower energy orientation) or antiparallel to it (higher energy orientation) [271]. When the nucleus is placed in a magnetic field, it stops spinning on its axis, exhibiting a characteristic wobbling motion (precession) [271]. If a radiofrequency field is now applied in a direction perpendicular to the magnetic field, and at a frequency that exactly matches the precessional frequency ("Larmor" frequency) of the nucleus, absorption of energy will occur and the nucleus will suddenly "flip" from its lower energy orientation to the higher energy orientation [271]. It can then relax back to the lower energy state through *spin-lattice relaxation* (*T*1), by transfer of energy to the assembly of surrounding molecules, or by *spin-spin relaxation* (*T*2), involving transfer of energy to a neighboring nucleus [271]. The change in the impedance of the oscillator coils caused by the relaxation is measured by the detector as a signal in the form of a decaying beat pattern, known as a *free induction decay* (FID) [271]. The signal is then converted to a ^{1}H-NMR spectrum by Fourier transformation.
Protons that are in the same magnetic environment are chemically equivalent. Each group of chemically equivalent protons gives rise to a signal [272,273]. The groups H's, CH_3 and CH_2 are usually equivalent, as well as symmetrical compounds such as benzene. The relative intensity (integration) of the signal is proportional to the relative number of protons responsible for such signal [272,273]. Instead of inform the absolute number of protons, it provides ratios of protons [272,273].
Protons that are not equivalent will absorb at different frequencies, which give rise to a different signal on the ^{1}H-NMR spectra [272,273]. The positions of the signals in a ^{1}H-NMR spectrum are based on how far they are from the signal of the reference compound [272,273]. The position of the signals depends on the chemical shift, which is measured in parts per million, ppm. The reference compound is at the zero position on the very left of the spectrum, and as the signal moves toward the left, the ppm values become larger [272,273]. The chemical

shift is influenced by the shielding effect (electron density) and electronegativity. For example, protons in electron dense environments sense a smaller effective magnetic field and therefore will require a lower frequency to come into resonance [272,273].

Each unit residue of the polymer has six carbon and seven hydrogen atoms which produce C–H linkages [274]. The peak at 2.2 ppm represents three protons of N-acetyl glucosamine and the peak at 3,5 ppm represents H2 proton of glucosamine residues [274,275]. The non-anomeric protons (H3-H4-H5-H6-H6'), connected to ring-skeleton, have similar electron densities and thus chemical shifts [274,275]. The signals of the non-anomeric protons partially overlap and produce a broad envelope of signals in the middle of the spectrum, which are observed around 4 ppm [274]. Anomeric proton H1 is observed at higher chemical shift due to its neighboring glycosidic and ring oxygen [274].

According to Hirai *et al*.[275] the D.D. of chitosan is determined from equation 2 by using the integral intensity of its CH_3 residue (I_{CH3}) and the sum of the integral intensities of H2, H3, H4, H5, H6, H6´ protons.

$$\mathbf{D.D.}\,(\%) = \left(\mathbf{1} - \frac{\frac{I_{CH3}}{3}}{\frac{I_{H2-H6}}{6}}\right) \times \mathbf{100} \qquad (2)$$

6.3.1. Experimental Procedure

To measure the D.D. of chitosan, a ^{1}H-NMR tube was prepared with a chitosan solution of 5 mg/ml in a DCl/D_2O solution (2%, w/v). The experiment was carried out in a Bruker Avance-III 400 MHz NMR spectrometer, under a static magnetic field of 9,4 T and at a temperature of 70°C. This temperature was chosen to avoid any interference of the solvent with the chitosan peaks.

The sample tube was inserted in the magnet and allowed to reach thermal equilibrium. The experiment for D.D. determination was a single pulse sequence with pre-saturation of the solvent with irradiation (ZGPR pulse sequence). The software used to analyze the spectrum was the Bruker Topsin 3.1.

The D.D. was calculated by using equation 2.

7. Experimental tests and methods for the evaluation of 3D dense chitosan-based product compositions

Several test methods (e.g. mechanical, chemical and biological tests) are available in science and engineering to identify the performance and characteristics of a given material or product. This chapter presents the different test methods used in this experimental study, in order to evaluate and characterize the intrinsic potential of each the chitosan-based compositions developed for applications in orthopedics.

7.1. Mechanical properties

7.1.1. Compression tests

Compressive tests determine the behavior of the materials under crushing loads, by estimating fundamental variables such as stress, stain and deformation [276]. By testing the material at compression, the compressive strength, the compressive stress and the compressive modulus of elasticity may all be determined.

During a compressive test, a specimen is loaded with a force that is applied perpendicularly to the cross section under consideration [276]. Compressive internal forces develop in the specimen and the intensity of such forces, on the various cross sections portions of the specimen, is called stress [276]. When a deformable body is subjected to stresses, it undergoes deformation. When a compressive test is performed, the deformation is normally accompanied by a reduction of the specimen's dimensions in the direction of the applied force [276]. The total deformation of a specimen under the force is called elongation, δ [276].

The compressive strength supported by a test specimen corresponds to the maximum compressive stress applied, before a first crack is detected [277]. In turn, the nominal compressive stress (σ_C) is the load (F) per unit area of minimum original cross section (A_0) carried by the test specimen at any given moment, as given by equation 3 [277].

$$\boldsymbol{\sigma_C = \frac{F}{A_0}} \tag{3}$$

The compressive strain is calculated according to equation 4, where *l* is the instantaneous length at any moment, after deformation, and *lo* is the original length of the material. It corresponds to the elongation, δ, per unit of the original length, *lo* [277].

$$\boldsymbol{\varepsilon_C = \frac{\delta}{lo} = \frac{l - lo}{lo}} \tag{4}$$

The compressive modulus of elasticity, E_C, is calculated by the slope of the initial linear portion of the stress-strain curve [277]. According to Hooke's law, there is a linear relationship between stress and strain, as long as the values of stress are below the yield point. The mathematical relation between σ_C, ε_C, and E_C is expressed by equation 5 [276].

$$E_c = \frac{\sigma_C}{\varepsilon_C} \quad (5)$$

The ASTM D695-10 Standard provides the guidelines for how to calculate the mechanical properties of unreinforced and reinforced rigid plastics (or composites) when compression tests are performed. This standard shall be followed for loads in compression at relatively low uniform rates of deformation [277].

7.1.1.1. Experimental procedure

Compression tests were performed at IST, according to the ASTM D695-10 Standard, at room temperature. It was used an Instron Universal Testing Machine (model 5566) and flat compression test plates from steel. The load cell was 10 kN and the loading rate was 1.5 mm/min. The results were processed using the Bluehill®2 software. For each specimen tested, the compressive modulus, the compressive strength and the compressive strain were determined from the corresponding load-displacement curve, according to the information presented in 7.1.1.
The number of specimens and dimensions will be addressed in the chapter 9 of the section D.

7.1.2. Flexural tests

The flexural test method measures the behavior of the materials when subjected to loads transverse to their main structural axis. This test provides information about the flexural stress-strain response of the material and estimates for the flexural stress, the flexural strain and the flexural modulus of elasticity.
The ASTM D790-15 Standard gives indications of how to determine the flexural properties of unreinforced and reinforced rigid plastics (or composites) when a three-point loading system is used to apply a load to a specimen. The test specimens must be solid and uniformly rectangular [278]. Figure 7.1 represents a schematization of a three point loading system. Briefly, a bar of rectangular cross section rests on two supports and is loaded by means of a loading nose midway between the supports. The distance between the two supports is called support span (*L*).

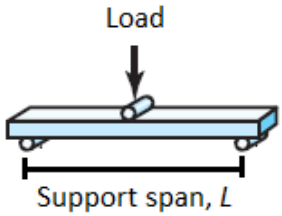

Figure 7.1. Example of a three-point loading system [279].

When a beam is subjected to external loads, shear forces and bending moments develop in the beam. Therefore, a beam must develop internal resistance to resist such forces[280]. The relationship between the bending moment on the cross section, bending stresses and the properties of the cross section allow to define the flexural formulas [280].
The flexural stress (σ_f) of the test specimen, at a given strain, is calculated according to equation 6. In this formula, *P* corresponds to the load at a given point on the load-deflection

curve, *b* is the specimen width, *d* is the specimen thickness and *L* is the support span [278]. The maximum flexural stress sustained by the test specimen, during the flexural test, is designated by flexural strength.

$$\boldsymbol{\sigma_f = \frac{3PL}{2bd^2}} \quad (6)$$

The flexural strain (ε_f) is the nominal fractional change in the length of an element in the outer surface of the specimen at the center of the support span, where the maximum strain occurs. It is calculated from the formula shown in equation 7. In this equation, the variable *D* is the maximum deflection of the center of the specimen, *d* is the specimen thickness specimen and *L* is the support span [278].

$$\boldsymbol{\varepsilon_f = \frac{6Dd}{L^2}} \quad (7)$$

Lastly, the flexural modulus of elasticity (E_B) is the ratio, within the elastic limit, of stress to corresponding strain (Hooke's law). To calculate this property, it was drawn a tangent to the steepest initial straight line portion of the load-deflection curve in order to obtain the slope of this tangent, *m*. Then, it was applied the formula of equation 8. Once again, *b* is the specimen width, *d* is the specimen thickness and *L* is the support span [278].

$$\boldsymbol{E_B = \frac{L^3 m}{4bd^3}} \quad (8)$$

7.1.2.1. Experimental procedure

Three point bending flexural tests were performed at IST, at room temperature, according to the ASTM D790-15 Standard. It was used an Instron Universal Testing Machine (model 5566) and a bending test aluminum fixture. The load cell was 10 kN and the loading rate was 0.1 mm/min. The results were processed using the Bluehill®2 software. For each specimen tested, the flexural modulus of elasticity, the flexural strength and flexural strain were calculated from the corresponding load-displacement curve, according to the equations presented in 7.1.2.
Number of specimens and dimensions will be addressed in the chapters 10, 11 and 12.

7.1.3. Hardness tests – Nanoindentation

Hardness is commonly defined as the resistance of the material against plastic deformation, usually by penetration [281]. This property gives a general indication of the strength of the material, and it is the result of a well-defined measurement procedure [279]. It is important to note that the hardness is not a fundamental property of a material; it represents a quantity measured on an arbitrary scale. Comparisons between different hardness scales are meaningful only through experimental verification. Additionally, correlation with fundamental parameters (e.g. yield stress) is valid only in the range used in the experiment [282].
Three different types of methods characterize the hardness tests: 1) scratch tests, 2) rebound tests and 3) indentation tests [283]. Indentation tests are the most commonly used method for evaluating the hardness of a material. They produce a permanent impression in the surface of the material. The force and size of the impression can be related to the hardness quantity and

the pressure (stress) used to create the impression can be related to both the yield and ultimate strengths of materials [283].

Indentation hardness tests are still divided in three classes: macroindentation, microindentation and nanoindentation. The division between micro and macro occurs for a load of approximately 2 N; microindentation hardness apply a load lower than 2 N and they are recommended to assess the hardness of a material at a microscopic scale. In the nanoindentation tests, the load is of the order of mN and the length scale of the penetration is measured in nanometers [282].

Macroindentation hardness tests include Brinell, Vickers and Rockwell and microindentation tests hardness include Knoop and Vickers (in these last two cases, the load used is lower than the load assigned to the macroindentation test).

Nanoindentation tests are performed using a computer-controlled depth-sensing indentation system that allows the measurement of small forces and displacements [282]. Since the size of the residual impression of the nanoindentation test is too small, it is very difficult to obtain a direct measure using optical instruments. Thus, very small volumes of a material can be studied and local characterization of microstructural features (e.g. coatings, matrix interface and grain boundary regions) can be obtained using this hardness-testing method [284].

The main goal of the nanoindentation tests is to extract the hardness and the elastic modulus of the specimen material from a load-displacement measurement [284]. The hardness measure is obtained by dividing the indentation load by the projected area of the contact. In turn, the elastic modulus (the indentation modulus) of the specimen can be determined from the slope of the unloading of the load-displacement response [284].

These measurements can be affected by the presence of indenter tip imperfections, especially when sharp points (pyramidal or cone shaped) were used to penetrate the surfaces [285]. To avoid such problems, the Berkovich indenter is usually used. Berkovich's three-sided pyramid indenter has the advantage that its edges are more easily constructed to meet at a single point, thus ensuring a more precise control over the indentation process [284,285]. Figure 7.2 shows a typical residual impression of this indenter in a specimen material.

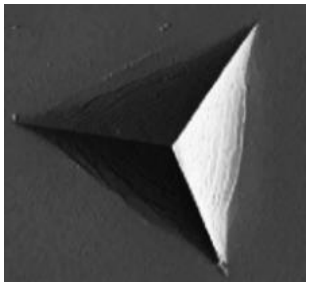

Figure 7.2. Example of a residual impression left on a metal sample by the Berkovich indenter [286].

The International Standard ISO 14577 covers the determination of the indentation hardness in metallic materials, using a Berkovich indenter [287]. According to this Standard [287]: a) the test specimen surface should be smooth and free from lubricants and contaminants, b) a hold period at a maximum indentation load should be applied for the instrument and the specimen to stabilize before the unloading segment begins and c) the indentations should be spaced at approximately three to five times the diameter of the residual impression obtained, to avoid

affecting the results by the presence of an edge or any previous residual impression in the specimen surface.

Figure 7.3 indicates the load/unload cycle of a nanoindentation test procedure. As the indenter penetrated the specimen, the test force, *F*, indentation depth, *h*, and time are recorded continuously during the load/unload cycle [287].

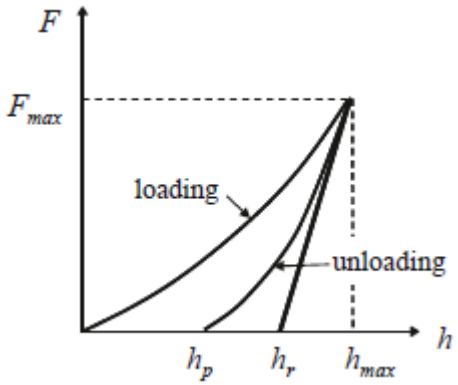

Figure 7.3. Parameters of a nanoindentation test procedure; *hp* is the depth of the residual impression, *hr* is the intercept of the tangent to the initial unloading curve, *hmax* is the maximum penetration beneath the specimen surface and *Fmax* is the maximum load applied to the indenter [287].

The indentation hardness H_{IT} is defined as the mean contact pressure, i.e., it is obtained dividing the maximum indentation load ($F_{\max}$) by the projected area of contact (A_P), according to equation 9 [287]. The area of contact is estimated from the depth of the penetration and the known geometry of the indenter – equation 10 [287].

$$\boldsymbol{H_{IT} = \frac{F_{max}}{A_P}} \tag{9}$$

$$\boldsymbol{A_P = 24,5 h_c^2} \tag{10}$$

In the Standard, h_c is the depth of contact of the indenter with the specimen, given by equation 11. The parameter ε corresponds to the intercept corrector factor, which is 0.75 for the pyramidal Berkovich indenter [287]. Still on this formula, h_r is the depth found from extrapolating the slope of the tangent of the initial unloading to the depth axis and h_{max} is the maximum penetration depth [287] as shown in Figure 7.3.

$$\boldsymbol{h_c = h_{max} - \varepsilon(h_{max} - h_r)} \tag{11}$$

The indentation modulus (E_{IT}) is calculated from the slope of the upper portion of the unloading curve during the initial stages of unloading (also called the contact stiffness), according to the method developed by Oliver and Pharr [287,288]. Equation 12 is then applied for the calculation of the E_{IT}.

$$\boldsymbol{E_{IT} = \frac{1-(\upsilon_s)^2}{\frac{1}{E_r} - \frac{1-(\upsilon_i)^2}{E_i}}} \tag{12}$$

The formula represented in equation 12 takes into account the fact that elastic displacements occur in both the specimen and the indenter. The elastic modulus and the Poisson's ratio of

the indenter are E_i and v_i, respectively [287]. For the specimen, v_s is the Poisson's ratio and E_r is the reduced modulus, which is given by Equation 13.

$$\boldsymbol{E_r = \frac{\sqrt{\pi}}{2C\sqrt{A_p}}} \quad (13)$$

In equation 13, A_p is the projected contact area and *C* is the compliance of the contact [287]. This last parameter is defined as the deflection of the indentation test instrument divided by the load [287,289]. The compliance of the instrument should be accurately determined to avoid errors into the load-displacement curve obtained for a particular specimen [289].

7.1.3.1. Experimental procedure

Nanoindentations tests were performed at IST, using a Dynamic Ultra Micro Hardness Tester from Shimadzu. The specimens were first smoothed with water sandpaper and then tested using a diamond Berkovich indenter. The results were processed using the DUH-211S software, according to the International Standard ISO 14577. The maximum load force was 200 mN and the load speed was 5 mN/second. For each load/unloading cycle, there was a hold time of 15 seconds. The elastic modulus was calculated by the software from the slope of the initial 30% of the unloading curve.

7.2. Microstructural properties

7.2.1. Scanning Electron Microscopy analysis

Scanning Electron Microscopy (SEM) analysis is used to scan a solid sample with a focused beam of high-energy electrons, generating a variety of signals at the surface of the specimens [290]. These signals provide information about the specimen's topography, microstructure and chemical compositions or its variations [290]. The signals generated during SEM analysis produce a two-dimensional image over the selected area on the specimen's surface. The images produced have high resolution, and the magnifications can vary from 5X to 300.000X [291].
Briefly, when the incident electrons are decelerated in the solid specimen, the resultant kinetic energy is dissipated in signals such as secondary electrons, backscattered electrons, diffracted backscattered electrons, photons, visible light and heat [290,292]. Secondary electrons are most valuable for showing morphology and topography on specimens while the backscattered electrons are most valuable for illustrating contrasts in composition in multiphase samples [290,292]. In turn, the X-rays generated are used for elemental analysis [290,292]. The X-ray spectrum emitted by the specimen provides both quantitative and qualitative information, allowing identification of which elements are present in the sample and its respective amount [293].

7.2.1.1. Experimental procedure

The SEM analysis was performed at IST. The analysis required the coating of all the tested specimens with a gold-palladium thin film, which made them electrically conductive. The specimens were then observed in a high resolution FEG-SEM from JEOL, model JSM-7001F,

using a beam energy of 5 kV to 15 kV. To analyze the specimens, magnifications from 20X to 6.000X have been recorded.
Some images obtained by SEM analysis were analyzed by ImageJ, an image processing program developed at the National Institutes of Health.

7.2.2. X-ray microtomography analysis

X-ray computed tomography (CT) is a well-established diagnostic tool which is routinely used in modern medicine. Beyond that, this nondestructive technique has become an important and common tool in industrial inspection and material sciences, for example, to search for defects in critical parts of airplanes, cars, engines, etc. [294]. To visualize and characterize the internal structure of materials, such as ceramics, composites, metals, bones and soft tissues, it is fundamental to obtain an image quality in terms of absolute contrast, homogeneity and artifacts reduction [294,295]. Therefore, the accuracy of reconstructed mass densities or attenuation coefficients is crucial [294].
X-ray microtomography (microCT) differs from conventional CT by combining a much smaller field-of-view with a high resolution detector [295]. It produces high resolution 3D images and applies differences in X-ray attenuation properties of the materials to reconstruct their 3D structure [294,295]. Four main steps explain the operation of microCT [294,296]:

1) X-rays are first emitted from the X-ray generator;
2) X-rays propagate through the sample where some of the photons are absorbed while others are transmitted to the detector, resulting in a projection image;
3) the sample can be rotated by 180° and 360° with a projection image being acquired at each defined angle position;
4 the projection images are reconstructed through image reconstruction algorithms.

7.2.2.1. Experimental Procedure

Morphologic studies and internal microstructure images were obtained using microCT equipment at IPLeiria, SkyScan 1174v2 from Brucker, without sample preparation or chemical fixation. Some acquisition scan parameters included the image pixel size of 7,76 µm, the source voltage/current of 50 kV/800 µA, the exposure time of 4500 ms and the rotation step of 0,9 degrees.
After scanning, the sample reconstruction procedure was performed using the NRecon reconstruction program version 1.7.0.4. CTAn program was used to analyze and quantify the fractions of the different materials in the specimens. CTVox program was used to do the 3D realistic visualization of the scanned specimens.

7.3. Physical properties

7.3.1. Differential Scanning Calorimetry analysis

Differential Scanning Calorimetry (DSC) is a thermoanalytical technique whose goal is to measure the difference in the amount of heat flow or the difference in temperatures between a test sample and an inert reference when both are raised and/or lowered in temperature, at

some constant temperature rate (°C/min) [297]. DSC allows quick measures on small sample masses, in wide temperature ranges with high accuracy. This technique is advantageous in areas such as the characterization of materials, quality control, stability investigations and evaluation of phase transitions [298].

Two types of DSC are available: the heat flux DSC and the power compensation DSC [299]. In the first case, the sample and the reference sample are positioned in the same single furnace. The heat flow is directed from the furnace to the samples [300]. If the heat capacity of the sample changes, a difference in temperature is generated, ΔT, which corresponds to the enthalpy change in the sample [297]. The ΔT is then converted into heat flow information, ϕ_m , through calibration experiments and mathematical equations built in the equipment software [297].

Regarding the power compensation DSC, the sample and the inert reference are heated independently, since it is intended that both are always at the same temperature [300]. When changes in the sample occur, extra heat, *Q,* (endothermic effect) or less heat, *Q,* (exothermic effect) will be needed to maintain the set temperature program and the zero temperature difference between sample and reference [300]. The heating power difference necessary for this to occur is converted into a proportional temperature difference, ΔT [299]. Once again, the heat flow rate, ϕ_m , is related with ΔT by a factor which come from the instrument calibration [299].

Commercial instruments provide a recorder output of the constant-pressure heat capacity, C_p, as a function of temperature – equation 14 [300,301].

$$\boldsymbol{C_p = \left(\frac{dQ}{dT}\right)_P = \left(\frac{\partial H}{\partial T}\right)_P} \tag{14}$$

The area detected in the DSC profile, between any two temperature limits, corresponds to the enthalpy change, ΔH, of the sample – equation 15 [300,301].

$$\boldsymbol{\Delta H = \int_{T1}^{T2} \left(\frac{\partial H}{\partial T}\right)_P dT = \int_{T1}^{T2} C_P \; dT} \tag{15}$$

As previously discussed, DSC allows the determination of important thermal characteristics of materials such as the following transition temperatures: melting temperature (T_m), vaporization temperature (T_v), glass transition temperature (T_g) and crystallization temperature (T_c) [302]. At the melting phase, the energy is spent in breaking down the rigid solid structure into a much less rigid structure, leading to a material's gain of energy (endothermic transition) [302]. Therefore, the sample requires a higher heat flow in order to increase its temperature at the same rate as the reference sample. A similar process takes place during the phase transformation from liquid to gas (vaporization) [302].

Glass transition is a reversible characteristic of amorphous materials (or amorphous regions within a semicrystalline material) due to a change in the heat capacity of the material [302]. The T_g corresponds to a temperature range in which the material change from a hard, rigid or "glassy" state to a more pliant, compliant or "rubbery" state [303]. Over this temperature range, the material undergoes a transition from a lower energy state to a higher energy state where its molecules/atoms become more mobile [302]. Generally, there is no peak, but in some studies a small endothermic relaxation peak is found in the DSC profile [297].

At a temperature between the T_g and the T_m, the crystallization of the material occurs. At or near the T_c, the material has gained enough energy so that its atoms/molecules could re-

arrange into a more stable and ordered state [302]. This is an exothermic process since the sample heater supplies less energy than the reference heater to maintain the same constant heating rate [302].

Figure 7.4 represents a DSC profile, where different phase transitions are exemplified, namely the T_g, T_c and T_m.

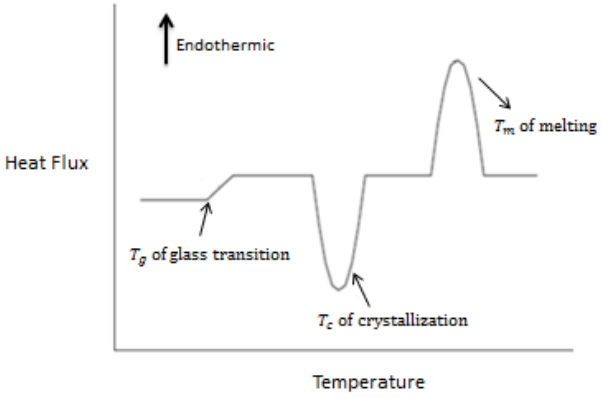

Figure 7.4. Example of a DSC profile [297].

7.3.1.1. Experimental procedure

The thermal properties of the specimens were analyzed using a DSC 200 F3 Maia® from NETZSCH, which uses the heat flux system. These tests were performed at IST.

The following setup has been configured for each DSC run:

- Isothermal period: 25°C for 10 minutes;
- Dynamic period: heating rate at 20°C /min to 200°C;
- Dynamic period: cooling rate at 20°C /min to 25°C;
- Isothermal period: 25°C for 10 minutes;
- Dynamic period: heating rate at 20°C /min to 300°C;
- Dynamic period: cooling rate at 20°C /min to 25°C;
- Isothermal period: 25°C for 10 minutes.

To perform this experiment, it was necessary to crush the specimens into small fragments using a mortar and pestle. Approximately 7 mg of each composition were introduced into an aluminum pan, to constitute the sample pan. The reference pan had nothing inside it.

7.3.2. Wettability – Contact Angle measurement

Wettability describes the tendency of one fluid to spread or adhere to a solid surface. It is then a measure of the preferential tendency of one of the fluids to wet (spread or adhere) the surface [304,305].

Wettability is governed by the interfacial tension between solid and liquid. It can be estimated by measuring the contact angle [306], which depends on the surface tension of the liquid. The surface tension of a liquid results from an imbalance of intermolecular attractive forces; for example, each molecule in the bulk liquid experiences cohesive forces with other molecules in all directions while the molecules exposed at the surface experience only net inward cohesive

forces [307]. As a result, the liquid voluntarily contracts its surface area to maintain the lowest free energy surface. This intermolecular force is called surface tension [307].

Several approaches can be used to estimate solid surface tensions, including direct force measurement, sedimentation of particles and contact angle [306]. Focusing on the contact angle approach, it represents the mechanical equilibrium of the drop under the action of three interfacial tensions: solid - vapor,γ_{sv}, solid - liquid, γ_{sl}, and liquid - vapor, γ_{lv} [306,307] It is then defined as the angle, θ, between the solid surface and the tangent to the liquid surface at the line of contact with the solid, according to equation 16 (Young's Equation) [308].

$$\boldsymbol{cos\theta = \frac{\gamma_{sv}-\gamma_{sl}}{\gamma_{lv}}} \quad (16)$$

The contact angle measurement is specific for a given solid-liquid system and depends on the environment conditions [309]. The chemical inhomogeneities or roughness of the solid substrate can influence this measure [310].

Small contact angles (less than 90°) indicate a solid surface with high wettability whereas large contact angles (more than 90°) indicate a surface with low wettability [308]. In the first case, the fluid will spread over a large area, occurring a complete or perfect wetting if the contact angle is 0° [307]. In turn, less wettability generally means that the solid surface is unfavorable for the fluid, thus it will tend to minimize its contact with the surface [307]. For superhydrophobic surfaces, it is considered that water contact angles are greater than 150°, revealing almost no contact between the liquid drop and the surface [307]. All these cases are represented in Figure 7.5. Note that contact angles of 180° are not found, since there is always some interaction between the liquid and the solid [308].

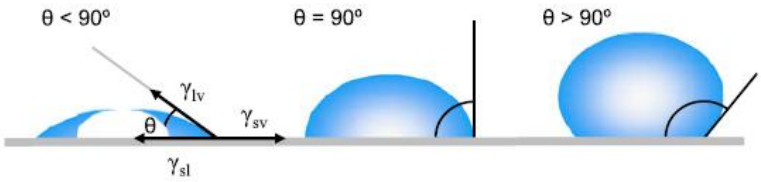

Figure 7.5. Examples of different contact angles formed by liquid drops on homogenous solid surfaces [307].

Forces of attraction between a liquid and a solid surface are called adhesive forces. A surface that is mainly composed by polar groups (e.g. hydroxyl groups) will have strong adhesive forces and low contact angles with polar liquids such as water [307]. This type of surface is called hydrophilic. On the other hand, if the surface is mainly composed by non-polar groups (e.g. polymer surfaces), it will not have good affinity to water and the contact angle will be large [307]. Such a surface is called hydrophobic. Therefore, the chemical compositions of the surfaces can be assessed by measuring their contact angles [307].

The fundamental property of liquid surfaces is that they tend to contract to the smallest possible area [311]. The contact angle is the boundary condition for the differential equation that states the normal stress jump across the liquid-vapor interface is balanced by the curvature of the interface [306,307]. For static situations in a gravitational field, this corresponds to the Laplace equation of capillary action, represented in equation 17. In this formula, ΔP is the pressure jump across the liquid-vapor interface, γ_{lv} is the liquid-vapor interfacial tension, and R_m is the mean curvature of the interface [308,309,311].

$$\Delta P = \frac{2\gamma_{lv}}{R_m} \quad (17)$$

An adequate technique to determine the contact angle is to determine the drop profile and to fit that shape to the appropriate version of equation 17, which has as fitting parameter the contact angle [309]. The contact angle is then the angle that the solid surface forms with the drop interface, at the triple point tangent where solid, liquid and vapor coexist. This methodology assumes that the contact angle is a material dependent boundary condition [309].

7.3.2.1. Experimental procedure

Contact angles were estimated analyzing the profile of a liquid drop placed on the surface of a solid (sessile drop technique), as represented in Figure 7.5. These tests were performed at IST.
To remove the residual water and ensure the reproducibility of the hydration state of the surfaces, the specimens were left in a vacuum oven, without temperature, for 3 hours. After the drying period of the specimens, they were left in the desiccator while the contact angle was determined experimentally.
Specimens were placed individually in the test chamber at room temperature. Using a micrometer syringe, a drop of pure water (3 - 4µL) was deposited in the specimen surface. The profile of each drop was analyzed from images collected during 180 seconds, using a video camera (JAI CV-A50), installed in a microscope (WildM3Z) and connected to a frame grabber (Data Translation DT3155). During the 180 seconds, 20 imagens were collected at instants 0, 1, 2, 3, 4, 5, 6, 8, 10, 12, 15, 20, 30, 40, 50, 60, 90, 120, 150 and 180 seconds.
The contact angles were obtained indirectly using the Laplace equation, as explained in chapter 7.3.2. In this work, it was used the algorithm developed by Cheng *et al.*[312], (Axisymmetric Drop Shape Analysis-Profile), which allows to theoretically adjust the Laplace curve to the drop profile.

7.4. Chemical properties

7.4.1. Fourier Transform Infrared Spectroscopy - Attenuated Total Reflection analysis

Infrared (IR) spectroscopy is a technique that relies on the vibrations of the atoms of a molecule. An infrared spectrum is normally obtained by passing infrared radiation through a sample and determining which fraction of the incident radiation is absorbed at a particular energy [313]. The energy at which any peak appears in an absorption spectrum corresponds to the frequency of a vibration of a part of a sample molecule [313].
Vibrational spectra appear as a band because a single vibrational energy change is accompanied by a number of rotational energy changes [314]. The frequency (or wavelength) of absorption depends on the relative masses of the atoms, the force constants of the bonds and the geometry of the atoms [314].
There are two types of molecular vibrations, namely bending and stretching [314,315]. The bending vibration involves the change of bond angles whereas the stretching vibration results in an increasing or in a decreasing of the interatomic distance [314,315]. Some bonds can stretch

in-phase (symmetrical) or out-of-phase (asymmetric) [315]. The latter case corresponds to stronger vibrations that will lead to an intense band. Additionally, if the molecule has different terminal atoms (e.g. HCN) then the stretching modes consist on different proportions of each of these groups (coupling) [315].

Infrared spectroscopy is a versatile experimental technique and it is possible to obtain spectra from solid or liquid samples [315]. Traditionally, Fourier-Transform Infrared Spectrometry (FTIR) is used to obtain the infrared spectrum [315]. When IR radiation goes through a sample, some radiation is absorbed and some is transmitted [315]. A detector measures the intensity of transmitted light as a function of its wavelength [315]. The signal obtained from the detector is an interferogram, which is analyzed using Fourier transforms to obtain an interpretable spectrum [315]. Band positions in IR spectra are presented as centimeter (cm^{-1}), as indicated in the examples of Table 7.1.

The technique of Attenuated Total Reflectance (ATR) spectroscopy is based on the concept of total internal reflection [315]. In this case, an infrared beam is directed to an optically dense crystal with a high refractive index at a certain angle [315,316]. This internal reflectance creates an evanescent wave that extends beyond the surface of the crystal into the sample [315,316]. The attenuated energy from each evanescent wave then exits the opposite end of the crystal and passes to the detector in the IR spectrometer, generating an infrared spectrum [315,316].

Table 7.1. Characteristic IR absorption frequencies of some functional groups [185,317].

Functional group		Type of vibration	Absorption range (cm^{-1})	Intensity
Alcohol	O-H	stretch, H-bonded	3.200-3.600	strong, broad
	O-H	stretch, free	3.500-3.700	strong, sharp
	C-O	stretch	1.050-1.150	strong
Alkane	C-H	stretch	2.850-3.000	strong
	-C-H	bending	1.350-1.480	variable
Alkene	=C-H	stretch	3.010-3.100	medium
	=C-H	bending	675-1.000	strong
	C=C	stretch	1.620-1.680	variable
Amine	N-H	stretch	3.300-3.500	medium
	C-N	stretch	1.080-1.360	medium-weak
	N-H	bending	1.600	medium
Acid	C=O	stretch	1.700-1.725	strong
	O-H	stretch	2.500-3.300	strong, very broad
	C-O	stretch	1.210-1.320	strong
Carbonyl	C=O	stretch	1.670-1.820	strong

7.4.1.1. Experimental procedure

ATR-FTIR was carried out at FCT/UNL using a Spectrum Two spectrometer (PerkinElmer) equipped with a UATR Polarization Accessory, using a single reflection diamond crystal. The software used in data collection, processing and results generation was the SpectruM® 10. Spectra were recorded between 4.000 cm^{-1} and 600 cm^{-1}, resulting in a total of 6 scans at 4 cm^{-1} resolution. The sample was clamped to the crystal surface by applying pressure to ensure a good optical contact between the sample and the crystal.

7.5. Biological properties

7.5.1. *In-vitro* Cytotoxicity tests

To limit animal experimentation to its minimum, it became essential to develop and standardize *in vitro* tests that can detect the toxicity of devices for human use, especially those in clinical applications [318,319]. In this sense, the *in vitro* cytotoxicity assays are performed to carry out an initial screening on the biocompatibility of any material proposed for implantation. It is only after its non-toxicity has been proven that the biocompatibility of the material can be further assessed, which includes the necessary *in vivo* tests [318]. Additionally, these assays limit the number of experimental variables, allowing significant data to be obtained more rapidly and with lower associated costs [318].

Toxicity involves the disturbance of cellular homeostasis, which produces negative effects on the cellular functions [320]. Essentially, it consists on morphological evaluations to quantify and highlight the cells that died or have undergone regressive phenomena after contact with the material [319]. Examples of toxicity evaluations in vitro include: cell death, reduced cell adhesion and proliferation, altered cellular morphology and reduced biosynthetic activity [321].

Cytotoxic tests were performed according to the International Standard ISO 10993-5 [322]. This standard does not focus on a specific test but rather it presents guidelines to choose appropriate tests for the toxicity evaluation. These guidelines include, for example, positive and negative control materials, number of replicates, extraction conditions, choice of cell lines and cell media and the different categories of the procedures [322]. Three categories of tests are listed in this Standard: extract test, tests by direct contact and tests by indirect contact [322,323]. In this work, the first two types were used.

Tests by direct contact or by extract allow both qualitative and quantitative assessment of cytotoxicity [322]. These methods specify, respectively, the incubation of cultured cells in direct contact with a material/device and in contact with extracts of a material/device [322]. In this work, the cell morphology and viability were analyzed qualitatively by the direct contact assay, through an optical microscope. In turn, a quantitative analysis of the cell viability was performed by the extract assay, through the 3-(4,5-dimethylthiazol-2-yl)-2,5-diphenyl-tetrazolium bromid (MTT) test.

MTT test is used to quantify the metabolic activity of cells [323]. In viable cells, the water-soluble yellow dye MTT is reduced to a dark purple (blue-magenta) colored formazan precipitate [324], as represented in Figure 7.6. The lipid soluble formazan product may be extracted with organic solvents and estimated by spectrophotometry [325]. The MTT-formazan production is then proportional to the number of metabolically viable cells [324,326].

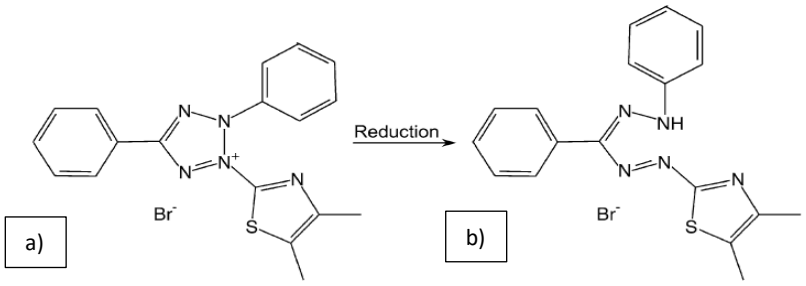

Figure 7.6. Chemical structure of MTT (a) and its reduced formazan product (b) [327].

MTT reduction occurs by oxidoreductases, which use nicotinamide adenine dinucleotide coenzyme (NADH) generated in the mitochondria [325]. Superoxide may also contribute to intracellular MTT reduction, whereas the cell surface oxidoreductases are responsible for extracellular MTT reduction [324].

7.5.1.1. Experimental procedure

The cytotoxic tests were performed according to International Standard ISO 10993-5 [322] at IST. In the extract assay, material triplicates were submersed in 90% (v/v) Dulbecco's Modified Iscove's Medium (DMEM, GIBCO®) supplemented with 10% (v/v) of Fetal Bovine Serum (FBS, Life Technologies) and left in the incubator (37°C, 21% O_2, 5% CO_2) for 24h. At the same time, mouse fibroblasts L929 were seeded in 12-well plates in order to achieve 80% of confluence, and were also left in the incubator. After the incubation time, the medium in contact with the cells was discarded and the leachings from the triplicates were added to the cells seeded in the well plates. Fresh medium was used as negative control and a piece of latex glove was used as positive control. The well plates were again incubated in the same conditions, for the same period of time. The cell viability was then quantified following the MTT (Sigma Aldrich) protocol. The relative quantification of cell viability was normalized to the negative control.
To perform the direct contact assay, L929 cells were seeded in well plates as previously described for the extract assay. Triplicates were placed on the top of the cell monolayer and incubated in the same conditions and period of time. Cell morphology and viability in contact with materials were then analyzed with the optical microscope Leica DMI3000B.

7.5.2. *In-vitro* Degradation tests

In vitro degradation tests of bioabsorbable polymeric implants, in simple aging media, are normally conducted to predict the *in vivo* performance of such polymers in the clinical situation [328].
Materials exposed to the body fluids may undergo changes in their physicochemical properties as a result of chemical, physical, mechanical, and biological interactions between the material and the surrounding environment [328]. In this sense, the International ISO Standard 10993-13 was outlined to determine the biological hazards from potential degradation products from polymer components of medical devices [329]. These products might come from a variety of sources since the polymeric device can contain residuals and leachables such as monomers, oligomers, solvents, catalysts, additives, fillers and processing aids [329]. This standard describes two test methods to generate degradation products: an accelerated degradation test as a screening method and a real-time degradation test in a simulated environment [329]. However, the *in vitro* degradation study of this thesis focused only on the determination of the mass and mechanical degradation profile of the chitosan-based materials, according to the information of the FDA guidance indicated in Appendix A.2.
Lysozyme is the primary enzyme responsible for the *in vivo* degradation of chitosan [129]. Inside the body, it leads to the release of amino sugars that can be processed by the metabolic system [129]. Lysozyme (or muramidase or *N*-acetylmuramichydrolase) is a strong basic protein known as a hydrolase that cuts the *β*-1-4 glycosidic bond of the polysaccharides architecture

[330]. It is found in almost all secretions, body fluids, and tissues of human and animal organisms, ranging from 4 to 13 mg/L in normal human serum while in tears this value is approximately 1300 mg/L [330–332]. Therefore, the *in vitro* degradation tests used a commercial source of lysozyme - recombinant human lysozyme. This lysozyme is produced in an animal-free production system and it presents higher bioactivity when compared with lysozyme from chicken egg white albumen [330].

7.5.2.1. Experimental Procedure

Degradation tests were performed at IST. Before initializing the experiment, the specimens were weighed in an analytical scale (w_i). Next, all the specimens were sterilized in 70% (v/v) ethanol for 24h, followed by overnight exposure to ultraviolet (UV) light.

The specimens were placed on 6 well plates, totally covered by an enzymatic solution or by a phosphate-buffered saline (PBS) control solution (Thermo Fisher). The enzymatic solution consisted in 500 mg/L of lysozyme (Lysobac™ from Sigma Aldrich). Additionally, a mixture of antibiotic-antymicotic (AA, Thermo Fisher) was added to each solution in the proportion 1:100, to prevent bacterial and fungal contamination. The well plates were incubated (37°C, 5% CO_2, fully humidified) throughout the study, and the medium was replaced every week.

The specimens were removed at defined degradation periods, the excess of water was removed with an absorbent paper and their wetted weight (w_w) was recorded to determine the swelling ratio, according to equation 18. The specimens were then dried at 40°C in a stove (humidity controlled and with air circulation) until their weight stabilizes. The weight loss was then calculated according to equation 19, where w_f is the final weight, after the degradation test.

$$\boldsymbol{Swelling\ Ratio}\ (\%) = \frac{(\boldsymbol{w_w - w_i})}{\boldsymbol{w_i}} \times \mathbf{100} \tag{18}$$

$$\boldsymbol{Weight\ Loss}\ (\%) = \frac{(\boldsymbol{w_i - w_f})}{\boldsymbol{w_i}} \times \mathbf{100} \tag{19}$$

To determine the loss of the mechanical properties at each degradation period, flexural tests were performed according to the experimental procedure described in chapter 7.1.2.1.

7.5.3. *In-vitro* Differentiation tests

Bone constitutes the supporting framework of the body, characterized by its rigidity and dynamic nature [333]. It protects internal organs and structures, provides maintenance of mineral homeostasis and acid-base balance, serves as a reservoir of growth factors and cytokines, and provides the environment for hematopoiesis within the marrow spaces [333,334].

The dynamic nature of the bone is achieved by a process of remodeling, which occurs in both cortical and trabecular bone [335]. Bone remodeling is a complex process by which old bone is replaced by new bone in response to physiologic stimulus (e.g. calcium levels and endocrine factors) or mechanical forces [334,335]. It depends on the concerted actions of osteoclasts (cells that destroy one) and osteoblasts (cells that form bone) as well as osteocytes within the bone matrix and osteoblast-derived lining cells that cover the surface of bone [335]. Osteocytes act as mechanosensors and orchestrators of the bone remodeling process whereas bone lining cells

play an important role in coupling bone resorption to bone formation [336]. Figure 7.7 represents the coordinated actions of these cells, which together form the temporary anatomical structure described as the "Basic Multicellular Unit [335,336].

Bone remodeling also occurs during the complex process of fracture healing that occurs as a response to injury, resulting in skeletal repair and skeletal function [337]. It follows a definable and spatial sequence of haematoma, inflammation, angiogenesis, chondrogenesis to osteogenesis and finally bone remodeling [338]. Therefore, the complex cascade of biologic events that characterize the fracture healing process repeats certain aspects that regulate the formation of skeleton tissue during the embryogenesis [339,340].

The formation of bone during the embryogenesis involves two mechanisms: intramembranous ossification and endochondral ossification [341]. In the first case, there is direct conversion of mesenchymal tissue into bone whereas in the second case, the MSCs first differentiate into cartilage, and then this cartilage is later replaced by bone [341].

.

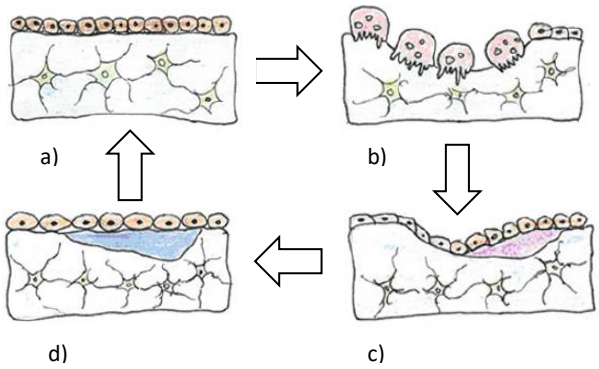

Figure 7.7. Schematization of the bone remodeling process: a) bone lining cells are activated, b) activated osteoclasts resorb the underlying bone, c) osteoclasts are replaced by osteoblasts and a new osteoid matrix is formed, d) mineralization of the osteoid matrix [333].

In this thesis, the osteogenic capacity of the chitosan-based specimens was assessed by their ability in promoting the *in vitro* osteoblastic differentiation of human bone marrow mesenchymal stem cells (hBMSC). It involved the assessment of hBMSC metabolic activity using the AlamarBlue® (AB) assay, the detection of the alkaline phosphatase (ALP) activity and the quantification of the expression of certain osteogenic marker genes by real-time reverse transcription polymerase chain reaction (RT-qPCR).

The AB is a cell viability reagent that works by using the reducing power of living cells. Metabolic active cells produce reducing equivalents that promote the conversion of resazurin to resorufin [342]. As the indicator dye accepts electrons, it changes from the oxidized, non-fluorescent, blue state to a reduced, fluorescent, pink state [342]. Therefore, the intensity of the fluorescence produced is proportional to the number of viable cells.

The ALP is a biochemical marker for osteoblast activity, playing an important role in skeletal mineralization [343]. It is an enzyme that catalyzes the hydrolysis of phosphate esters at an alkaline environment, resulting in an organic radical and an inorganic phosphate [344]. The detection method uses *p*-nitrophenyl phosphate that is hydrolyzed by ALP into a yellow colored product [344]. The rate of the reaction is directly proportional to the enzyme activity.

The RT-qPCR is a sensitive technique which has become the method of choice for gene expression analysis. In this method, messenger RNA (mRNA) is first transcribed into complementary DNA (cDNA) by reverse transcriptase [345]. Gene-specific PCR primers are then

used to amplify a segment of the cDNA of interest [345]. The reaction is followed in real time by double-stranded DNA intercalating agents (e.g. SYBR® Green 1) or by fluorescent probes (e.g. Taqman®).The fluorescence intensity measured is proportional to the product accumulation, i.e. the amount of amplified DNA [346].

For the analysis of a RT-qPCR experiment, a threshold level of fluorescence is chosen in the exponential phase of the PCR, and the number of cycles required to reach such level is called threshold level (C_T) [345]. Two methods are available to quantify the RT-qPCR results: the relative quantification method ($2^{-\Delta\Delta CT}$ method) and the absolute quantification method [346]. The first method, used in this thesis, consists in determining the relative expression levels of a target relative to a reference control such as a sample at time zero [346]. The amount of the target gene in the sample is normalized to an endogenous housekeeping gene and relative to the normalized calibrator [346].

In this thesis, the osteogenic differentiation was confirmed by assessing gene expression using RT-qPCR. A subset of genes was selected, including Runt-related transcription factor 2 (Runx2), ALP, alpha-1 type I collagen (COL1A1) and Osteocalcin. Runx2 is a central and early osteoblastic gene that regulates a broad spectrum of other genes involved in osteoblastic differentiation [347,348]. The gene encoding ALP is expressed early and indicates cellular activity and differentiation, as reported previously [347,348]. COL1A1 is an early gene that encodes the expression of type 1 collagen, which is an important component of bone ECM [347,348]. In turn, Osteocalcin is expressed late, being an osteoblast-specific gene that has a significant up-regulation role in both matrix synthesis and mineralization [347,348]. Lastly, glyceraldehyde-3-phosphate dehydrogenase (GAPDH) was used as housekeeping gene since it is expressed in all cells.

7.5.3.1. Experimental procedure

The osteogenic differentiation experiment was performed at IST. hBMSCs were seeded on top of the specimens at a density of 20.000 cells per specimen. The osteogenic medium consisted of StemPro® Osteogenisis Differentiation Kit (Thermo Fisher Scientific). Before subjecting the hBMSCs to the osteogenic medium, they were first expanded on the surface of the specimens in a culture media which consisted of DMEM + 10% FBS (MSC qualified) + 1% AA for 7 days.

The experiments were performed in an incubator (37°C, 5% CO_2) under a humidity controlled environment in static conditions. Throughout the experiments, the culture medium was changed every 3 days, until the end of the experiments.

AB assay

hBMSC metabolic activity was monitored at days 1, 7, 14 and 21 by the AB reagent, according to the manufacturer's protocol (Thermo Fisher Scientific).

Samples were incubated at each time point with a 10% v/v AB solution (diluted in culture media) for 2,5 hours. For zero control, AB was added to wells containing only specimens and media. After the incubation time, 200 µL aliquots were pipetted in triplicates into 96-well plates and the AB fluorescence intensity was measured using the plate reader Infinite®200 PRO (TECAN) with an excitation wavelength of 560nm and an emission wavelength of 590nm.

The cells were refeed with fresh medium and placed in the incubator to be analyzed at the next reading point.

The fluorescence intensity results were calculated from the fluorescence detected for the specimens tested with cells, at a certain culture time, minus the fluorescence intensity detected for the control.

RT-qPCR

After 21 days of cell culture (14 days of osteogenic differentiation), the expression of osteogenic marker genes was evaluated by qPCR. Total RNA was isolated using the RNeasy mini kit (Qiagen). RNA concentration was quantified in a NanoDrop, after which RNA was reverse-transcribed to cDNA using the IScript cDNA synthesis kit (BioRad). cDNA was amplified with a RT-qPCR equipment (StepOne, Applied Biosystems) with the Fast SYBR Green Master Mix (Life Technologies) and the primers (Life Technologies) indicated in Table 7.2. The relative expression of the genes was obtained following the $2^{-\Delta\Delta CT}$ method. GAPDH was used a housekeeping gene and the gene expression at day 0 was used as a baseline.

Table 7.2. List of primers sequence used in the quantification of the osteogenic differentiation.

Primers	Sequence
GAPDH	For: 5' AAC AGC GAC ACC CAC TCC TC Rev: 5'CAT ACC AGG AAA TGA GCT TGA CAA
Runx2	For: 5' AGA TGA TGA CAC TGC CAC CTC TG Rev: 5' GGG ATG AAA TGC TTG GGA ACT
ALP	For: 5' ACC ATT CCC ACG TCT TCA CAT TT Rev: 5' AGA CAT TCT CTC GTT CAC CGC C
COL1A1	For: 5' CAT CTC CCC TTC GTT TTT GA Rev: 5' CCA AAT CCG ATG TTT CTG CT
Osteocalcin	For: 5' TGT GAG CTC AAT CCG GCA TGT Rev: 5' CCG ATA GGC CTC CTG AAG C

ALP activity

ALP activity was detected using a colorimetric ALP kit (QuantiChrom™, BioAssays Systems), according to the manufacturer's protocol. After 7 days of osteogenic differentiation, the specimens were washed with PBS (Gibco) and were incubated in a lysis buffer (0.1% Triton X-100 in PBS) by shaking for 1 hour at room temperature. The lysis solution was added to a *p*-nitrophenyl phosphate solution from the ALP kit. The absorbance was measured at 405 nm for each sample using the plate reader Infinite®200 PRO (TECAN).

7.6. Statistical analysis

The results of the experimental tests are shown in graphs and/or tables. When the results are presented in the form mean ± standard deviation (SD), samples *t*-tests were performed for statistical comparisons between two groups. In all statistical evaluations, statistical significance was set at the level of 0,05 under the assumption of the null hypotheses (H0: the means of the two groups are equal). Therefore, if the p-value ≤ 0,05 the null hypothesis is rejected. The statistical evaluations with p-value ≤ 0,05 are visually labelled with a line and an asterisk*.

8. Sterilization methods on 3D dense chitosan-based product compositions

Sterilization eliminates or destroys all forms of microbial life including the more resilient forms such as bacterial spores, mycobacteria, nonenveloped (non-lipid) viruses, and fungi [349]. Therefore, materials implanted either into the human or animal body must be sterile to avoid infection that can lead to illness or even death [350].

Sterilization of medical devices is generally the last phase in their manufacturing process. It should occur when the medical device is packaged to guarantee sterility during handling, transport and storage.

The choice of the sterilization method depends on several factors including the type of material to be sterilized, the quantity and type of microorganisms involved, the classification of the item and the availability of sterilization methods [349]. Table 8.1 shows the different physical, chemical and gas vapor sterilization methods.

The FDA guidance "Submission and Review of Sterility Information in Premarket Notification (510(k)) Submissions for Devices Labeled as Sterile" classifies the established sterilization methods into two categories [351]:

- Category A: methods that have a long history of safe and effective use, thus consensus standards for development, validation and routine control are recognized by the FDA. Examples: dry heat, steam heat, EtO and ionizing radiation.
- Category B: methods for which there are no FDA-recognized dedicated consensus standards, but there is published information regarding development, validation and routine control. Examples: hydrogen peroxide, ozone and flexible bag systems (e.g. diffusion method).

Table 8.1. Sterilization methods.

Physical Methods	Chemical Methods
▪ Steam under pressure ▪ Dry heat ▪ Filtration ▪ Ultraviolet radiation ▪ Ionizing radiation (e.g. gamma and electron beam)	▪ Peracetic acid ▪ Glutaraldeyde ▪ Ethylene oxide ▪ Hydrogen peroxide vapor ▪ Plasma gas ▪ Ozone

Since it is difficult to clearly verify the sterility of large lots of medical devices that underwent an industrial-scale sterilization process, validation studies are used to determine the security assurance level (SAL) [350]. The SAL is defined as “the probability of a single viable microorganism occurring in or on a product after sterilization” [350,352]. The accepted definition of sterility is a chance of 1 in 1 million that the implant will remain nonsterile or a SAL of at most 10^{-6} [350,352]. However, FDA recommends a SAL of 10^{-3} if the medical device is only in contact with intact skin [352].

To validate the sterilization method, it is necessary to quantify the bioburden, i.e. the number of viable microorganisms present in the device after the manufacturing process [353]. The bioburden quantification is expressed in terms of colony forming units (CFU) [353]. The next step

is to perform fractional-run sterilization studies to determine the rate of killing [350,352]. In this case, product samples (in packages) are exposed to different fractions of the desired sterilization process or dose [350,352]. Samples are then tested for sterility, and the number of surviving microorganisms is reported graphically on a semi-logarithmic scale to extrapolate the exposure time or dose required to achieve a 10^{-6} SAL [350,352]. The exposure time (or dose) necessary to reduce the microorganism population by 90% or $1\log_{10}$ is designed by the decimal reduction time (D-value) [352]. This parameter allows to determine the limit sterilization exposure time, necessary to achieve the SAL from a given bioburden [352]. In this way, excess sterilization can be avoided since it may damage the medical device.
The efficiency of the sterilization can be monitored by biological and chemical indicators (or dosimeters, in case of radiation dose) [352]. In the first case, the indicators inform when certain sterilization parameters have been reached while in the second case, the indicators provide direct evidence that the sterilization process conditions can effectively kill spores [352].
The International Standard ISO 11737-1 is defined to determine the bioburden of the medical devices and products, whereas the International Standard ISO 11737-2 indicates how to validate the sterilization process.[354,355].
The sterilization methods used in this thesis and their main guidelines are described in chapter 8.1 and the experimental procedures are described in chapter 8.2. In this case, the validation guidelines were not strictly followed, since the aim was not to confirm the sterility of the products but to see whether the different sterilization methods could affect the physical, mechanical and cytotoxic characteristics of the chitosan-based compositions.

8.1. Sterilization method's guidelines

8.1.1. Steam (autoclaving) sterilization

Steam sterilization is a quick, effective, nontoxic and simple method that destroys microorganisms by an irreversible denaturation of enzymes and structural proteins [350,356]. However, it is only recommended for products that do not suffer from heat or water damage [357]. For example, most liquids, metals, glass and some heat resistant plastic materials such as polytetrafluoroethylene (PTFE), PP and celluloses (papers) can be sterilized by this technique [358]. Further attention should be given to the permeability of the package since it can influence the sterilization process [357].
The power of steam is due to its latent heat of vaporization (e.g. approximately 540 calories per gram) and temperature [357]. After steam contacts the device surface, it condenses and raises the temperature, decreasing the volume of steam, which establishes a negative pressure that draws in more steam. This occurs until a temperature equilibrium is reached [357].
The primary process variables of this sterilization are temperature, steam pressure and length of exposure [356,357]. The pressure is mainly used to obtain the required steam temperature and will vary directly with the temperature applied [356]. A typical steam sterilization process generally lasts 15 to 30 minutes at a temperature of 121°C [350,357]. It involves several steps: 1) loading, 2) pre-evacuation to remove air prior before the admission of steam, 3) heat-up, 4) exposure, 5) cool-down and 6) drying [357].
The validation for the steam sterilization in medical devices can be found in the International Standard ISO 17665-1:2006 and ISO 17665-2:2009 [359,360]. More specifically, Part 1 provides

three different approaches for microbial lethality assessment, which are: overkill, biological indicator/ bioburden and bioburden [359].

8.1.2. Gamma irradiation sterilization

Gamma irradiation is one of the most common used sterilization techniques on pharmaceuticals and medical devices because of its high penetration capacity, uniform and time dependent dose and absence of toxic residues [361]. It is a safe method since the gamma rays' energies are not high enough to induce radioactivity in the irradiated products.

This sterilization method uses ionizing radiation from a cobalt-60 isotope source, which emits gamma rays [350,356] measured in kiloGrays (kGy). In this case, the radiation generates mutations in the DNA of the microorganisms, thus altering their replication capabilities [356].

The radiation processing facility should be made of concrete and the cell walls of the irradiation chamber should be ticker (~170 cm) [362]. Control of sterilization is maintained between two different areas of the building (sterile and non-sterile), divided by a conveyor that runs through these two areas [362]. The materials are exposed to the sealed cobalt 60 isotope source, where the conveyor system is used to transport materials through the cell in carriers that hold the product [362]. The goal is to ensure that the entire dose is uniformly delivered [350]. Dosimeters are placed with the materials to monitor the radiation doses during the entire process. It documents that the minimum dose required for sterilization was delivered as well as the maximum dose for product integrity was not exceeded [350]. Dose mapping is therefore an important parameter that measures the variation of delivered dose within the radiation containers, and therefore should be determined *a priori* [363].

Validation procedures for the sterilization by gamma radiation are described in the International Standard ISO 11137, which is divided in three parts (ISO 11137-1:2006, ISO11137-2:2013 and ISO 11137-3:2006) [363]. More specifically, Part 2 describes three methods for the measurement of the radiation dose: Method 1 and 2 involve the determination of bioburden and multiple dose analyses in several product units, whereas the last method - designated by Method VD_{max} - substantiates the suitability of a predetermined dosage level, specifically 25 kGy (for product bioburdens less than or equal to 1.000 CFU) or 15 kGy (for product bioburdens less than or equal to 1,5 CFU) [364].

8.1.3. Ethylene oxide sterilization

Sterilization by EtO is an efficient technique, compatible with most implant and packaging materials [350]. This is a gaseous method with high diffusivity and permeability, low volatility and moderate chemical reactivity [350,365]. One particular advantage is to avoid heat and radiolytic stress often associated to sterilization with steam or radiation [366].

The lethal effect of EtO is due to the alkylation (replacement of a hydrogen atom with an alkyl group) of side chains of enzymes, DNA and RNA, which interfere with the normal cellular metabolism and reproductive processes of the microorganisms [366]. However, strict regulations limit its use since it is a toxic, explosive, flammable and (suspected) carcinogenic gas [349]. To reduce some of the EtO limitations, it is mixed with inert gases (e.g. nitrogen, N_2, and carbon dioxide, CO_2) and special attention is given to the facility design and environmental control [350,366].

The sterilizing efficiency of EtO depends on the concentration of the gas, the humidity, the exposure time, the temperature, and the load density [356]. Briefly, the implants, conditioned in a gas-permeable packaging, are loaded into a sterilization chamber. Initial vacuum is drawn to remove air and the gas mixture is injected at a certain EtO concentration (recommendation: 400 – 650 mg/L) [350,366]. The relative humidity in the chamber should be between 30%-90% and the typical operational temperature should be between 35°C-60°C. These two last parameters are crucial for the gas diffusion [350,366]. The sterilization is maintained at a sufficient time to achieve the required 10^{-6} SAL and this exposure time depends, primarily, on the gas concentration and temperature [350,366]. Following the exposure, an aeration period is necessary to remove the EtO residues, which are toxic [350,366]. This process can be performed in the sterilizer or in a separate aeration chamber or room, under specific conditions (e.g. temperature, rate and number of air changes, etc.) [366]. The aeration time depends on these conditions as well as on the characteristics of the sterilized and packaging material, the sterilizing conditions, the load being aerated and the acceptable limits of the residues for the intended use of the medial device [366]. A typical industrial EtO sterilization cycle involves an exposure time of 4 hours and an additional aerated time of 12 hours [349].
Appropriate sterilization conditions must be determined experimentally for each type of product, according to the International Standard ISO 11135:2014 [366,367]. This standard provides three approaches for microbial lethality assessment, that are: overkill, biological indicator/ bioburden and bioburden [367].

8.1.4. Ozone sterilization

As indicated previously, FDA considers the sterilization by ozone as a non-traditional technique. The first ozone sterilizer for medical devices (STERIZONE 125L, TSO_3) was licensed by Health Canada in 2002 and by FDA in 2003 as a faster economical alternative to low-temperature sterilization [368,369].
The antimicrobial activity of ozone is due to its oxidizing capacity that impairs the cellular components of the microorganisms [370]. Two mechanisms have been identified: 1) ozone oxidizes sulfhydryl groups and amino acids of enzymes, peptides and proteins and 2) ozone oxidizes polyunsaturated fatty acids to acid peroxides [371].
Ozone is produced when oxygen is energized and split into two monatomic molecules. The monatomic oxygen molecules then collide with oxygen molecules to form ozone [369]. It is easily soluble in water and has a longer half-life in the gaseous state. In water, ozone quickly degrades in oxygen. These characteristics make it an excellent candidate to be used as a sterilizing agent[368,370].
The mechanism of ozone sterilization involves two identical half-sterilization periods, where vacuum is created through water vapor, followed by humidification of devices and ozone generation and exposition[369]. Ozone is created in a specific enclosed generator when admitted oxygen is subjected to an electrical discharge [369,372]. The entire process takes approximately 4,5 hours at a temperature between 30°C - 35°C [369,372]. When it is complete, the residual ozone and water vapor are removed from the sterilized chamber into the catalytic converter to transform ozone into oxygen [372]. This last step uses ventilation to remove the ozone from the chamber [369]. Therefore, no toxic/hazardous residues are produced in the end of this sterilization process, which only requires medical-grade oxygen and only releases

oxygen and water into the air. This means that no aeration and cool down time are required. [372]

Like the other sterilization techniques, sterilization parameters, including the ozone dose, should be defined to assure a 10^{-6} SAL. Therefore, the bioburden of the products should be determined and the process must be monitored using biological and chemical indicators that are specific to ozone sterilization [372]. The validation of the ozone sterilization must be done in accordance with the International Standard ISO 14937:2009 [373].
Many devices can be sterilized by ozone: stainless steel, titanium, ceramic, polyvinyl chloride (PVC), PP, PTFE, among others [369,372]. However, due to its great oxidizing capacity and the humidity level used in the process, several other materials cannot be used. Examples include natural rubber, latex, textile fabrics and copper [369,372]. Additionally, this sterilization process was not approved for devices intended to be in contact with human body for more than 24 hours [369]. To overcome all these limitations, a new system that combines H_2O_2 and ozone has been developed by TSO_3 and, presently, it is commercialized in Europe and Canada by 3M™ and is under evaluation by the FDA [369]. The idea under this new system is to facilitate ozone penetration into challenging devices and to enable the use of lower concentrations of ozone [369].

8.2. Experimental procedure

In this study, the objective of testing different sterilizations methods was not exactly to determine if the methods are effective in the actual sterilization, but instead to ascertain if the methods affect the physical and mechanical properties of the chitosan-based specimens. Therefore, the parameters used in each sterilization method were defined according to standard values of validated sterilizations used for this type of orthopedic products/biomaterials.

8.2.1. Steam (autoclaving) sterilization

Steam sterilization was performed in Altakitin S.A. (Loures, Portugal), following the sterilization protocol that this company uses for the materials required for the production and/or conditioning of its non-metallic medical devices (e.g. bone grafts, bone cements and injectable bone substitutes).
The exposure cycle of this sterilization process occurred at 121°C for 20 minutes, and the drying cycle lasted 20 more minutes.
The specimens to sterilize were conditioned in falcon tubes of 15 ml, composed of polypropylene. The tubes were not completely enclosed, to allow the diffusion of the heat steam to its interior.

8.2.2. Gamma radiation sterilization

Gamma irradiation sterilization was performed in Campus Tecnológico e Nuclear (CTN) - Instituto Superior Técnico (Loures, Portugal). The sterilization protocol was the same used by Altakitin S.A., in the sterilization of its injectable bone substitute that has chitosan in its

composition (k-IBS ®). The specimens were conditioned in Tyvek sterilization pouches, which were heat-sealed.
The specimens were exposed to 15 kGy, at a dosage rate of 4 kGy/h. The sterilization process occurred at room temperature (approximately 21°C), and the exposure time was 3 hours.

8.2.3. Ethylene oxide sterilization

Sterilization by EtO was performed in Estereobato (Mora, Portugal), following the validated sterilization protocol that this company uses for the sterilization of certain biomaterials and medical devices such as prosthesis and surgical instruments. The specimens were conditioned in Tyvek sterilization pouches, which were heat-sealed.
Pure EtO was mixed with nitrogen with a purity of 98%, to increase the pressure inside the chamber (injected amount was 2,5 times the volume of the sterilization chamber). Before the EtO exposure, the relative humidity was 60% and the chamber pressure was 700 mbar. The specimens were exposed to 19,75 kg of EtO, which results in a concentration of approximately 600 mg/L. Exposure to EtO occurred for 4 hours, at a temperature of 54°C (chamber temperature). The final aeration period took 3 hours and consisted in an injection of nitrogen and then several injections of sterile air and vacuum, to reduce the EtO levels.

8.2.4. Ozone sterilization

Ozone sterilization was performed in Brasil Ozônio (São Paulo, Brasil), using equipment developed by this company. To sterilize the 3D chitosan-based specimens a validated protocol for other medical devices was followed. The specimens were conditioned in Tyvek sterilization pouches, which were heat-sealed.
In this sterilization, four cycles were performed. Each cycle comprised the establishment of vacuum inside the chamber, the admission of ozone gas with humidity between 91-95% and temperature between 30°C - 35°C and a stabilization of the sterilization conditions for a period of 20 minutes. A new cycle was repeated after emptying the chamber. In total, the four sterilization cycles took 140 minutes.

SECTION D: Development and experimental evaluation of 3D dense chitosan-based compositions for orthopedic applications

9. Preliminary studies: production process optimization and materials selection

Preliminary tests were performed to optimize critical parameters of the production process of 3D dense chitosan-based specimens and to select the materials for such production. The production process adopted in this study was developed by Oliveira *et al.*[109] whose study in described is chapter 3.3.1.1.

9.1. Optimization of the production process

9.1.1. Optimization experiments

The optimization of the production process was still required to improve and systematize future productions, reducing its duration and maintaining the quality and the appearance of the produced specimens - dense and easily processable from the chitosan block that is obtained in the end of the drying phase. Besides the parameters that were optimized by Oliveira *et al.*[109] other parameters were analyzed in this optimization study.

To test the production process, a 3% (w/v) chitosan from Altakitin SA, with an average M_W of 490 kDa, a viscosity of 970 cP and 92% D.D. was used. Further reagents used in the optimization experiments were:

- Acetic acid (glacial) from Carlo Erba Reagents;
- NaOH 50% (w/w) solution from Liqual, Lda;
- Deionized water produced by reverse osmosis at Altakitin S.A.;
- Glycerol from LabChem (purity > 99,5%);
- L-Ascorbic acid from Panreac;
- Ammonia solution 25% (v/v) from Quimitécnica.

The results of the optimization studies are described and discussed in the following chapters.

9.1.1.1. Blends of chitosan

Previous studies indicated that higher mechanical properties were obtained when chitosan was blended with 10% (w/v) glycerol [109,175]. Therefore, tests were performed to assess differences between the specimens produced with and without this plasticizer. The results indicated that it was not possible to produce chitosan-only specimens since the obtained blocks were brittle and ended up breaking. Figure 9.1 shows the appearance of these blocks.

Figure 9.1. Example of chitosan block produced without the addition of plasticizers.

This result may be related to the strong intermolecular forces that the chitosan chains feel after the precipitation phase. Such interactions have made the chains stiffer and less ductile, producing a brittle specimen. As consequence of this analysis, all the following optimizations used 10% (w/v) glycerol.

9.1.1.2. Dissolution acid

Several studies have been published using chitosan as a raw material. Among these studies, acetic acid is, by far, the most used acid in the dissolution of chitosan [17,374–378]. Therefore, it could be assumed *a priori* that 2% (v/v) of acetic acid is effective in the dissolution of 3% (w/v) of chitosan. However, to analyze the efficiency of other acids, the dissolution of chitosan was tested in a 2% (w/v) aqueous ascorbic acid solution. This is a biocompatible organic acid that promotes the formation of collagen in fibrous tissues, teeth, bones, connective tissue, capillaries and skin [379]. In respect to its capacity to aid chitosan dissolution, it is believed that ascorbic acid not only provides the necessary protons for the dissolution, but also that it can act as a potential cross-linker, improving the final properties of the chitosan material [380].
However, as shown in the figure below, the production of specimens failed since it was not possible to obtain integral specimens, capable of being shaped into any geometry. The precipitation with NaOH resulted in a hydrogel with many cracks, possibly explained by the new conformation of the chitosan's backbone chain, promoted by this organic acid. This may be related with the lack of freedom that the chitosan chains feel while being entangled with a bigger conjugated salt anion. Therefore, during the basic precipitation of the polymer, the homogeneity among the layers is affected due to a more rigid hydrogel causing a less efficiency in NaOH diffusion within the medium (heterogeneous precipitation). As a consequence, the next optimization studies used acetic acid as the dissolution agent, since it produces better results.

Figure 9.2. Final aspect of specimens produced by dissolving chitosan in an ascorbic acid solution.

9.1.1.3. Dissolution temperature

Air retention during dissolution is another factor that plays an important role in the reproducible production of 3D dense chitosan specimens. Thus, to reduce the viscosity of the solution, two different dissolution temperatures were: 30°C and 50°C. To avoid possible damages on the chitosan's polymeric chain, temperatures above 50°C were not considered. Although the dissolution temperature of 50°C greatly helped to reduce the air bubbles entrapped in the solution, in the end a lower dissolution volume was obtained for the same proportion of chitosan, acid and water due to solvent evaporation. For this reason, all future dissolutions were performed at a temperature of 30°C.

9.1.1.4. Type of mold

After the drying phase, the goal is to obtain consistent dense chitosan blocks, able to be transformed into chitosan specimens with the desired dimensions. Hence, it was crucial to find a mold for the solution freezing that would not only assure the appropriate dimensions for these final structures, but would also ease its removal prior to the precipitation step. Examples of different tested materials are shown in Figure 9.3. Besides the examples on this figure, a dialysis membrane was also tested as a mold for the solution. However, the dialysis membrane, as well as many other materials, had the same problem – the outer layers of the hydrogel were destroyed once removed from the mold. This problem was avoided by using a Tetra Pak® mold, since its inner material reduces the friction between the mold and the frozen solution, allowing a smooth and straightforward removal of the mold without damaging the outer layer of the hydrogel.

Figure 9.3. Examples of different materials tested as molds for the production of dense chitosan specimens.

9.1.1.5. Freezing temperature

Freezing cracks that are sometimes generated during the freezing process may cause imperfections in the outer layers of the hydrogel. Figure 9.4 a) reflects these imperfections. To avoid these cracks, three different freezing temperatures were tested: -20°C, -25°C and -30°C. An improved result was observed when the temperature is reduced to -30°C, as seen in Figure 9.4 b). This observation could be explained by a faster freezing process that yields a more random growth of water crystals (small crystals with different orientations), which reduces the possibility of larger areas of "oriented crystals" that may give in to cracks. Therefore, all the future productions used -30°C as the freezing temperature.

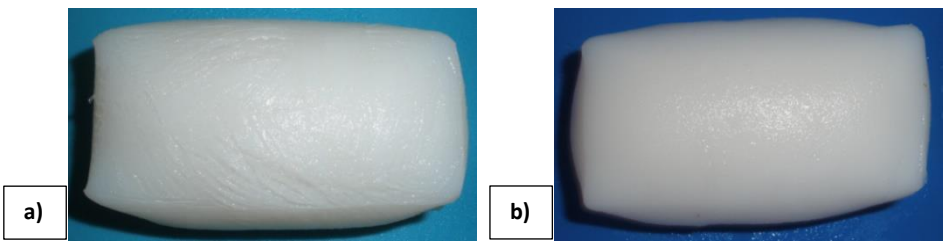

Figure 9.4. Hydrogel obtained when the freezing temperature was a) -20°C and b) -30°C.

9.1.1.6. Precipitation method

To shorten the production time of the 3D dense chitosan specimens, a different precipitation method was tested. In this new method, the chitosan solution was poured inside a dialysis

tubing membrane from regenerated cellulose (Spectra/Por®1, Spectrum Labs) and it was left suspended in a close environment, in contact with a gaseous ammonia atmosphere (the ammonia solution was placed in petri dishes), as shown in Figure 9.5. The idea behind using ammonia as a precipitation method is not only to avoid the freezing phase, since the dialysis membrane gives a 3D shape to the solution, but also to shorten the washing phase, since ammonia is a slightly weaker base than NaOH.

The concentration of the ammonia solution used in this experiment was 25% (v/v). Since ammonia is highly volatile, it diffused in the chitosan solution for the neutralization of amine groups [381]. Although the precipitation of the solution did occur, this process took approximately one week and the hydrogel looked brittle and fluffy. Therefore, the precipitation agent used hereinafter remained the NaOH solution.

Figure 9.5. Precipitation method using a gaseous ammonia atmosphere in an isolated environment.

9.1.2. Parameters selected for the production process

Table 9.1 indicates the parameters tested and optimized in this study. New experiments considered the parameters selected.

Table 9.1. Critical production process parameters and their optimization.

Parameter	Optimization	Selection
Production Stage 1: Dissolution		
Blends of chitosan	Dissolution of chitosan with and without a plasticizer	Use plasticizers
Type of acid	Ascorbic acid was tested, in addition to acid acetic	Use acetic acid
Dissolution temperature	Temperatures of 30°C and 50°C were tested, in addition to the dissolution at room temperature	Use 30°C
Production Stage 2: Molding		
Type of molds	Molds from different materials/ geometries were tested	Use rectangular Tetra Pak® molds (117 mm × 47 mm × 37 mm)
Production Stage 3: Freezing		
Freezing temperature	Temperatures -25°C and -30°C were tested, in addition to the temperature at -20°C	Use -30°C
Production Stage 4: Precipitation		
Precipitation method	Ammonia atmosphere was tested, in addition to the NaOH solution	Use NaOH solution

9.2. Preliminary tests on the production and evaluation of candidate materials for chitosan-based implants

9.2.1. Production of specimens

The production process parameters optimized in the previous study were tested in this stage, to assess the machining capabilities of the resulting blocks and to understand if the production process is influenced by the addition of different materials, aiming to constitute chitosan-based specimens with different compositions.

Three different plasticizers were added to the dissolution stage of the optimized production process: 10% (w/v) glycerol, 10% (w/v) sorbitol and 10% (w/v) ethylene glycol. The chitosan, glycerol and other reagents used in this production process are described in chapter 9.1.1. Sorbitol (no crystallizable solution, 70%) and ethylene glycol were purchased from Carlo Erba Reagents. The plasticizers used were according to the European Pharmacopoeia, except for the ethylene glycol (analytical grade reagent).

The blocks were shaped in a conventional milling machine and cut with a handsaw into specimens with average dimensions of 14 mm × 12 mm × 7 mm (all faces were smooth and uniform). Figure 9.6 shows two specimens obtained by blending chitosan with glycerol.

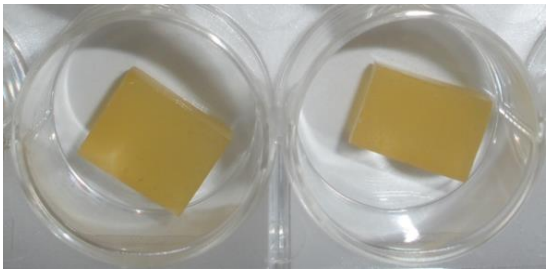

Figure 9.6. Examples of 3D dense chitosan specimens produced by adding 10% (w/v) glycerol.

Differences in the behavior of the specimens were noted only during the precipitation stage; the sorbitol hydrogels were faster to dive into the NaOH solution, possibly because precipitation was faster, or it simply happened because sorbitol has a higher density than glycerol. Despite this difference, the precipitation stage lasted 48h in both situations and both hydrogels were precipitated at the end of that time.

The specimens produced with ethylene glycol showed problems during the shaping process and, as a consequence, local fractures appeared during the machining process. Despite these local imperfections, all the specimens were visually similar.

9.2.2. Experimental evaluation of preliminary specimens

9.2.2.1. Compression tests

Four specimens of each composition were tested to compression, according to the experimental procedure described in chapter 7.1.1.1. Figure 9.7 shows the stress-strain curves that represent the behavior of the three types of specimens during the compression test. Figure 9.8 a) and b) show the results of the compressive tests, namely the compressive modulus and the compressive strength. For the compressive strength results, the maximum

stress for each specimen was measured on the first load decay observed in the respective stress-strain curves.

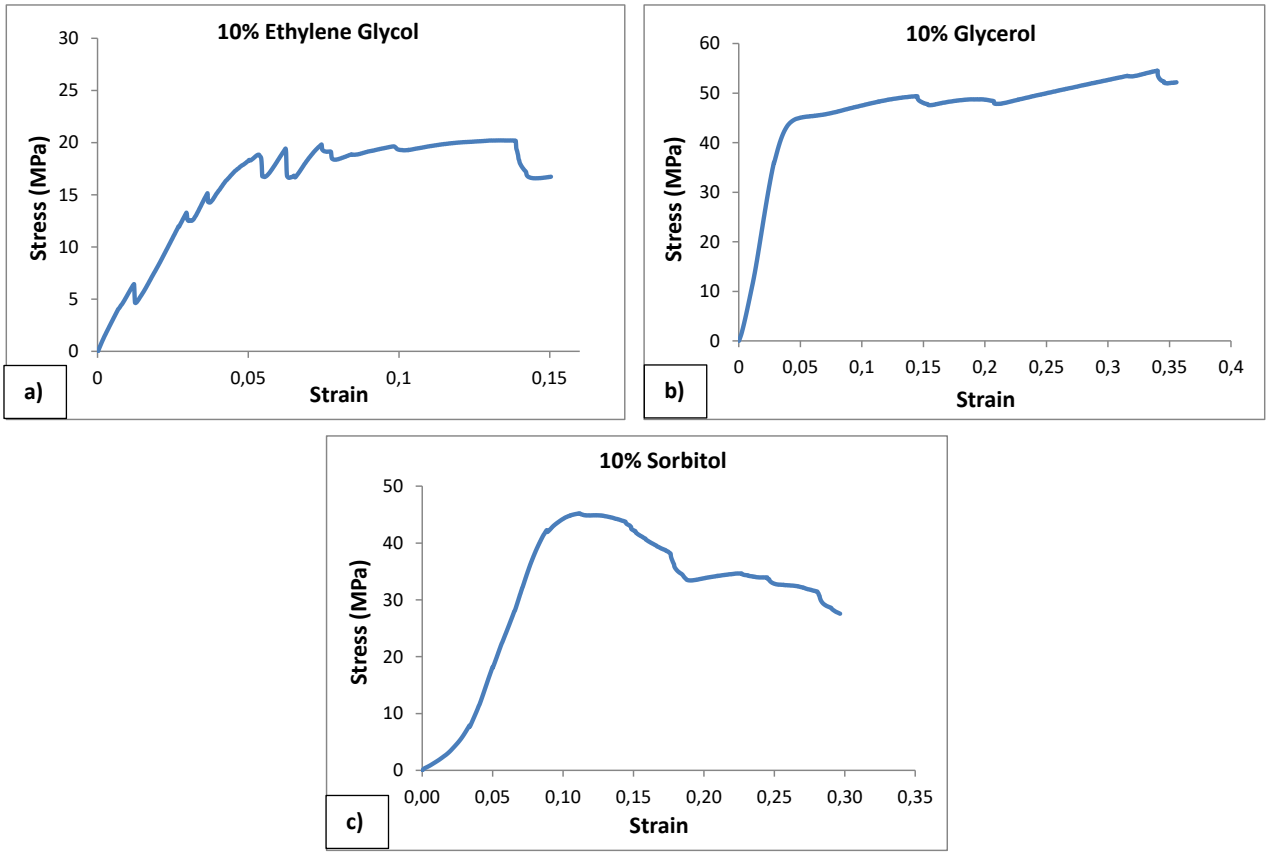

Figure 9.7. Stress-strain curves obtained for one specimen obtained by blending chitosan with a) 10% ethylene glycol, b) 10% glycerol and c) 10% sorbitol.

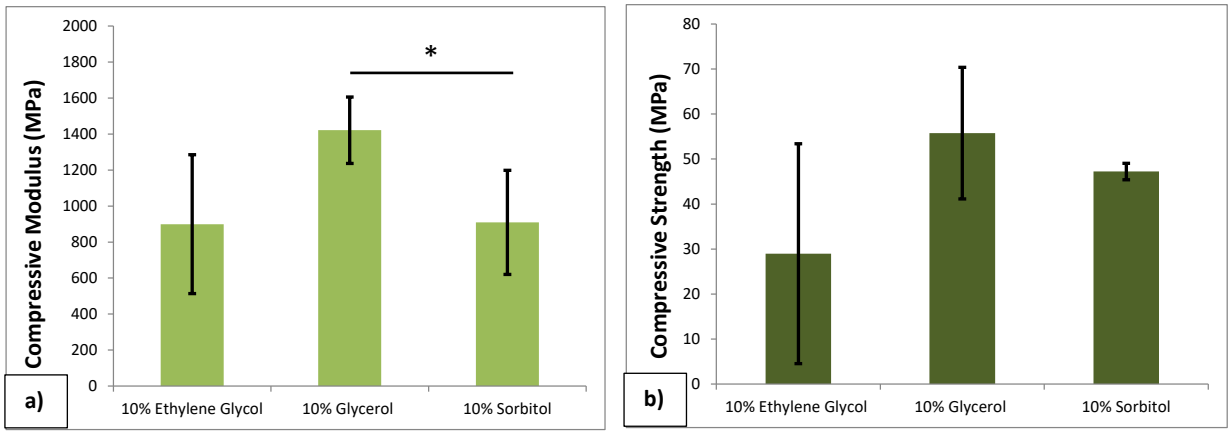

Figure 9.8. Results of the a) compressive modulus and b) compressive strength (*p-value < 0,05).

The stress-strain curves indicate a different mechanical response of the specimens under the compressive loading. The ethylene glycol curve exhibits several load decays even for low loading, indicating some crack initiation since the beginning of the test. This is also the material which exhibit lower stress and strain values. The other materials reveal higher stress before the first crack occurs, indicating higher compressive strength values. The 10% glycerol specimens are the ones who exhibited higher strain before cracking occurs.

In general, the specimens that present higher elasticity and strength are the ones produced with 10% glycerol, according to the results depicted in Figure 9.8 (compressive modulus of 1421 MPa and compressive strength of 56 MPa). On the other hand, the specimens produced with 10% ethylene glycol show lower mean values of these two properties.

9.2.2.2. SEM analysis

SEM analyses were performed using the experimental procedure described in chapter 7.2.1.1. Figure 9.9 to Figure 9.11 show the SEM images on the surfaces of the different specimens.

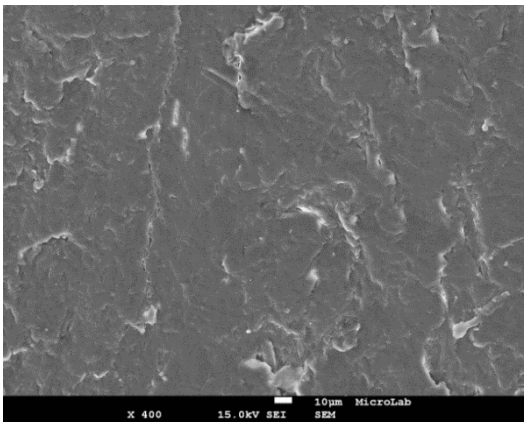

Figure 9.9. SEM image (400X) of specimen produced by blending chitosan with 10% ethylene glycol.

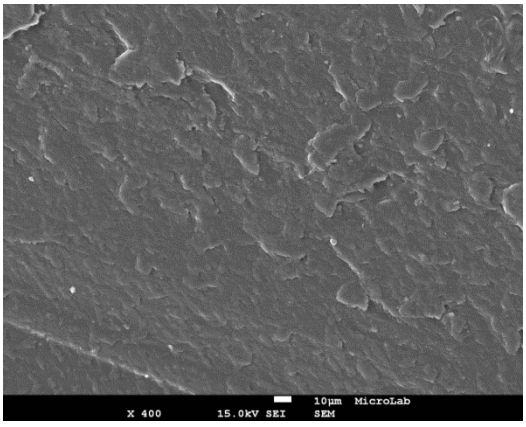

Figure 9.10. SEM image (400x) of a specimen produced by blending chitosan with 10% glycerol.

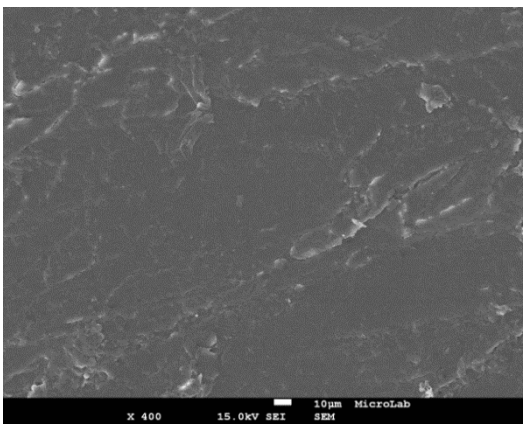

Figure 9.11. SEM image (400X) of specimen produced by blending chitosan with 10% sorbitol.

The SEM images revealed that the specimens are mostly dense and do not have significant pores.

9.2.2.3. DSC tests

DSC tests were performed according to the procedure described in chapter 7.3.1.1. Figure 9.12 to Figure 9.14 represent the DSC curve of heat flux versus temperature obtained for each type of chitosan blend.

In addition, Figure 9.15 shows a DSC run for the chitosan powder, where the maximum temperature for the second dynamic heating period was 350°C, instead of 300°C.

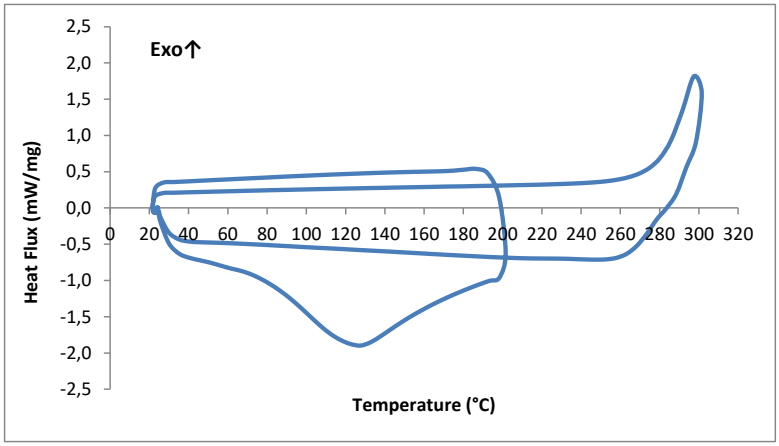

Figure 9.12. DSC of a specimen produced by blending chitosan with 10% ethylene glycol.

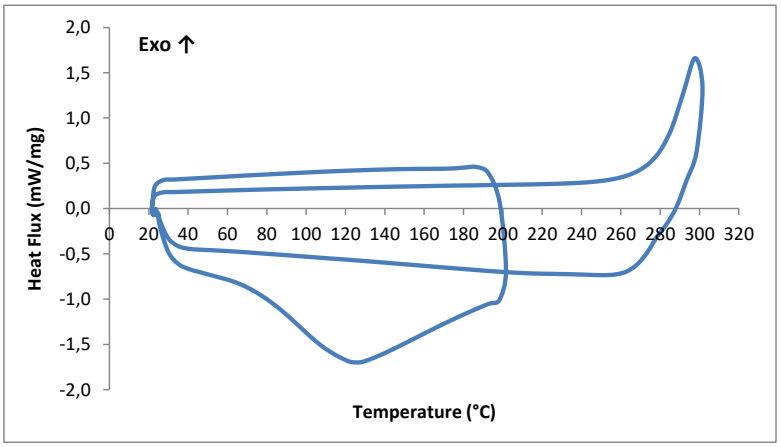

Figure 9.13. DSC of a specimen produced by blending chitosan with 10% glycerol.

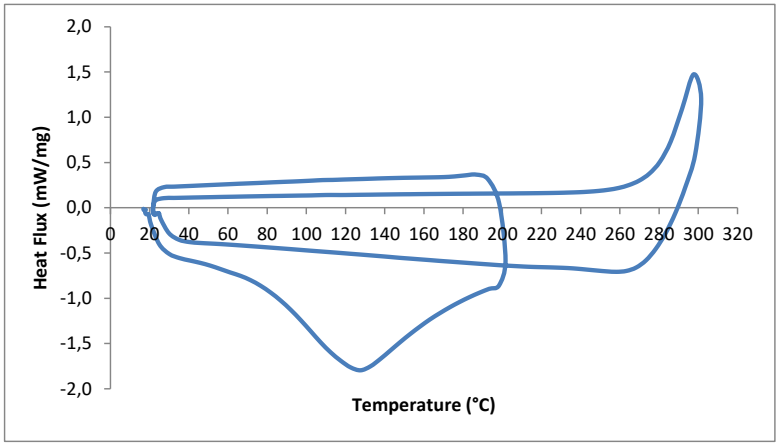

Figure 9.14. DSC of specimen produced by blending chitosan with 10% sorbitol.

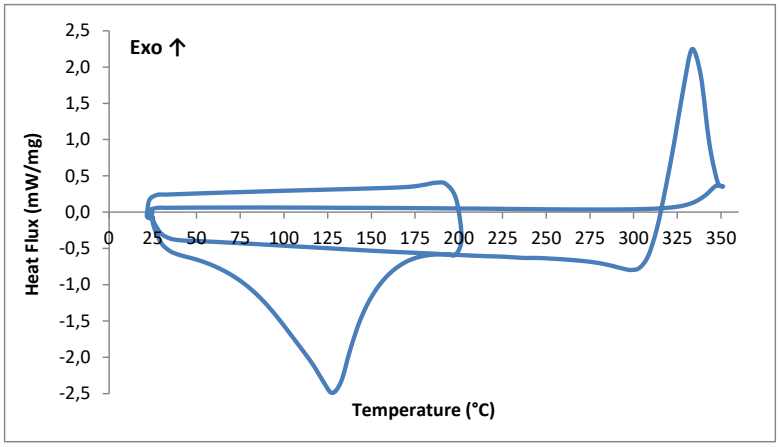

Figure 9.15. DSC to the chitosan powder.

The endothermic peak observed on the first dynamic heating run, for all the tested samples, corresponds to the vaporization of water. The wideness of this peak shows that the water is strongly attached to the material, and this occurs for all compositions, including the chitosan powder (this peak is not so wide).

To easily identify the differences between all the DSC tests performed, the final dynamic heating period, from all the materials, are compared in Figure 9.16.

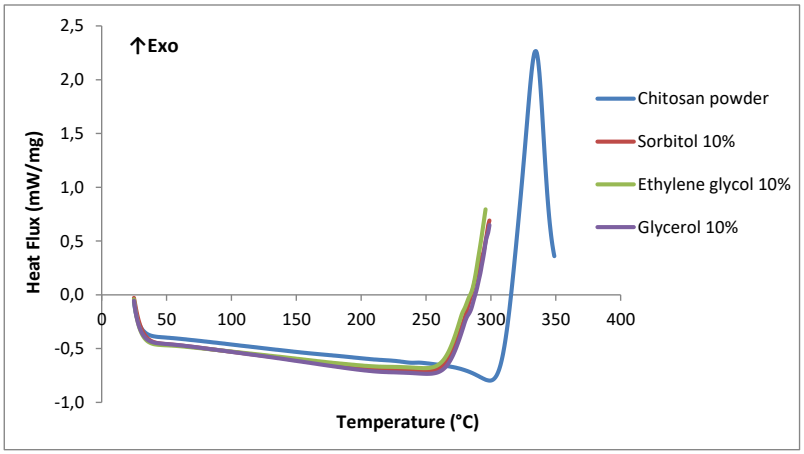

Figure 9.16. Comparison of all the lasted heating curves, from all the DSC runs.

In the second dynamic heating run, the temperature was raised by 20°C/min to a maximum of 300°C (or 350°C, in the case of the chitosan powder). The results show an exothermic peak approximately at 260°C for all experiments performed on chitosan specimens, which corresponds to the thermal degradation of chitosan. For the chitosan powder, this peak is observed at 300°C.

9.2.2.4. Cytotoxic tests

For the cytotoxic test, two groups of triplicates of each composition, were first sterilized with ethanol (70%, v/v) followed by overnight UV exposure. The cytotoxic tests were then performed according to the methodology described in chapter 7.5.1.1. Figure 9.17 presents the results of the cell viability performed by the extract assay.

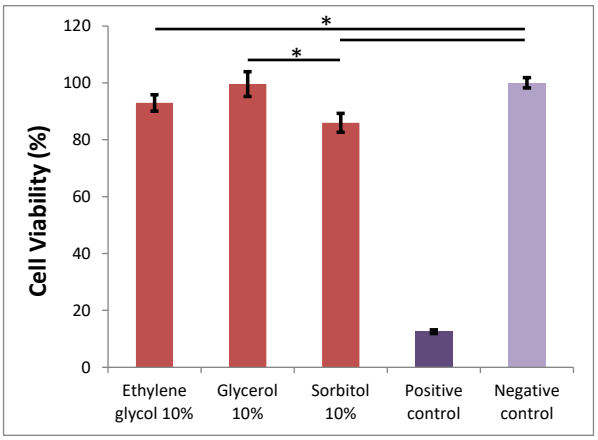

Figure 9.17. Results of the cytotoxic assay by extract dilution - MTT test (*p-value < 0,05).

According to the results in Figure 9.17, the percentage of viable cells is greater than 80%, and in the case of the glycerol specimen, the mean percentage reaches the value obtained for the negative control, prepared by placing the cells only in contact with fresh medium. Comparing the three compositions, the percentage of viable cells is lower for the sorbitol specimens, especially when compared with the results of the glycerol specimens and the negative control (p-value of 0,01 and 0,009, respectively). However, the cell viability is still greater than 80%.
The results of the direct contact assay are shown in Figure 9.18, Figure 9.19 and Figure 9.20. The specimens' positions in the cell medium are identified in these figures.

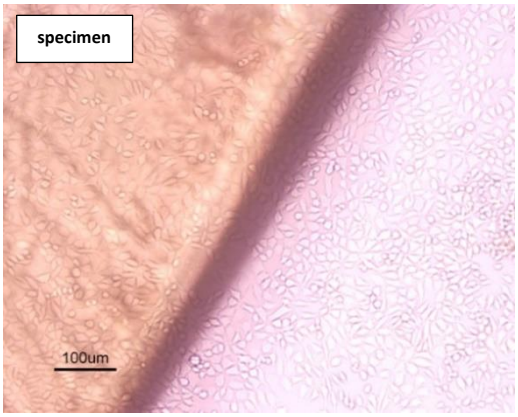

Figure 9.18. Direct contact assay for a specimen produced by blending chitosan with 10% ethylene glycol.

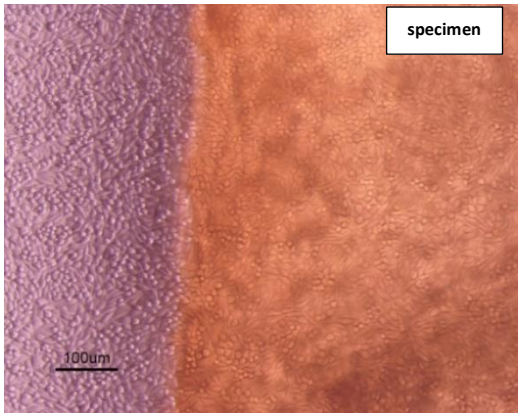

Figure 9.19. Direct contact assay for a specimen produced by blending chitosan with 10% glycerol.

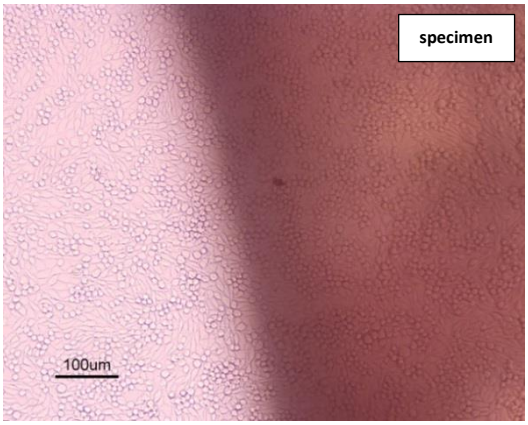

Figure 9.20. Direct contact assay for a specimen produced by blending chitosan with 10% sorbitol.

The results of the direct contact assay show that the cells grew around and on the surface of all the specimens, without any morphologic disorder.

9.2.3. Selection of the candidate materials

The goal of this experimental evaluation was to understand the effect of materials other than glycerol in the optimized production process. At the same time, the effects of these materials on the chitosan specimens' processability and on their final properties were assessed.

Since plasticizers improve the processability of chitosan specimens, reducing its brittle behavior, the selection focused on this group of materials. Although other materials such as lipids and oligosaccharides can act as plasticizers, two other polyols were selected for this study. Polyols are described as being more effective since their plasticizing effect results in a structure similar to the polymer matrix [382]. Among several candidates (e.g. sorbitol, mannitol, xylitol, ethylene glycol, propylene glycol and PEG), focus was given to sorbitol and ethylene glycol. These compounds were selected because they differ from the molecular weight of glycerol and do not have long molecules which may difficult the penetration of the plasticizer through the polymer matrix.

Preliminary chitosan-based specimens were successfully produced and machined when 10% (w/v) of each of the three plasticizers (glycerol, sorbitol and ethylene glycol) were blended to chitosan. However, difficulties were found during the shaping process of the ethylene glycol specimens.

Compression tests:

The compression test results are in accordance with what has been described in the literature for the chitosan films; the presence of glycerol improves the dynamics of the polymer chains, relieving the limitations in local motion caused by the presence of strong intermolecular interactions, hence modifying the properties of the polymer [187]. Interactions between glycerol and chitosan occur by hydrogen bonding on specific polymer sites, which facilitates the stress transfer to the reinforcement phase, resulting in a material with improved mechanical properties [383].

Studies found no difference on the mechanical properties between chitosan films prepared by the addition of glycerol and sorbitol [382,384] . However, the statistical analysis performed on the results of Figure 9.8 a) indicated statistical significance between the stiffness mean values of the glycerol and sorbitol specimens (p-value = 0,03).

The specimens produced by adding ethylene glycol to the composition presented higher standard deviation in the two mechanical properties measured: compressive modulus and compressive strain. This may be related with material imperfections that, consequently, promoted the appearance of material imperfections during the shaping phase. These imperfections resulted in several points of stress decay, shown in the respective stress-strain curve – Figure 9.7 a).

Oliveira *et al.*[175] performed compression tests on dense circular chitosan specimens produced by adding 10% (w/v) glycerol to a chitosan with high M_W, DD and viscosity (800 kDa, 90% DD and 1.200 cP, respectively). They obtained a mean compressive modulus of 600 MPa and a mean compressive strength of 75 MPa. The preliminary results of this thesis indicated higher mean compressive modulus (1.421 MPa) for the glycerol specimens but lower compressive strength (56 MPa). These differences could be related with the different geometries of the tested specimens as well as the type of chitosan material used in each of the studies.

SEM analysis:

The SEM analysis shown in Figure 9.9 to Figure 9.9 revealed that the specimens are dense and only some pores are visible in the interior of the specimens, eventually due to the air retention. Comparing the images obtained for the three compositions, no relevant differences were observed in the porosity of the specimens.

DSC tests:

The DSC analyses indicated that the different compositions do not alter the capacity of water holding and the strength of the water-polymer interaction in the plasticized specimens. Variations would be observed if another chitosan material, with different D.D., was also used for the production of the plasticized specimens. The endothermic peak associated to the chitosan powder indicates residual water (absorbed moisture) [385].

The thermal degradation of chitosan powder occurred at a higher temperature, when compared with the plasticized specimens. This shift towards a higher degradation temperature may occur since the polymeric chains that compose this polysaccharide are in its native state, and did not suffer from any type of action that may alter its ordered structure. In the native state, there are two types of strong attraction forces operating in chitosan: intramolecular and intermolecular forces via hydrogen bonding or hydrophobic interactions [13,385]. Therefore chitosan undergoes a process of self-cross-linked structure that greatly influences its thermal properties [385]. On the other hand, the polymeric structure of the plasticized specimens was altered during the production process. The molecular interactions established between both

plasticizers and water with chitosan weakens the strong intermolecular bonds that exist in native chitosan, which explains their lower thermal resistance. This effect was also observed in thermal studies on plasticizer films [386,387]. In this thesis, no differences were found in the degradation temperature between the different plasticized specimens. In turn, Matet *el al*. [387] found differences when they studied different plasticized chitosan films, and concluded that sorbitol films had a slower thermal degradation when compared with glycerol films [387]. The degradation temperatures observed in this study are consistent with the results on published studies [388].

The results did not reveal a stepwise increase on temperature, characteristic of a Tg. This suggests that chitosan requires a higher temperature for their molecules to become more mobile, which goes beyond its degradation temperature. According to Schut *et al.*[389], several factors can influence the mobility of the polymers' chains and therefore the Tg: the molecular weight (chain ends are more mobile), chemical structure (stiffness of the chain and interactions with other chains), diluents or plasticizers (increase the free volume), cross links and crystallization (limit the chain mobility). In case of plasticizers, as previously described, these interact with the polymer chains, promoting its mobility [388,390]. They intersperse themselves among the polymers' chains (spacing them apart), acting as internal lubricants by reducing the frictional forces between polymer chains. By breaking the polymer-polymer interactions, the free volume increases and the Tg lowers [388]. Therefore, if the Tg was observed, it was expected that it would occur at a lower temperature for the plasticized specimens when compared to the chitosan powder.

The literature reports different values for the Tg of chitosan, obtained either by DSC or by other techniques (e.g. Dynamic Mechanical Thermal Analysis, DMTA, and Thermogravimetric Analysis, TGA) [391–393]. In some cases, the Tg is not even detected [391,394]. Gartner *et al.*[385] suggested that the residual water impairs the determination of the chitosans' Tg, hypothesizing that the complex structure of chitosan via local dynamics (secondary or β-relaxation phenomena) explains the dispersion of results in the literature.

Cytotoxic tests:

The main goal of these tests was to investigate whether the different stages of the production process would change the biocompatibility of chitosan specimens and to understand if the addition of plasticizers would cause this effect. For the extract assay, the results shown in Figure 9.17 revealed that there is cell activity, which points out that no cytotoxic substances had been released in the medium during the extract assay. According to the ISO 10993-5, if cell viability is reduced to < 70 % of the blank, the material has cytotoxic potential [322], which did not happen in this study. In addition to the extract assay, the results of the direct contact assay reinforce the conclusions obtained for the extract assay, i.e. the blends of chitosan with ethylene glycol, glycerol and sorbitol are not cytotoxic for the cells. The results of these tests are in accordance with published cytotoxic studies performed on chitosan membranes and films [395,396].

Material selection:

The addition of different plasticizers to the production process allowed to obtain dense chitosan specimens that were easily shaped and tested. However, the machining of the ethylene glycol blocks caused local imperfections that resulted in lower mechanical properties when the resulting specimens were tested to compression. The materials blended to the chitosan did not alter the cytotoxic and the thermal properties of the specimens. According to

the results, the blends with glycerol and the sorbitol seemed more appropriate for further evaluations.

9.3. Selection of the chitosan material

9.3.1. Strategies used to obtain chitosan

To ensure the reproducibility of the experiments, it was crucial to guarantee the necessary amount of chitosan, assuring the properties defined in chapter 3.3.1.1. A manual production of chitosan was attempted, to obtain at least 1,5 kg of material. The manual production of chitosan followed the industrial production protocol of Altakitin S.A., but on a smaller scale. The initial step was to produce chitin, according to the schematization of the Figure 3.1. Figure 9.21 shows the result of the first deproteinization step. In this case, 1 M NaOH solution is used to extract the proteins from the previously demineralized crushed shrimp shells. Figure 9.22 shows the final step of the chitin production, which consisted in the filtration and washing of the chitin with acetone after the discoloration step.

Figure 9.21. Chitin production: first deproteinization step.

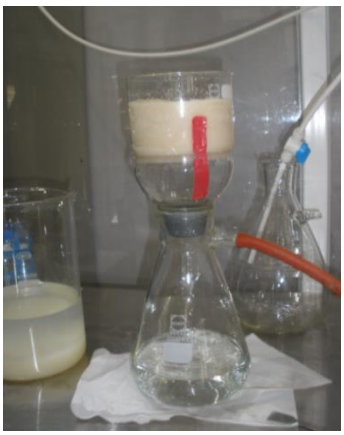

Figure 9.22. Chitin production: filtration after the discoloration step.

The chitosan production followed the schematization in Figure 3.2, according to the industrial production protocol of Altakitin S.A. Figure 9.23 shows the first deacetylation reaction that

occurred at 80°C when a 50% (w/w) solution of NaOH was added to the chitin. This step was repeated to obtain chitosan with D.D. of 90%.

Figure 9.23. Deacetylation reaction.

Two batches of chitosan were produced in the end of two completed manual production processes, yielding merely 320 g of chitosan, from an initial weight of 1.200 g of crushed shrimp shells. Since the manual production was long and extremely time consuming, a market search was conducted to identify manufacturing companies that sell chitosan to use in further experiments. From this search, only two sellers met the criteria defined for the desired chitosan: medical grade, 90% D.D. and viscosity around 1.000 cP. These companies were Primex (Iceland) and Heppe Medical Chitosan (Germany). Different chitosan batches were then acquired from these two companies.

9.3.2. Selection of the chitosan batch

To select the final chitosan material, the optimized production process was tested using six different chitosan batches. These productions were performed by adding only 10% (w/v) glycerol to the dissolution stage. Table 9.2 indicates the characteristics of the tested batches.
The conformity of the different chitosan batches to the production process is explained in Table 9.2; if a certain process stage was reached successfully, this is referred as “Yes” in this table, otherwise, it is referred as “No”. Two specimens were produced in the end of successful shape stages. These correspond to the production processes that used chitosan batches 2, 3 and 5.
The values of D.D. and viscosity are presented according to the product certificate of analysis, except for the mixture of the batch 3. In this case, the properties of the chitosan were assessed based on the experimental procedures described in chapters 6.1.1 and 6.1.2.

Table 9.2. Properties and conformity of the different chitosan batches to the optimized production process.

Chitosan Batch	Company	Properties			Conformity with the production process			
		DD (%)	Viscosity (Cp)	M_w (kDa)	Dissolution stage	Precipitation stage	Drying stage	Shape stage
1	Primex	87 *	992 *	856	No	-	-	-
2	Primex	95 *	570 *	910	Yes	Yes	Yes	Yes
3	Primex/ Altakitin	89	800	704	Yes	Yes	Yes	Yes
4	Heppe	91 *	568 *	608	Yes	Yes	Yes	No
5	Heppe	88 *	1.210 *	834	Yes	Yes	Yes	Yes
6	Heppe	98 *	1.040 *	700	Yes	Yes	Yes	No

*according to the certificate of analysis

The final selection was based on the mechanical properties of the produced specimens. In this case, flexural tests were performed according to the procedure described in chapter 7.1.2.1. In Table 9.3, the mean flexural modulus, flexural strength and the maximum flexural strain are compared for each type of chitosan successfully processed in the end of the production process. The tested specimens had average dimensions of 20 mm × 12 mm × 3,5 mm.

Table 9.3. Flexural properties (mean properties) of the chitosan specimens produced with different chitosan batches.

Chitosan Batch	Flexural modulus (MPa)	Flexural strength (MPa)	Flexural strain (%)
2	1.543	37	3,8
3	1.509	52	5,8
5	866	38	6,5

According to the results of the previous table, the chitosan mixture of batch 3 shows a better combination between the mechanical strength, the stiffness and the deformation until fracture. In this case, the combination of two types of chitosan, one with high M_W and another with medium M_W, provides a good relationship between mechanical strength (due to the long chains) and flexibility (due to the mobility of the shorter chains). Identical results were obtained by Oliveira *et al.*[109,175].

Several factors may explain why it was not possible to work with certain chitosan materials. The methodology used for the companies to perform both the chemical extraction of chitin and the deacetylation of chitin into chitosan, the origin of the material, the polydispersity index and the techniques used to characterize the chitosan material are among the potential factors. For example, the chitosan from Primex and Altakitin comes from the same shrimp species (*Pandalus borealis)* whereas the chitosan from Heppe comes mainly from crab shells [397]. The first two companies indicate the origin of chitosan in the certificate of analysis of their products, but the same does not happen with Heppe.

To prove differences between the purchased batches, the D.D. of each batch was confirmed by ^{1}H-NMR, according to the experimental procedure described in chapter 6.3.1. The results were 77% for batch 1, 86% for batch 2, 93% for batch 4, 90% for batch 5 and 96% for batch 6. Figure 9.24 and Figure 9.25 show the ^{1}H-NMR spectrum of the batch 1 and batch 2, respectively.

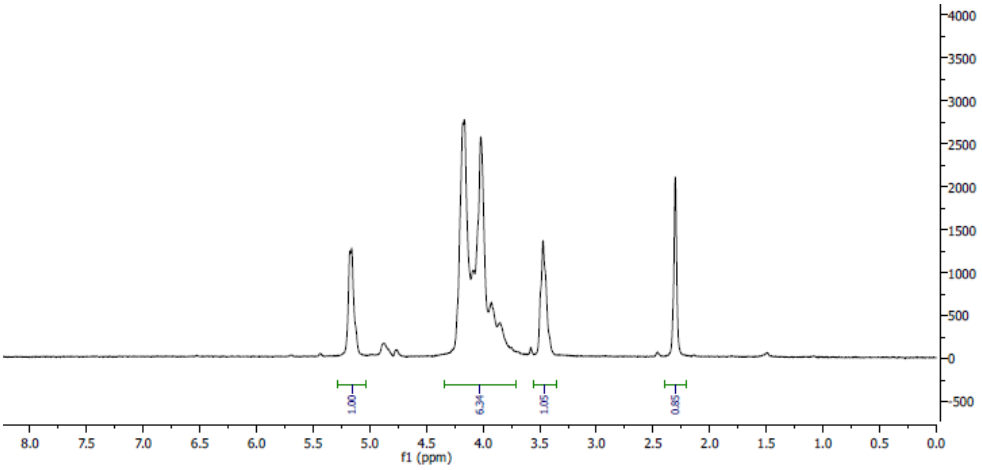

Figure 9.24. ^{1}H-NMR spectrum of the chitosan batch 1.

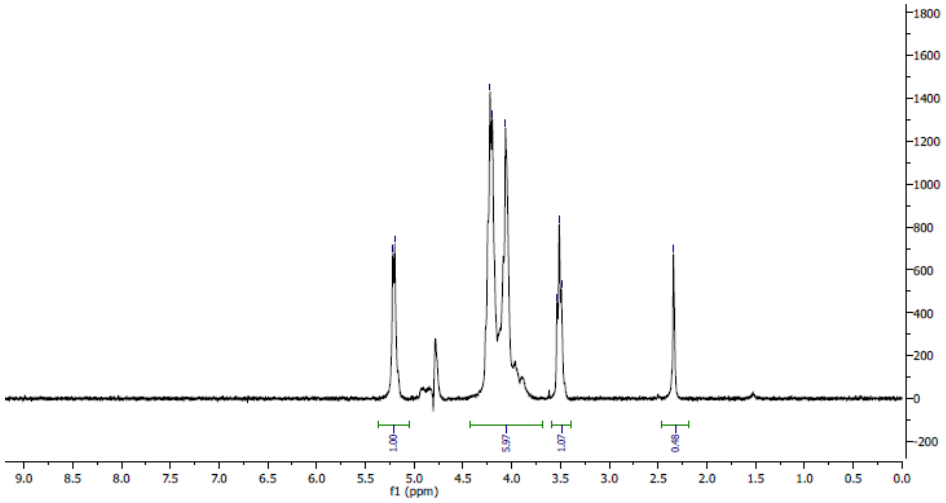

Figure 9.25. ^{1}H-NMR spectrum of chitosan batch 2.

Therefore, the D.D. values determined by ^{1}H-NMR did not match with the analysis certificate of the batches acquired from Primex, being substantially lower. After contacting the company, it became clear that the D.D. of their products is determined by colloidal titration, which explains the differences found (rapid detection method but with less specificity).

9.4. Conclusion - optimized method and materials for future productions

The optimization study altered some variables in the production process described in chapter 3.3.1.1. Therefore, the specimens produced in the next chapters followed the steps described below:

1 – Dissolution stage: dissolve 3% (w/v) chitosan in 2% (v/v) acetic acid solution, at 30°C, using a mechanical stirring system. Add a plasticizer in this stage;

2 – Molding stage: pour the solution in Tetra Pak® molds and leave it at rest until all the air bubbles disappear (approximately 24 hours);

3 – Freezing stage: freeze the molds at -30°C for 24 hours to yield chitosan solutions with a pre-defined 3D geometry;

4 – Precipitation stage: remove the frozen solutions from the molds and immerse them into a NaOH 10% (w/v) solution for 48 hours. At the end of this process, mold-shaped chitosan hydrogels are obtained;

5 – Washing stage: wash the hydrogels intensively until reaches neutral pH, for approximately 6 days;

6 – Drying stage: dry the hydrogels at 40°C in a temperature controlled stove with circulating air, for approximately 5 days. At the end of this process, dense chitosan blocks are obtained with the average dimensions of 30 mm × 17 mm × 12 mm;

7 – Shaping stage: shape the chitosan blocks into the desired geometry, using conventional machining processes.

The optimized production process was tested by adding, independently, sorbitol and ethylene glycol to the dissolution process, in addition to glycerol. The goal was to evaluate not only the suitability of the production process to other materials, but also to study the effect of these plasticizers on the produced specimens. The results lead to following conclusions:

a) it was possible to dissolve and process all the materials, under the defined production conditions, obtaining 3D dense chitosan specimens capable of being machined and tested;

b) the results obtained do not rule out a particular plasticizer *a priori.* However, only two plasticizers were selected for the next experiments – glycerol and sorbitol. This decision considered the surface imperfections of the ethylene glycol specimens, which lead to the dispersion of results for the compression modulus and the compression strength, and also for not being approved as a pharmaceutical compound, according to current regulations.

This optimization study also selected the chitosan batch 3 as the most adequate for future productions. It was possible to dissolve the chitosan from this batch and to produce blocks able to be shaped by a milling machine. Additionally, the specimens originated by this chitosan batch allowed a better combination of mechanical properties determined by flexural tests.

These preliminary experiments also proved that the addition of plasticizers to the dissolution stage may interfere with the polymeric chain of chitosan, improving the processability and machinability of the chitosan dense blocks into specimens with the desired geometry. This result was important since it was not possible to produce specimens composed only with chitosan. In this case, brittle and non-uniform specimens were obtained, which easily broke when machining. To further study the effect of plasticizers, or even other materials (e.g. ceramics) on the final properties of chitosan specimens, a more intensive study is required to determine the influence of different concentrations.

The reagents used in future studies and experiments were the same used in this chapter, including the glycerol and sorbitol.

10. Mechanical behavior of different chitosan blends in the development of bioabsorbable implant products

To produce 3D dense chitosan implant products for orthopedic applications, it is essential that the final composition of such structures guarantees adequate stiffness and strength, able to comply with the bone tissue requirements. With this goal in mind, a study was planned to improve the mechanical behavior of the produced specimens by blending chitosan with different types of materials (plasticizers and ceramics), in the early stages of the development process. The mechanical evaluation was performed through flexural tests and nanoindentation tests. Complementary tests were performed through SEM and microCT analysis. After these tests, a final composition was selected for each type of material studied.

10.1. Blend chitosan with plasticizers

10.1.1. Production of rectangular specimens

According to the results of the preliminary studies, two plasticizers were selected to optimize the final composition of the chitosan blocks: glycerol and sorbitol. Therefore, three different concentrations of these plasticizers were added on the dissolution stage of the production process described in chapter 9.4. The concentrations were:

- Glycerol: 5% (w/v), 10% (w/v) and 15% (w/v);
- Sorbitol: 5% (w/v), 10% (w/v) and 15% (w/v);

Regardless of the plasticizer type and concentration level, the obtained chitosan blocks had the same appearance and brown color, as shown in Figure 10.1 and Figure 10.2.

Figure 10.1. Examples of 3D dense chitosan blocks obtained after blending chitosan with 15% glycerol.

Figure 10.2. Examples of 3D dense chitosan block obtained after blending chitosan with 15% sorbitol.

Each block was processed using a conventional milling machine (Optimum MF4). A 16 mm end mill cutting tool of high speed steel (HSS) was used at a low cutting speed to thin out each block into specimens with rectangular cross-section of 25 mm × 12 mm × 4 mm (average dimensions). Figure 10.3 shows examples of the specimens obtained after the shaping phase. The surface of the specimens was smooth and uniform.

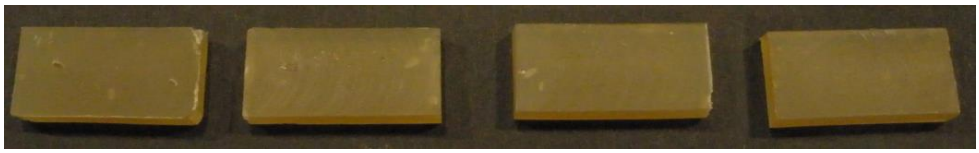

Figure 10.3. Specimens produced by blending chitosan with 5% sorbitol.

10.1.2. Results of the experimental evaluation

10.1.2.1. Flexural tests

Flexural tests were performed to study the mechanical behavior of the plasticizer specimens produced, according to the procedure described in chapter 7.1.2.1. Four specimens were tested for each plasticizer blend, except for the 10% and 15% sorbitol compositions. In this case, only three were tested (one specimen broke at the beginning of the test). Figure 10.4 exemplifies a three point flexural test running.

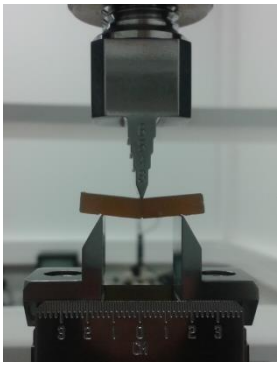

Figure 10.4. Three point flexural test of a specimen produced by blending chitosan with 10% glycerol.

The behavior of two plasticizers (the 10% compositions) to the imposed load is represented in the stress-strain curves of Figure 10.5.

The flexural modulus, flexural strength and the maximum flexural strain results obtained for each analyzed composition are indicated in Figure 10.6 to Figure 10.8. The statistical evaluations considered for the graph bars were performed only for pairs of plasticizers tested under the same concentration level. The remaining results are indicated in the Appendix A.3.

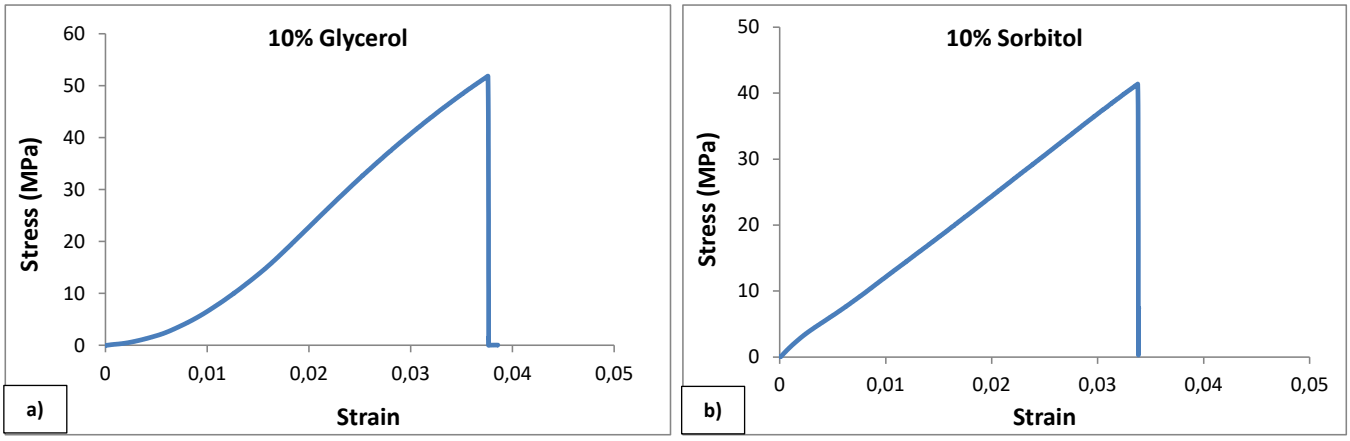

Figure 10.5. Stress-strain curves obtained for specimens composed by a) 10% glycerol and b) 10% sorbitol.

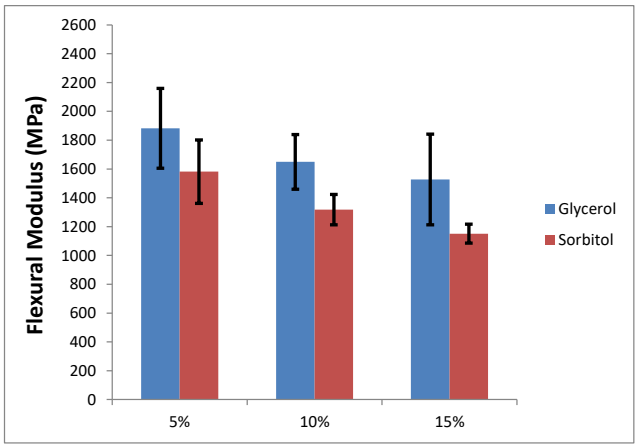

Figure 10.6. Flexural modulus obtained for the specimens produced with different blends of chitosan with plasticizers.

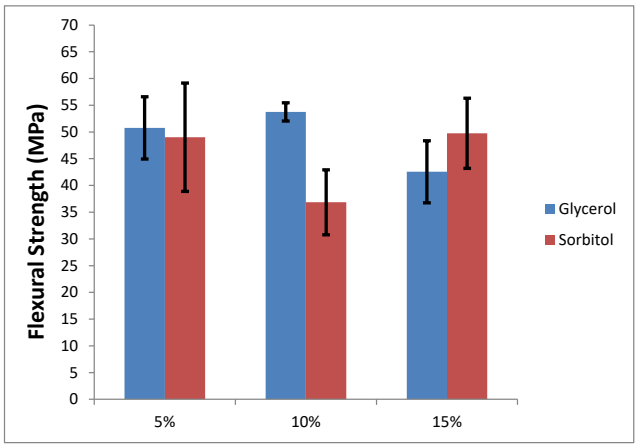

Figure 10.7. Flexural strength obtained for the specimens produced with different blends of chitosan with plasticizers.

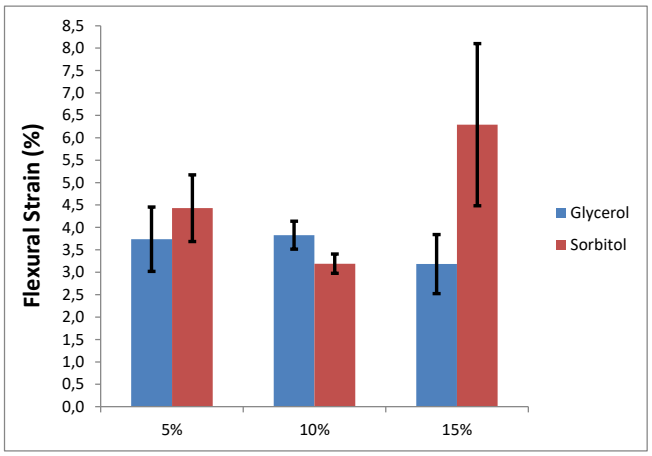

Figure 10.8. Flexural strain obtained for the specimens produced with different blends of chitosan with plasticizers.

The stress-strain curves reveal identical behavior of the two compositions when subjected to transverse loading. The fracture of the specimens occurred with practically no plastic deformation. During the tests, crack initiation was observed at the bottom of the specimens, where higher tensile stresses develop. Crack propagation quickly occurred giving rise to specimens' fracture with a brittle surface.

The results show that the mean flexural modulus decreased with the increasing concentration of plasticizers, but the same was not observed for the flexural strength and maximum flexural strain results. Globally, the 10% glycerol composition revealed better combination of these three mechanical properties.

For the flexural strength, the highest mean value was obtained for the 10% composition (54 MPa), while the specimens with 15% sorbitol presented higher maximum flexural strain values. However, for all the assessed properties, the statistical tests revealed weak evidence that the means of the two groups of plasticizers with the same concentration reflect a true difference between the populations from which the groups were sampled (p-value > 0,05).

10.1.2.2. Nanoindentation tests

Nanoindentation tests were performed according to the procedure described in chapter 7.1.3.1. In average, 8 indentations were made for each plasticizer/concentration specimen. Figure 10.9 presents the indentation hardness values whereas Figure 10.10 shows the indentation modulus.

The statistical evaluations considered in the graph bars were performed only for pairs of plasticizers tested under the same concentration level. The remaining results are indicated in the tables in the Appendix A.3.

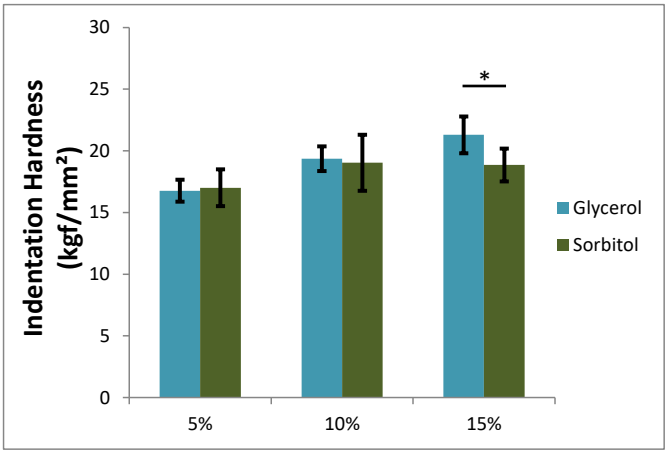

Figure 10.9. Indentation hardness obtained for the specimens produced with different blends of chitosan with plasticizers (*p-value < 0,05).

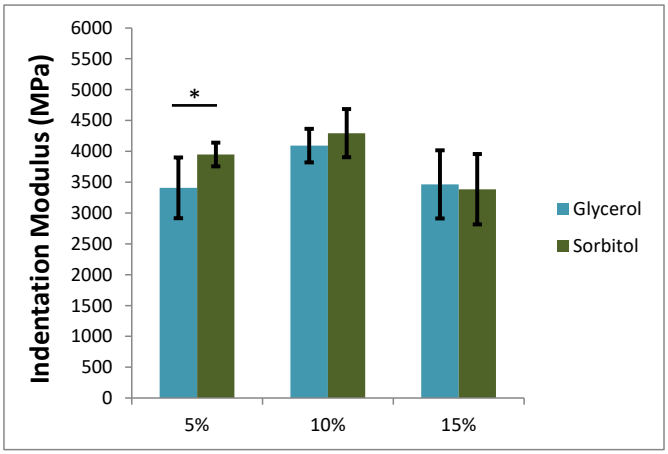

Figure 10.10. Indentation modulus obtained for the specimens produced with of chitosan with plasticizers (*p-value < 0,05).

The mean indentation hardness value increases with increasing concentration of glycerol. Similar results were obtained for sorbitol concentrations, although the 10% and 15% concentrations of this plasticizer have practically the same mean value. The highest mean value for the indentation hardness was obtained for 15% glycerol, which stands out from the corresponding concentration of sorbitol (p-value = 0,0039). In this case, the nanoindentation hardness was 21,3 kgf/mm^2.

Comparing the results of the indentation modulus among themselves, the highest mean value was obtained for 10% sorbitol. If the analysis is only restricted to the values obtained for glycerol, the highest mean value is for the composition of 10% glycerol, with indentation modulus being 4.093 MPa. The *t*-tests performed to all concentration pairs of glycerol and to all concentration pairs of sorbitol reveal that there is strong evidence that the mean values of both 10% concentrations are different from the other compositions (5% and 15%).

10.1.2.3. microCT analysis

MicroCT analysis was performed for one specimen of each plasticizer composition, according to the experimental procedure described in chapter 7.2.2.1. Table 10.1 indicates the quantitative (percentage) evaluation of closed pores (non-connected cavities) that were present in the specimens. Additionally, Figure 10.11 shows images (frontal plane, x0z) from the interior of the 10% plasticizers' blends, obtained after applying the volume rendering reconstruction software (CTVox).

Table 10.1. Quantification of the closed pores present in all plasticized specimens.

Content (w/v) of plasticizer material in the specimen (%)		**microCT analysis: Closed pores (%)**
Glycerol	5	0,31
	10	0,75
	15	1,20
Sorbitol	5	0,21
	10	0,63
	15	0,53

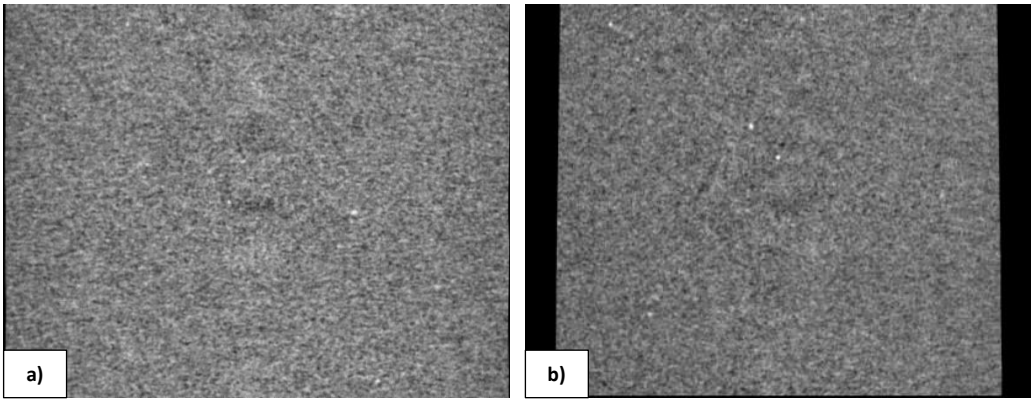

Figure 10.11. Frontal (x0z) images of specimens produced by blending chitosan with a) 10% glycerol and b) 10% sorbitol, obtained through microCT analysis.

The results in Table 10.1 reveal that the specimens produced either by adding glycerol or sorbitol are dense, showing a maximum porosity level of 1,20%. Figure 10.11 shows the inner structure of the specimens, revealing a continuous material with few black areas (pores).

10.1.3. Discussion

The preliminary results presented in chapter 9 showed that the addition of glycerol and sorbitol favors the processability of chitosan specimens. To optimize the composition that helps to improve, at the same time, the processability and the mechanical properties of the final specimens, it was necessary to study concentrations beyond 10%. Therefore, two other concentrations were selected for this study: 5% and 15%.

Flexural tests:

The mechanical properties of the bulk specimens were tested at flexion, contrary to what happened in the preliminary study where the specimens were tested to compression (chapter 9). This change occurred to more easily perceive the behavior of specimens until break, namely their ductility. For both plasticizers, the mean flexural modulus value was higher for lower concentrations of plasticizers than higher concentrations, which was more evident for the sorbitol condition. The effect of the plasticizer concentration on both the mean flexural strength and flexural strain values was not so evident. Comparing each plasticizer alone, the highest mean values for the flexural modulus, strength and strain were obtained, respectively, for the 5% glycerol, 10% glycerol and 15% sorbitol compositions. Despite these results, it can be stated that the 10% glycerol composition has lower dispersion of results, especially in the flexural strength. Additionally, it was the best combination of flexural results.

One 10% sorbitol specimen and one 15% sorbitol specimen broke at the beginning of the flexural tests. This may be related with small pores at the surface of the specimens, which are favorable sites of cracks initiation and propagation, or due to small defects resulting from the shaping process.

Several studies report that the strength of chitosan films decreases as the content of glycerol increases, contrary to what happens with the elongation at break [390,398,399]. This occurs because glycerol penetrates through the polymer matrix, interfering with the polymer chains and promoting the polymer mobility [398,399]. The results in this thesis are in accordance with such findings.

Chen and Zhao [382] tested the mechanical properties of chitosan films produced with glycerol and sorbitol and did not find major differences on their mechanical properties. They concluded that sorbitol may also act like glycerol due to its similar carbon structure with hydroxyl groups along the polymer chain [382]. However, Srinivasa *et al.*[384] reported that sorbitol films are more flexible than films plasticized with glycerol, which are in accordance with the results found in this thesis when the 15% compositions are compared.

Nanoindentation tests:

In this study, the indentation hardness and the indentation modulus were determined by the Oliver and Pharr method, as described in chapter 7.1.3. This method assumes that the contact between the material surface and the tip is purely elastic, and therefore the material undergoes purely elastic recovery during the unloading [400]. However, for most polymers and testing conditions, the indentation of the material is influenced by viscoelasticity, which manifests itself as a change in depth for a constant applied load [284,400]. This effect leads to an

increase in the contact stiffness, as a result of poor non-linear curve fitting of the unloading data, and theoretically invalid fitting exponents [401] . To minimize this effect, it was imposed a hold time of 15 seconds between each loading and unloading cycle. However, if the hold period is too short or the unloading rate is too low, the estimation of the contact stiffness is compromised as well [400,402]. Additionally, other phenomena can affect the measurements such as the thermal drift and the sinking-in or pilling-up around the indenter, which depends of the strain-hardening properties of the material, the indentation size effect, the residual stresses, among others [403,404]. The presence of these effects, during the indentation tests, cause the overestimation of the elastic modulus of the material when compared with the values of the elastic modulus determined using conventional macroscale mechanical testing [401]. These phenomena may also explain other different trends between the flexural and the indentation modulus: the flexural modulus decreases as glycerol concentration increases in the specimens, contrary to what has been observed in the indentation studies. These observations may occur due the previously mentioned factors (e.g. viscoelasticity), or because the specimens are denser on their surface (fewer pores) as the concentration of glycerol increases.
Different studies have been published on the determination of the modulus and hardness of chitosan materials, measured by nanoindentation. However, most of them are focused primarily in films and porous structures. Mishra and Kannan [405] analyzed four different chitosan/PVA polymer composite films used in a titanium implant coating and they registered hardness values from 0,20 to 0,35 GPa and indentation modulus from 10 to 35 GPa, according to the concentration of PVA and the water content of the samples. Converting the values in Figure 10.9 and Figure 10.10 to GPa, the results of the nanoindentation resulted in hardness and modulus values varying from 0,16 to 0,21 GPa and 3,4 to 4,3 GPa, respectively. However, comparing the results obtained in this thesis with results obtained in other studies, for chitosan compositions or even other polymers, may lead to misinterpretations. Indentation hardness and modulus are influenced by potential variations in microstructure, semicrystalline morphology, anisotropy, molecular weight, crosslinking density, etc. [406], as well as the conditions of the experiments (e.g. maximum load and loading speed).

microCT analysis:

The microCT tests were carried out in this stage with the purpose of observing the internal microstructure of the specimens and quantifying their porosity. The results indicate a lower porosity level under the conditions of the microCT equipment (image pixel size of 7,76 µm). Although the values presented in Table 10.1 lack experimental validity, obtainable if more specimens were analyzed by microCT, the values range indicate that all the specimens exhibit high density and have no significant pores. The low porosity level is also observed in the images of Figure 10.11. These results are in accordance to the SEM analysis performed in the preliminary tests (Figure 9.9 to Figure 9.11).

Plasticizer selection:

The chitosan blend with 10% glycerol was selected for the next study.

10.2. Blend chitosan with ceramics

10.2.1. Selection of the ceramic materials

The materials that were selected for this study included different calcium phosphate-based ceramic materials, namely:

- HA powder (acronym used: HA);
- biphasic powder mixture of 70% HA: 30% β-TCP (acronym used: HA-TCP);
- biphasic granules mixture of 70 % HA: 30% β-TCP (acronym used: granules).

This selection included ceramics with different particle dimensions and compositions. Since biphasic mixtures are widely used in bone graft substitutes they were included in this study in addition to pure HA. All the ceramic materials were produced by Altakitin S.A.

The powders had a particle size distribution of 7 µm (d0,9) whereas the granules size ranged from 75 µm to 125 µm. Figure 10.12, Figure 10.13 and Figure 10.14 show the particle size distribution of the three ceramic materials.

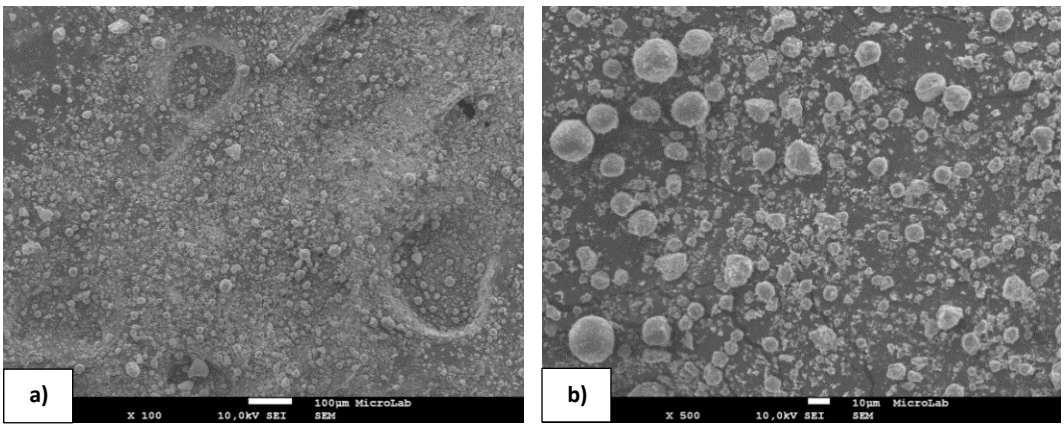

Figure 10.12. SEM images of the HA particles, using a) 100X magnification and b) 500X magnification.

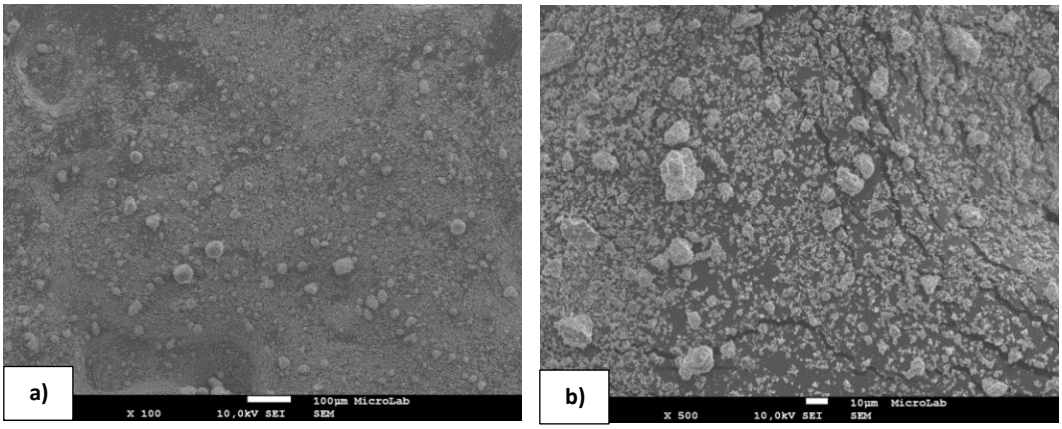

Figure 10.13. SEM images of the HA-TCP particles, using a) 100X magnification and b) 500X magnification.

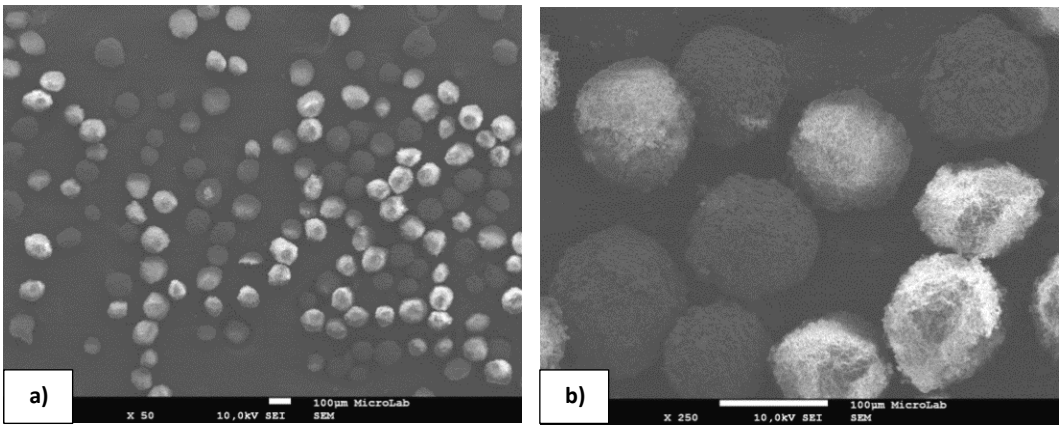

Figure 10.14. SEM images of the granules particles, using a) 100X magnification and b) 250X magnification.

The previous figures show a homogeneous distribution of the different particles, in which the powders have variable dimensions while the spherical granules have uniform dimensions.

10.2.2. Production of rectangular specimens

New specimens were produced by adding HA, HA-TCP and granules to the production process described in chapter 9.4. The production of these specimens included the addition of 10% (w/v) of glycerol, according to the results of the previous study. The concentration levels of the three ceramics took into account the desired amount of these materials on the final weight of each block. Therefore, the different concentrations of each ceramic material were:

- HA: 5% (w/w), 10% (w/w), 15% (w/w)
- HA-TCP: 5% (w/w), 10% (w/w), 15% (w/w)
- Granules: 5% (w/w), 10% (w/w), 15% (w/w)

The new blocks had all white color but had a different aspect if the material added to chitosan was either HA and HA-TCP or the granules. In this case, the blocks produced with granules were slightly rough while the other blocks were smoother. Examples are shown in Figure 10.15.

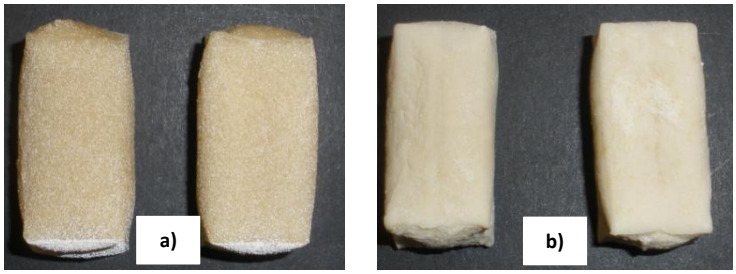

Figure 10.15. Examples of blocks produced by blending chitosan with: a) 10% granules and b) 10% HA.

In general, the dispersion of the ceramics was more difficult for the 15% concentrations and for the powders than for the granules, but in none of the situations were noticed different concentration gradients during the production stages (no sedimentation). To confirm a uniform dispersion of ceramic particles, two blocks of the highest concentration level (15%) were cut in two distinct zones, near the bottom and near the top of the blocks. The blocks studied were produced by blending either HA or granules to chitosan. SEM analyses were

performed in the resultant cross sections, and the dispersion of the ceramic particles was analyzed using the image analysis software ImageJ. Figure 10.16 and Figure 10.17 show the images assessed by this software.

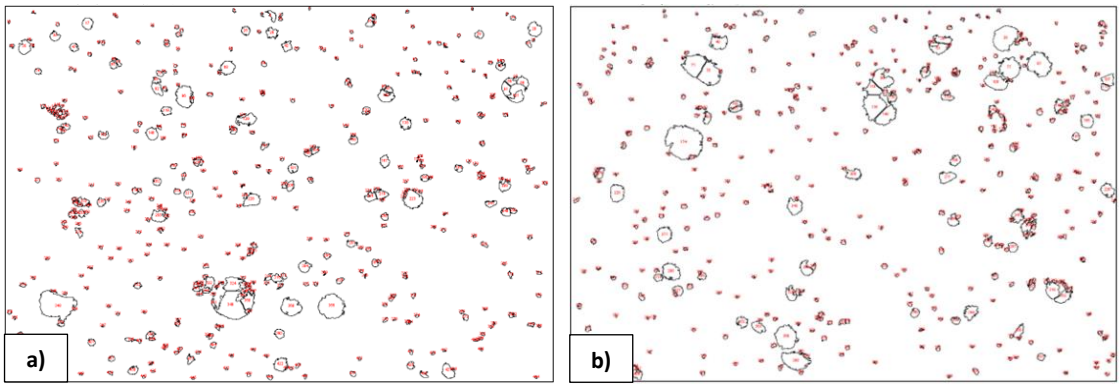

Figure 10.16. Analysis of different cuts of the block produced with HA, through the ImageJ software: a) bottom part cross section (445 particles counted) and b) top part cross section (414 particles counted).

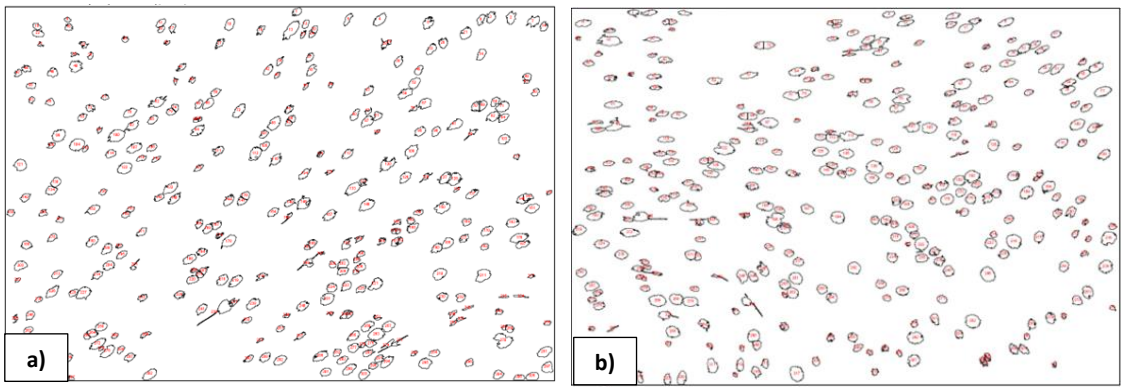

Figure 10.17. Analysis of different cuts of the block produced with granules, through the ImageJ software: a) bottom part cross section (309 circular particles counted) and b) top part cross section (323 circular particles counted).

The results of the previous figures indicate an evenly distribution of particles in the bottom and top part of the blocks. For example, 309 circular particles were counted on the bottom cross section while 323 particles were counted on the top cross section of the block composed by 15% granules (Figure 10.17).

Once again, specimens of rectangular cross section were machined using a conventional milling machine, with the average dimensions 25 mm × 12 mm × 4 mm. These ceramic specimens revealed the same color and surface characteristics of the respective blocks, as represented in Figure 10.18. However, manual machining caused small damages of the specimens, especially in their vertices and face transitions.

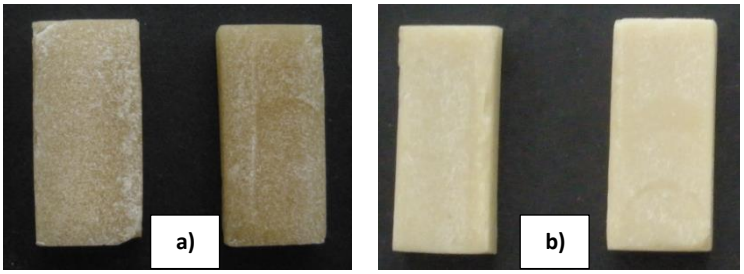

Figure 10.18. Examples of specimens produced by blending chitosan with: a) 10% HA and b) 10% granules.

10.2.3. Results of the experimental evaluation

10.2.3.1. Flexural tests

Flexural tests were performed to four specimens of each ceramic blend, according to the procedure described in chapter 7.1.2.1. The behavior of the 10% ceramic compositions to the imposed load is represented in the stress-strain curves indicated in Figure 10.19. Figure 10.20, Figure 10.21 and Figure 10.22, which show, respectively, the flexural modulus, the flexural strength and the maximum flexural strain results. The statistical evaluations considered in the graph bars were performed only for pairs of ceramics tested under the same concentration level. The remaining results are presented in the Appendix A.3.

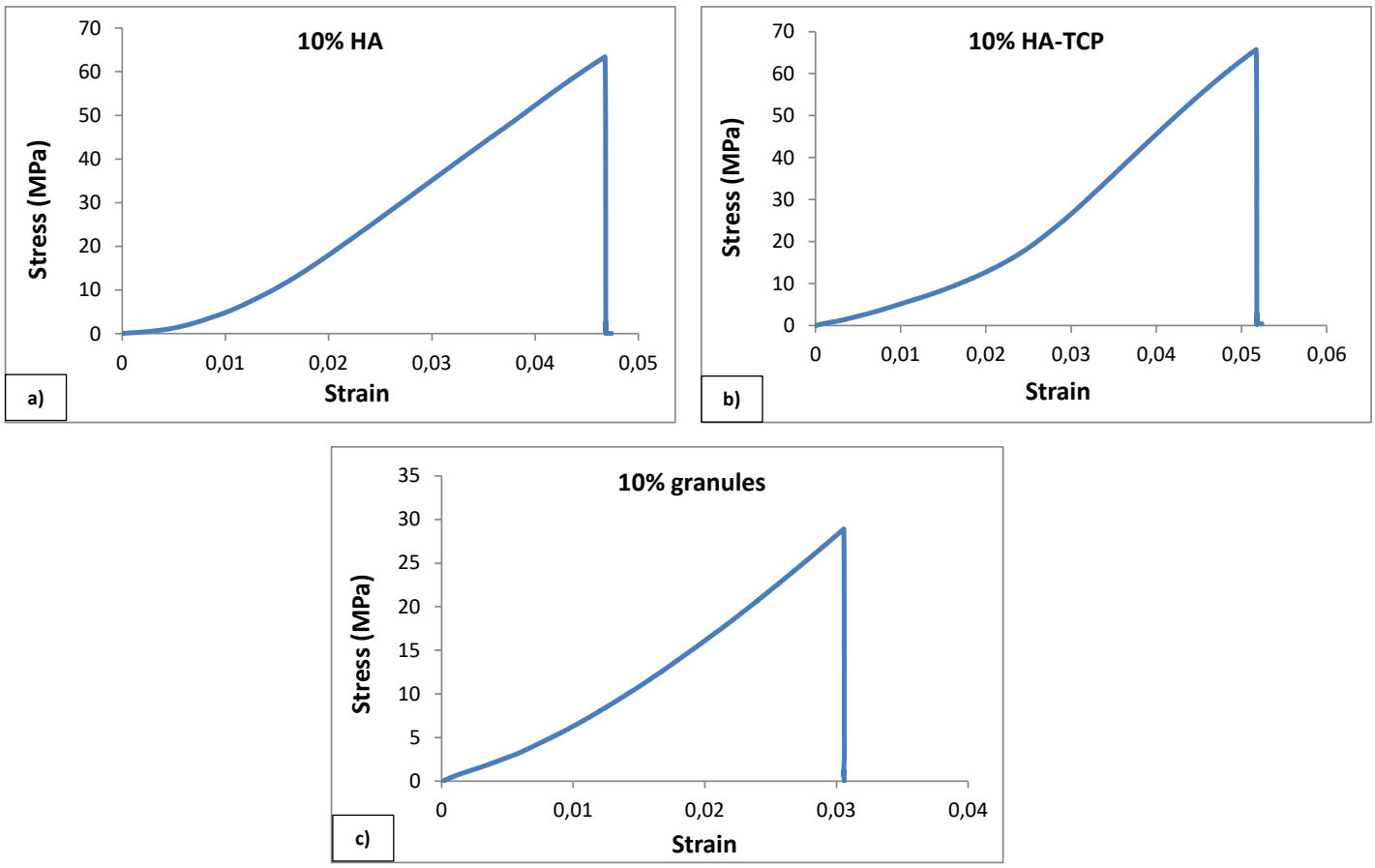

Figure 10.19. Stress-strain curves obtained for one specimen composed by a) 10% HA, b) 10% HA-TCP and c) 10% granules.

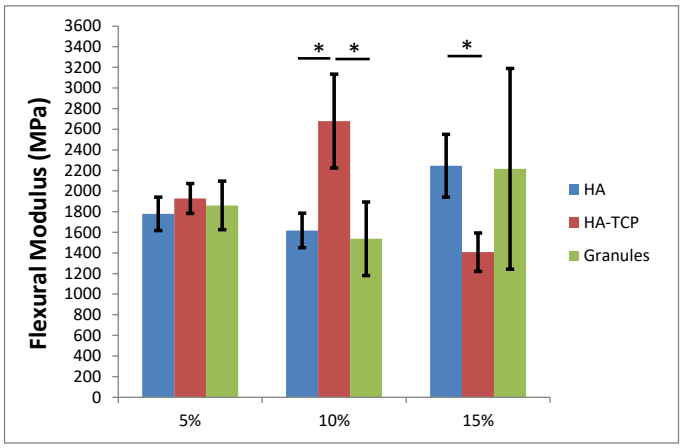

Figure 10.20. Flexural modulus obtained for the specimens produced with different blends of chitosan with ceramics (*p-value < 0,05).

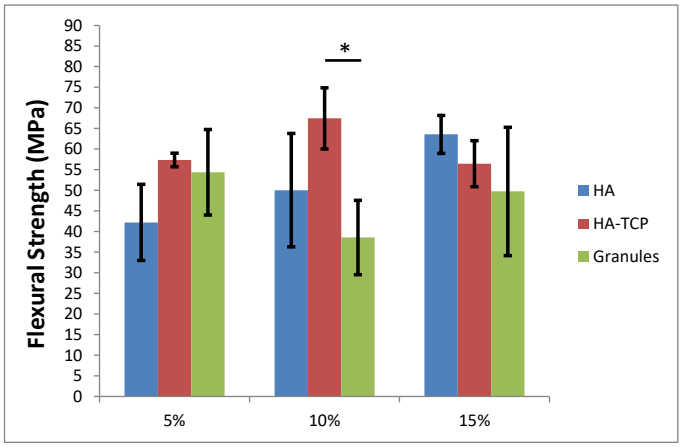

Figure 10.21. Flexural strength obtained for the specimens produced with different blends of chitosan with ceramics (*p-value < 0,05).

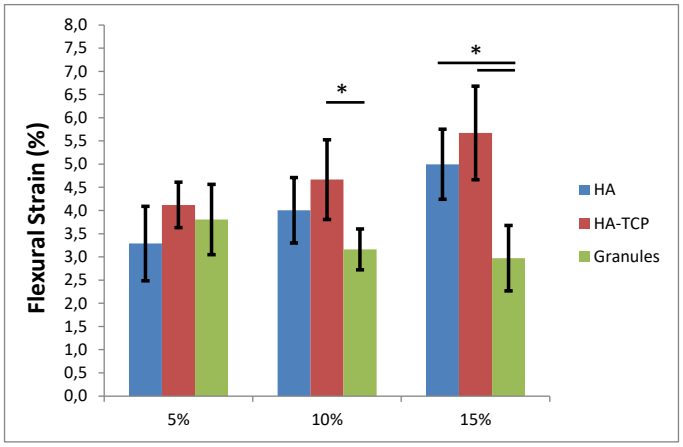

Figure 10.22. Flexural strain obtained for the specimens produced with different blends of chitosan with ceramics (*p-value < 0,05).

The stress-strain curves reveal that the fracture of the specimens occurred with practically no plastic deformation, as happened for the plasticizer specimens (chapter 10.1.2.1.) The crack initiation was observed at the bottom of the specimens and quickly propagated giving rise to specimens' fracture with a brittle surface.

The mean flexural modulus results (Figure 10.20) were similar for all 5% ceramic blends. However this was not observed for the other concentrations. The highest mean value was obtained for the 10% HA-TCP and for the 15% HA and 15% granules - 2679 MPa, 2245 MPa and 2215 MPa, respectively. Moreover, the mean flexural modulus was similar for these last two ceramics in each concentration level. Adding HA-TCP to the specimens increases their flexural modulus, reaching a maximum mean value for the 10% concentration. On the other hand, the HA-TCP granules revealed lower mean value at 10% concentration, but a higher mean value for the 15% concentration, which is accompanied by a large dispersion of results.

The results in Figure 10.21 indicate that the higher value for the HA-TCP and HA was attained for the 10% and 15% concentrations – 68 MPa and 64 MPa, respectively. These results follow the same trend observed for the flexural modulus results except for the granules, whose highest mean value was obtained for the 5% concentration (54 MPa). However, the *t*-tests performed on all the observations of this ceramic material revealed that there is weak evidence that the means obtained, for each concentration, reflect a true difference between the populations from which the groups were sampled. Therefore, the mean flexural strength obtained for the 5% granules is not truly different from the other mean values, obtained for the other concentrations of this ceramic material.

Regarding the maximum flexural strain (Figure 10.22), the mean value increases with increasing concentrations of HA and HA-TCP, but the opposite observation is made for the granules. The highest mean value (5,7%) was obtained for 10% HA-TCP blend.

10.2.3.2. Nanoindentation tests

Nanoindentation tests were performed according to the procedure described in chapter 7.1.3.1. In average, 8 indentations were performed for each chitosan blend with ceramics. The results are indicated in the next figures. The statistical evaluations considered in the graph bars were performed only for pairs of ceramics tested under the same concentration level. The remaining results are presented in the Appendix A.3.

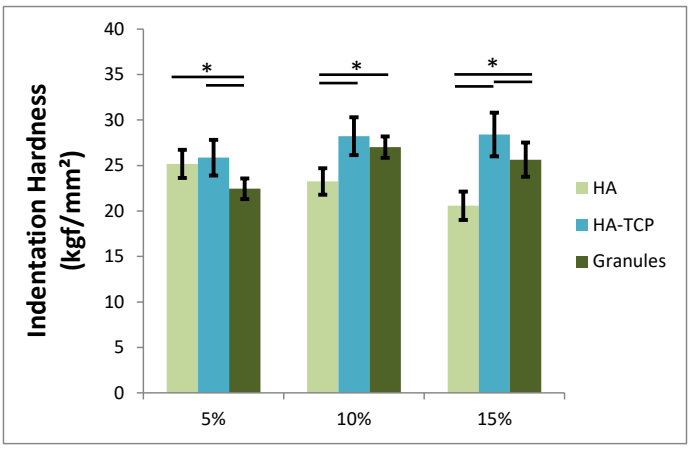

Figure 10.23. Indentation hardness obtained for the specimens produced with different blends of chitosan with ceramics (*p-value < 0,05).

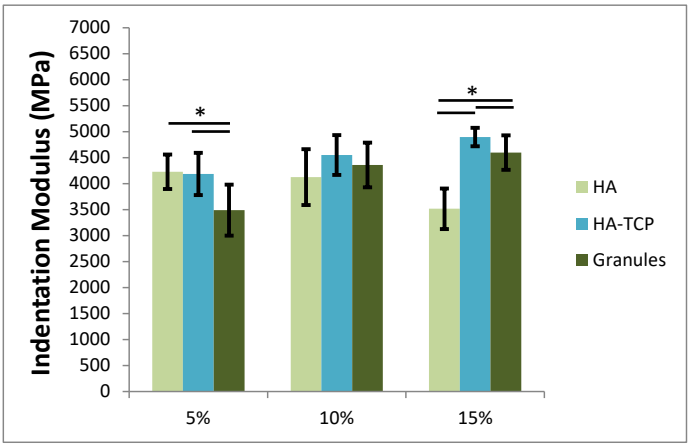

Figure 10.24. Indentation modulus obtained for the specimens produced with different blends of chitosan with ceramics (*p-value < 0,05).

The nanoindentation results reveal that the highest mean values were obtained for the 10% and 15% concentrations of HA-TCP. The indentation hardness (Figure 10.23) of the chitosan-based specimens increases with increasing concentrations of HA-TCP, remaining practically the same for the 10% and 15% concentrations (~28 kgf/mm^2). The opposite observation is made for the HA, whose increasing content promotes a decrease in the measured hardness. For the granules, the indentation hardness increases until 10% concentration (~23 kgf/mm^2), and then decreases slightly.

The indentation modulus results (Figure 10.24) indicate higher mean values for increased content of HA-TCP and granules in the specimens. Once again, an opposite observation is made for the specimens with increasing content of HA. Like in the hardness evaluation, the highest mean value was obtained for the concentration of 15% HA-TCP (4.896 MPa), followed by the concentration of 10% (4.550 MPa).

10.2.3.3. microCT analysis

The microCT analyzes were performed in one specimen of each ceramic blend, according to the experimental procedure described in chapter 7.2.2.1. Table 10.2 shows the results of the quantitative study, where the percentage of ceramic dispersed and closed pores were assessed.

Table 10.2. Quantification of closed pores and dispersion of ceramic material in all specimens with ceramics.

Content (w/w) of ceramic material in the specimen (%)		microCT analysis:	
		Ceramic dispersed (%)	Closed pores (%)
HA	5	0,34	0,36
	10	0,07	1,63
	15	0,13	1,57
HA-TCP	5	4,50	2,17
	10	11,08	0,08
	15	15,73	3,09
Granules	5	0,68	1,65
	10	0,49	2,99
	15	1,41	6,90

The results of previous table show that, globally, the porosity increases as more ceramic material is added to the specimens and the granules specimens have higher porosity while the HA specimens have lower porosity. The initial theoretical percentage of ceramic dispersed in the specimens was only confirmed for the composition with HA-TCP.
Figure 10.25 shows images (frontal plane, x0z) from the interior of each 10% ceramic blend, obtained after applying the volume rendering reconstruction software. Larger areas of black color are perceptible in the granules image (Figure 10.25 c), confirming the higher level of porosity of these specimens when compared to the remaining. In this case, it was easier for the operator to define a second grey threshold, which represents the ceramic material added.

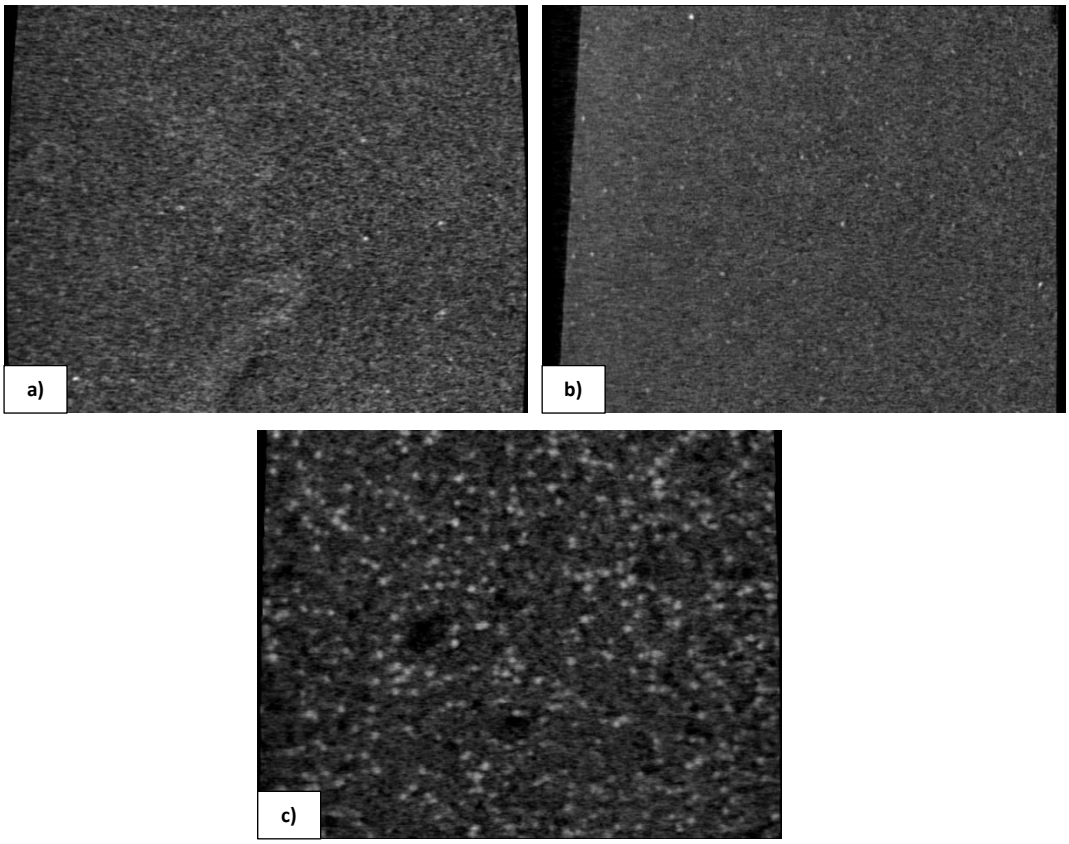

Figure 10.25. Frontal (x0z) images of specimens produced by blending chitosan with a) 10% HA, b) 10% HA-TCP and c) 10% granules, obtained through microCT analysis.

10.2.4. Discussion

To reach the properties of the synthetic polymers described in Table 2.3 (chapter 2.3.1.), the properties of the blend selected previously were improved by adding different concentrations (5%, 10% and 15%, w/w) of calcium phosphate-based ceramic materials: HA and a biphasic mixture of 70% HA and 30% β-TCP with two different particle sizes. Therefore, the improvements were carried on from the plasticizer blend optimized in the previous study (blend of chitosan with 10% glycerol) to continue to take advantage from the plasticizer effect of chitosan specimens.
Contrary to the previous observations, which reveal similar aspect between the different chitosan blends with glycerol and sorbitol, the new specimens had different surface characteristics if the material blended with chitosan-glycerol was either HA and HA-TCP or the

granules. Spherical particles were noted on the surface of the specimens with granules and these surfaces were slightly rough. Despite the increased difficulty to disperse the 15% concentrations, the specimens did not reveal different concentration gradients of the ceramic materials, confirmed by image analysis on the cuts performed on the top and on the bottom of the blocks. The existence of this gradient would render the specimens as non-homogeneous and would have a negative impact in their mechanical behavior. In situations where the dispersion was more difficult, faster mixing velocity was required, which may have introduced more air bubbles into the solutions, leading to increased porosity.

Manual machining caused damages in some parts of the specimens, which were promoted by the brittle characteristics of the ceramic specimens.

Flexural tests:

The mean flexural modulus and flexural strength values were obtained for the 10% HA-TCP blend. This may indicate an optimal homogenization of this powder concentration in the specimens. On the other hand, the maximum mean flexural strength value was obtained for the 15% HA-TCP blend. However, the statistical tests revealed weak evidence that the means of the 10% HA-TCP and 15% HA-TCP groups reflect a true difference between the populations from which the groups were sampled (p-value > 0,05).

The results were expected to be similar for the HA and HA-TCP blends. However, the two means are only similar for the 5% concentration and 15% concentration (in this latter case, only for the flexural strength property). Once again, the better homogenization of the HA-TCP in the specimens could explain such observations.

The results also indicated that it is difficult to benefit from ceramic particles with larger sizes, since the increase concentration of the granules led to the dispersion of results, which are more evident in the flexural modulus and flexural strength measures.

Comparing all the results obtained in this study, the specimens produced with 10% HA-TCP present better results for the two main properties assessed; flexural modulus of 2,7 GPa and flexural strength of 67 MPa. Comparing these results with the results obtained for the specimens produced with 10% glycerol, the flexural modulus increased by 60% and the flexural strength by 25%.

Hu *et al.*[407] produced a composite for the development of small circular rods via *in situ* precipitation by blending chitosan with HA. They reported a flexural strength and modulus of 86 MPa and 3,4 GPa. In this thesis, these two values were slightly lower. Hasirci, *et al.*[408] studied the behavior of different polymer materials used in the construction of bioabsorbable plates and reported a flexural strength higher than 60 MPa for PLGA and higher than 100 MPa for PLA. Therefore, the flexural strength obtained for 10% HA-TCP blend is comparable to the value obtained by Hu *et al.*[407], for the PLGA polymer.

Nanoindentation tests:

For both the indentation hardness and indentation modulus measures, the highest mean values were obtained for the 15% HA-TCP blend followed by the 10% HA-TCP blend. However, the populations of these two groups are statistically different for the indentation modulus (p-value = 0,0438). While the increase of the HA-TCP concentration may favor a less optimal distribution of the powder in the specimen, which contributes to the reduction of the elasticity of the bulk material, in the case of the indentation tests, it may contribute to increase the indentation hardness and the indentation modulus of the nanostructure surface of such specimens [404]. In addition to the reasons explained in chapter 10.1.3. that may contribute to

the overestimation of the indentation modulus (e.g., sinking-in is likely to occur when the indentation is made on ceramic materials [403]), the nanoindentations were performed after viewing and choosing the indentation area, which most of the time did not present significant defects.

Comparing the nanoindentation results of the 10% HA-TCP blend with the results obtained for the chitosan blends with 10% glycerol (chapter 10.1.), it is observed that the mean hardness value increased by 44% and the mean indentation modulus by 11%.

Several publications are available on the study of the micro- or nanoindentation hardness of chitosan/HA porous composite materials. Danilchenko *et al.*[409] studied non-porous formulations and found that the micro hardness (Hardness Vickers, HV) varied from 0.12 to 0.22 GPa, according to the HA content. Although these results correspond to micro hardness evaluations, studies report that the nanoindentation hardness is about 10%-30% larger in magnitude than the micro hardness since nanoindentation uses the projected contact area at full load instead of the residual projected area measured by the diagonal lengths of an indentation [281]. Katti *et al.*[410] performed nanoindentation studies on a scaffold formulation with chitosan/montmorillonite/HA, using a 100 µN load. They found a mean indentation hardness and modulus of 0,47 GPa and 9,4 GPa, respectively. For mixtures only with chitosan/HA, these values were 0,38 GPa and 7,6 GPa, respectively. The results obtained in this thesis (0,28 GPa and 4,6 GPa, respectively, for the 10% HA-TCP blend) were lower if compared with the results obtained by Katti *et al.* [410] However, this comparison is merely for informative purposes since the material structures are different and the indentations were not made under the same force.

microCT analysis:

The microCT analysis showed that the samples have more porosity as the ceramic material dispersed in the specimens increases. However, the porosity observed for 10% HA-TCP was lower than the porosity of 5% HA-TCP, which may indicate an optimal dispersion of this HA-TCP concentration in the specimens. However, the results lack experimental validity, which could be achieved if more specimens were analyzed by microCT.

The porosity level of the ceramic specimens (Table 10.2) was higher than the porosity obtained for the plasticized-only specimens (Table 10.1). This may be related with air retention, as consequence of the higher rotation speed employed to uniformly disperse the ceramic materials in the solution.

Two levels of grey scales were distinguished in the CTAn program. Considering the limitation of the technique and the operator conditionings, namely in the definition of the material threshold it was only possible to quantify the granules distribution. Additionally, the possibility of image reconstruction failures (e.g. ring and beam hardening artifacts) is not completely ruled out. These failures may have led to operator errors, for example, in the voids definition in the images.

Ceramic selection:

The chitosan-glycerol blend with 10% HA-TCP was selected for further experiments.

10.3. Conclusion

The main goal of this study was to improve the mechanical properties of 3D dense chitosan-based specimens though the optimization of their compositions. In the first part of this work,

three different glycerol and sorbitol concentrations were added to the dissolution stage of the production process. The mechanical performance of these specimens was tested at flexion and the nanoindentation hardness and modulus were determined through a Berkovich indenter. Based on the results obtained, the chitosan blend with 10% glycerol was chosen for the next study. This composition presented the highest combination of all measured properties – flexural modulus, flexural strength, flexural strain, indentation hardness and indentation modulus.

In the second part of this work, three different concentrations of ceramic materials were blended to chitosan together with the optimized plasticizer concentration. These consisted in HA, HA-TCP and granules. These last two materials differ in their particle size. According to the results of the flexural and nanoindentation tests, the selected composition was 10% HA-TCP. In this case, the highest mean values for the flexural modulus and flexural strength were, respectively, 2,7 GPa and 67 MPa, increasing by 60% and by 25%, respectively, if compared with the results obtained for the specimens produced by adding only 10% glycerol. These values agree with the mechanical properties associated to the current bioabsorbable implants (Table 2.3), which reveal the potential of the chitosan blends in the development of chitosan-based product implants.

The level of specimens' porosity was also quantified through the microCT tests, proving that these are mostly dense and therefore their mechanical properties will not be compromised.

11. Biological behavior of the chitosan-based compositions selected for the development of bioabsorbable implant products

The blends studied and selected in the previous chapter were biologically evaluated to define its degradation profile (that results from the immersion of the produced specimens in a lysozyme solution) and to analyze the ability of MSCs to undergo *in vitro* osteogenic differentiation when they are placed into contact with these materials.
The goal of this study is to confirm the good biological properties of chitosan-based compositions and to detect if there are differences in the biological behavior of the chitosan blends produced with and without the ceramics.

11.1. Production of rectangular specimens

Two groups of specimens with rectangular cross section were produced according to the production process described in chapter 9.4., using the materials selected in chapter 10. The specimens produced by blending chitosan with 10% (w/v) glycerol are described as Ch+Gly and the specimens produced by blending chitosan with 10% (w/v) glycerol and 10% (w/w) of HA-TCP are described as Ch+Gly+HA-TCP. The resulting blocks were shaped (stage 7) by a computer numerical control (CNC) milling machine (Mikron VCE 500) to the dimensions of 25mm × 12 mm × 4 mm using a hard metal cutting tool (end mill) with 8 mm of diameter. The spindle rotation was 800 rpm and the tool travelling at an axial speed was 800 mm/min.
The resulting specimens showed a good appearance and surface finish and they were smooth to the touch. Figure 11.1 shows one specimen from each composition.

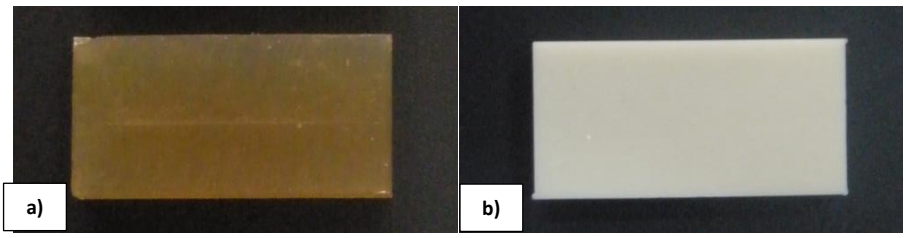

Figure 11.1. Examples of specimens with different compositions: a) Ch+Gly and b) Ch+Gly+HA-TCP.

Additionally, groups of small rectangular specimens were cut in a conventional milling machine using a slitting saw cutting tool from HSS. From one original specimen, six small specimens with average dimensions of 7,2 mm × 5 mm × 4 mm were obtained as depicted in Figure 11.2.

Figure 11.2. Examples of small Ch+Gly+HA-TCP specimens.

The specimens of the previous figure were engineered to be used in the differentiation tests described in chapter 11.3.
A control group of PLA specimens was also produced by a rapid prototyping machine (Ultimaker 2), as shown in Figure 11.3. These bulky specimens were produced for the degradation tests to simulate the behavior of this synthetic polymer under the same degradation conditions used to study the chitosan-based specimens. Therefore, the PLA specimens were produced with the same dimensions: 25 mm × 12 mm × 4 mm. The print speed was 60 mm/s, the travel speed 120 mm/s, the layer height 0,1 mm and the printing temperature was 200°C. Note that the PLA used as control is not a medical grade material, as reported by the Ultimaker technical sheet.

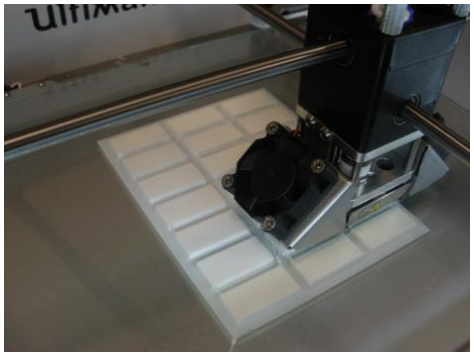

Figure 11.3. Production of PLA specimens by rapid prototyping machine (3D printing).

11.2. Degradation behavior

The degradation tests were performed according to the procedure described in chapter 7.5.2.1. Two degradation periods were defined for this study: 12 weeks and 24 weeks. The lysozyme was weekly replaced, to guarantee continuous activity, with the pH always remaining close to 7, which did not impair the lysozyme activity. In the end of each degradation period, four specimens from each of the three compositions (Ch+Gly, Ch+Gly+HA-TCP and PLA) were removed from both the lysozyme solution and the PBS solution, and their wet weight, dry weight and their flexural properties were determined.
Figure 11.4 shows the swelling ratio results at the end of the degradation periods. The statistical evaluations were performed only for groups of materials tested under the same degradation condition. The remaining statistical results are indicated in the Appendix A.4.

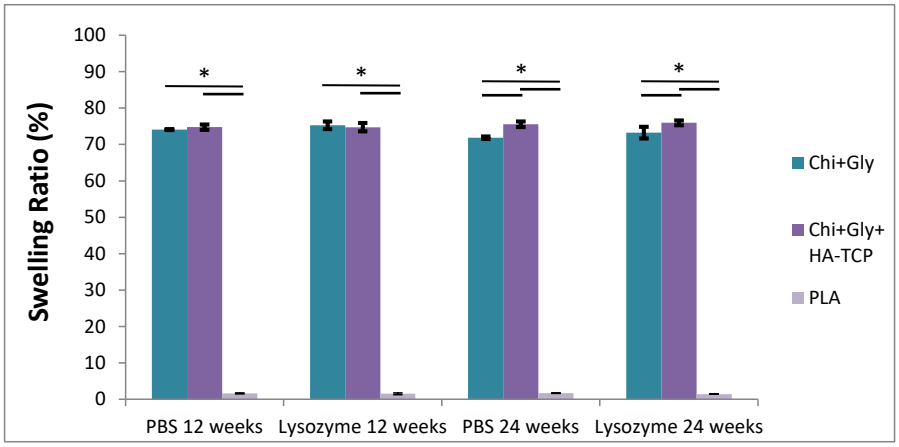

Figure 11.4. Swelling ratio of the PLA and the chitosan-based specimens after 12 and 24 weeks of degradation (*p-value < 0,05).

According to the results in the last figure, the swelling ratio is approximately 75% for the Ch+Gly and Ch+Gly+HA-TCP specimens assessed and under all the degradation conditions. However, the mean swelling capacity is statistically significant (p-value < 0,05) when the values obtained for Ch+Gly and Ch+Gly+HA-TCP specimens are compared in week 24. However, the mean values remain above 70%. Therefore, these specimens are hygroscopic and their liquid absorption capacity did not change over time. As consequence of this process, the specimens increased their dimensions. In turn, the swelling capacity of the PLA specimens is negligible (lower than 1,5%).

Figure 11.5 shows the results of the weight loss of the specimens dried for 120 hours, after the two degradation periods. The statistical evaluations were performed only for groups of materials tested under the same degradation condition. The remaining statistical results are indicated in the Appendix A.4.

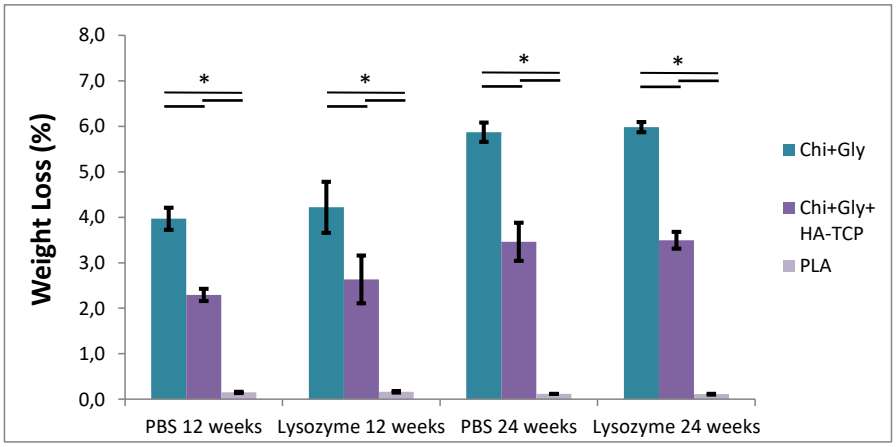

Figure 11.5. Weight loss of the PLA and the chitosan-based specimens after 12 and 24 weeks of degradation (*p-value < 0,05).

The mean weight loss is approximately 4% and 6% for the Ch+Gly specimens, and 2,5% and 3,5% for the Ch+Gly+HA-TCP specimens after, respectively, 12 weeks and 24 weeks of degradation (Figure 11.5). These values are registered at the end of each of the periods, regardless of the type of degradation solution used. In these cases, no statistical significance is found between the means obtained for the same specimens but which were studied under

different degradation solutions. However, there is an increase in the weight loss between week 12 and week 24, for all the specimens. This increase is proportional in both chitosan-based compositions, being smaller for the Ch+Gly+HA-TCP composition. Therefore, the statistical evaluations reject the hypothesis that the two means are equal when the analysis considers the same degradation condition of the material in different degradation periods (see results on Appendix A.4.). The weight loss of the PLA specimens is negligible (lower than 0,2%), as happened in the determination of its swelling capacity.
Figure 11.6 shows the visual appearance of two Ch+Gly and Ch+Gly+HA-TCP specimens after 24 weeks of degradation.

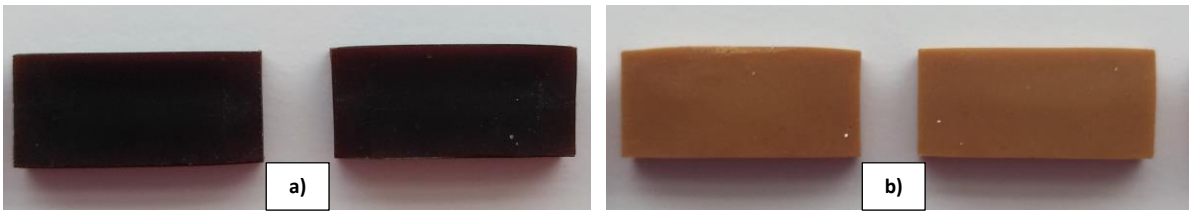

Figure 11.6. Examples of the a) Ch+Gly and b) Ch+Gly+HA-TCP specimens after 24 weeks of degradation in the lysozyme solution.

In general, the specimens are darker after drying in the stove, which is more noticeable for the lysozyme condition and after 24 weeks of degradation than after 12 weeks of degradation. This was particularly evident for the Ch+Gly specimens. Also, only for Ch+Gly specimens studied over 24 weeks, small cracks appeared on their surface during the drying however these cracks were no longer observed at the start of the flexural tests. In this case, the cracks disappeared as the specimens absorbed moisture.
Figure 11.7, Figure 11.8 and Figure 11.9 show the results of the flexural modulus, the flexural strength and the maximum flexural strain, respectively. The flexural properties of the specimens are compared with the properties of the controls, which were not subjected to any type of treatment. The statistical evaluations considered in the graph bars are performed only for groups of materials which were assessed under the same degradation condition and for the control pairs. The remaining results are shown in the Appendix A.4.
The behavior of the Ch+Gly and Ch+Gly+HA-TCP specimens under load is similar to the behavior represented in the stress-strain curves of Figure 10.5 and Figure 10.19, respectively. The same is valid for the PLA specimens.

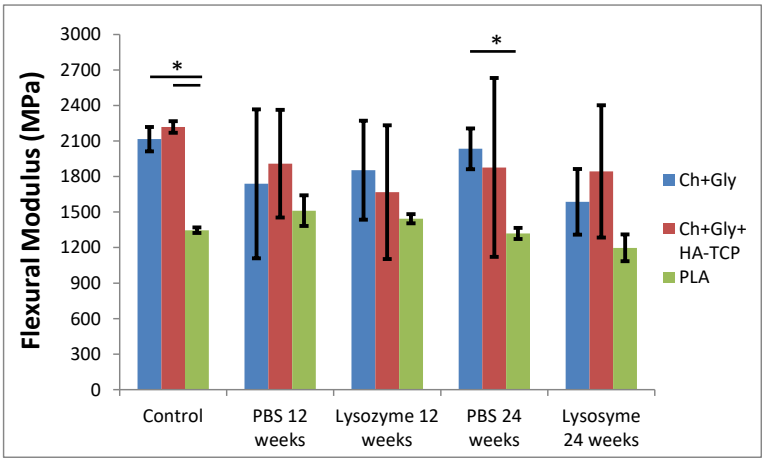

Figure 11.7. Flexural modulus of the PLA and chitosan-based specimens left on the degradation solutions for 12 and 24 weeks (*p-value < 0,05).

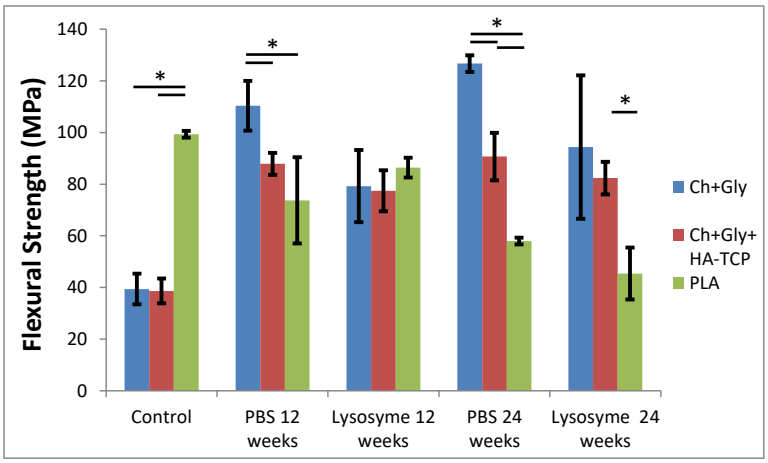

Figure 11.8. Flexural strength of the PLA and chitosan-based specimens were left on the degradation solutions for 12 and 24 weeks (*p-value < 0,05).

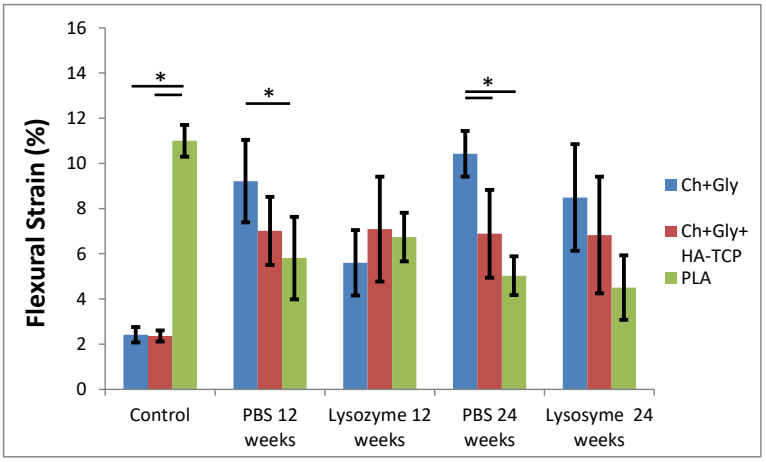

Figure 11.9. Flexural strain of the specimens that were left on the degradation solutions for 12 and 24 weeks (*p-value < 0,05).

In the beginning of the flexural tests, one Ch+Gly+HA-TCP specimen left in the lysozyme solution for 24 weeks broke, probably related with the cracks referred above.

According to Figure 11.7, similar mean values are obtained for the flexural modulus of the two chitosan-based specimens, regardless of the type of degradation solution used in the study

(PBS or lysozyme). The mean flexural modulus values of the specimens subjected to degradation are lower than the values of the control specimens.

The flexural strength and the flexural strain have increased considerably when the specimens were left for some time in the degradation solutions, as shown in Figure 11.7 and Figure 11.8, respectively. For example, the mean flexural strength increases more than 2 times and 3 times in the Ch+Gly compositions which were studied for 24 weeks, respectively, in the lysozyme and PBS solutions. Almost all these values differ significantly from the values obtained for the control specimens, as indicated in the Appendix A.4. In both cases, the mean results are higher for the Ch+Gly specimens, especially those immersed in the PBS solution for 24 weeks (mean flexural strength of 126 MPa and mean flexural strain of 10,4%).

In general, higher dispersion of results is associated to the flexural modulus, strength and strain measurements of the specimens that were left in the degradation solutions when compared to the controls. This is especially evident for the flexural modulus.

Regarding the PLA specimens, the mean flexural modulus did not significantly alter after the degradation periods, when compared with the control. The exception is the result obtained for the specimens submersed in the PBS for 12 weeks: the statistical evaluation rejects the hypothesis of equal means. Both the mean flexural strength and flexural strain greatly reduce when compared with the control, especially for the specimens tested at 24 weeks of degradation. In both evaluated mechanical properties, there was a decrease in the measurements between week 12 and week 24 (p-value $< 0,05$), for the specimens tested in the lysozyme solution. For example, in this case, the mean flexural strength reduced from 99 MPa to 45 MPa.

11.3. Osteoinduction behavior

To evaluate the osteoinduction capacity of the chitosan-based specimens, different tests were performed according to the methodologies described in chapter 7.5.3.1. To perform these tests, all the specimens were sterilized with ethanol (70%, v/v) followed by UV exposure (overnight).

For the AB assay, three small specimens (see Figure 11.2) were assessed in each time point. Additionally, one small specimen from each composition was used as control.

Figure 11.10 shows the results obtained in the AB experiment. The statistical evaluations represented in this figure were performed only for the materials tested at the same time point. The remaining statistical results are indicated in the Appendix A.4., where only the data of two consecutive cell culture times were considered.

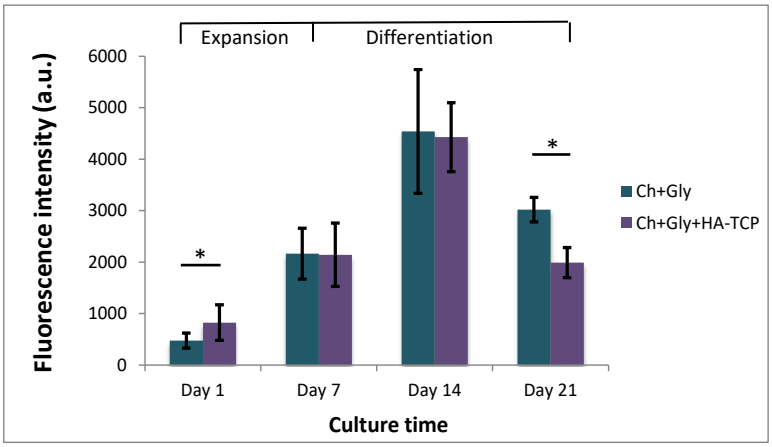

Figure 11.10. AB results of MSCs on chitosan-based specimens as a function of culture time (*p-value < 0,05).

As observed in the previous figure, the metabolic activity of the cells increased throughout the experiment and reached maximum values on day 14 (after 7 days of MSCs expansion), for both compositions. In day 1, the metabolic activity of the Ch+Gly+HA-TCP specimens was higher than the Ch+Gly specimens (p-value = 0.018), but then the values of the two compositions remained at the same level in the next two readings. In day 21, the metabolic activity decreased, being lower for the Ch+Gly+HA-TCP composition. In this case, it decreased by 55%.

Gene expression was determined by RT-qPCR at day 21 of the experiment, after 7 days of MSCs expansion and 14 days of MSCs differentiation). Three specimens from each composition were used. Figure 11.11 shows the results of the expression of the genes Runx2, ALP, COL1A1 and Osteocalcin.

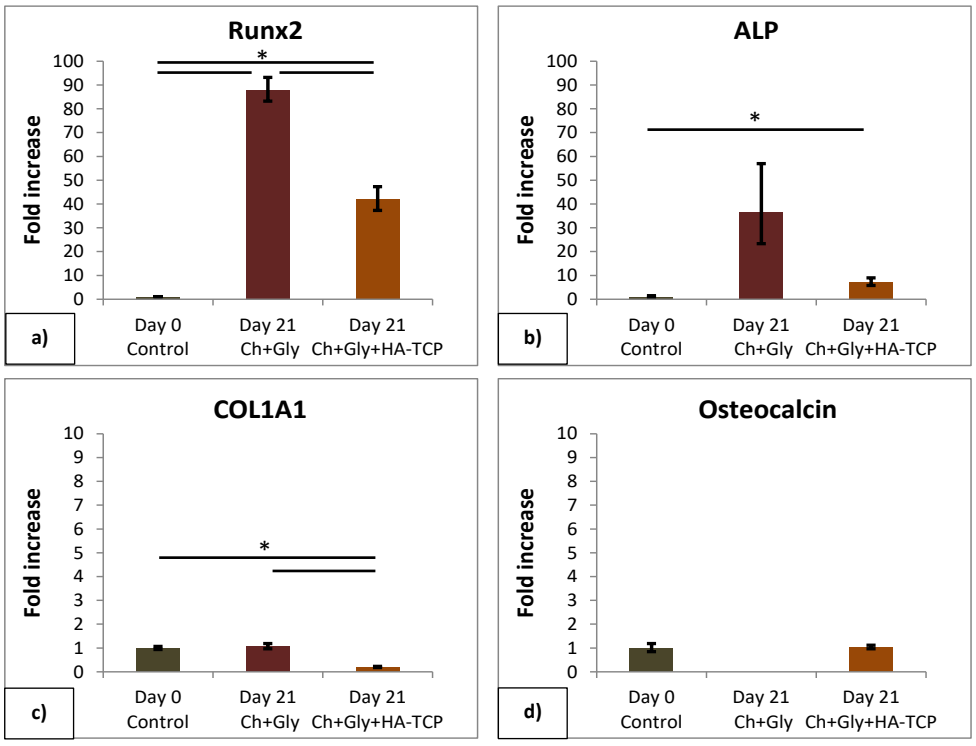

Figure 11.11. Results of gene expression, presented as fold chance from undifferentiated (day 0) expression level (*p-value < 0,05).

The results of the previous figure indicate higher levels of Runx2 and ALP, contrary to what was observed for the expression of COL1A1 and Osteocalcin. The expression of Runx2 and ALP was higher when the cells were cultured on the Ch+Gly specimens.
The ALP activity was assessed using one small specimen of Ch+Gly and Ch+Gly+HA-TCP. Small control specimens, one from each composition, were used as control (not exposed to MSCs). The ALP activity registered was 0,635 µmol/(L.min) for the Ch+Gly composition and 0,387 µmol/(L.min) for the Ch+Gly+HA-TCP composition.

11.4. Discussion

Two groups of specimens were produced in this study: Ch+Gly and Ch+Gly+HA-TCP. In this case, all the specimens were machined by a CNC milling machine, which reduced the variability on the surface finish, observed when the machining was performed manually.
Degradation behavior:
The degradation study used a lysozyme concentration of 500 mg/L to accelerate the study and to make the study conditions approximate the conditions of an *in-vivo* study.
The weight loss results were lower for the Ch+Gly+HA-TCP composition. The ceramic materials did not dissolve under the degradation solutions and their presence difficulted the access of the lysozyme to the glycosidic bond sites of chitosan chain. Pu *et al.*[411] found that the addition of ceramics to the composition of small chitosan rods has contributed to slow the degradation rate of such specimens, especially on the first days of the experiment. After a degradation period of 6 weeks, the authors observed a mean weight loss higher than 6%, for both rod compositions. In this thesis, the specimens were placed on the degradation solutions for a period four times longer, but even so, they did not register the same level of mass loss when compared to the mentioned study.
The PLA used in this study does not degrade if immersed either in PBS or lysozyme solutions, which indicates that this polymer takes more time than chitosan-based compositions to start to degrade in the tested conditions. Several factors affect the PLA reactivity to water and therefore its degradation rate - particle size, crystallinity, residual lactic acid concentration, molecular weight, water diffusion, etc. [412]. For example, Savioli Lopes *et al.*[412] indicate that the complete resorption rate for high molecular weight PLA can vary from 2 to 8 years.
The weight loss promoted by the PBS solution corresponds to the loss of material due to normal hydrolysis. Since the two blends have glycerol in their composition, the PBS solution can promote, for example, the extraction of the free glycerol or the glycerol that is not strongly connected to the chitosan chain. When the PBS solution is supplemented with the lysozyme, both the normal and the enzymatic hydrolysis are expected to occur [332]. Halim *et al.*[184] proposed a list of events for the chitosan degradation by the lysozyme. First the lysozyme permeates into the chitosan structure and then it acts by cleavage of the β(1–4) glycosidic bonds to form low M_w chitosan, chito-oligomers and N-acetyl-D-glucosamine residues. The low Mw fragments remain in the bulk materials until they are small enough to dissolve. When the small fragments are released into the media, the weight loss occurs, and the chitosan is totally degraded to the smallest structure. This stage depends on the D.D. of chitosan, hence chitosan with a higher D.D. requires more time for the fragmentation to occur. Therefore, in this thesis, the lysozyme may have transformed the chitosan chain into small fragments, but these fragments were not small enough to dissolve. Consequently, the lysozyme did not contribute

to significantly increase the weight loss of the chitosan-based specimens after 24 weeks of degradation. The lower lysozyme activity is explained by the high D.D. of the chitosan used in the specimens (89%). The fragmentation of the polymer chain may also be related with the small cracks observed on Ch+Gly specimens, after drying them in the stove.

There are several publications referring that lysozyme efficiently degrades chitosan, especially if the specimens have a low Mw and D.D. [413,414]. In this area, published studies are mainly focused on chitosan-based films, membranes, microspheres and scaffolds. The exception is the study performed by Oliveira *et al.*[175]. These authors studied the degradation of small cylindrical plasticized and non-plasticized dense chitosan structures (14 mm diameter and 6.5 mm height), and they found a higher weight loss for the non-plasticized structures after 8 weeks on degradation solutions. The mean weight loss was approximately 15% for the specimens immersed in lysozyme (Lysobac), and lower than 10% for the specimens left on the control (PBS) solutions. For the specimens produced with glycerol, the weight loss was much lower, even though there were still differences between the two degradation conditions. Generally, the degradation studies vary among themselves by the different configurations of the chitosan-based products, the lysozyme concentration, the frequency of the lysozyme replacement/renovation and the study period. For example, the studies cited previously did not focus on the degradation of chitosan-based products for more than 12 weeks. Additionally, only a few studies reported the origin of the lysozyme, which generally is from chicken egg white.

The flexural tests were performed to assess the loss of mechanical properties after the two degradation periods. The results (Figure 11.7 to Figure 11.9) indicate a decrease in the mean flexural modulus values, whereas the opposite trend was observed for the mean flexural strength and strain results. This may occur since the water acts as a plasticizer as it permeates into the structure of the specimens, promoting polymer chain re-orientations and crosslinks. In the context of these observations, González-Campos *et al.*[415] reported that water affects the molecular dynamics of chitosan films, a subject that was further explored by Fundo *et al.*[416], who studied the relationship between molecular mobility and the properties in chitosan/glycerol films by NMR. They found that water presented transverse relaxation (spin-spin T2) 10 times higher than the glycerol, for the same film. This is related with the availability of binding sites in the polymer chain that are preferentially occupied with glycerol, leaving the water molecules free to move in the system. The effect on the mechanical properties was increasing elongation at break and decreasing tensile strength. However, in this thesis, both the elongation and strength increase, which may indicate new molecular rearrangements (polymer/polymer, polymer/plasticizer, plasticizer/plasticizer) during the drying process, thus improving the mechanical strength of the materials. It would be interesting to compare the mechanical properties between the wet and dried specimens, to understand if this effect on the mechanical properties is observed in both situations.

In general, lower dispersion of results was obtained for the control specimens when compared to the specimens left in the degradation solutions. This was particularly evident for the flexural modulus, which may indicate that the elasticity of the chitosan-based specimens can alter more easily when they are placed inside the human body. Additionally, the control specimens analyzed in this study did not show the dispersion of results as observed in the flexural experiments described in chapter 10. This may be related with the machining process that was used.

The mean flexural strength and flexural strain values were higher for the Ch+Gly specimens. This observation indicates a greater ability of the water molecules to exert a plasticizing effect, which preferably occurred in the Ch+Gly composition left in the PBS solution. Statistical significances were found for the flexural strength and flexural strain means of the Ch+Gly specimens tested after 12 weeks of degradation in PBS and after 12 weeks of degradation in lysozyme. In turn, no statistical significance was found when the results of PBS and lysozyme are statistically compared between week 12 and 24.

According to Rokannen [417], current bioabsorbable implants lose most of their strength after 30 to 120 days in *in-vivo* environments and are resorbed after 6 to 12 months (SR-PGA) or 2 to 5 years (SR-PLLA), depending on size and composition. This information is also present in Table 2.3. Therefore, the behavior of chitosan-based specimens is distinguished from synthetic materials since chitosan compositions do not lose strength for at least 6 months.

Two studies assessed the effect of degradation solutions on the mechanical properties of dense chitosan specimens. Pu *et al.*[411] produced small dense rods of chitosan and chitosan/HA via *in situ* precipitation and tested the mechanical properties after 6 weeks of immersion in a solution consisting only of PBS. Thus, these authors did not study the effect of lysozyme in these specimens. They found that chitosan-only compositions showed a greater weight loss (6,6%) and fractured before the bending tests. On the other hand, the compositions with HA presented a bending strength of 51 MPa, which represents a reduction of 60% from the initial value. Oliveira *et al.*[175] also analyzed the strength and stiffness of the materials before and after the degradation period, and registered a reduction of these properties after 8 weeks of degradation. For the plasticized specimens, the authors registered a reduction on the compressive modulus, from the initial average value of 328 MPa to 112 MPa, after 8 weeks of immersion in the solution containing lysozyme.

Osteoinduction behavior:

The metabolic activity results (Figure 11.10) indicated a decrease between days 14 and 21. This decrease may not be directly related with cell death but rather by changes in the cell metabolism as a result of attaining a certain level of differentiation. According to Zachari *et al.* [418], the AB method relies on metabolic pathways that can be affected by the reducing capacity of individual cells or by agents affecting mitochondrial activity that have a direct reducing effect on resazurin. Therefore, AB reduction may not indicate a direct cell dysfunction [342]. To understand the effect of certain redox potentials profiles during osteogenesis of MSCs, Imhoff and Hansen [419] measured different intracellular couples. The authors found, by studying the effect of glutathione redox state, that osteogenic cells remain reduced during the initial periods of differentiation and then rapidly oxidize during terminal differentiation. As a conclusion, these authors referred that cellular differentiation is controlled by specific regulatory elements and therefore it is important to understand what types of dysregulations or redox changes could directly influence the differentiation of stem cells. Eble and Rezende [420] reported that the ECM regulation in the cells use reactive oxygen species as physiologically signalizing molecules, being crucial for cell signaling and redox-regulation, instead of just causing oxidative stress and damage.

Frohbergh *et al.*[421] studied the metabolic activity by the AB assay of two types of genipin-chitosan scaffolds (with and without HA), during osteogenic differentiation. The authors found that by day 10 the metabolic activity of murine MSCs decreased on all scaffolds, remaining at the same level until day 21. The AB fluorescence reached 70.000 a.u., considering an initial cell

seeding of 500.000 cells per scaffold. Through fluorescence microscopy, the authors realized that the cell number did not decrease over time and suggested that the observed decrease in AB fluorescence might indicate an enhancement of cellular quiescence/differentiation rather than a loss of cell numbers/viability.

The results in Figure 11.11 revealed promising gene expression results, i.e. the MSCs were induced to differentiate into osteoblastic lineage with high expression of Runx2 and ALP genes. Lower levels of COL1A1 and Osteocalcin may indicate that 14 days of *in vitro* cell differentiation may not be sufficient to initiate ECM synthesis and bone mineralization, under the established culture conditions. The cell culture conditions could be improved with a dynamic culture system provided by a bioreactor [422]. García-Gareta *et al*.[423] indicate that it is still necessary to develop a consistent *in vitro* model of osteoinductivity; important factors to take into account are cell type (stem cells, osteoprogenitor cells, fully differentiated cells, co-culture of different cell types), culture conditions (media with or without osteogenic or angiogenic factors, calcium/phosphate enriched media, static or dynamic culture, mechanical stimulation, electrical stimulation, timeframe) and which output parameters should be measured at the end and throughout the culture period. As reported in this thesis, Wang *et al*.[424] observed lower levels of COL1A1 when they studied chitosan/collagen composite microbeads for tissue regeneration using MSCs.

Surprisingly, lower levels of gene expression were detected for the Ch+Gly+HA-TCP composition. In general, the biomaterial-cell interactions depend on surface characteristics such as chemistry, topography and surface physics [425]. The surface characteristics regulate the ionic exchange dynamics, protein adsorption and the cellular activity of attachment, proliferation and differentiation [425]. Under physiological conditions, this dissolution process strongly depends on the nature of the calcium phosphate material [425,426]. HA is more stable thermodynamically than TCP, therefore HA is less soluble [425]. Amorphous materials dissolve faster than its crystalline equivalents and the larger the exposed surface to the environment, the faster the biomaterials dissolves [425,426]. Therefore, micro- and macro-porosity play an important role in the dissolution process of calcium phosphates as well as the presence of concavities and channels [425,426]. Smaller particle size and the presence of certain additives (e.g. carbonate and silicate) can also accelerate the dissolution of the material [425,426]. However, Barradas *et al*.[427] stated that it is still necessary to determine if free ions are in fact the trigger for the osteogenic differentiation or simply they are the template where the onset of bone formation can occur.

Yuan *et al.*[428] implanted different calcium phosphates in muscles of dogs to assess their osteoinduction behavior. They found lower bone formation in materials without micropores, composed by HA rather than HA/TCP and with higher sintering temperatures. Revisiting the properties of calcium phosphates used in this thesis, the mixture HA-TCP had a particle size distribution, d0.9, of 7 µm and the sintering temperature used to prepare them was 1.110°C. Therefore, these parameters may also have contributed to a lower expression level of the genes in the Ch+Gly+HA-TCP compositions.

Other authors reported differences in the osteogenic differentiation in materials composed with ceramics. Puvaneswary *et al*.[429] produced tricalcium phosphate-chitosan-fucoidan (TCP-Ch-Fu) scaffolds for tissue engineering applications. They determined a high level of Osteocalcin release (ng/ml) in the TCP-Ch-Fu scaffold seeded with hMSCs when compared with that in the TCP-Ch scaffolds (in osteogenic and normal media). At day 14, the gene expression

of ALP, Runx2 and COL1A1 was also higher for the TCP-Fu-Ch scaffold cultured in osteogenic media. Comparing all the assessed genes, the expression of COL1A1 was lower, being at the same level of the expression (fold increase relative to GAPDH) obtained in this thesis.
Finally, the osteoinduction capacity of the specimens was determined by measuring the ALP activity. Since ALP is expressed at the early stages of the MSC differentiation towards osteogenic lineage, this thesis focused on the ALP activity at day 14 (day 7 of differentiation). The results confirmed the capacity of the two compositions in promoting osteogenesis, with a higher enzymatic activity being recorded for the Ch+Gly composition (0,635 µmol/L.min). These results are in accordance with the results obtained in the RT-qPCR experiments. Weir and Xu[430] studied the response of hBMSCs to a high-strength calcium phosphate cement scaffold prepared with chitosan. They found a significant increase in ALP on day 8 (normalized to DNA concentration), which was higher for the calcium phosphate cement without chitosan. As a conclusion, these authors stated that such results were likely caused by ion activities promoted by the continued setting and dissolution of the mixture of tetracalcium phosphate and dicalcium phosphate anhydrous, used in the composition of calcium cement. Therefore, the dissolution of ions from calcium phosphates accelerates the ALP activity, which may have not happened in the ALP activity study of this thesis.

11.5. Conclusion

The *in vitro* degradation and osteoinduction behavior of the Ch+Gly and Ch+Gly+HA-TCP compositions were studied to anticipate their *in vivo* performance.
The assessment of the degradation profile is essential for the selection of the composition that best meets the biodegradation requirements, necessary for the development of new bioabsorbable implants. For example, for the success of the ACL reconstruction, it is crucial that the implant maintains its integrity and high fixation strength as healing occurs. According to the information in chapter 5.1.4, for bone-tendon-bone graft fixation, healing occurs between 4 and 12 weeks after surgery. Based on the results obtained over 24 weeks of degradation, both compositions do not compromise the development of implants for the intended application. The resulting degradation from the specimens' immersion on the enzymatic (lysozyme) and non-enzymatic (PBS) solutions was determined by measuring the changes relative to the initial weight and initial mechanical properties. In both situations, the mass loss was not substantial and the mechanical properties were not compromised; the flexural strength and flexural strain even increased for both compositions, after the 24 weeks of degradation.
Differentiation tests were also performed to determine the osteoinduction capacity of the chitosan-based compositions, i.e. their capacity in inducing the bone-forming cell lineage from MSCs. The osteoinductive potential of the chitosan-based specimens was determined over 21 days (7 days of expansion and 14 days of osteogenic differentiation). The response of the two compositions allows inferring that they promote the differentiation of MSCs into osteoblastic lineage, which is fundamental for the biological integration of the implant material into the body. The osteoinduction capacity was verified in all the tests performed i.e. AB assay, ALP activity and gene expression by RT-qPCR.
Comparing all the results obtained in this chapter, the composition that revealed a better biological behavior is the Ch+Gly composition; despite losing more weight over time, in

relation to Ch+Gly+HA-TCP, it showed better mechanical performance after degradation and it revealed higher osteogenic potential. Therefore, Ch+Gly is the most interesting composition to be used *in vivo*. Nonetheless, it is important to mention that both compositions have achieved such performance values, allowing both them to be tested *in vivo*.

To analyze the effect that the ceramic materials used in the specimens can exert on the MSCs, new experiments and analyzes must be carried out, including, for example, the study of specimens produced with amorphous ceramics with smaller particle dimensions.

As a final remark, it must be taken into account that *in vivo* behavior of the materials can be different from *in vitro* behavior. For example, the *in vivo* degradation of bioabsorbable materials depends on the foreign body responses and the action of many more enzymes in addition to lysozyme. The calcium and phosphate levels in the cell culture medium can vary without being regulated, which normally does not happen in an *in vivo* environment.

12. Sterilization of the chitosan-based compositions selected for the development of bioabsorbable implant products

To study the effect of the different sterilization methods (steam, EtO, gamma irradiation and ozone) on the chitosan-based compositions, different tests and analysis were performed to determine if the sterilization method affects their final properties, compromising their *in vivo* behavior. This study was performed in sterilized and non-sterilized specimens for comparison.

12.1. Sterilization of rectangular specimens

The sterilizations were performed on two types of specimens with rectangular cross section: Ch+Gly and Ch+Gly+HA-TCP. These specimens were produced as explained in chapter 11.1., having the same final dimensions (25mm × 12 mm × 4 mm and 7,2 mm × 5 mm × 4 mm) and appearance. In this study, the small specimens (see Figure 11.2) were used for the cytotoxic tests.

The specimens were sterilized through four different sterilization methods, according to the procedures described in chapter 8.2: steam, EtO, ozone and gamma irradiation. Visually, the Ch+Gly+HA-TCP specimens sterilized by steam presented a slight yellowish colour. In addition, the specimens sterilized by EtO suffered internal cracks probably due to the several cycles of sterile air and vacuum, necessary to reduce the EtO levels on the specimens. Both compositions suffered from this effect, because they have lost about 1,5% of initial weight. However these cracks were only visible in the Ch+Gly compositions due to their transparency – Figure 12.1. The other specimens did no change their appearance after sterilization.

Figure 12.1. Example of a specimen sterilized by EtO, exhibiting internal cracks.

The specimens were all sterilized in the same week to guarantee the same time frame between the sterilization and the experimental tests described next.

12.2. Results of the experimental evaluation

12.2.1. Flexural tests

Flexural tests were performed in four specimens from each composition, according to the procedure described in chapter 7.1.2.1. The results (flexural modulus, flexural strength and maximum flexural strain) are shown in the figures below. The statistical evaluations shown in

these figures were performed only for pairs of materials sterilized under the same method and for the non-sterilized pairs. The remaining results are indicated in the Appendix A.5.
The behavior of two compositions (non-sterilized and sterilized) under load is similar to the behavior represented in the stress-strain curves of Figure 10.5 and Figure 10.19, respectively, for the Ch+Gly and Ch+Gly+HA-TCP compositions.

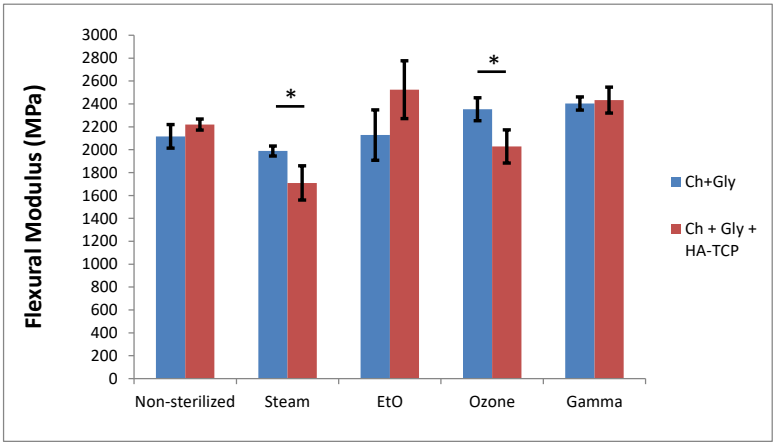

Figure 12.2. Flexural modulus obtained for each sterilized and non-sterilized specimens (*p-value < 0,05).

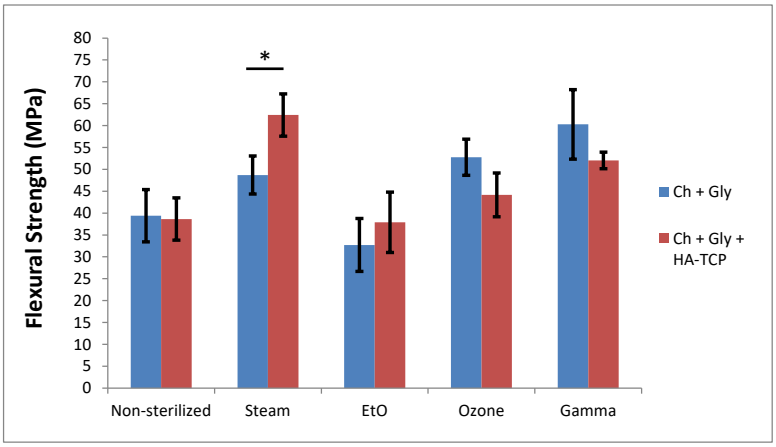

Figure 12.3. Flexural strength obtained for each sterilized and non-sterilized specimens (*p-value < 0,05).

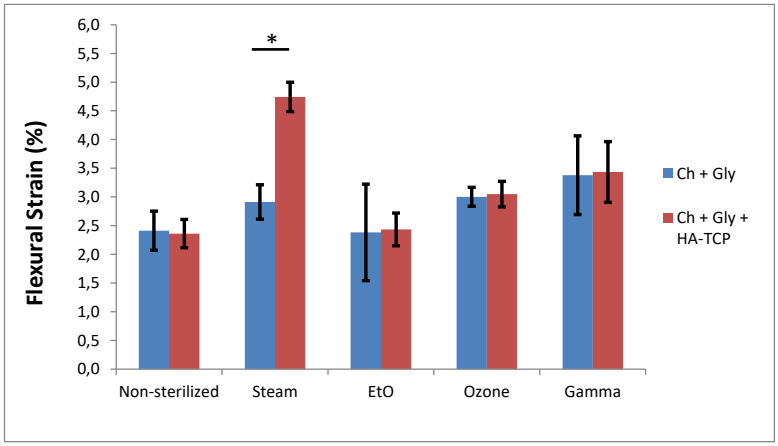

Figure 12.4. Flexural strain obtained for each sterilized and non-sterilized specimens (*p-value < 0,05).

Analyzing the results of the flexural tests, it is notorious that the mean flexural modulus of the two compositions is only statistically different for the steam and ozone sterilizations (p-value =

0,043 and p-value = 0,022, respectively). In general, the mean stiffness modulus increases for the Ch+Gly specimens after the gamma and ozone sterilizations (2.404 MPa and 2.353 MPa, respectively), whereas this property increases for the Ch+Gly+HA-TCP specimens after the gamma and EtO sterilizations (2.434 MPa and 2.525 MPa, respectively).

Regarding the flexural strength, the mean values have completely opposite trends for steam and EtO sterilizations, especially for the Ch+Gly+HA-TCP composition; the flexural strength increases and slightly decreases, respectively, when compared with the non-sterile compositions. For the specimens sterilized by ozone and gamma irradiation, the mean flexural strength has improved overall. The highest mean values are obtained for the Ch+Gly specimens sterilized by gamma irradiation (60 MPa) and for Ch+Gly+HA-TCP specimens sterilized by steam (62 MPa).

Regarding the maximum flexural strain, the results followed the trend observed in the flexural strength. However, comparing the flexural strain values obtained for the sterilized specimens with the values obtained for the respective controls, statistical significance (p-value < 0,05) is found for the Ch+Gly+HA-TCP specimens sterilized by steam, ozone and gamma irradiation (see Appendix A.5.).

12.2.2. Nanoindentation tests

Nanoindentation tests were performed according to the procedure described in chapter 7.1.3.1. On average, 8 indentations were performed on each sterilized and non-sterilized specimen.

The results are indicated in Figure 12.5 (indentation hardness) and Figure 12.6 (indentation modulus). The statistical evaluations considered in the graph bars were performed only for pairs of materials sterilized under the same sterilization method and for the non-sterilized pairs. The remaining results are presented in the Appendix A.5.

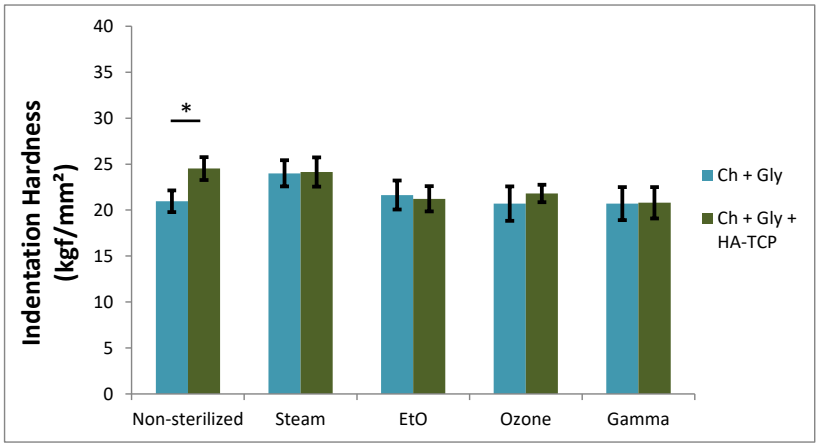

Figure 12.5. Indentation hardness obtained for each sterilized and non-sterilized specimens (*p-value < 0,05).

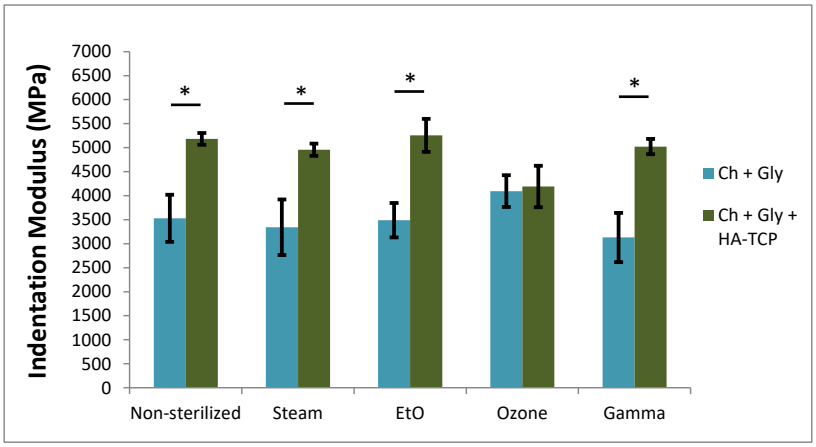

Figure 12.6. Indentation modulus for each sterilized and non-sterilized specimens (*p-value < 0,05).

Indentation hardness results indicate that sterilizations promote the same effect on the two tested compositions. No statistical significance is found between the two compositions, except for the two non-sterilized compositions. When compared with the controls, statistical significance is found for the Ch+Gly+HA-TCP compositions sterilized through EtO, ozone and gamma irradiation (p-value <0,05). In this case, the indentation hardness has decreased by 13%, 11% and 15%, respectively. For the Ch+Gly compositions, the average indentation hardness did not change when sterilized, except for the specimens sterilized by steam, which has increased (p-value = 0,0004). The highest mean indentation hardness was obtained for the Ch+Gly+HA-TCP specimens sterilized by steam (24 kgf/mm^2).

Regarding the indentation modulus results, statistical significance (p-value < 0,05) is found when the two compositions are compared in all the sterilizations conditions, except for the ozone sterilization. The same is observed for the non-sterilized compositions. When comparing the values obtained for the sterilized and non-sterilized compositions, higher statistical significances are found for the Ch+Gly+HA-TCP composition (see Appendix A.5.). The highest mean indentation modulus is obtained for the Ch+Gly+HA-TCP specimens sterilized by EtO (5256 MPa).

12.2.3. SEM analysis

SEM analysis was performed according to the experimental procedure described in chapter 7.2.1.1. The analysis intended to visualize both the outer surface of the specimens before and after the different sterilization methods (400X magnification), as well as the fracture surfaces that resulted from the flexural tests (20X or 50X magnification). The SEM images obtained for each sterilized and non-sterilized specimens are shown in Figure 12.7 to Figure 12.16.

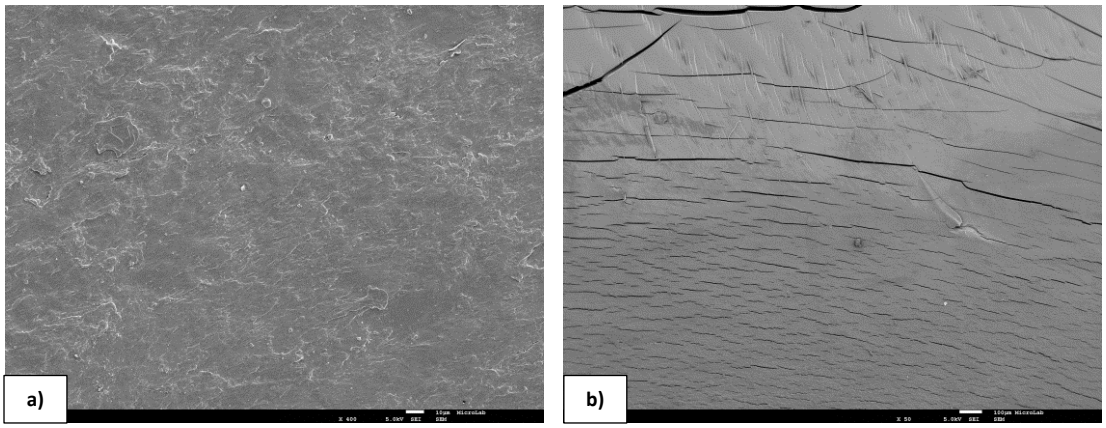

Figure 12.7. Non-sterilized Ch+Gly specimen: SEM images of the a) outer surface (400X) and b) fracture surface (50X) after the flexural tests.

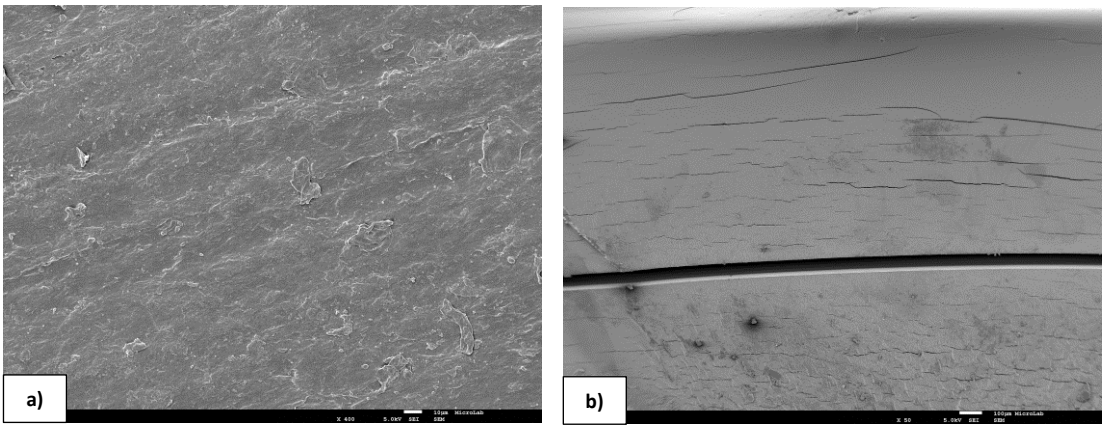

Figure 12.8. Sterilization by steam on a Ch+Gly specimen: SEM images of the a) outer surface (400X) and b) fracture surface (50X) after the flexural tests.

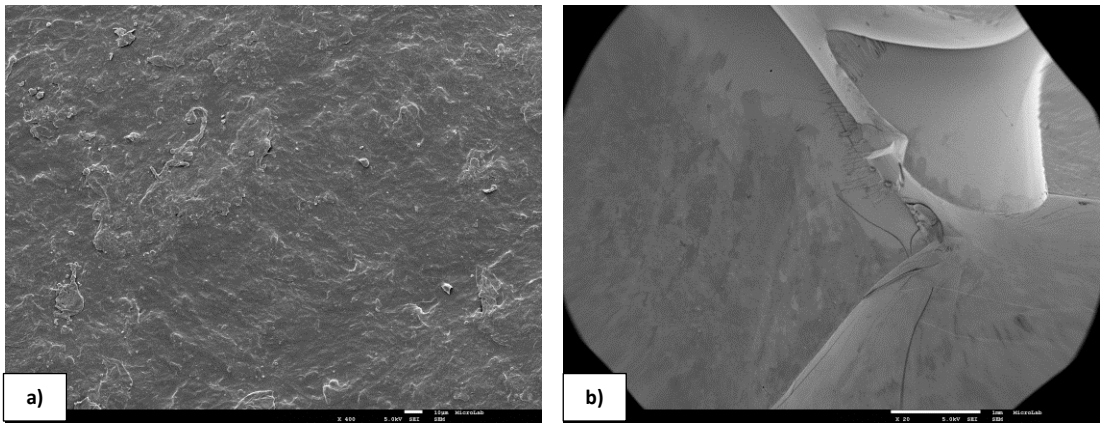

Figure 12.9. Sterilization by EtO on a Ch+Gly specimen: SEM images of the a) outer surface (400X) and b) fracture surface (20X) after the flexural tests.

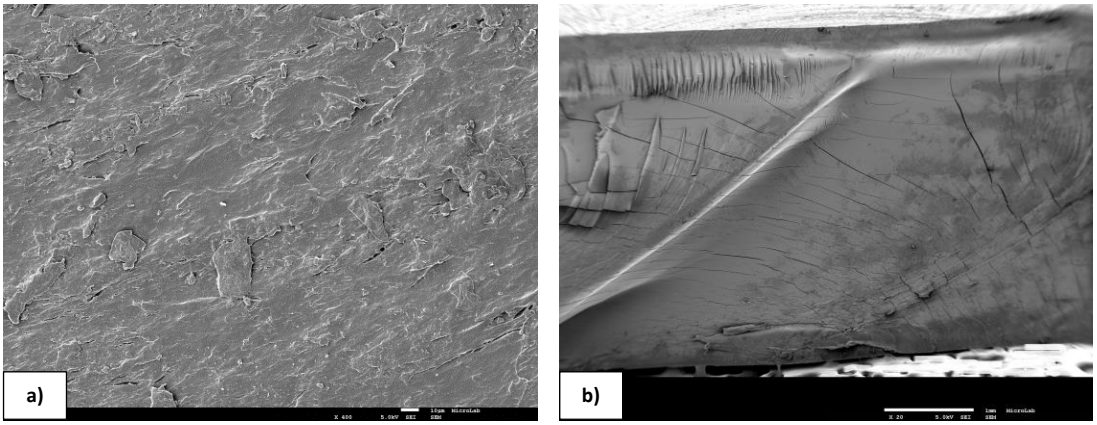

Figure 12.10. Sterilization by ozone on a Ch+Gly specimen: SEM images of the a) outer surface (400X) and b) fracture surface (20X) after the flexural tests.

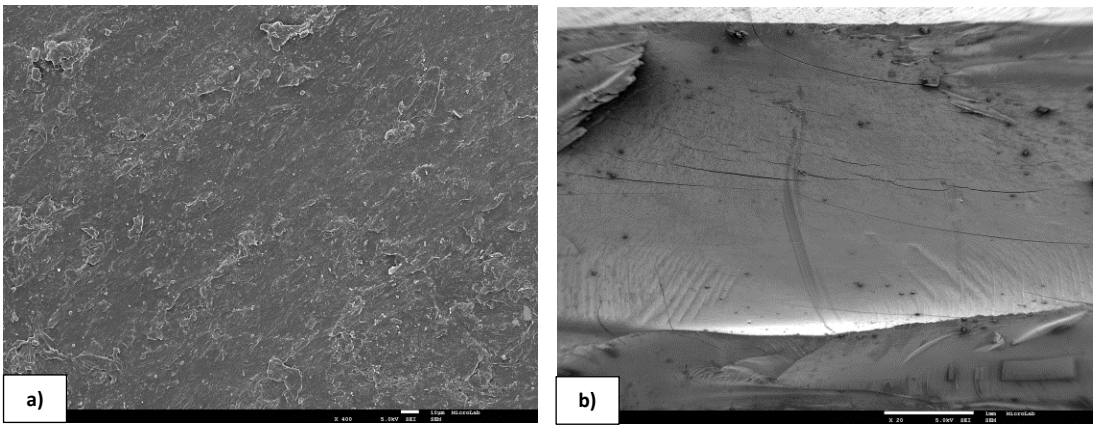

Figure 12.11. Sterilization by gamma irradiation on a Ch+Gly specimen: SEM images of the a) outer surface (400X) and b) fracture surface (20X) after the flexural tests.

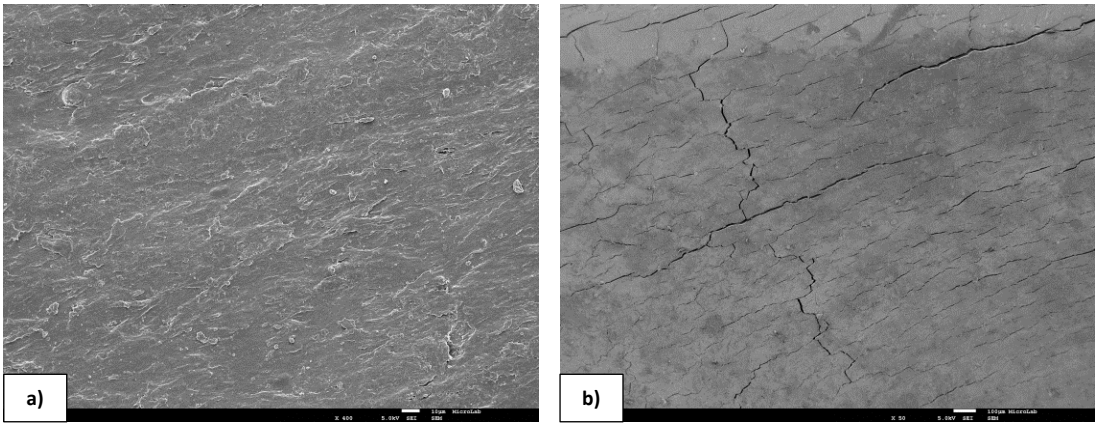

Figure 12.12. Non-sterilized Ch+Gly+HA-TCP specimen: SEM images of the a) outer surface (400X) and b) fracture surface (50X) after the flexural tests.

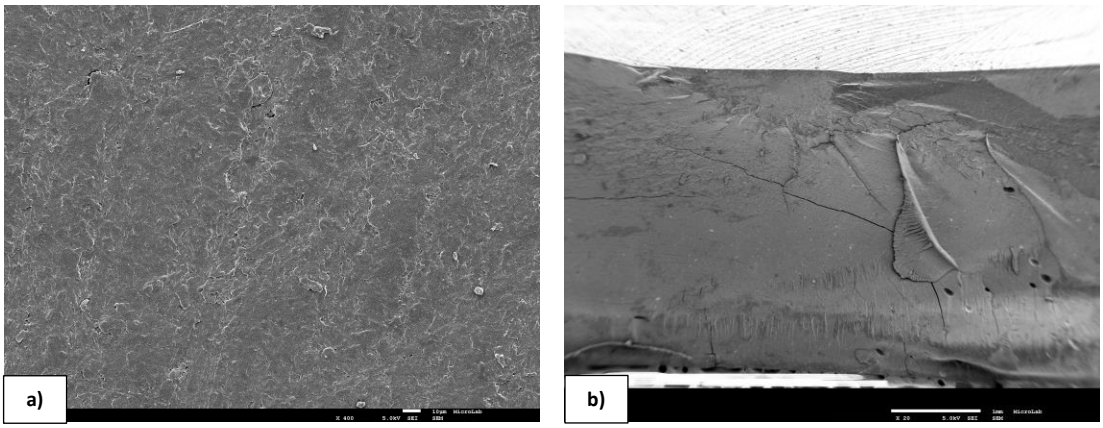

Figure 12.13. Sterilization by steam on a Ch+Gly+HA-TCP specimen: SEM images of the a) outer surface (400X) and b) fracture surface (20X) after the flexural tests.

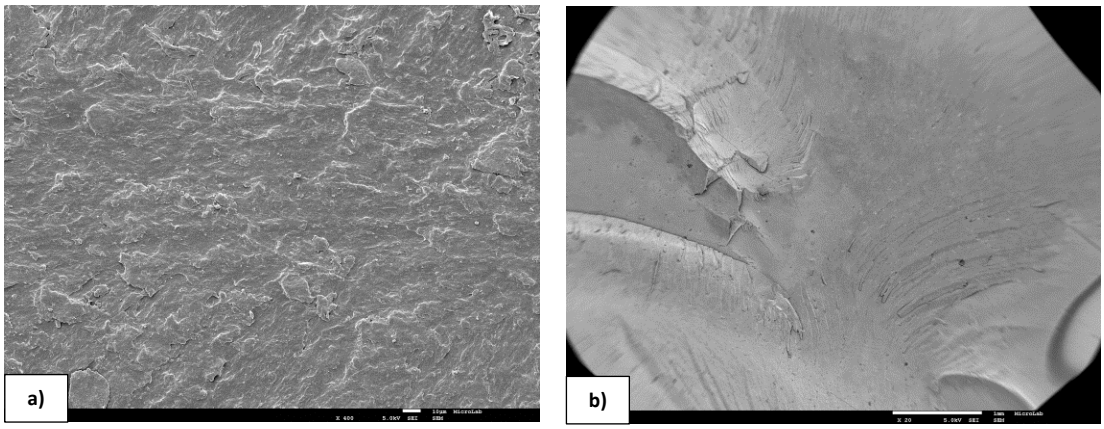

Figure 12.14. Sterilization by EtO on a Ch+Gly+HA-TCP specimen: SEM images of the a) outer surface (400X) and b) fracture surface (20X) after the flexural tests.

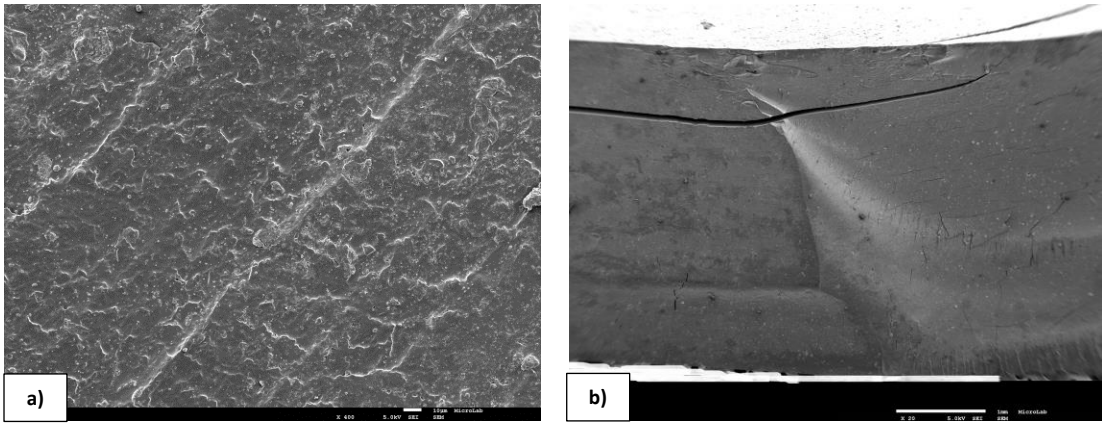

Figure 12.15. Sterilization by ozone on a Ch+Gly+HA-TCP specimen: SEM images of the a) outer surface (400X) and b) fracture surface (20X) after the flexural tests.

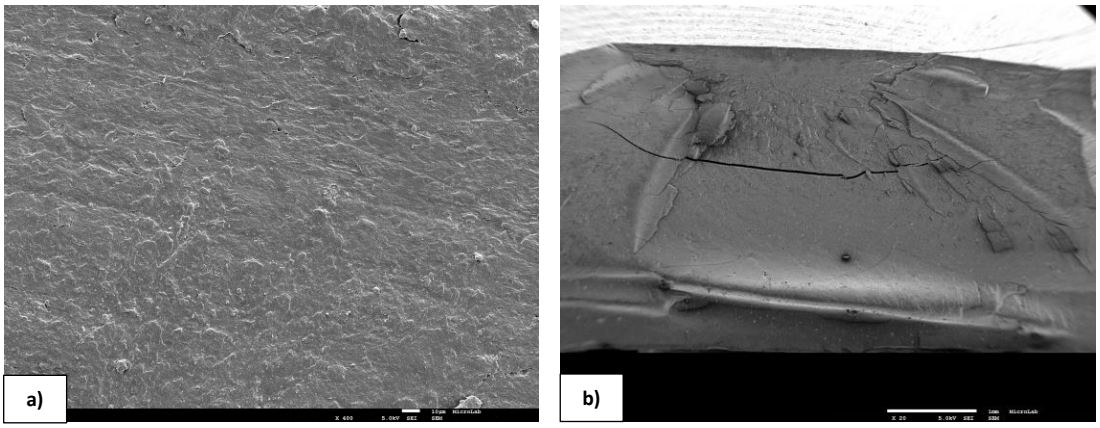

Figure 12.16. Sterilization by gamma irradiation on a Ch+Gly+HA-TCP specimen: SEM images of the a) outer surface (400X) and b) fracture surface (20X) after the flexural tests.

Comparing the outer surfaces of all the specimens, shown in previous figures, no differences are found in terms of roughness, density or porosity. Only the specimens sterilized by EtO do not reveal a well-defined fracture zone, as a result of the imposed load during the flexural tests. The fracture occurred diagonally, throughout the specimen. In the other cases the fracture occurred in the middle of the specimens, both for the non-sterilized and sterilized specimens. The images that show the fracture surface (images on the right) reveal different fracture cracks for the non-sterilized specimens. Transverse cracks are mostly present on the Ch+Gly specimens (Figure 12.7 b) whereas these do not have a specific direction in the Ch+Gly+HA-TCP specimens (Figure 12.12 b). For the sterilized Ch+Gly+HA-TCP specimens, fewer cracks and pores are noticeable. No additional defects are visible next to the cracks.

12.2.4. Contact Angle measurement

Contact angles were determined according to the experimental procedure described in chapter 7.3.2.1. To test the wettability of the Ch+Gly and Ch+Gly+HA-TCP specimens, the profile of four water drops was analyzed on the surface of two sterilized specimens of each composition. In addition, the profile of four water drops on the surface of two non-sterilized specimens of each different composition was also tested. Figure 12.17 shows the evolution of the mean contact angle during the 180 seconds of the analysis.

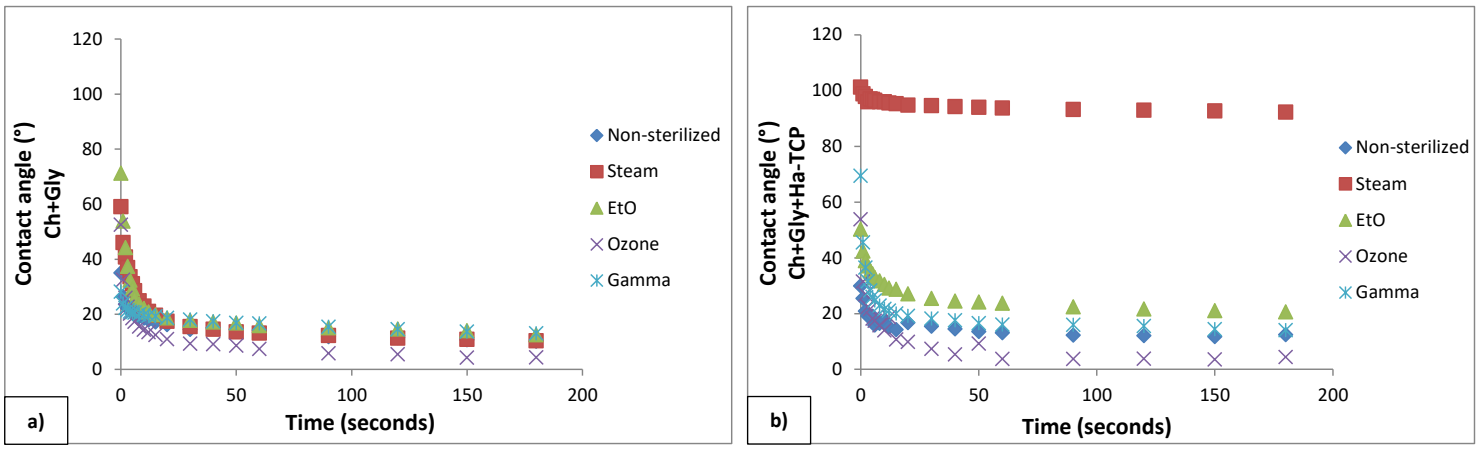

Figure 12.17. Mean contact angle recorded at each time for the sterilized and non-sterilized specimens: a) Ch+Gly composition, b) Ch+Gly+Ha-TCP composition.

The results indicate that most of the specimens have a hydrophilic surface, showing the same wettability profile during the 180 seconds of evaluation. The exception is the Ch+Gly+HA-TCP composition sterilized by steam that reveals an unfavorable wetting surface (hydrophobic surface). In this case, the drop fluid tended to minimize the contact with the surface and forms a compact droplet, as shown in Figure 12.18 b).

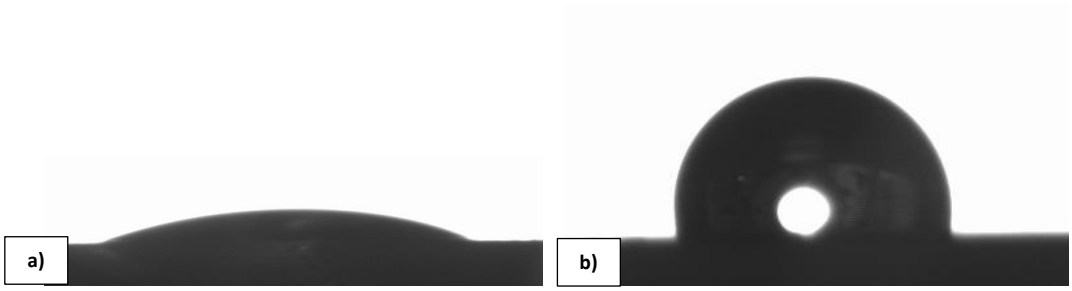

Figure 12.18. Water droplet profile at the end of the contact angle tests on the surfaces of specimens sterilized by steam: a) Ch+Gly composition, b) Ch+Gly+HA-TCP composition.

Figure 12.19 represents the mean contact angle measured during the last 60 seconds of the experiment, for all the assessed sterilized and non-sterilized specimens. The statistical evaluations considered in the graph bars were performed only for pairs of materials sterilized under the same sterilization method and for the non-sterilized pairs. The remaining results are presented in the Appendix A.5.

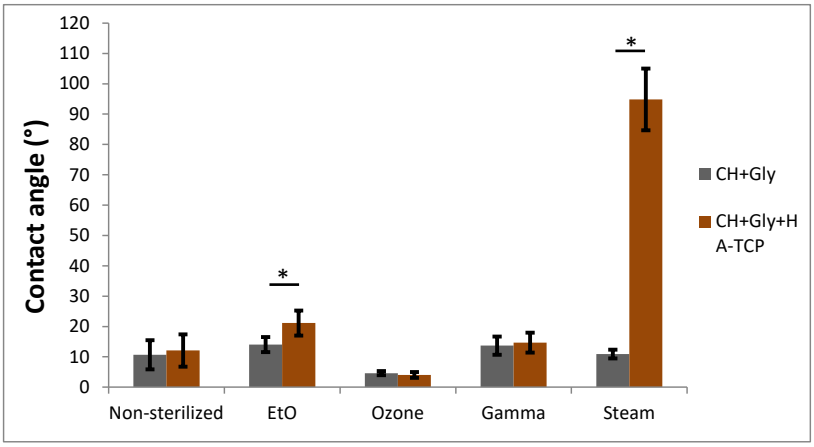

Figure 12.19. Mean contact angle obtained for each non-sterilized and sterilized specimens (last 60 seconds).

Comparing the results obtained for the non-sterilized and sterilized specimens, from each composition, the statistical evaluations do not indicate statistical significance only for both specimens sterilized by gamma irradiation.

12.2.5. ATR-FTIR analysis

ATR-FTIR analyses were performed according to the experimental procedure described in chapter 7.4.1.1. These analyzes were performed on a single specimen of each composition that was sterilized by steam, EtO, gamma irradiation or ozone. Non-sterilized specimens were also used as comparison.

Figure 12.20 shows the spectra referring to the Ch+Gly and Ch+Gly+HA-TCP specimens. Each spectra set contains different colors, which identifies the sterilization method used and the controls.

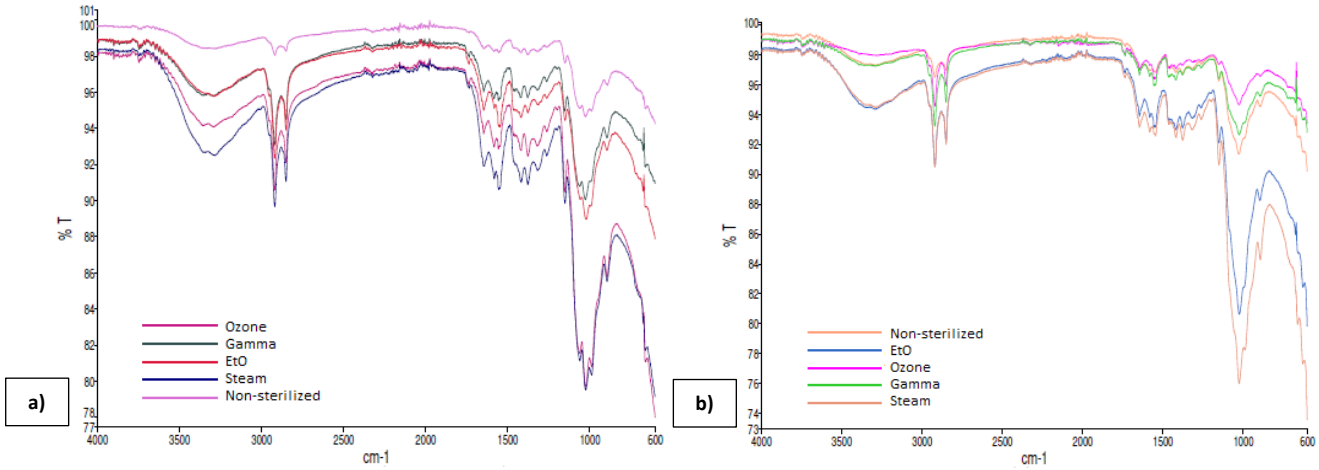

Figure 12.20. ATR-FTIR corresponding to the a) Ch+Gly composition and b) Ch+Gly+HA-TCP composition.

The ATR-FTIR spectra of Figure 12.20 a) and b) reveal similar bands between all the sterilized and non-sterilized specimens, regardless of their composition. These different bands are registered in the same wave number, thus they do not shift due to new chemical interactions. Therefore, the results do not reveal chemical changes on the surface of the specimens after sterilization.

12.2.6. Cytotoxicity tests

For the cytotoxic test, only two groups of triplicates (smaller specimens – see Figure 11.2) from both compositions, were left in ethanol (70%, v/v) overnight without any sterilization treatment (the non-sterilized specimens). The sterilized specimens were used directly in the cytotoxic tests. These tests were performed according to the methodology described in chapter 7.5.1.1. Figure 12.21 presents the results of the cell viability performed by the extract assay, through the MTT test. The statistical evaluations considered in the graph bars were performed only for pairs of materials sterilized under the same sterilization method and for non-sterilized pairs. The remaining results are presented in the Appendix A.5.

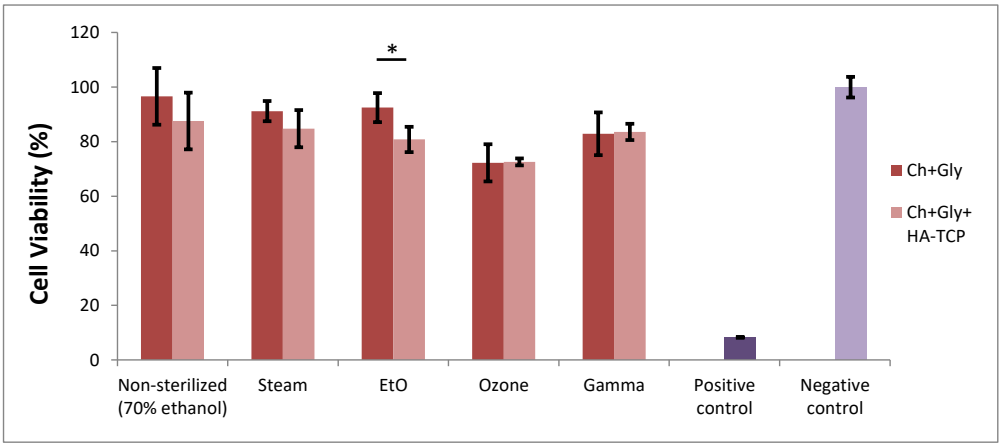

Figure 12.21. Results of the cytotoxic assay by extract dilution - MTT test (*p-value<0,05).

The results of the previous table show that the mean cell viability percentage is slightly higher for the Ch+Gly compositions. However, statistical significance between the means of the two compositions is found only for the specimens sterilized by EtO (p-value = 0,047). For the steam, EtO and gamma irradiation sterilizations, the cell viability is higher than 80%, which means that no significant cytotoxic substances were released from the specimens into the medium. On the other hand, the cell viability detected from the extracts obtained for the specimens sterilized with ozone was around 70%, which may indicate that these specimens are cytotoxic for the cells.

The results of the direct contact are shown in the next set of figures. The specimens are properly identified and they are distinguished in the areas where the color is darker and/or translucent.

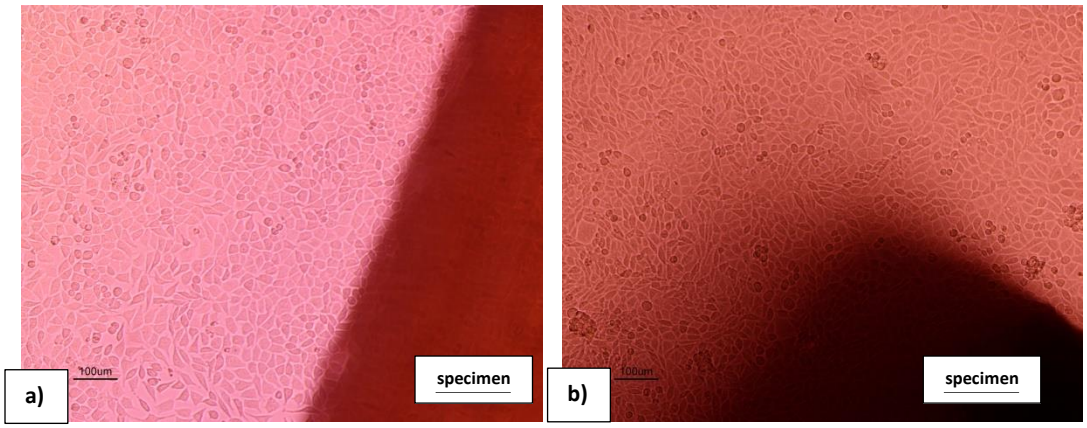

Figure 12.22. Direct contact assay to non-sterilized specimens (70% ethanol): a) Ch+Gly and b) Ch+Gly+HA-TCP.

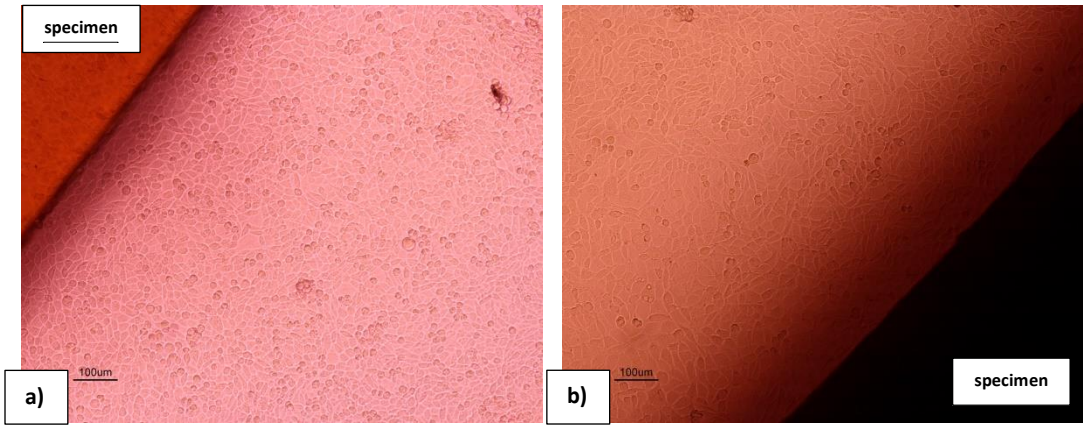

Figure 12.23. Direct contact assay to specimens of each composition that were sterilized by steam: a) Ch+Gly and b) Ch+Gly+HA-TCP.

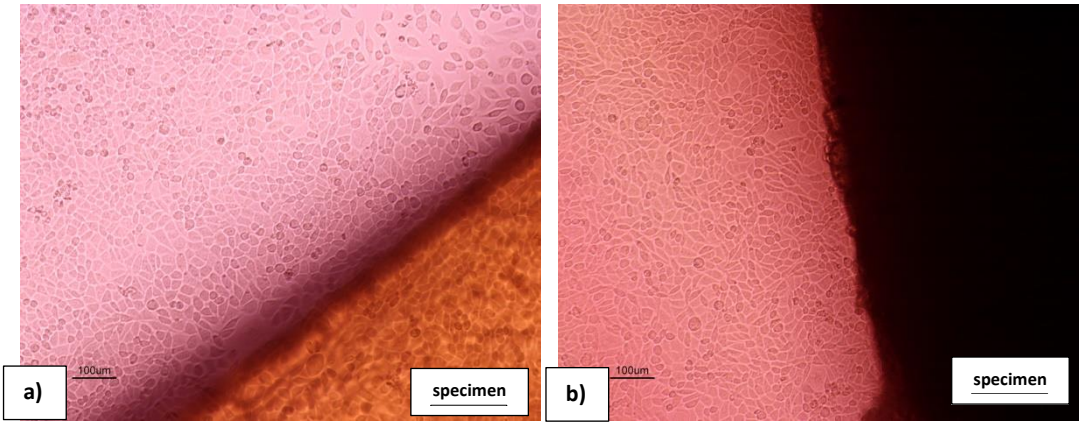

Figure 12.24. Direct contact assay to specimens of each composition that were sterilized by EtO: a) Ch+Gly and b) Ch+Gly+HA-TCP.

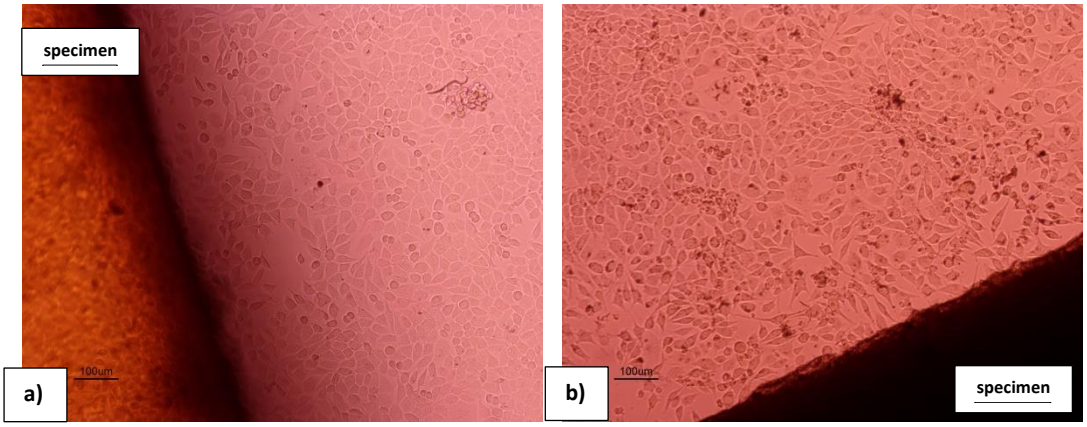

Figure 12.25. Direct contact assay to specimens of each composition that were sterilized by ozone: a) Ch+Gly and b) Ch+Gly+HA-TCP.

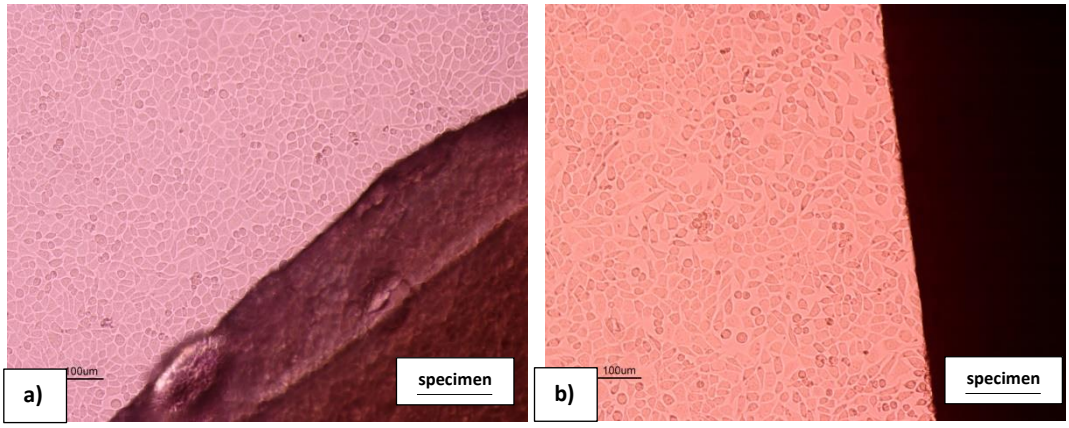

Figure 12.26. Direct contact assay to specimens of each composition that were sterilized by gamma irradiation: a) Ch+Gly and b) Ch+Gly+HA-TCP.

The results of the direct contact assay show cells on the surface and around the specimens. However, the cells around the specimens sterilized with ozone show morphologic disorders; the cells are no longer disc-shaped and are no longer concentrated next to the specimens. This observation may indicate cytotoxic effects on the cells.

12.3. Discussion

Sterilization requires validation to ensure the method's efficacy when applied to a certain material. However, this study did not focus on the sterility of the specimens assessed but rather if undesirable responses could happen if a certain sterilization method is applied to the chitosan-based compositions. With this goal in mind, four sterilization methods were selected: steam, EtO, ozone and gamma irradiation.

The EtO and steam sterilizations resulted in changes on the appearance of the specimens. In the first case, the Ch+Gly+HA-TCP specimens showed a yellowish colour, contrary to what happened with the remaining specimens, probably as a result of the Maillard reaction. According to Leceta *et al.*[431], Maillard reaction is promoted at higher temperatures and it involves the formation of conjugates between the carbonyl group with the amine group of chitosan. On the other hand, the specimens sterilized by EtO presented internal cracks as a result of the "dynamic" aeration process. Possibly, these cracks are avoidable if the aeration process takes place in a controlled environment with air circulation (time-consuming process).

Flexural tests:

The sterilization can cause different effects on the mechanical properties of the chitosan-based specimens. The increase of crosslinking density may explain the increase in the bonding strength, which explains the higher flexural modulus after a certain sterilization method [432,433]. However, if chain scission also occurs, the flexural strength may decrease [434]. This could have happened for the specimens sterilized by EtO. The polymer chain scission, resulting in a lower M_w, may also be accompanied by rearrangements in the structure by crosslinks between chains [435], which explain the situations in which the flexural strength increases without the increase in flexural modulus, as observed for the steam sterilizations. As reported by Lim *et al*.[433], the steam sterilization may involve an initial depolymerization of chitosan followed by interchain crosslink.

Overall, only gamma irradiation improves substantially the three properties, which happened for both compositions. Note that the results of the flexural tests performed on the non-sterilized chitosan-base specimens did not fully agree with the results presented in chapter 10, especially for the Ch+Gly+HA-TCP composition. In this case, the mean values for the flexural modulus, strength and strain decreased and approached the values of the non-sterilized Ch+Gly composition. The reason may be the machining process used, that guarantees exactly the same finish and dimensions for all the specimens, which was not easily guaranteed by manual machining. In addition, the Ch+Gly+HA-TCP specimens could have higher residual stresses introduced by the high speed of the machining process (CNC), which diminished their mechanical properties when compared with the results obtained for these specimens in the chapter 10.2.

Some studies analyze the effect of sterilization on the mechanical properties of biomaterials composed by chitosan. Yamaguchi *et al.*[434] produced cylindrical composites of chitosan and HA and studied their behavior after different steam sterilization temperatures. They found that the strain at failure and the bending strength increased with the temperature, but the modulus of elasticity decreased. These observations were much more evident for temperatures higher than 90°C. The results of these two studies are similar to the results obtained in this thesis, after the steam sterilization.

Nanoindentation tests:

Overall, the nanoindentation results do not change when the sterilized and non-sterilized specimens are compared. However, some statistical significance was found, especially for the Ch+Gly+HA-TCP compositions. Rearrangements in the microstructure of these specimens could lead to a decrease of the indentation hardness after the EtO, ozone and gamma irradiation sterilizations. It was also registered a decrease of the indentation modulus for the Ch+Gly+HA-TCP compositions sterilized by ozone. Since the surface of these specimens has become extremely hydrophilic after ozone sterilization (see the contact angle results), the absorbed water on their surface may have influenced these measures.

Comparing the mean indentation hardness results with the mean flexural strength results, only the Ch+Gly composition sterilized by steam became, at the same time, stronger and harder after the sterilization, when compared with non-sterilized results. Additionally, the results of these last specimens differ from the nanoindentation results obtained in chapter 10. Once again, this may be related with the machining process, as explained previously.

SEM analysis:

The SEM analysis on the fracture surface revealed differences between the compositions. The non-sterilized specimens showed crack propagation along all fracture surfaces, which are fairly smooth, characteristical of a typical brittle fracture. The cracks found have the same direction for the Ch+Gly composition, contrary to what happened for the Ch+Gly+HA-TCP composition, which propagated in different directions, probably due to the presence of ceramic material. The fracture surfaces of the sterilized specimens revealed a microstructure alteration since the crack propagation was not observed along the entire surface. This alteration may be related to the increase in the strength of the material, promoted by the sterilization. In this case, a larger crack was observed but almost no other cracks were present. These observations were more evident in the ozone and gamma sterilization for the Ch+Gly+HA-TCP composition, and in the steam sterilization for the Ch+Gly composition. Additionally, the fracture toughness probably increased for the sterilized specimens, deduced by the reduction in the number of cracks. However, to confirm this hypothesis, specific tests should be made to calculate the fracture toughness of the material before and after the sterilization, according to the available standards.

Contact angle measurement:

The contact angle measurements were performed to assess if the wettability of the materials' surface changed with sterilization, since such alterations may compromise the cell-implant biological interaction. Published studies indicate that polymers with enhanced hydrophilic properties promoted cell spreading and adhesion [436].

Changes on the surface occurred only for the Ch+Gly+HA-TCP composition sterilized by steam. In this case, the surface has become hydrophobic. The same result was found when Lim *et al.* [433] sterilized chitosan powder samples. They observed that specimens produced with such powders had lower affinity for water when the powder was exposed to autoclave. As explained in chapter 7.3.2, less wettability generally indicates that the solid surface is unfavorable for the fluid, and therefore it will tend to minimize its contact with the surface [307]. Comparing the SEM images of the non-sterilized surface and the surface sterilized by steam, for the Ch+Gly+HA-TCP composition, no noticeable changes are observed between their roughnesses which may promote this behavior of the water molecules. Therefore, the observed effect might be caused by the strong hydrogen bonds that have been established

after this sterilization process, which is so stable that prevents the formation of new hydrogen bonds between the water molecules and the surface (the water drop prefers to bond with itself). Other possibility is a significant reduction of the free hydroxyl groups in the treated surface which decreased its polarity (water affinity). This phenomenon might be promoted by the humid heat, allowing chemical reactions between neighbor chains (e.g. formation of ether and peroxide residues).

Regarding the ozone sterilization, the addition of polar hydrophilic groups to the surface (oxygen) led to a lower contact angle. For both compositions, the contact angle stayed below 5°, which characterize the sterilized surfaces as superwetting; the water spreads on it completely.

ATR-FTIR analysis:

The ATR-FTIR spectra did not reveal chemical changes on the surface of the two compositions caused by the different sterilization methods. However, some bands have different intensities, which may simply be related with poor contact between the specimen and the crystal, resulting in a lowest penetration depth of the evanescent wave.

According to the information provided by Shen *et al.*[432], the characteristic bands of chitosan at 3.450 cm^{-1}, 2.920 cm^{-1}, 1.660 cm^{-1}, 1.590 cm^{-1}, 1.380 cm^{-1} and 1.150–1.040 cm^{-1} correspond to hydroxyl group, CH_2 stretching vibration of pyranose ring, C=O in amide group, NH_2 in amino group, CH_3 in amide group and –C–O–C– in glycosidic linkage, respectively – all visible in Figure 12.20. The bands related with the ceramic material match with some bands of chitosan. The vibration of phosphate group occurs at 560 - 600 cm^{-1} and at 1.000–1.100 cm^{-1} (intensive bands) and the carbonate group forms weak peaks at 870–880 cm^{-1} and more intensive bands at 1.460–1.530 cm^{-1} [437]. In this sense, it is difficult to state (due to natural limitations of the technique) if any significant chemical change was promoted by the sterilization techniques in the specimens surfaces.

Cytotoxicity tests:

As already explained, tests were not performed to confirm the efficiency of the various sterilization methods' parameters in the elimination of the potential contamination level of the specimens. The goal was to assess the eventual cytotoxic effects caused by the different sterilization methods on the two chitosan-based compositions.

Higher cell viability was found for the Ch+Gly composition, which demonstrates the biocompatibility and antimicrobial power of chitosan materials, when they have higher D.D. Probably the addition of calcium phosphate may have hindered the availability of certain chitosan functional groups, responsible for such behavior. However, the cell viability detected from the extracts of the sterilized specimens with ozone was around 70%, which may indicate cytotoxicity. According to the ISO 10993-5, reduction of cell viability by more than 30% is considered a cytotoxic effect [322]. This observation may indicate that the oxidation effect promoted by the ozone sterilization was not able to inactivate the potential microorganisms present in the chitosan-bases specimens. Another possible explanation for this observation includes a direct oxidation effect on mouse fibroblasts L929 cells as a side effect of this sterilization. The images from the direct contact test (Figure 12.25) clearly show the real effect of the ozone sterilization; the cells grew around the chitosan-based specimens with morphologic disorders. This observation is not so clear for the other compositions, which supports the claim already made that the other sterilized specimens do not present cytotoxic effects to the cells.

Galante *et al.*[438] produced chitosan-tripolyphosphate hydrogel nanoparticles and sterilized them by applying different ozone cycles. In this case, the samples were effectively decontamined when 8 or 10 ozone pulses were applied. However, a slight reactivity was detected in the cells when the cytotoxic tests were performed. The cytotoxic results obtained in this thesis and by Galante *et al.*[438] indicated, respectively, that either 4 or 8 pulses may cause slight reactivity on the cells when chitosan-based materials are sterilized by ozone.
Note that the specimens used as control were also sterilized with 70% ethanol, to avoid potential contamination inside the incubator. Although this solvent is not considered a sterilizing agent, but instead a good disinfectant, it is concluded that the specimens may not be heavily contaminated by microorganisms, since the viability of the cells was also higher than 80% in this case.

12.4. Conclusion

For the development of successful medical devices, it is extremely important to study and define a cost-effective sterilization process where sterility is achieved without exerting harmful effects on the materials. Therefore, it is crucial to find an effective terminal sterilization method that does not compromise the biological, chemical and mechanical properties of the medical devices.
Chitosan is extremely sensible to sterilization. In this field, different publications are available, but none focused on the study of the sterilization effects in dense chitosan-based compositions. Normally these studies involve chitosan-based hydrogels, scaffolds, films, among others. Therefore, in this thesis, steam, EtO, ozone and gamma irradiation were employed for the sterilization of chitosan-based specimens. Among these methods, only ozone sterilization is considered a non-traditional method by the FDA. Several tests were then performed to evaluate the behavior of the two chitosan-based compositions, before and after the sterilization. These tests included flexural, nanoindentation, contact angle and cytotoxicity tests. Additionally, SEM analyses and ATR-FTIR were performed, respectively, to detect alterations on the microstructure and on surface chemistry of the sterilized compositions.
The flexural tests revealed that the mean values for the flexural modulus, the flexural strength and the flexural strain only increased for the specimens sterilized by a gamma irradiation dose of 15 kGy. However, in general, the different sterilization methods have increased the strength of the material, except for the specimens sterilized by EtO. In this case, the procedure employed during the EtO sterilization caused damage in its internal structure.
The results of the contact angle and cytotoxic tests reinforced the suitability of gamma irradiation on the sterilization of chitosan-based compositions. In the first case, the specimens maintained their hydrophilic behavior except for the steam sterilization on the Ch+Gly+HA-TCP composition. For the ozone sterilization, the introduction of oxygen-containing functional groups on the surface of the specimens strongly increased their wettability, which ultimately could favor the cell interactions with the material. However, the cytotoxic tests revealed cell viability close to 70% and disturbances on the morphology of the cells when direct contact tests were performed. Additionally, the steam sterilization made the surface of the Ch+Gly+HA-TCP compositions hydrophobic. For these reasons, it can be considered that the ozone and steam are not suitable for the sterilization of the Ch+Gly and Ch+Gly+HA-TCP

specimens, because it changes the non-cytotoxic and hydrophilic behavior of the material into a less friendly matrix which interacts negatively with the cells.
Overall, this study confirmed that the properties of the two chitosan-based compositions are not strongly impaired by the different sterilization methods, with greater advantages if sterilization is achieved by gamma irradiation instead.

13. Development of bioabsorbable screws based on the chitosan-based compositions selected

The machining capabilities of the dense chitosan-based compositions, selected as described in the previous chapters, were further tested for the development of screws for the ACL reconstruction surgery. To attain this goal, different machining steps were necessary to replicate a geometry that was based on the opinion of an orthopedist.

13.1. Characteristics of bioabsorbable screws

Orthopedic screws are commonly used for internal fracture fixation, to hold two or more objects [439]. The device converts the torque applied during its insertion into a compressive force between the two components that it is placed through [440]. An overview of the functional parts of a screw can be seen in Figure 13.1. It consists of different functional parts:

- the head serves as an attachment for the screw driver [439,440];
- the shaft (not represented in the figure below) is the smooth portion of the screw between the head and the threaded region [439].
- the thread is defined by its core diameter (minimum diameter of the screw across the base of the thread), its thread diameter (outside diameter that corresponding to the widest diameter of the screw) and its pitch (distance between adjacent threads) [439,440]. It provides the main support of the screw [439,440].
- the tip of the screw is the end opposite to the head [439].

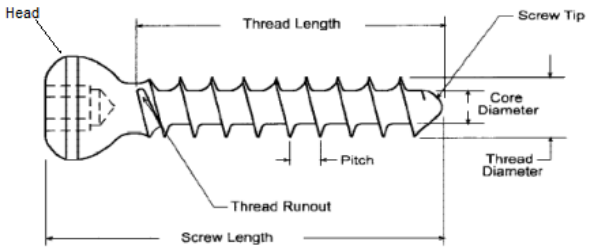

Figure 13.1. Exemplification of the functional parts of the screw [441].

In ACL reconstruction surgery, the interference screw is considered the *gold standard* fixation mechanism, being widely used in the fixation of BPTB grafts [215]. Its purpose is to hold the graft in a drilled bone tunnel while the tissues heal. For more information regarding the ACL reconstruction surgical procedure consult the chapter 5.1.4. Also, in chapter 2.1., the Figure 2.1 exemplifies two different interference screws used in those surgeries.

Currently, several companies manufacture interference screws to use in the ACL reconstruction surgery (see Table 2.2). There are a large number of variables in interference screw designs between the different companies [442]. Examples include size availabilities (diameter, length), shape (tapered/conical, cylindrical), thread profile (Buttress, V-shaped), thread pitch (constant, variable), screw head (round head, tapered head, flat head/headless), screw head design (hexagonal, triangular, quadrangular, six-stars, pentalobe, trilobe), tip profile (self-tapping, nonself-tapping) and materials (metal, bioabsorbable) [442].

The main characteristics of graft fixation in ACL reconstruction are strength and stiffness [215,443]. The literature refers that the normal ACL undergo forces of up to 500 N during daily living activities, thus the graft fixation mechanism should be able to withstand forces greater than this amount [443]. Therefore, the interference screw must be [215]:

- Strong enough to avoid failure;
- Stiff enough to restore load displacement response and allow biological incorporation of the graft into the bone tunnels;
- Secure enough to resist slippage under cyclic loading.

Several factors may influence the potential failures of interference screws [215,442]:

- Incorrect screw size and diameter (e.g. graft/screw tunnel mismatch);
- Tunnel/screw divergence (the direction of the screw is not parallel to the axis of the bone tunnel);
- Graft advancement, graft translocation, graft fracture and laceration of tensioning sutures;
- Bone mineral density (larger diameter interference screw should be used for fixation in the proximal tibia than that used for fixation on the distal femur since the bone mineral density is higher on the femur side).

According to Antoniac *et al.*[442], interference screws must minimize tissue laceration and shear stress on the graft, while maximizing insertion torque pullout strength. Additionally, if the screw is manufactured from a bioabsorbable material, it must not cause inflammatory reactions and the absorption rates must be correlated to osteointegration. One important aspect to take into consideration is that the screwdriver design has to be designed to avoid the screw breakage during insertion, to minimize the insertion torque and to distribute it along the entire screw length [444].

The literature includes different biomechanical studies, whose purpose is to establish relationships between various screw design parameters and the fixation strength, pullout strength, compressive forces or insertion torque [215,442,443]. However, the conclusions of these studies are influenced by the type of material/specimens (human, sawbones, bovine, ovine, porcine) used in the experiments [215,442,443].

13.2. Experimental development process of the screw

13.2.1. Screw geometry

The goal of this work was not to obtain a new design for the chitosan-based screw in the ACL reconstruction, but instead to test the machining capabilities of chitosan-based compositions, reproducing the screw geometry of a bioabsorbable implant currently being used in this surgery.

To better understand the choice of a particular bioabsorbable screw for the ACL reconstruction, an interview was conducted with an orthopedic surgeon, who is a specialist in the treatment of the ACL and other knee injuries in the Portuguese private healthcare sector.

Focus was given to four current designs: the two models presented in Figure 2.1 of chapter 2.1. (headless or full thread screws), and the round heads versions of those models. The feedback collected from the interview established the following selection criteria:

- preference for headless screws;
- the contact area between the screw and the graft must be as large as possible;
- screws must not have sharp edges.

Comparing the four proposed geometries, the surgeon's preference was the headless geometry of ComposiTCP®60, whose 2D model is indicated in Appendix A.6. In this case, the thread filament is less pointed, which avoids lacerations of the graft. However, the introduction of a more flattened crest, as well as a thread angle may favor the behavior of the screw. These two changes, exemplified in the screw drawing of Figure 13.2, promote an increasing contact area between the screw and the graft.

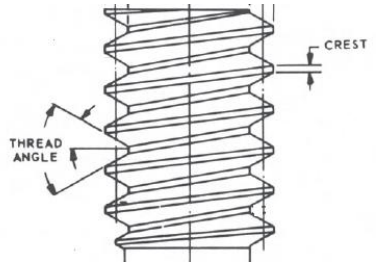

Figure 13.2. Components of the screw – thread angle and crest [440].

The final geometry of the chitosan-based screws included a conical end without the thread. This design makes it easier to point the screw in the correct direction before screwing it.

13.2.2. Production of rods

Two groups of rods were produced from the compositions selected in chapter 10, according to the production process described in chapter 9.4. Therefore, Ch+Gly blocks were produced by adding 10% (w/v) glycerol and the Ch+Gly+HA-TCP blocks were produced by adding 10% (w/v) glycerol and 10% (w/w) of HA-TCP to the stage 1 of the production process.

The shaping of the blocks into rods (stage 7 of the production process) took three machining steps. First, the blocks were divided longwise, resulting in two parts with non-uniform geometry. The goal was to avoid the central part of the blocks, which shrunk slightly in the center after drying. Next, the parts were round manually using a whetstone grinding machine. The last step involved the use of a conventional lathe machine for the final uniformity of the rod diameter. All the rods had a diameter of 6,5 mm and an average length of 28 mm.

13.2.3. Production of screws

The screws were shaped by a CNC milling machine based on the previously selected geometry. Due to the impossibility to obtain rods with dimensions that allow a faithful reproduction of the selected screw geometry, a scale-down of the original model was made on the chitosan-based screws. The opinion of the orthopedic surgeon was also considered in this stage, leading to some changes in the original geometry. These changes included the definition of a thread angle, flattened crest and a conical end of the screw free of threads, as reported previously.

For the shaping of the screws, it was necessary to construct a nylon holding system that, at the same time, centered and fixed the rods and contained the vibration of the machining process. The rod was introduced inside the tunnel structure represented in Figure 13.3 and the machining was performed only on the material that remained outside. As shown in Figure 13.4 a), for each final screw, about 1/3 of the rod material was not machined.

A 22 mm disc milling cutter from HSS was used at a cutting speed of 138 mm/minute (rotation speed of 2.000 rpm), following a helical cutting path. The feed per tooth was 3 µm. During this process, a jet of cold air was continuously directed to the surface of the material, to avoid heating and differences in their consistency that could lead to failure. Additionally, this jet of cold air also allowed cleaning the material and the cutting tool (chips removal) throughout the machining process.

The machined screws presented the following final dimensions: thread diameter of 6,5 mm, pitch length of 2,1 mm, thread angle of 20°, crest length of 0,5 mm and conical length of 3 mm. The thread length varied between 10 and 20 mm. Figure 13.4 b) shows a Ch+Gly+HA-TCP screw with a thread length of 17 mm.

The original screw model (Appendix A.6.) has a pentalobe shape and it is perforated for the screwdriver to extend throughout the entire screw. However, in the chitosan-based screws, only a simple hole (1,7 mm of diameter) was drilled as a proof of concept.

All the Ch+Gly and Ch+Gly+HA-TCP screws produced are represented, respectively, in Figure 13.5 and Figure 13.6.

Figure 13.3. Nylon holding system.

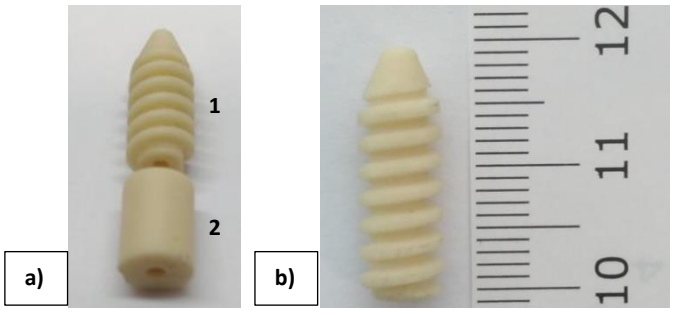

Figure 13.4. a) Screw after the machining process (zone 1) and material that remained in the holding system (zone 2); b) Example of a screw length.

Figure 13.5. Ch+Gly screws.

Figure 13.6. Ch+Gly+HA-TCP screws.

13.2.4. Discussion

Before transforming the chitosan-based blocks into screws, it was first necessary to shape them into rods through three machining steps. The first step, i.e. the cutting of the blocks in two equal parts, was fundamental since it avoided the central part of the block. Preliminary test rods were machined from the core material of the blocks. However, these rods bent slightly shortly after their production which may indicate that the blocks were not completely dry or even had defects on their center. Previously, the Ch+Gly and Ch+Gly+HA-TCP specimens were obtained from the blocks simply by reducing their size until they reached the rectangular plate format with average dimensions of 25 mm × 12 mm × 4 mm. Therefore, if the central core of the block was not completely dry, the plate format ensured that the drying process that was still occurring was efficient and controlled (large area and low volume). This is why the bending effect was not evident in the previous studies. When the blocks were shaped into rods, all the material was wasted except for the core material, which might not be totally dry and solid. As a consequence, these core materials changed their drying rate when exposed to atmospheric conditions (humidity and temperature), thus leading to the new conformations of the rod materials.

Since the blocks dried faster on the surface than on its core, traction forces may have been generated from the inside to the outside of the blocks. This may also explain why some fissures were observed in the preliminary rods, visible shortly after their machining.

The screws were successfully obtained from the two types of blocks tested: Ch+Gly and Ch+Gly+HA-TCP. The screws obtained from the ceramic compositions revealed less surface imperfections and fissures than the other screws.

The screws were obtained after a time-consuming phase of material preparation, to reach the circular shape of the rods. Even though the experimental procedure used for the screws preparation was adequate for this work stage, it might not be suitable for an industrialization phase, which requires mass production. Different strategies may solve this problem:

- Use of circular molds, with smaller diameters (e.g. Tetra Pak® molds or molds from materials with low friction coefficient). The goal is not only to optimize the drying process, but also to avoid waste of material. From the chitosan-based circular blocks,

the screws can be obtained either by material removal technologies (e.g. CNC machining) or by forging the material by applying impact.

- Introduce the hydrogel directly in a mold that reproduces the geometry of the desired screw. During the drying stage, compression can be applied on the mold with the following goals: forcing the exit of water, to counteract the tensile forces that can be generated during the drying of the material and to obtain an approximate shape of the screw. After this stage, the resulting block would be machined to fine-tune the desired geometry of the screw.

13.3. Conclusion

Several screws were produced from the selected chitosan-based compositions: Ch+Gly and Ch+Gly+HA-TCP. The geometry was successfully reproduced in these two compositions. Nonetheless the Ch+Gly revealed some imperfections that may reveal less resistance of this composition to the forces imposed during the machining process, when compared with the Ch+Gly+HA-TCP composition.

The screws were obtained through different machining stages, necessary to convert the blocks into rods and the rods into screws. These stages were time-consuming, especially in obtaining of the rods, and involved the preparation of different tools and machines. Therefore, these screws lose competitiveness if this experimental procedure is reproduced in the industrialization phase. Several solutions may be employed to increase the competitiveness of the chitosan-based screws, such as the use of circular molds and eventually process the screws by forging.

It must be stressed out that both compositions allowed the use of several techniques of shaping, which proves its versatility and widens the range of possible geometries.

SECTION E: Final conclusion and future directions

14. Conclusion and future directions

Bioabsorbable implants play an important role in the treatment of musculoskeletal disorders since they are able to reduce the problems associated with the rigid fixation implants, such as the stress shielding effect caused by metals, avoiding the need for a second surgery after the biological consolidation. However, problems such as lack of mechanical strength and inflammatory reactions motivate the continuous research in this field, in order to achieve a bioabsorbable implant with optimal mechanical properties and improved biological features.
Therefore, the main goal of this work was to produce and characterize 3D dense chitosan-based specimens to be used as bioabsorbable fixation devices for orthopedic applications. To achieve this goal, this work was divided in several tasks:

a) The current market of bioabsorbable orthopedic implants was studied, to understand the key features that characterize such implants and the developments that have been made on their properties over the past years. The problems that are still associated with these implants were explored, focusing in all orthopedic areas, and the potential for new improvements were explored, under the current and future research strategies.
Based on the information collected, and with the help of experts, the ACL reconstruction was selected as a candidate application to benefit from the development of a new bioabsorbable implant. Although there is room for mechanical and biological improvements of the current implants, the economic analysis developed in this thesis showed that a bioabsorbable implant that only improves the biological behavior, by reducing the complications that cause pain and stiffness symptoms, will have an economic benefit for the society. Therefore, the economic model developed in this thesis supports the research and development of new bioabsorbable implants based on chitosan, since this polymer is biodegradable, it offers good biological properties (biocompatibility, biodegradability, etc.) and it promotes bone formation.

b) Several challenges are associated with chitosan, namely the development of tridimensional structures with controllable and predictable performance. Therefore, the production process of 3D dense structures for orthopedic applications was optimized from a process developed in a previous study. Critical production stages were optimized (dissolution, molding, freezing and precipitation) to obtain processable chitosan blocks without structural defects and with properties that do not vary in each production batch. For this optimization step, it was crucial to select the chitosan material to work.

c) To produce chitosan-based implants with appropriate strength and stiffness, essential for the successful treatment of orthopedic injuries, different blends of chitosan with other materials were tested. Blends with different concentrations of plasticizers (glycerol and sorbitol) and blends with different concentrations of ceramic materials (HA and HA-TCP) were tested to determine their flexural modulus, strength, strain and hardness. Two compositions were chosen, within each group of materials, according to the best set of mechanical properties assessed. Another key aspect for the selection of the materials was their ease-to-shape features, which widened the scope of possible shapes that the 3D dense products can undergo. The compositions selected were Ch+Gly (chitosan + 10% glycerol) and Ch+Gly+HA-TCP (chitosan + 10% glycerol + 10% biphasic mixture HA -β TCP).

d) *In vitro* degradation tests and *in vitro* differentiation tests were performed to understand if the mechanical properties of the selected compositions are maintained for at least 6 months after the implantation in the human body and to understand if these materials are able to interplay positively with the surrounding tissues, promoting bone formation. The results from the biological tests confirmed the potential of these two compositions in promoting the healing of the tissues without losing their mechanical performance. The results indicated a superior biological response of the Ch+Gly composition when compared with the Ch+Gly+HA-TCP composition.

e) A critical attribute of implantable medical devices is their sterility, since they must be free of viable microorganisms. However, care should be taken when a sterilization method is chosen, since it can affect negatively the properties of the materials. Therefore, different sterilization methods were applied to the selected chitosan-based compositions to subsequently test the effects of each of the sterilizations on the short-term properties of those materials. The results indicated that the selected compositions do not alter significantly their properties, identifying the gamma irradiation at 15 kGy as the one that less change causes in the mechanical, physical and cytotoxic behavior in both compositions. For this sterilization condition, both compositions had similar responses in all the measured properties.

f) Screws were machined from the Ch+Gly and Ch+Gly+HA-TCP compositions. Different machining procedures were used to transform the blocks into screws. The two compositions allow the use of machining conditions, being the Ch+Gly+HA-TCP composition the one with the best mechanical behavior, which favors the reproduction of the selected geometry without the appearance of imperfections or defects in the material. The results proved the versatility of the 3D dense chitosan-based compositions, which are capable of being machined into simple rectangular plates or in more complex geometries like the screws.

Overall, the goals of this thesis were attained (see chapter 1). The following table summarizes the main outputs of this thesis, considering the key-properties desired for the chitosan products in orthopedics:

Table 14.1. Summary of the results obtained in this thesis (++ goal is surpassed; + goal is achieved; +/- goal requires improvements; - goal not attained).

Key-properties for the chitosan bioabsorbable products	Properties attained	Comments
Processable	+	Two chitosan-based compositions were selected based on their mechanical and ease-to-shape features. Rectangular plates and screws were shaped successfully, through different machining methodologies.
Suitable strength and stiffness	+	The mechanical properties of the two chitosan-based compositions are comparable to the properties of the PLDLA (Table 2.3) and attain the values reported by Hasirci, *et al.*[408], who studied the behavior of PLGA and PLA bioabsorbable plates, after the biodegradation and sterilization processes.
Suitable biodegradation profile	++	The two-chitosan materials do not degrade and do not lose mechanical properties in 6 months of *in vitro* degradation.

Key-properties for the chitosan bioabsorbable products	Properties attained	Comments
Sterilizable without compromising its properties	++	The matrix of the chitosan-based compositions is not impacted by different sterilization conditions and even benefits when the sterilization is performed by gamma irradiation.
Not cytotoxic	++	The materials blended to chitosan do not alter the biocompatibility of the material.
Promote bone formation	+	The two chitosan-based compositions revealed osteoinduction properties in *in vitro* evaluations.

For the chitosan-based implants to be available and to be a reality in the market of bioabsorbable orthopedic implants they must initially provide secure fixation and have appropriate mechanical properties; have a gradual degradation as biologic fixation is established and be metabolized; not cause inflammation or other toxic response; be sterilized and easily processed into a final product that has an acceptable shelf life. Therefore, to accomplish all these goals, it is still necessary:

i) to ensure that the blocks are completely dry on their inside. The blocks dry faster on their surface than on their core. The introduction of pressure (compression force) on the blocks, during this stage, may counteract the traction forces that may have been generated inside the blocks. However, it must be considered that the blocks are hydrogels at the beginning of the drying and thus are susceptible to deformation during the first days inside the stove. A controlled and gradual compression force, especially in the later drying stages, may solve this problem. Completely dry materials are easily achieved if they dry in such a way that hot air circulates equally on all their sides and if other molds, with smaller dimensions (e.g. thickness), are used.

ii) to define rules for the chitosan properties in the development of bioabsorbable implants in order to mitigate the risk of batch to batch inconsistencies of the raw material (intrinsic variability due to its biological origin). These rules go through the establishment of the origin of the material, the methods for the determination of its properties (e.g. M_w and D.D.) and the working ranges in such properties;

iii) to perform further *in vitro* tests, to assess the biocompatibility of the sterilized specimens. The goal would be to study the effect of the sterilization on the long-term degradation behavior of the chitosan-based compositions (minimum 12 months) and the potential side effects on the cells differentiation, which may hinder osteogenesis. Additional *in vitro* tests should include hemocompatibiliy, genotoxicity, among others, as reported in the International Standard ISO 10993;

iv) to study the mechanical behavior of hydrated specimens to understand if their dry properties change in *in vivo* conditions;

v) to study the scale-up production of precursors of final shaped chitosan-based medical implants. Based on the selected orthopedic application (ACL reconstruction), outline a business model that includes the projections for the operational costs, sales projections, revenues, etc.

Explore different production alternatives, such as "*in house*" production or outsourcing the production to other companies;

vi) to validate the sterilization, the packaging, the production process, the shelf life of the product and perform the risk analysis. These stages are necessary to outline the technical documentation, necessary to obtain the CE mark.

REFERENCES

1. Institute for Health Metrics and Evaluation. The Global Burden of Disease: Generating Evidence, Guiding Policy. WA:IHME; 2013.
2. Bill F, Foundation MG. Global , regional , and national incidence , prevalence , and years lived with disability for 301 acute and chronic diseases and injuries in 188 countries , 1990 – 2013 : a systematic analysis for the Global Burden of Disease Study 2013. The Lancet. 2015,386,1990–2013.
3. March L, Smith EUR, Hoy DG, Cross MJ, Sanchez-Riera L, Blyth F, Buchbinder R, Vos T, Woolf AD. Burden of disability due to musculoskeletal (MSK) disorders. Best Practice and Research: Clinical Rheumatology. 2014,28(3),353–66.
4. Bevan S. Economic impact of musculoskeletal disorders (MSDs) on work in Europe. Best Practice & Research Clinical Rheumatology. 2015,29(3),356–73.
5. Mukherjee DP, Pietrzak WS. Biabsorbable Fixation: Scientific, Technical and Clinical Concepts. Journal of Craniofacial Surgery. 2011,22(2),679–89.
6. Ciccone II WJ, Motz C, Bentley C, Tasto JP. Bioabsorbable Implants in Orthopaedics: New Developments and Clinical Applications. Journal of the American Academy of Orthopaedic Surgeons. 2001,9(5),280–8.
7. Amini AR, Wallace JS, Nukavarapu SP. Short-Term and Long-Term Effects of Orthopedic Biodegradable Implants. Journal of Long-Term Effects of Medical Implants. 2012,21(2),93–122.
8. Inion OY. White Paper: An Introduction to Biodegradable Polymers as Implant Materials. Tampere, Finland;
9. Venkatesan J, Vinodhini PA, Sudha PN, Kim S-K. Chitin and chitosan composites for bone tissue regeneration. 1st ed. Vol. 73, Advances in food and nutrition research. Elsevier Inc.; 2014. 59-81.
10. Liu X, Ma L, Mao Z, Gao C. Chitosan-Based Biomaterials for Tissue Repair and Regeneration. Advances in Polymer Science. 2011,(April),81–128.
11. Alvarenga ES De. Characterization and Properties of Chitosan. In: Biotechnology of Biopolymers. 2006. p. 91–108.
12. Venkatesan J, Kim S-K. Chitosan composites for bone tissue engineering--an overview. Marine drugs. 2010,8(8),2252–66.
13. Sarasam A, Madihally S V. Characterization of chitosan-polycaprolactone blends for tissue engineering applications. Biomaterials. 2005,26(27),5500–8.
14. Oh DX, Hwang DS. A biomimetic chitosan composite with improved mechanical properties in wet conditions. Biotechnology progress. 2013,29(2),505–12.
15. Muzzarelli R a. a. Chitins and chitosans for the repair of wounded skin, nerve, cartilage and bone. Carbohydrate Polymers. 2009,76(2),167–82.
16. Di Martino A, Sittinger M, Risbud M V. Chitosan: a versatile biopolymer for orthopaedic tissue-engineering. Biomaterials. 2005,26(30),5983–90.
17. Pillai CKS, Paul W, Sharma CP. Chitin and chitosan polymers: Chemistry, solubility and fiber formation. Progress in Polymer Science. 2009,34(7),641–78.
18. Rokkanen P, Böstman O, Hirvensalo E, Partio E., Mäkelä E., Pätiälä H, Vihtonen K. Bioabsorbable implants in orthopaedics. Current Orthopaedics. 1999,13(3),223–8.
19. Rokkanen PU, Bökstman O, Hirvensalo E, Mäkeläk EA, Partio EK, Pätiälä H, La T, Vainionpää S, Vihtonen K, Törmälä P. Bioabsorbable fixation in orthopaedic surgery and traumatology. Biomaterials. 2000,21(24),2607–13.
20. Navarro M, Michiardi A, Castaño O, Planell JA. Biomaterials in orthopaedics. Journal of the Royal Society, Interface. 2008,5(27),1137–58.
21. Hofmann GO. Biodegradable implants in traumatology : a review on the state-of-the-art. Archives of Orthopaedic and Trauma Surgery. 1995,114,123–32.
22. Nair LS, Laurencin CT. Biodegradable polymers as biomaterials. Progress in Polymer Science. 2007,32(8-9),762–98.
23. Lewallen EA, Riester SM, Bonin CA, Kremers HM, Dudakovic A, Kakar S, Cohen RC, Westendorf JJ, Lewallen DG, van Wijnen AJ. Biological Strategies for Improved Osseointegration and Osteoinduction

of Porous Metal Orthopedic Implants. Tissue Engineering: Part B. 2015,21(2),218–30.

24. Harwood PJ, Stewart TD. Mechanics of musculoskeletal repair devices. Orthopaedics and Trauma. 2016,In Press,1–9.
25. Taljanovic MS, Jones MD, John RT, Benjamin JB, Sheppard JE, Hunter TB. Fracture Fixation. RadioGraphics. 2003,23(6),1569–90.
26. Suchenski M, McCarthy MB, Chowaniec D, Hansen D, McKinnon W, Apostolakos J, Arciero R, Mazzocca AD. Material properties and composition of soft-tissue fixation. Arthroscopy. 2010,26(6),821–31.
27. Hutmacher D, Hürzeler MB, Schliephake H. A review of material properties of biodegradable and bioresorbable polymers and devices for GTR and GBR applications. The International Journal of Oral and Maxillofacial Implants. 1996,11(5),667–78.
28. Eglin D, Alini M. Degradable polymeric materials for osteosynthesis: tutorial. European Cells and Materials Journal. 2008,16,80–91.
29. Kohane DS, Langer R. Polymeric Biomaterials in Tissue Engineering. Pediatric Research. 2008,63(5),487–91.
30. Pietrzak WS. Principles of Development and Use of Absorbable Internal Fixation. Tissue Engineering. 2000,6(4),425–33.
31. Oliveira NG, Pinto LF V, Reis L, Rodrigues A. Competitiveness of chitosan-based implants. Ciência & Tecnologia dos Materiais. 2014,26(2),77–88.
32. Dhillon M, Lokesh A. Bioabsorbable implants in orthopaedics. Indian Journal of Orthopaedics. 2006,40(4),205–9.
33. Agrawal CM. Biodegradable Polymers for Orthopaedic Applications. Reis RL, Cohn D, editors. Polymer Based Systems on Tissue Engineering , Replacement and Regeneration. Dordrecht: Springer; 2002. 25-36.
34. Waris E, Konttinen Y, Ashammakhi N, Suuronen R, Santarvita S. Bioabsorbable fixation devices in trauma and bone surgery : current clinical standing. Expert Review of Medical Devices. 2004,1(2),229–40.
35. The U.S. Market for Medical Devices. Opportunities and Challenges for Swiss Companies. Swiss Business Hub. Chicago, USA; 2011.
36. Orthopedic Implants - A Global Market Overview [Internet]. Market Publishers. 2011 [cited July 7, 2016]. Available at:

    https://pdf.marketpublishers.com/iexperts/orthopedic_implants_a_global_market_overview.pdf
37. Sports Medicine Market worth 8.3 Billion USD by 2020 [Internet]. Markets and Markets. Available at: http://www.marketsandmarkets.com/PressReleases/sports-medicine-devices.asp
38. $5.7B by 2020: 10 trends in the orthopedic trauma fixation devices market [Internet]. Becker's Healthcare. 2014 [cited July 7, 2016]. Available at: http://www.beckersspine.com/orthopedic-a-spine-device-a-implant-news/item/21863-5-7b-by-2020-10-trends-in-the-orthopedic-trauma-fixation-devices-market.html
39. Trauma Fixation – US Analysis and Market Forecasts (Executive Summary). Global Data. London, UK.; 2013.
40. GlobalData. Spinal Fusion – Global Analysis and Market Forecasts. London, UK.; 2014.
41. Zhang Z, Ortiz O, Goyal R, Kohn J. 13 Biodegradable Polymers. Ebnesajjad S, Modjarrad K, editors. Handbook of Polymer Applications in Medicine and Medical Devices. Elsevier Inc.; 2014. 303-336 p.
42. Sheikh Z, Najeeb S, Khurshid Z, Verma V, Rashid H, Glogauer M. Biodegradable Materials for Bone Repair and Tissue Engineering Applications. Materials. 2015,8(9),5744–94.
43. Maurus PB, Kaeding CC. Bioabsorbable Implant Material Review. Operative Techniques in Sports Medicine. 2004,12(3),158–60.
44. Middleton JC, Tipton AJ. Synthetic biodegradable polymers as orthopedic devices. Biomaterials. 2000,21(23),2335–46.
45. Santoro M, Perale G. 6. Using synthetic bioresorbable polymers for orthopedic tissue regeneration. In: Jenkins M, Stamboulis A, editors. Durability and Reliability of Medical Polymers. Woodhead Publishing; 2012. 119–39.
46. Törmälä P, Pohjonen T, Rokkanen P. Bioabsorbable polymers: materials technology and surgical applications. Proceedings of the Institution of Mechanical Engineers, Part H: Journal of Engineering

Manufacture. 1998,212(2),101–11.

47. Sugih AK, Picchioni F, Heeres HJ. Experimental studies on the ring opening polymerization of p-dioxanone using an Al(OiPr)3-monosaccharide initiator system. European Polymer Journal. 2009,45(1),155–64.

48. Laine K. Rotational Melt Spinning as a Manufacturing Method For Tissue Engineering Scaffolds (Master Dissertation). Tampere University of Technology; 2013.

49. Wang M. Developing Bio-Stable and Biodegradable Composites for Tissue Replacement and Tissue Regeneration. In: Materials Research Society Symposium Proceedings. San Francisco, CA; USA; 1-5 Apr.; 2002. 83–93.

50. Suwanprateeb J, Trongtong P. Radiation enhanced modification of HDPE for medical applications. Journal of Materials Science: Materials in Medicine. 2003,14(10),851–5.

51. Kurtz SM. Chapter 6 – Chemical and Radiation Stability of PEEK. In: Kurtz SM, editor. PEEK Materials Handbook. 1st Ed. Oxford: Elsevier; 2012. 75–9.

52. Savvidis P, Givissis P, Papalois A, Apostolou T, Christodoulou A. Is the Use of Bioabsorbable Materials in Orthopaedic Surgery Associated with Infections? Review of the Literature. International Journal of Orthopaedics. 2015,2(2),238–42.

53. Gajjar CR, King MW. Degradation Process. In: Resorbable Fiber-Forming Polymers for Biotextile Applications. Cham: Springer; 2014. 7–11. (SpringerBriefs in Materials).

54. Pietrzak WS, Sarver D, Verstynen M. Bioabsorbable Implants - Practical Considerations. Bone. 1996,19(1),109–19.

55. Kontakis GM, Pagkalos JE, Tosounidis TI, Melissas J, Katonis P. Bioabsorbable materials in orthopaedics. Acta Orthopaedica Belgica. 2007,73(2),159–69.

56. Pietrzak WS. Bioabsorbable Polymer Applications in Musculoskeletal Fixation and Healing. In: Pietrzak WS, editor. Musculoskeletal Tissue Regeneration Biological Materials and Methods. Human Press; 2008. 509–29.

57. Ambrose CG, Clanton TO. Bioabsorbable Implants : Review of Clinical Experience in Orthopedic Surgery. Annals of Biomedical Engineering. 2004,32(1),171–7.

58. Wuisman PIJM, Smit TH. Bioresorbable polymers: heading for a new generation of spinal cages. European Spine Journal. 2006,15(2),133–48.

59. Qiu Q-Q, Sun W-Q, Connor J. 4.410. Sterilization of Biomaterials of Synthetic and Biological Origin. In: Ducheyne P, Healy KE, Hutmacher DW, Grainger DW, Kirkpatrick CJ, editors. Comprehensive Biomaterials - Volume 4: Biocompatibility, Surface Engineering, and Delivery of Drugs, Genes and Other Molecules. Boston, USA: Elsevier; 2011. 127–44.

60. Peltoniemi H, Ashammakhi N, Kontio R, Waris T, Salo A, Lindqvist C, Grätz K, Suuronen R. The use of bioabsorbable osteofixation devices in craniomaxillofacial surgery. Oral Surgery, Oral Medicine, Oral Pathology, Oral Radiology, and Endodontology. 2002,94(1),5–14.

61. Ibrahim AMS, Koolen PGL, Kim K, Perrone GS, Kaplan DL, Lin SJ. Absorbable Biologically Based Internal Fixation. Clinics in Podiatric Medicine and Surgery. 2015,32(1),61–72.

62. Kmettya Á, Bárány T, Karger-Kocsis J. Self-reinforced polymeric materials: A review. Progress in Polymer Science. 2010,35(10),1288–310.

63. Törmälä P, Vasenius J, Vainionpää S, Laiho J, Pohjonen T, Rokkanen P. Ultra-high-strength absorbable self-reinforced polyglycolide (SR-PGA) composite rods for internal fixation of bone fractures: in vitro and in vivo study. Journal of Biomedical Materials Research - Part A. 1991,25(1),1–22.

64. Francois E, Dorcemus D, Nukavarapu S. Biomaterials and scaffolds for musculoskeletal tissue engineering. In: Nukavarapu S, Freeman J, Laurencin C, editors. Regenerative Engineering of Musculoskeletal Tissues and Interfaces. Cambridge, UK: Woodhead Publishing; 2015. 1–23.

65. Tan L, Yu X, Wan P, Yang K. Biodegradable Materials for Bone Repairs: A Review. Journal of Materials Science & Technology. 2013,29(6),503–13.

66. Kohn D, Rose C. Primary stability of interference screw fixation. Influence of screw diameter and insertion torque. The American Journal of Sports Medicine. 1994,22(3),334–8.

67. Weiler A, Hoffmann RF, Siepe CJ, Kolbeck SF, Südkamp NP. The influence of screw geometry on hamstring tendon interference fit fixation. The American Journal of Sports Medicine. 2000,28(3),356–9.

68. Gaweda K, Walawski J, Węgłowski R, Krzyzanowski W. Comparison of bioabsorbable interference

screws and posts for distal fixation in anterior cruciate ligament reconstruction. International orthopaedics. 2009,33(1),123–7.

69. Parsons E, Yu J, Pedroza AD, Kaeding CC. In vivo degradation characteristics of bioabsorbable cross-pins in anterior cruciate ligament reconstruction. The Knee. 2013,20(4),281–6.

70. Shen C, Jiang S-D, Jiang L-S, Dai L-Y. Bioabsorbable versus metallic interference screw fixation in anterior cruciate ligament reconstruction: a meta-analysis of randomized controlled trials. Arthroscopy. 2010,26(5),705–13.

71. Pereira H, Pereira HMD, Correlo VM, Silva-Correia J, Oliveira JM, Reis RL, Reis Ceng RL, Espregueira-Mendes J. Migration of "bioabsorbable" screws in ACL repair. How much do we know? A systematic review. Knee surgery, sports traumatology, arthroscopy : official journal of the ESSKA. 2013,21(4),986–94.

72. Dhawan A, Ghodadra N, Karas V, Salata MJ, Cole BJ. Complications of bioabsorbable suture anchors in the shoulder. The American journal of sports medicine. 2012,40(6),1424–30.

73. Nho SJ, Provencher MT, Seroyer ST, Romeo A. Bioabsorbable anchors in glenohumeral shoulder surgery. Arthroscopy. 2009,25(7),788–93.

74. Park MJ, Hsu JE, Harper C, Sennett BJ, Huffman GR. Poly-L/D-lactic acid anchors are associated with reoperation and failure of SLAP repairs. Arthroscopy. 2011,27(10),1335–40.

75. Pearce Mccarty III l., Buss DD, Datta MW, Freehill MQ, Giveans MR. Complications Observed Following Labral or Rotator Cuff Repair with Use of Poly-L-Lactic Acid Implants. The Journal of Bone and Joint Surgery. 2013,95(6),507–11.

76. Givissis PK, Stavridis SI, Papagelopoulos PJ, Antonarakos PD, Christodoulou AG. Delayed Foreign-body Reaction to Absorbable Implants in Metacarpal Fracture Treatment. Clinical Orthopaedics and Related Research. 2010,468(12),3377–83.

77. Yang T, Huang C, Lu Y, Chen H, Lin C, Huang C. Delayed foreign body reaction after fixation of distal radius fracture with biodegradable implant. Formosan Journal of Musculoskeletal Disorders. 2012,3(1),27–30.

78. Camathias C, Gögüs U, Hirschmann MT, Rutz E, Brunner R, Haeni D, Vavken P. Implant failure after biodegradable screw fixation in osteochondritis dissecans of the knee in skeletally immature patients. Arthroscopy. 2015,31(3),410–5.

79. An J, Jia P, Zhang Y, Gong X, Han X, He Y. Application of biodegradable plates for treating pediatric mandibular fractures. Journal of Cranio-Maxillofacial Surgery. 2015,43(4),515–20.

80. Laurencin CT, Ambrosio AMA, Borden MD, Cooper JA. Tissue Engineering: Orthopedic Applications. Annual Review Biomedical Engineering. 1999,1,19–46.

81. Huang J, Guo ZX. Biomechanical and biochemical compatibility in innovative biomaterials. In: Boutrand J-P, editor. Biocompatibility and performance of medical devices. Philadelphia, Pa: Woodhead Publishing Limited; 2012. 37–61.

82. Kroeze RJ, Helder MN, Govaert LE, Smit TH. Biodegradable Polymers in Bone Tissue Engineering. Materials. 2009,2(3),833–56.

83. Tang X, Thankappan SK, Lee P, Fard SE, Harmon MD. Polymeric Biomaterials in Tissue Engineering and Regenerative Medicine. In: Kumbar A, Laurencin C, Deng M, editors. Natural and Synthetic Biomedical Polymers. 1st Ed. Burlington, MA, USA: Elsevier Inc.; 2014. 351–71.

84. Lyles MB, Hu JC, Varanasi VG, Hollinger JO, Athanasiou KA. Bone tissue engineering. In: Nukavarapu S, Freeman J, Laurencin C, editors. Regenerative Engineering of Musculoskeletal Tissues and Interfaces. Cambridge, UK: Woodhead Publishing; 2015. 97–134.

85. Patel JM, Dunn MG. Cartilage tissue engineering. In: Nukavarapu S, Freeman J, Laurencin C, editors. Regenerative Engineering of Musculoskeletal Tissues and Interfaces. Cambridge, UK: Woodhead Publishing; 2015. 135–60.

86. Kwansa AL, Freeman JW. Ligament tissue engineering. In: Nukavarapu S, Freeman J, Laurencin C, editors. Regenerative Engineering of Musculoskeletal Tissues and Interfaces. Cambridge, UK: Woodhead Publishing; 2015. 161–93.

87. Ramos D, Peach MS, Mazzocca AD, Yu X, Kumbar SG. Tendon tissue engineering. In: Nukavarapu S, Freeman J, Laurencin C, editors. Regenerative Engineering of Musculoskeletal Tissues and Interfaces. Cambridge, UK: Woodhead Publishing; 2015. 195–217.

88. Tollemar V, Collier ZJ, Mohammed MK, Lee MJ, Ameer GA, Reid RR. Stem cells , growth factors and scaffolds in craniofacial regenerative medicine. Genes & Diseases. 2016,3(1),56–71.

89. Ashman O, Phillips AM. Treatment of non-unions with bone defects: Which option and why? Injury. 2013,44,S43–5.

90. Zhao L, Weir MD, Xu HHK. An injectable calcium phosphate-alginate hydrogel-umbilical cord mesenchymal stem cell paste for bone tissue engineering. Biomaterials. 2010,31(25),6502–10.

91. Heino TJ, Hentunen TA. Differentiation of Osteoblasts and Osteocytes from Mesenchymal Stem Cells. Current Stem Cell Research & Therapy. 2008,3(2),131–45.

92. Quarto R, Giannoni P. Bone Tissue Engineering: Past-Present-Future. In: Gnecchi M, editor. Mesenchymal Stem Cells Methods and Protocols. 2nd editio. Humana Press; 2008. 21–33.

93. Calori GM, Donati D, Di Bella C, Tagliabue L. Bone morphogenetic proteins and tissue engineering: future directions. Injury. 2009,40 Suppl 3,S67–76.

94. Koort JK, Mäkinen TJ, Suokas E, Veiranto M, Jalava J, Aro HT, Koort JK, Mäkinen TJ, Suokas E, Veiranto M, Jalava J. Sustained release of ciprofloxacin from an osteoconductive poly (DL) -lactide implant. Acta Orthopaedica. 2008,79(295–301).

95. Balasundaram G, Webster TJ. An Overview of Nano-Polymers for Orthopedic Applications. Macromolecular Bioscience. 2007,7(5),635–42.

96. Khojasteh A, Behnia H, Naghdi N, Esmaeelinejad M, Alikhassy Z, Stevens M. Effects of different growth factors and carriers on bone regeneration: a systematic review. Oral surgery, oral medicine, oral pathology and oral radiology. 2013,116(6),e405–23.

97. Boccaccini AR, Erol M, Stark WJ, Mohn D, Hong Z, Mano JF. Polymer/bioactive glass nanocomposites for biomedical applications: A review. Composites Science and Technology. 2010,70(13),1764–76.

98. Niemela T, Niiranen H, Kellomaki M, Tormala P. Self-reinforced composites of bioabsorbable polymer and bioactive glass with different bioactive glass contents . Part I : Initial mechanical properties and bioactivity. Acta Biomaterialia. 2005,1(2),235–42.

99. Erol-Taygun M, Zheng K, Boccaccini AR. Nanoscale Bioactive Glasses in Medical Applications. International Journal of Applied Glass Science. 2013,4(2),136–48.

100. Jr ABN, Sousa SLS de, Barros RRM de, Pereira KKY, Iezzi G, Piattelli A. Influence of Implant Surfaces on Osseointegration. Brazilian Dental Journal. 2010,21(6),471–81.

101. Bosco R, Beucken J Van Den, Leeuwenburgh S, Jansen J. Surface Engineering for Bone Implants: A Trend from Passive to Active Surfaces. Coatings. 2012,2(3),95–119.

102. Duan K, Wang R. Surface modifications of bone implants through wet chemistry. Journal of Materials Chemistry. 2006,16(24),2309–21.

103. Guastaldi FPS, Yoo D, Marin C, Jimbo R, Tovar N, Zanetta-barbosa D, Coelho PG. Plasma Treatment Maintains Surface Energy of the Implant Surface and Enhances Osseointegration. International Journal of Biomaterials. 2013,2013,1–6.

104. Zhou T, Zhu Y, Li X, Liu X, Yeung KWK, Wu S, Wang X, Cui Z, Yang X, Chu PK. Surface functionalization of biomaterials by radical polymerization. Journal of Progress in Materials Science. 2016,83,191–235.

105. Popelut A, Rooker SM, Leucht P, Medio M, Brunski JB, Helms J a. The acceleration of implant osseointegration by liposomal Wnt3a. Biomaterials. 2010,31(35),9173–81.

106. Hur W, Park M, Lee JY, Kim MH, Lee SH, Park CG, Kimc S-N, Min HS, Min HJ, Chai JH, Lee SJ, B SK, Choi TH, Choy Y Bin. Bioabsorbable bone plates enabled with local , sustained delivery of alendronate for bone regeneration. Journal of Controlled Release. 2016,222,97–106.

107. Augat P, Robioneck PB, Abdulazim A, Wipf F, Lips KS, Alt V, Schnettler R, Heiss C. Fixation performance of an ultrasonically fused, bioresorbable osteosynthesis implant: A biomechanical and biocompatibility study. Journal of Biomedical Materials Research Part B: Applied Biomaterials. 2016,104(1),170–9.

108. Schneider M, Stadlinger B, Loukota R, Eckelt U. Three-dimensional fixation of fractures of the mandibular condyle with a resorbable three-dimensional osteosynthesis mesh. British Journal of Oral & Maxillofacial Surgery. 2011,50(5),470–3.

109. Oliveira NG, Rodrigues A, Reis L, Pinto LF V. Trends in Bioabsorbable Osteosynthesis Devices: Introduction to a Novel Production Process of Chitosan-Based Implants. Journal of Chitin and Chitosan Science. 2013,1(3),210–20.

110. Wang Z, Hu Q, Cai L. Chitin Fiber and Chitosan 3D Composite Rods. International Journal of Polymer Science. 2010,2010,1–7.

111. Mokhtarzadeh A, Alibakhshi A, Hejazi M, Omidi Y, Ezzati J, Dolatabadi N. Bacterial-derived

biopolymers : advanced natural nanomaterials for drug delivery and tissue engineering. Trends in Analytical Chemistry. 2016,82,367–84.

112. Bhubalan K, Lee W-H, Sudesh K. Biodegradable Polymers of Natural Origin: Polyhydroxyalkanoate. In: Domb AJ, Kumar N, Ezra A, editors. Biodegradable Polymers in Clinical Use and Clinical Development. Hoboken, NJ, USA: John Wiley & Sons; 2011. 247–315.

113. Martin DP, Williams SF. Medical applications of poly-4-hydroxybutyrate: a strong flexible absorbable biomaterial. Biochemical Engineering Journal. 2003,16(2),97–105.

114. Williams SF, Rizk S, Martin DP. Poly-4-hydroxybutyrate (P4HB : a new generation of resorbable medical devices for tissue repair and regeneration. Biomed Tech (Berl). 2013,58(5),439–52.

115. Chen G-Q, Wu Q. The application of polyhydroxyalkanoates as tissue engineering materials. Biomaterials. 2005,26(33),6565–78.

116. Bezwada RS. From Biostable to Biodegradable Polymers for Biomedical Applications. Polymeric Materials: Science and Engineering. 2009,101,1044–5.

117. Farraro KF, Kim KE, Woo SL, Flowers JR, Mccullough MB. Revolutionizing orthopaedic biomaterials: The potential of biodegradable and bioresorbable magnesium-based materials for functional tissue engineering. Journal of Biomechanics. 2014,47(9),1979–86.

118. Walker J, Shadanbaz S, Woodfield TBF, Staiger MP, Dias GJ. Magnesium biomaterials for orthopedic application: a review from a biological perspective. Journal of biomedical materials research Part B, Applied biomaterials. 2014,102(6),1316–31.

119. Denkena B, Lucas a. Biocompatible Magnesium Alloys as Absorbable Implant Materials – Adjusted Surface and Subsurface Properties by Machining Processes. CIRP Annals - Manufacturing Technology. 2007,56(1),113–6.

120. Seitz J, Eifler R, Bach F, Maier HJ. Magnesium degradation products: effects on tissue and human metabolism. Journal of Biomedical Materials Research Part A. 2014,102(10),3744–53.

121. Chen Y, Xu Z, Smith C, Sankar J. Recent advances on the development of magnesium alloys for biodegradable implants. Acta Biomaterialia. 2014,10(11),4561–73.

122. Windhagen H, Radtke K, Weizbauer A, Diekmann J, Noll Y, Kreimeyer U, Schavan R, Stukenborg-Colsman C, Waizy H. Biodegradable magnesium-based screw clinically equivalent to titanium screw in hallux valgus surgery: short term results of the first prospective, randomized, controlled clinical pilot study. Biomedical engineering online. 2013,12(1),62.

123. Brar HS, Wong J, Manuel M V. Investigation of the mechanical and degradation properties of Mg-Sr and Mg-Zn-Sr alloys for use as potential biodegradable implant materials. Journal of the mechanical behavior of biomedical materials. 2012,7,87–95.

124. Zheng YF, Gu XN, Witte F. Biodegradable metals. Materials Science and Engineering: R: Reports. 2014,77,1–34.

125. Wang YB, Xie XH, Li HF, Wang XL, Zhao MZ, Zhang EW, Bai YJ, Zheng YF, Qin L. Biodegradable CaMgZn bulk metallic glass for potential skeletal application. Acta biomaterialia. 2011,7(8),3196–208.

126. Perrone GS, Leisk GG, Lo TJ, Moreau JE, Haas DS, Papenburg BJ, Golden EB, Partlow BP, Fox SE, Ibrahim AMS, Lin SJ, Kaplan DL. The use of silk-based devices for fracture fixation. Nature Communications. 2014,5,1–9.

127. Clinical Trials database [Internet]. Available at: clinicalstrials.gov.

128. Hamed I, Özogul F, Regenstein JM. Industrial applications of crustacean by-products (chitin, chitosan, and chitooligosaccharides): A review. Trends in Food Science & Technology. 2016,48,40–50.

129. Rodríguez-Vázquez M, Vega-Ruiz B, Ramos-Zúñiga R, Saldaña-Koppel DA, Quiñones-Olvera LF. Chitosan and Its Potential Use as a Scaffold for Tissue Engineering in Regenerative Medicine. BioMed Research Internationa. 2015,2015(821279),1–15.

130. Synowiecki J, Al-khateeb NA. Production , Properties , and Some New Applications of Chitin and Its Derivatives. Critical Reviews in Food Science and Nutrition. 2003,43(2),145–71.

131. Revathi M, Saravanan R, Shanmugam A. Production and characterization of chitinase from Vibrio species , a head waste of shrimp Metapenaeus dobsonii (Miers , 1878) and chitin of Sepiella inermis Orbigny , 1848. Advances in Bioscience and Biotechnology. 2012,3(August),392–7.

132. Gortari MC, Hours RA. Biotechnological processes for chitin recovery out of crustacean waste: A mini-review. Electronic Journal of Biotechnology. 2013,16(3).

133. Merzendorfer H. Chitin. In: Gabius H-J, editor. The sugar code: fundamentals of glycosciences.

Weinheim, Germany: John Wiley & Sons; 2009. 217–30.

134. Arbia W, Arbia L, Adour L, Amrane A. Chitin Extraction from Crustacean Shells Using Biological Methods - A Review. Food Technology and Biotechnology. 2013,51(1),12–25.

135. Domard A. A perspective on 30 years research on chitin and chitosan. Carbohydrate Polymers. 2011,84,696–703.

136. Kaur S, Dhillon GS. Recent trends in biological extraction of chitin from marine shell wastes: a review. Critical Reviews in Biotechnology. 2015,35(1),44–61.

137. Ribeiro R, Faria R, Rodrigues L, Neto DS, Frederico L, Faria E De. Modelling Computational study of polymorphic structures of α- and β- chitin and chitosan in aqueous solution. Journal of Molecular Graphics and Modelling. 2016,63,78–84.

138. Rinaudo M. Chitin and chitosan: Properties and applications. Progress in Polymer Science. 2006,31(7),603–32.

139. Croisier F, Jérôme C. Chitosan-based biomaterials for tissue engineering. European Polymer Journal. 2013,49(4),780–92.

140. Kumirska J, Weinhold MX, Thöming J, Stepnowski P. Biomedical Activity of Chitin/Chitosan Based Materials - Influence of Physicochemical Properties Apart from Molecular Weight and Degree of N-Acetylation. Polymers. 2011,3(4),1875–901.

141. Kurita K. Chitin and chitosan: functional biopolymers from marine crustaceans. Marine biotechnology (New York, NY). 2006,8(3),203–26.

142. Chatelet C, Damourb O, Domard A. Influence of the degree of acetylation on some biological properties of chitosan films. Biomaterials. 2001,22(3).

143. Aranaz I, Mengíbar M, Harris R, Paños I, Miralles B, Acosta N, Galed G, Heras Á. Functional Characterization of Chitin and Chitosan. Current Chemical Biology. 2009,3,203–30.

144. Ngo D, Vo T, Ngo D, Kang K, Je J, Pham HN, Byun H, Kim S. Biological effects of chitosan and its derivatives. Food Hydrocolloids. 2015,51,200–16.

145. Sundaram M. N, Mony U, Jayakumar R. Chitin and Chitosan as Hemostatic Agents. In: Mark HF, editor. Encyclopedia of Polymer Science and Technology. John Wiley & Sons; 2016. 1–12.

146. Madureira AR, Sarmento B, Pintado M. Current State of the Potential Use of Chitosan as Pharmaceutical Excipient. In: Thakur VK, Thakur MK, editors. Handbook of Polymers for Pharmaceutical Technologies: Biodegradable Polymers. Beverly, MA: Scrivener Publishing; 2015. 275–97.

147. Younes I, Rinaudo M. Chitin and Chitosan Preparation from Marine Sources. Structure, Properties and Applications. Marine Drugs. 2015,13(3),1133–74.

148. M H, K Y, S I, M H. Chitosan induces apoptosis via caspase-3 activation in bladder tumor cells. Japanase Journal of Cancer Research. 2001,92(4),459–66.

149. Cheung RCF, Ng TB, Wong JH, Chan WY. Chitosan: An Update on Potential Biomedical and Pharmaceutical Applications. Marine Drugs. 2015,13(8),5156–86.

150. Badylak SF. Naturally occurring scaffold materials. In: Atala A, Lanza R, Thomson JA, Nerem RM, editors. Principles of Regenerative Medicine. 1st editio. Burlington, MA, USA; 2008. 594–603.

151. Al-Qadi S, Grenha A, Remuñán-López C. Chitosan-Based Systems for Mucosal Delivery of Biopharmaceuticals. In: Sarmento B, Neves J das, editors. Chitosan-Based Systems for Biopharmaceuticals: Delivery, Targeting and Polymer Therapeutics. 1st editio. Chichester, United Kingdom: Wiley; 2012. 181–209.

152. Anitha A, Sowmya S, Kumar PTS, Deepthi S, Chennazhi KP, Ehrlich H, Tsurkan M, Jayakumar R. Chitin and chitosan in selected biomedical applications. Progress in Polymer Science. 2014,39(9),1644–67.

153. Zargar V, Asghari M, Dashti A. A Review on Chitin and Chitosan Polymers: Structure, Chemistry, Solubility, Derivatives, and Applications. ChemBioEng Reviews. 2015,2(3),204–26.

154. Rasmussen RS, Morrissey MT. Chitin and Chitosan. In: Barrow C, Shahidi F, editors. Marine Nutraceuticals and Functional Foods. 1st editio. Boca Raton: CRC Press; 2007. 155–80.

155. Heppe Medical Chitosan [Internet]. [cited January 1, 2016]. Available at: https://www.gmp-chitosan.com/

156. Kraska RC, McQuate RS, Soni MG. ChitoClear® Shrimp-Derived Chitosan. Food Usage Conditions for General Recognition of Safety - GRAS Notification for ChitoClear® Shrimp-Derived Chitosan. Siglufjordur; 2012.

157. European Pharmacopeia - Chitosan Hydrochloride. 2005.

158. Fernandez JG, Ingber DE. Unexpected Strength and Toughness in Chitosan-Fibroin Laminates Inspired by Insect Cuticle. Advanced Materials. 2012,24(4),480–4.

159. Dornish M, Kaplan DS, Arepalli SR. Regulatory Status of Chitosan and Derivatives. In: Sarmento B, Neves J das, editors. Chitosan-Based Systems for Biopharmaceuticals Delivery, Targeting and Polymer Therapeutics. 1st editio. Chichester: Wiley; 2012. 463–81.

160. GRAS Notices - FDA [Internet]. [cited January 1, 2016]. Available at:

https://www.accessdata.fda.gov/scripts/fdcc/?set=GRASNotices&sort=GRN_No&order=ASC&type=basic&search=chitosan

161. Levengood SL, Zhang M. Chitosan-based scaffolds for bone tissue engineering. Journal of Materials Chemistry B Materials for Biology and Medicine. 2014,2(21),3161–84.

162. Chesnutt BM, Yuan Y, Buddington K, Haggard WO, Bumgardner JD. Composite chitosan/nano-hydroxyapatite scaffolds induce osteocalcin production by osteoblasts in vitro and support bone formation in vivo. Tissue Engineering Part A. 2009,15(9),2571–9.

163. Thein-Han WW, Misra RDK. Biomimetic chitosan–nanohydroxyapatite composite scaffolds for bone tissue engineering. Acta Biomaterialia. 2009,5(41182–1197).

164. Kong L, Gao Y, Cao W, Gong Y, Zhao N, Zhang X. Preparation and characterization of nano-hydroxyapatite/chitosan composite scaffolds. Journal of Biomedical Materials Research Part A. 2005,75(2),275–82.

165. Ahmed EM. Hydrogel: Preparation, characterization, and applications: A review. Journal of Advanced Research. 2015,6(2),105–21.

166. Park D-J, Choi B-H, Zhu S-J, Huh J-Y, Lee B-YKS-H. Injectable bone using chitosan-alginate gel/mesenchymal stem cells/BMP-2 composites. Journal of Cranio-Maxillofacial Surgery. 2005,33(1),50–4.

167. Dyondi D, Webster TJ, Banerjee R. A nanoparticulate injectable hydrogel as a tissue engineering scaffold for multiple growth factor delivery for bone regeneration. Internacional Journal of Nanomedicine. 2013,8,47–59.

168. Wise JK, Alford AI, Goldstein SA, Stegemann JP. Comparison of uncultured marrow mononuclear cells and culture-expanded mesenchymal stem cells in 3D collagen-chitosan microbeads for orthopedic tissue engineering. Tissue Engineering Part A. 2014,20(1-2),210–24.

169. Dhivya S, Saravanan S, Sastry TP, Selvamurugan N. Nanohydroxyapatite-reinforced chitosan composite hydrogel for bone tissue repair in vitro and in vivo. Journal Nanobiotechnology. 2015,13(40),1–13.

170. Suh JF, Matthew HWT. Application of chitosan-based polysaccharide biomaterials in cartilage tissue engineering: a review. Biomaterials. 2000,21(24),2589–98.

171. Yan L-P, Wang Y-J, Ren L, Wu G, Caridade SG, Fan J, Oliveira T, Wang L-Y, Ji P, Oliveira JM, Mano F, Reis RL. Genipin-cross-linked collagen/chitosan biomimetic scaffolds for articular cartilage tissue engineering applications. Journal of Biomedical Materials Research - Part A. 2010,95(2),465–75.

172. Silva JM, Georgi N, Costa R, Sher P, Reis RL, Blitterswijk CA Van, Karperien M, Mano JF. Nanostructured 3D Constructs Based on Chitosan and Chondroitin Sulphate Multilayers for Cartilage Tissue Engineering. Plos One. 2013,8(2),1–11.

173. R J, LSM T, PJ D, M K, CA van B, ZY Z, J F. Injectable chitosan-based hydrogels for cartilage tissue engineering. Biomaterials. 2009,30(13),2544–51.

174. Park H, Choi B, Hu J, Lee M. Injectable chitosan hyaluronic acid hydrogels for cartilage tissue engineering. Acta Biomaterialia. 2013,9(1),4779–86.

175. Oliveira NG, Sirgado T, Reis L, Pinto LF V., Silva CL, Ferreira FC, Rodrigues A. In vitro assessment of three dimensional dense chitosan- based structures to be used as bioabsorbable implants. Journal of the Mechanical Behavior of Biomedical Materials. 2014,40,413–25.

176. Szymańska E, Winnicka K. Stability of Chitosan - A Challenge for Pharmaceutical and Biomedical Applications. Marine Drugs. 2015,13(4),1819–46.

177. Praxedes APP, Silva AJC da, Silva RC da, Lima RPA, Tonholo J, Ribeiro AS, Oliveira IN de. Effects of UV irradiation on the wettability of chitosan films containing dansyl derivatives. Journal of Colloid and Interface Science. 2012,376(1),255–61.

178. Dimonie D, Dima SO, Petrache M. Influence of centrifugation on the molecular parameters of

chitosan solubilized in weakly acidic aqueous solutions. Digest Journal of Nanomaterials and Biostructures. 2013,8(4),1799–809.

179. The United States Pharmacopeia, USP 34–NF 29; Rockville; 2011.

180. Weinholda MX, C.M. J, Sauvageaua, Kumirskab J, Thöminga J. Studies on acetylation patterns of different chitosan preparations. Carbohydrate Polymers. 2009,78(4),678–84.

181. Viljoen J., Steenekamp J., Marais AF, Kotzé AF. Effect of moisture content, temperature and exposure time on the physical stability of chitosan powder and tablets. Drug Development and Industrial Pharmacy. 2014,40(6),730–42.

182. Kerch G, Korkhov V. Effect of storage time and temperature on structure, mechanical and barrier properties of chitosan-based films. European Food Research and Technology. 2011,232(1),17–22.

183. Harding SE. Some observations on the effects of bioprocessing on biopolymer stability. Journal of Drug Targeting. 2010,18(10),732–40.

184. Halim AS, Keong LC, Zainol I, Hazri A, Rashid A. Biocompatibility and Biodegradation of Chitosan and Derivatives. In: Sarmento B, Neves J das, editors. Chitosan-Based Systems for Biopharmaceuticals Delivery, Targeting and Polymer Therapeutics. 1st editio. Chichester,: Wiley; 2012. 57–74.

185. França R, Mbeh DA, Samani TD, Tien C Le, Mateescu MA, Yahia L, Sacher E. The effect of ethylene oxide sterilization on the surface chemistry and in vitro cytotoxicity of several kinds of chitosan. Journal of Biomedical Materials Research Part B: Applied Biomaterials. 2013,101(8),1–12.

186. Yoshida CMP, Junior ENO, Franco TT. Chitosan Tailor-Made Films: The Effects of Additives on Barrier and Mechanical Properties and Science. Packaging Technology and Science. 2009,21,161–70.

187. Quijada-Garrido I, Laterza B, Mazón-Arechederra JM, Barrales-Rienda JM. Characteristic Features of Chitosan/Glycerol Blends Dynamics. Macromolecular Chemistry and Physics. 2006,207(19),1742–51.

188. El-Hefian EA, Nasef MM, Yahaya AH. Chitosan-Based Polymer Blends: Current Status and Applications. Journal- Chemical Society of Pakistan. 2014,36(1),11–27.

189. Berger J, Reist M, Mayer JM, Felt O, Peppas NA, Gurny R. Structure and interactions in covalently and ionically crosslinked chitosan hydrogels for biomedical applications. European Journal of Pharmaceutics and Biopharmaceutics. 2004,57(1),19–34.

190. Mi F-L, Shyu S-S, Wong T-B, Jang S-F, Lee S-T, Lu K-T. Chitosan-polyelectrolyte complexation for the preparation of gel beads and controlled release of anticancer drug. II. Effect of pH-dependent ionic crosslinking or interpolymer complex using tripolyphosphate or polyphosphate as reagent. Journal of Applied Polymer Science. 1999,74(5),1093–107.

191. Lin J, Horn H, Henry J. Comparative Effectiveness Hits Medical Devices. 2010.

192. Ijzerman MJ, Steuten LMG. Early Assessment of Medical Technologies to Inform Product Development and Market Access. A Review of Methods and Applications. Applied Health Economics and Health Policy. 2011,9(5),331–47.

193. Markiewicz K, Til JA Van, Ijzerman MJ. Medical Devices Early Assessment methods: Systematic Literature Review. International Journal of Technology Assessment in Health Care. 2014,30(2),137–46.

194. Russel LB, Siegal JE, Daniels N, Gold MR, Luce BR, Mandelblatt JS. Cost-Effectiveness Analysis as a Guide to Resource Allocation in Health: Roles and Limitations. In: Gold MR, Siegal JE, Russell LB, Weinstein MC, editors. Cost-Effectiveness in Health and Medicine. New York: Oxford University Press; 1996. 3–24.

195. Mccabe C, Claxton K, Culyer AJ. The NICE Cost-Effectiveness Threshold. What it is and What that Means. Pharmacoeconomics. 2008,26(9),733–44.

196. Garber AM, Weinstein MC, Torrance GW, Kamlet MS. Theoretical Foundations of Cost-Effectiveness Analysis. In: Gold MR, Siegal JE, Russell LB, Weinstein MC, editors. Cost-Effectiveness in Health and Medicine. New York: Oxford University Press; 1996. 25–53.

197. Fuchs S, Olberg B, Panteli D, Perleth M, Busse R. HTA of medical devices: Challenges and ideas for the future from a European perspective. Health policy. 2016,1–15.

198. Cosh E, Girling A, Lilford R, Mcateer H, Young T. Investing in new medical technologies: A decision framework. Journal of Commercial Biotechnology. 2007,13(4),263–71.

199. Mandelblatt JS, Fryback DG, Weinstein MC, Russel LB, Gold MR, Hadorn DC. Assessing the Effectiveness of Health Interventions. In: Gold MR, Siegal JE, Russel LB, Weinstein MC, editors. Cost-Effectiveness in Health and Medicine. New York: Springer; 1996. 135–75.

200. Vallejo-torres L, Steuten LMG, Buxton MJ, Girling AJ, Lilford RJ, Young T. Integrating health economics modeling in the product development cycle of medical devices: A Bayesian approach. International Journal of Technology Assessment in Health Care. 2016,4(2008),459–64.

201. Vallejo-Torres L, Steuten L, Parkinson B, Girling AJ, Buxton MJ. Integrating Health Economics Into the Product Development Cycle: A Case Study of Absorbable Pins for Treating Hallux Valgus. Medical Decision Making. 2011,31(4),596–610.

202. Weiler A, Hoffmann RFG, Stähelin AC. Biodegradable Implants in Sports Medicine: The Biological Base. Arthroscopy. 2000,16(3),305–21.

203. Park H, Temenoff JS, Mikos AG. Biodegradable Orthopedic Implants. In: Bronner F, Farach-Carson MC, Mikos AG, editors. Engineering of Functional Skeletal Tissues Vol 3. London: Springer; 2007. 55–68.

204. Lord B, Grice J. Anterior cruciate ligament reconstruction - evolution and current concepts. Orthopaedics and Trauma. 2014,29(1),12–23.

205. Vavken P, Murray MM. ACL Injury Epidemiology. In: Murray MM, Vavken P, Fleming BC, editors. The ACL Handbook Knee Biology, Mechanics and Treatment. New York: Springer; 2013. 3–17.

206. Duffee AR, Hewett TE, Kaeding CC. Patient-Related Risk Factors for ACL Graft Failure. In: Marx RG, editor. Revision ACL Reconstruction Indications and Technique. New York: Springer; 2014. 1–10.

207. Bogunovic L, Yang JS, Wright RW. Anterior Cruciate Ligament Reconstruction: Contemporary Revision Options. Operative Techniques in Sports Medicine. 2013,21(1),64–71.

208. Murray MM. History of ACL Treatment and Current Gold Standard of Care. In: Murray MM, Vavken P, Fleming BC, editors. The ACL Handbook Knee Biology, Mechanics and Treatment. New York: Springer; 2013. 19–28.

209. Wilde J, Bedi A, Altchek DW. Revision Anterior Cruciate Ligament Reconstruction. Sports Health. 2014,6(6),504–18.

210. Pereira H, Sevivas N, Pereira R, Monteiro A, Sampaio R, Oliveira JM, Reis RL, Espregueira-Mendes J. Systematic Approach from Porto School. In: Siebold R, Dejour D, Zaffagnini S, editors. Anterior Cruciate Ligament Reconstruction A practical surgical guide. Springer; 2014. 367–86.

211. Cohen M, Arliani GG, Astur DC, Kaleka CC. Diagnosis of Failed ACL Reconstruction. In: Marx RG, editor. Revision ACL Reconstruction Indications and Technique. New York: Springer; 2014. 23–32.

212. Knee [Internet]. Orthopaedic Associates of Muskegon. Available at: http://www.oamkg.com/specialties/knee-specialty/knee-acl-reconstruction.html

213. Bonasia DE, Amendola A. Graft choice in ACL reconstruction. In: Bonnin M, Amendola A, Bellemans J, MacDonald S, Ménétrey J, editors. The Knee Joint Surgical Techniques and Strategies. Paris: Springer; 2012. 173–81.

214. Christel P. Graft Choice in ACL Reconstruction: Which One and Why? In: Sanchis-Alfonso V, Monllau JC, editors. The ACL-Deficient Knee A Problem Solving Approach. London: Springer; 2013. 105–12.

215. Milano G, Petersen W, Hoeher J, Paessler HH, Akoto R, Campana V, Saccomanno MF, Siebold R. Fixation. In: Siebold R, Dejour D, Zaffagnini S, editors. Anterior Cruciate Ligament Reconstruction A Practical Surgical Guide. Springer; 2014. 215–56.

216. Chen G, Wang S. Comparison of single-bundle versus double-bundle anterior cruciate ligament reconstruction after a minimum of 3-year follow-up: a meta-analysis of randomized controlled trials. International Journal of Clinical and Experimental Medicine. 2015,8(9),14604–14.

217. Brophy RH, Wright RW, Matava MJ. Cost Analysis of Converting From Single-Bundle to Double-Bundle Anterior Cruciate Ligament. The American Journal of Sports Medicine. 2009,37(4),683–7.

218. Maak TG, Delos D, Cordasco FA. Preoperative Planning for Revision ACL Reconstruction. In: Marx RG, editor. Revision ACL Reconstruction Indications and Technique. New York: Springer; 2014. 63–74.

219. Chahal J, Lee A, Heard W, Bach Jr BR. A Retrospective Review of Anterior Cruciate Ligament Reconstruction Using Patellar Tendon 25 Years of Experience. The Orthopaedic Journal of Sports Medicine. 2013,1(3),1–7.

220. Mather III RC, Hettrich CM, Dunn WR, Cole BJ, Bach BR, Huston LJ, Reinke K, Spindler KP, Iii RCM, Hettrich CM, Dunn WR. Cost-Effectiveness Analysis of Early and Delayed Reconstruction for Anterior Cruciate Ligament Tears. The American Journal of Sports Medicine. 2014,42(7),1583–91.

221. A.Gottlob C, Baker Jr CL, Pellissier JM, Lisa Colvin. Cost effectiveness of Anterior Cruciate Ligament Reconstruction in Young Adults. Clinical Orthopaedics and Related Research. 1999,357,272–82.

222. Mather III RC, Koenig L, Kocher MS, Dall TM, Gallo P, Scott DJ, Jr BRB, Group K, Spindler KP. Societal

and Economic Impact of Anterior Cruciate Ligament Tears. The Journal of Bone and Joint SurgerY. 2013,95(1),1751–9.

223. Paxton ES, Kymes SM, Brophy RH. Cost-Effectiveness of Anterior Cruciate Ligament Reconstruction. Preliminary Comparison of Single-Bundle and Double-Bundle Techniques. The American Journal of Sports Medicine. 2010,38(12),2417–25.

224. Genuario JW, Faucett SC, Boublik M, Schlegel TF. A Cost-Effectiveness Analysis Comparing 3 Anterior Cruciate Ligament Graft Types. Bone-Patellar Tendon-Bone Autograft, Hamstring Autograft, and Allograft. The American Journal of Sports Medicine. 2012,40(2),307–14.

225. Nagda SH, Altobelli GG, Bowdry KA, Brewster CE, Lombardo SJ. Cost Analysis of Outpatient Anterior Cruciate Ligament Reconstruction. Autograft versus Allograft. Clinical Orthopaedics and Related Research. 2010,468(5),1418–22.

226. Saltzman BM, Cvetanovich GL, Nwachukwu BU, Mall NA, Bush-Joseph CA, Bach BR. Economic Analyses in Anterior Cruciate Ligament Reconstruction. A Qualitative and Systematic Review. The American Journal of Sports Medicine. 2016,44(5).

227. Emond CE, Woelber EB, Kurd SK, Ciccotti MG, Cohen SB. Comparison of the Results of Anterior Cruciate Ligament Reconstruction Using Bioabsorbable Versus Metal Interference Screws. The Journal of Bone and Joint Surgery. 2011,93(6),572–80.

228. Stener S, Ejerhed L, Sernert N, Laxdal G, Kartus LR-CJ. A Long-Term, Prospective, Randomized Study Comparing Biodegradable and Metal Interference Screws in Anterior Cruciate. Radiographic Results and Clinical Outcome. The American Journal of Sports Medicine. 2010,38(8),1598–605.

229. Kaeding C, Farr J, Kavanaugh T, Pedroza A. A Prospective Randomized Comparison of Bioabsorbable and Titanium Anterior Cruciate Ligament Interference Screws. Arthroscopy. 2005,21(2),147–51.

230. Myers P, Logan M, Stokes A, Watts M. Bioabsorbable Versus Titanium Interference Screws With Hamstring Autograft in Anterior Cruciate Ligament Reconstruction: A Prospective Randomized Trial With 2-Year Follow-up. Arthroscopy. 2008,24(7),817–23.

231. Byford S, Raftery J. Perspectives in economic evaluation. The BMJ. 1998,316(7143),1529–30.

232. Torrance GW, Siegel JE, Luce BR. Framing and Designing the Cost-Effectiveness Analysis. In: Gold MR, Siegel JE, Russel LB, Weinstein MC, editors. Cost-Effectiveness in Health and Medicine. New York: Oxford University Press; 1996. 54–81.

233. George MS, Dunn WR, Spindler KP. Current concepts review: revision anterior cruciate ligament reconstruction. Am J Sports Med. 2006,34(12),2026–37.

234. Barker JU, Drakos MC, Maak TG, Warren RF, Williams III RJ, Allen AA. Effect of Graft Selection on the Incidence of Postoperative Infection in Anterior Cruciate Ligament Reconstruction. The American Journal of Sports Medicine. 2010,38(2),281–6.

235. Whitehead TS. Failure of Anterior Cruciate Ligament Reconstruction. Clinics in Sports Medicine. 2013,32(1),177–204.

236. Samitier G, Marcano AI, Alentorn-Geli E, Cugat R, Farmer KW, Moser MW. Failure of Anterior Cruciate Ligament Reconstruction. The Archives of Bone and Joint Surgery. 2015,3(4),220–40.

237. Eck CF Van, Schreiber VM, Liu TT, Fu FH. The anatomic approach to primary, revision and augmentation anterior cruciate ligament reconstruction. Knee Surgery, Sports Traumatology, Arthroscopy. 2010,18(9),1154–63.

238. Stevenson WW, Johnson DL. Revision ACL Reconstruction. In: Fu FH, Cohen SB, editors. Current Concepts in ACL Reconstruction. Thorofare: Slack Incorporater; 2008. 325–40.

239. Fabricant PD, McCarthy MM, Pearle AD, Ranawat AS. Biomechanics and Etiology of ACL Graft Failure. In: Marx RG, editor. Revision ACL Reconstruction Indications and Technique. New York: Springer; 2014. 33–42.

240. Maletis GB, Inacio MCS, Funahashi TT. Analysis of 16,192 Anterior Cruciate Ligament Reconstructions From a Community-Based Registry. The American Journal of Sports Medicine. 2013,41(9),2090–8.

241. Andernord D, Desai N, Björnsson H, Ylander M, Karlsson J, Samuelsson K. Patient Predictors of Early Revision Surgery After Anterior Cruciate Ligament Reconstruction: A Cohort Study of 16,930 Patients With 2-Year Follow-up. The American Journal of Sports Medicine P. 2014,43(121-127).

242. CM H, WR D, EK R, Group M, KP S. The Rate of Subsequent Surgery and Predictors Following ACL Reconstruction: Two- and Six-year Follow-up from a Multicenter Cohort. The American Journal of Sports Medicine. 2014,41(7),1534–40.

243. Kamath G V, Redfern JC, Greis PE, Burks RT. Revision Anterior Cruciate Ligament Reconstruction. The American Journal of Sports Medicine. 2011,39(1),199–217.

244. Røtterud JH, Sivertsen EA, Forssblad M, Engebretsen L, Årøen A. Effect of Meniscal and Focal Cartilage Lesions on Patient-Reported Outcome After Anterior Cruciate Ligament Reconstruction. A Nationwide Cohort Study From Norway and Sweden of 8476 Patients With 2-Year Follow-up. The American Journal of Sports Medicine. 2013,41(3),535–43.

245. Mauro CS, Irrgang JJ, Williams BA, Harner CD. Loss of Extension Following Anterior Cruciate Ligament IKDC Criteria. Arthroscopy. 2008,24(2),146–53.

246. Sonnery-Cottet B, Lavoie F, Ogassawara R, Kasmaoui H, Scussiato RG, Kidder JF, Chambat P. Clinical and Operative Characteristics of Cyclops Syndrome After Double-Bundle Anterior Cruciate Ligament Reconstruction. Arthroscopy. 2010,26(11),1483–8.

247. Heijne A, Werner S. A 2-year follow-up of rehabilitation after ACL reconstruction using patellar tendon or hamstring tendon grafts: a prospective randomised outcome study. Knee Surgery, Sports Traumatology, Arthroscopy. 2010,18(6),805–13.

248. Drogset JO, Grøntvedt T, Tegnander A. Endoscopic Reconstruction of the Anterior Cruciate Ligament Using Bone-Patellar Tendon-Bone Grafts Fixed With Bioabsorbable or Metal Interference Screws A Prospective Randomized Study of the Clinical Outcome. The American Journal of Sports Medicine. 2005,33(8),1160–5.

249. MARSGroup. Descriptive Epidemiology of the Multicenter ACL Revision Study (MARS) Cohort. The American Journal of Sports Medicine. 2010,38(10),1979–86.

250. Kartus J, Fernandez F, Siebold R. Postoperative Complications: Solutions? In: Siebold R, Dejour D, Zaffagnini S, editors. Anterior Cruciate Ligament Reconstruction A Practical Surgical Guide. Springer; 2014. 463–73.

251. Galal A, Abdul-Maksoud S, Al-Kandary S, Abdul-Salam S, Awad A. Anterior cruciate ligament reconstruction: Magnetic resonance imaging and factors influencing outcome. The Egyptian Journal of Radiology and Nuclear Medicine. 2011,42(2),193–200.

252. Laupattarakasem P, Laopaiboon M, Kosuwon W, Laupattarakasem W. Meta-analysis comparing bioabsorbable versus metal interference screw for adverse and clinical outcomes in anterior cruciate ligament reconstruction. Knee Surgery, Sports Traumatology, Arthroscopy. 2014,22(142-153).

253. Mascarenhas R, Saltzman BM, Sayegh ET, Verma NN, Cole BJ, Bush-Joseph C, Bach Jr BR. Bioabsorbable Versus Metallic Interference Screws in Anterior Cruciate Ligament Reconstruction: A Systematic Review of Overlapping Meta-analyses. Arthroscopy. 2015,31(3),561–8.

254. Edgar CM, DeBerardino T, Arciero R. Two-Stage ACL Revision: Indications and Technique. In: Marx RG, editor. Revision ACL Reconstruction Indications and Technique. New York: Springer; 2014. 127–38.

255. Leonardi AB de A, Junior AD, Severino NR. Bone Tunnel Enlargement on Anterior Cruciate Ligament Reconstruction. Acta Ortopédica Brasileira. 2014,22(5),240–4.

256. Wilson TC, Kantaras A, Atay A, Johnson DL. Tunnel Enlargement After Anterior Cruciate Ligament Surgery. The American Journal of Sports Medicine. 2004,32(2),543–9.

257. Ellman MB, Rosenthal MD, Thiel GS Van, Sherman SL, Provencher M. Rehabilitation of Revision ACL Reconstruction.

258. Freedman JA. ACL Reconstruction Post-Operative Rehabilitation Protocol.

259. Monte Carlo Simulation [Internet]. Palisade Corporation. [cited November 28, 2016]. Available at: http://www.palisade.com/risk/monte_carlo_simulation.asp

260. Prodromos CC, Rogowski J, Joyce BT. The Economics of Anterior Cruciate Ligament Reconstruction. In: Prodromos CC, editor. The Anterior Cruciate Ligament: Reconstruction and Basic Science. Second edi. Philadelphia,: Elsevier; 2018. 79–83.

261. Viswanath DS, Ghosh T, Prasad DHL, Dutt NVK, Rani KY. Introduction. In: Viscosity of Liquids Theory, Estimation, Experiment, and Data. Dordrecht: Springer; 2007. 1–8.

262. El-hefian EA, Yahaya AH. Rheological study of chitosan and its blends: An overview. Maejo International Journal of Science and Technology. 2010,4(02),210–20.

263. Viscometer [Internet]. ChemEurope. [cited March 27, 2017]. Available at: http://www.chemeurope.com/en/encyclopedia/Viscometer.html#Rotation_viscometers

264. Kienzle-Sterzer CA, Rodriguez-Sanchez D, Rha CK. Flow behavior of a cationic biopolymer: Chitosan. Polymer Bulletin. 1985,13(1),1–6.

265. Wang W, Xu D. Viscosity and flow properties of concentrated solutions of chitosan with different degrees of deacetylation. International Journal of Biological Macromolecules. 1994,16(3),14–7.

266. Anchisi C, Maccioni AM, Meloni MC. Physical properties of chitosan dispersions in glycolic acid. Il Farmaco. 2004,59(7),557–61.

267. Zhang J, Xia W, Liu P, Cheng Q, Tahirou T, Gu W, Li B. Chitosan Modification and Pharmaceutical/Biomedical Applications. Marine Drugs. 2010,8(1),1962–87.

268. Berat P, Kitosan M, Kaedah M, Intrinsik K, Yacob N, Talip N, Mahmud M, Aizam N, Mat I, Akma N, Fabillah NA. Determination of viscosity-average molecular weight of chitosan using intrinsic viscosity measurement. Journal of Nuclear and Related Technologies. 2013,10(1),39–44.

269. Striegel AM, Yau WW, Kirkland JJ, Bly DD. Background. In: Modern Size-Exclusion Liquid Chromatography: Practice of Gel Permeation and Gel Filtration Chromatography. Second edi. New Jersey: John Wiley & Sons,; 2009. 1–17.

270. An Introduction to Gel Permeation Chromatography and Size Exclusion Chromatography. 2015.

271. Atta-ur-Rahman, Choudhary MI, Atia-tul-Wahab. The Basics of Modern NMR Spectroscopy. In: Solving problems with NMR spectroscopy. Second Edi. San Diego: Elsevier Academic Press; 2016. 1–34.

272. Hardinger S. Proton nuclear magnetic resonance spectroscopy (H-NMR). 2006.

273. Hardinger S. Proton Nuclear Magnetic Resonance (H-NMR) Spectroscopy. 2006.

274. Kasaai MR. Determination of the degree of N -acetylation for chitin and chitosan by various NMR spectroscopy techniques: A review. Carbohydrate Polymers. 2010,79(4),801–10.

275. Hirai A, Odani H, Nakajima A. Determination of degree of deacetylation of chitosan by 1H NMR spectroscopy. Polymer Bulletin. 1991,26(1),87–94.

276. Ghavami P. Stress and Strain. In: Mechanics of Materials An Introduction to Engineering Technology. Springer; 2015. 143–62.

277. ASTM International. ASTM D695-10 Standard Test Method for Compressive Properties of Rigid Plastics. 2010.

278. ASTM D790- 15. Test Methods for Flexural Properties of Unreinforced and Reinforced Plastics and Electrical Insulating Materials. 2016.

279. Kalpakjian S, Schmid S. Mechanical Behavior, Testing, and Manufacturing Properties of Materials. In: Kalpakjian S, Schmid S, editors. Manufacturing Engineering & Technology. 7th Edition. Upper Saddle River: Pearson; 2014. 56–87.

280. Ghavami P. Bending Stresses in Beams. In: Mechanics of Materials An Introduction to Engineering Technology. Springer; 2015. 215–26.

281. Qian L, Li M, Zhou Z, Yang H, Shi X. Comparison of nano-indentation hardness to microhardness. Surface & Coatings Technology. 2005,195(2-3),264–71.

282. Meyers MA. Hardness. In: Mechanical behavior of materials. Second edit. New York: Cambridge University Press; 2009.

283. Labossiere PE. Mechanical Properties and Performance of Materials. Seattle; 2007.

284. Fischer-Cripps AC. Nanoindentation Testing. In: Nanoindentation. Third edit. New York: Springer; 2011. 21–37.

285. Briscoe BJ, Fiori L, Pelillo E. Nano-indentation of polymeric surfaces. Journal of Physics D: Applied Physics. 1998,31(19),2395–405.

286. Deng X, Chawla N, Chawla KK, Koopman M. Deformation behavior of (Cu , Ag)-Sn intermetallics by nanoindentation. Acta Materialia. 2004,52(14),4291–303.

287. Fischer-Cripps AC. Nanoindentation Test Standards. In: Nanoindentation. Third edit. New York: Springer; 2011. 181–98.

288. Oliver WC, Pharr GM. Measurement of hardness and elastic modulus by instrumented indentation: Advances in understanding and refinements to methodology. Journal of Materials Research. 2004,19(1).

289. Fischer-Cripps AC. Nanoindentation Instrumentation. In: Nanoindentation. Third edit. New York: Springer; 2011. 199–211.

290. Ludwig Reimer. Introduction to Scanning Electron Microscopy. In: Hawkes PW, editor. Scanning Electron Microscopy Physics of Image Formation and Microanalysis. Second edi. Heidelberg: Springer; 1998. 1–12.

291. Scanning Electron Microscopy [Internet]. Laboratory Testing Inc. [cited January 1, 2017]. Available at: https://www.labtesting.com/services/materials-testing/metallurgical-testing/sem-analysis/

292. Swapp S. Scanning Electron Microscopy (SEM) [Internet]. Science Education Resource Center at Carleton College. Available at:

http://serc.carleton.edu/research_education/geochemsheets/techniques/SEM.html

293. Girão AV, Caputo G, Ferro MC. Application of Scanning Electron Microscopy-Energy Dispersive X-Ray Spectroscopy (SEM-EDS). In: Comprehensive Analytical Chemistry. 2017. 153–68.

294. Hanke R, Fuchs T, Salamon M, Zabler S. X-ray microtomography for materials characterization. In: Hübschen G, Altpeter I, Tschuncky R, Herrmann H-G, editors. Materials Characterization Using Nondestructive Evaluation (NDE) Methods. Woodhead P. Cambridge, USA: Woodhead Publishing; 2016. 45–79.

295. MicroCT [Internet]. Scanco Medical. [cited May 1, 2016]. Available at: http://www.scanco.ch/en/support/faq-general.html

296. How does a micro-CT scanner work? [Internet]. Micro Photonics Inc. [cited May 1, 2016]. Available at: https://www.microphotonics.com/how-does-a-microct-scanner-work/

297. Zhou P, Labuza TP. Differential Scanning Calorimetry. In: McSweeney PLH, Fuquay JW, Fox PF, editors. Encyclopedia of Dairy Sciences. Second edi. Elsevier; 2011. 256–63.

298. Höhne GW., Hemminger WF, Flammersheim H-J. Introduction to Differential Scanning Calorimetry. In: Differential Scanning Calorimetry. Second edi. Springer; 2003. 1–7.

299. Höhne GW., Hemminger WF, Flammersheim H-J. Types of Differential Scanning Calorimeters and Modes of Operation. In: Differential Scanning Calorimetry. Second edi. Springer; 2003. 9–30.

300. Fortunato A. DSC: history, instruments and devices. In: Pignatello R, editor. Drug–biomembrane interaction studies: The application of calorimetric techniques. Cambridge, UK: Woodhead Publishing Limited; 2013. 169–212.

301. Phase Transitions and Differential Scanning Calorimetry [Internet]. Chemistry 75. 2010. p. 1–12. Available at: http://www.dartmouth.edu/~pchem/75/pdfs/DSC.pdf

302. Lukas K, Lemaire PK. Differential scanning calorimetry: Fundamental overview. Resonance. 2009,14(8),807–17.

303. Petrica M, Duscher B, Koch T, Archodoulaki V-M. Studies on Tribological Behavior of PEEK and PE-UHMW. In: Proceedings of the Regional Conference Graz 2015 – Polymer Processing Society PPS. 2016. p. 070001 1–5.

304. Djebbar T, Donaldson EC. Wettability. In: Petrophysics. Fourth edi. Elsevier; 2016. p. 319–57.

305. Sinez V, Thomy V, Dufour R. 1. Nanotechnologies for Synthetic Super Non-wetting surfaces. In: Nanotechnologies for Synthetic Super Non-wetting surfaces. Hoboken: John Wiley & Sons; 2014. 1–12.

306. Kwok DY, Neumann AWU. Contact angle measurement and contact angle interpretation. Advances in Colloid and Interface Science. 1999,81(3),167–249.

307. Yuan Y, Lee TR. Contact Angle and Wetting Properties. In: Bracco G, Holst B, editors. Surface Science Techniques. Springer; 2013. 3–34.

308. Barnes G, Gentle I. Capillarity and the mechanics of surfaces. In: Interfacial Science An Introduction. 2nd editio. New York: Oxford University Press; 2011. 10–42.

309. Decker EL, Frank B, Suo Y, Garoff S. Physics of contact angle measurement. Colloids and Surfaces A: Physicochemical and Engineering Aspects. 1999,156(1-3),177–89.

310. Snoeijer JH, Andreotti B. A microscopic view on contact angle selection. Physics of Fluids. 2008,20(5),1–11.

311. Birdi KS. Capillarity and Surface Forces (Liquids). In: Surface and Colloid Chemistry: Principles and Applications. Boca Raton: CRC Press; 2010. 9–38.

312. Cheng P, Li D, Boruvka L, Rotenberg Y, Neumann AW. Automation of Axisymmetric Drop Shape Analysis for Measurements of Interfacial Tensions and Contact Angles. Colloids and Surfaces. 1990,43(2),151–67.

313. Stuart B. Introduction to Infrared Spectroscopy. In: Ando DJ, editor. Infrared Spectroscopy: fundamentals and applications. Chichester: John Wiley & Sons; 2004. 1–14.

314. Silverstein RM, Webster FX, Kiemle DJ. Infrared Spectrometry. In: Spectrometric Identification of Organic Compounds. 7th editio. Danvers: John Wiley & Sons; 2005. 72–110.

315. Stuart B. Experimental Methods. In: Ando DJ, editor. Infrared Spectroscopy: fundamentals and applications. Chichester: John Wiley & Sons; 2004. 15–44.

316. PerkinElmer. FT-IR Spectroscopy Attenuated Total Reflectance (ATR) [Internet]. PerkinElmer Life and Analystical Sciences. 2005. 1–5. Available at: http://www.utsc.utoronto.ca/~traceslab/ATR_FTIR.pdf

317. Hanson J. Characteristic IR Absorption Frequencies [Internet]. 2002 [cited July 20, 2010]. Available at: http://www2.ups.edu/faculty/hanson/Spectroscopy/IR/IRfrequencies.html

318. Rogero SO, Lugão AB, Ikeda TI, Cruz ÁS. Teste in vitro de Citotoxicidade: Estudo Comparativo entre Duas Metodologias. Materials Research. 2003,6(3),317–20.

319. Pizzoferrato A, Ciapetti G, Stea S, Cenni E, Arciola CR, Granchi D, Lucia Savarino. Cell culture methods for testing Biocompatibility. Clinical Materials. 1994,15(3),173–90.

320. Marques AP, Cruz HR, Coutinho OP, Reis RL. Effect of starch-based biomaterials on the in vitro proliferation and viability of osteoblast-like cells. Journal of Materials Science: Materials in Medicine. 2005,16(9),833–42.

321. Kirkpatrick CJ, Mittermayer C. Theoretical and practical aspects of testing potential biomaterials in vitro. Journal of Materials Science: Materials in Medicine. 1990,1(1),9–13.

322. International Standard ISO 10993-5. Biological evaluation of medical devices - Part 5: Tests for in vitro cytotoxicity. 2009.

323. Kirkpatrick CJ, Bittinger F, Wagner M, Köhler H, Kooten TG van, Klein CL, Otto M. Current trends in biocompatibility testing. Proceedings of the Institution of Mechanical Engineers, Part H: Journal of Engineering in Medicine. 1998,212(2),75–84.

324. Stepanenko AA, Dmitrenko V V. Pitfalls of the MTT assay: Direct and off-target effects of inhibitors can result in over/underestimation of cell viability. Gene. 2015,574(2),193–203.

325. Stockert JC, Blázquez-Castro A, Cañete M, Horobin RW, Villanueva Á. MTT assay for cell viability: Intracellular localization of the formazan product is in lipid droplets. Acta Histochemica. 2012,114(8),785–96.

326. Mosmann T. Rapid colorimetric assay for cellular growth and survival: application to proliferation and cytotoxicity assays. Journal of Immunological Methods. 1983,65(1-2),55–63.

327. Kupcsik L. Estimation of Cell Number Based on Metabolic Activity: The MTT Reduction Assay. In: Stoddart MJ, editor. Mammalian Cell Viability Methods and Protocols. New York: Springer; 2011. 13–9.

328. Azevedo H, Reis R. Understanding the Enzymatic Degradation of Biodegradable Polymers and Strategies to Control Their Degradation Rate. In: Reis RL, Román JS, editors. Biodegradable Systems in Tissue Engineering and Regenerative Medicine. CRC Press; 2004. 177–202.

329. International Standard ISO 10993-13. Biological evaluation of medical devices - Part 13: Identification and quantification of degradation products from polymeric medical device. Geneva, Switzerland; 2010.

330. Lesnierowski G, Kijowski J. Lysozyme. In: Huopalahti R, López-Fandiño R, Anton M, Schade R, editors. Bioactive Egg Compounds. Heidelberg: Springer; 2007. 33–42.

331. Hankiewicz JAN, Swierczek EWA. Lysozyme in human body fluids. Clinica Chimica Acta. 1974,57(3),205–9.

332. Lim SM, Song DK, Oh SH, Sin D, Lee-Yoon, Bae EH, Lee JH. In vitro and in vivo degradation behavior of acetylated chitosan porous beads. Journal of Biomaterials Science, Polymer Edition. 2012,19(4),37–41.

333. Kini U, Nandeesh BN. Physiology of Bone Formation, Remodeling, and Metabolism. In: Fogelman I, Gnanasegaran G, Wall H van der, editors. Radionuclide and Hybrid Bone Imaging. Berlin: Springer; 2012. 29–57.

334. Clarke B. Normal Bone Anatomy and Physiology. Clinical Journal of the American Society of Nephrology. 2008,3(S131–S139),131–9.

335. Sims NA, Gooi JH. Bone remodeling: Multiple cellular interactions required for coupling of bone formation and resorption. Seminars in Cell & Developmental Biology Bone remodeling. 2008,19(5),444–51.

336. Florencio-Silva R, Rodrigues G, Sasso-Cerri E, Simões MJ, Cerri PS. Biology of Bone Tissue: Structure, Function , and Factors That Influence Bone Cells. BioMed Research International. 2015,2015,1–17.

337. Dimitriou R, Tsiridis E, Giannoudis P V. Current concepts of molecular aspects of bone healing. Injury.

2005,36(12),1392–404.

338. Arvidson K, Abdallah BM, Applegate LA, Baldini N, Cenni E, Gomez-Barrena E, Granchi D, Kassem M, Konttinen YT, Mustafa K, Pioletti DP, Sillat T, Finne-Wistrand A. Bone regeneration and stem cells. Regenerative Medicine Review Series. 2011,15(4),718–46.

339. Schindeler A, Mcdonald MM, Bokko P, Little DG. Bone remodeling during fracture repair: The cellular picture. Seminars in Cell & Developmental Biology. 2008,19(5),459–66.

340. Tsiridis E, Upadhyay N, Giannoudis P. Molecular aspects of fracture healing: Which are the important molecules? Injury. 2007,38(S1),S11–25.

341. Gilbert. SF. Osteogenesis: The Development of Bones. In: Developmental Biology. 6th editio. Sunderland: Sinauer Associates; 2000. 432–6.

342. Rampersad SN. Multiple applications of alamar blue as an indicator of metabolic function and cellular health in cell viability bioassays. Sensors. 2012,12(9),12347–60.

343. Golub EE, Boesze-Battaglia K. The role of alkaline phosphatase in mineralization. Current Opinion in Orthopaedics. 2007,18(5),444–8.

344. Alkaline Phosphatase Assay Kit. Abnova. 2015.

345. Wagner EM. Monitoring Gene Expression: Quantitative Real-Time RT-PCR. In: Freeman LA, editor. Lipoproteins and Cardiovascular Disease Methods and Protocols. Totowa, NJ: Humana Press; 2013. p. 19–45.

346. Arya M, Shergill IS, Williamson M, Gommersall L, Arya N, Patel HR. Basic principles of real-time quantitative PCR. Expert Review of Molecular Diagnosis. 2005,5(2),209–19.

347. Kirkham GR, Cartmell SH. Genes and Proteins Involved in the Regulation of Osteogenesis. In: N Ashammakhi RR& EC, editor. Topics in Tissue Engineering. Biomaterials and Tissue Engineering Group; 2007. 1–22.

348. Westhrin M, Xie M, Olderoy M, Sikorski P, Strand BL, Standal T. Osteogenic differentiation of human mesenchymal stem cells in mineralized alginate matrices. PLoS ONE. 2015,10(3),1–16.

349. Murray PR, Rosenthal KS, Pfaller MAeditors. Sterilization, Disinfection, and Antisepsis. In: Medical Microbiology. Eighth Edi. Elsevier; 2015. 11–4.

350. Anderson JM, Bevacqua B, Cranin AN, Graham LM, Hoffman AS, Klein M, Kowalski JB, Morrissey RF, Obstbaum SA, Ratner BD, Schoen FJ, Sirakian A, Whittlesey D. Implants and Devices. In: Ratner BD, Hoffman AS, Schoen FJ, Lemons JE, editors. Biomaterials Science: An Introduction to Materials in Medicine. London: Academic Press; 1996. 415–56.

351. Submission and Review of Sterility Information in Premarket Notification (510(k)) for Devices Labeled as Sterile. Guidance for Industry and Food and Drug Administration Staff. 2016.

352. Lerouge S. Introduction to sterilization: definitions and challenges. In: Lerouge S, Simmons A, editors. Sterilisation of biomaterials and medical devices. Cambridge, UK: Woodhead Publishing; 2012. 1–19.

353. Sandle T. Bioburden determination. In: Pharmaceutical Microbiology Essentials for quality assurance and quality control. Cambridge, UK: Woodhead Publishing; 2016. 81–91.

354. International Standard 11737-1. Sterilization of medical devices- Microbiological methods - Part 1: Determination of a population of microorganisms on products. Geneva, Switzerland; 2006.

355. ISO 11737-2 Sterilization of medical devices -Microbiological methods - Part 2: Tests of sterility performed in the definition, validation and maintenance of a sterilization process. Geneva, Switzerland; 2009.

356. Methods of sterilization [Internet]. The International Pharmacopeia. 2016 [cited January 16, 2017]. Available at: http://apps.who.int/phint/2016/index.html#d/b.7.5.9

357. Rogers WJ. Steam and dry heat sterilization of biomaterials and medical devices. In: Lerouge S, Simmons A, editors. Sterilisation of biomaterials and medical devices. Philadelphia: Woodhead Publishing; 2012. 20–55.

358. Rogers W. Steam Sterilisation of Healthcare Products and Polymers. In: Sterilization of Polymer Healthcare Products. 1st editio. Shrewsbury: Rapra Technology; 2005. 5–18.

359. International Standard 17665-1. Sterilization of health care products - Moist heat - Part 1: Requirements for the development, validation and routine control of a sterilization process for medical devices. Geneva; 2006.

360. Technical Specification ISO 17665-2. Sterilization of health care products - Moist heat - Part 2: Guidance on the application of ISO 17665-1. Geneva; 2009.

361. Türker NS, Özer AY, Kutlu B, Nohutcu R, Sungur A, Bilgili H, Ekizoglu M, Özalp M. The Effect of Gamma Radiation Sterilization on Dental Biomaterials. Tissue Engineering and Regenerative Medicine. 2014,11(5),341–9.

362. Rogers W. Radiation Sterilisation. In: Sterilization of Polymer Healthcare Products. 1st editio. Shrewsbury: Rapra Technology; 2005.

363. Parsons BJ. Sterilisation of healthcare products by ionising radiation: principles and standards. Lerouge S, Simmons A, editors. Sterilisation of biomaterials and medical devices. Philadelphia: Woodhead Publishing; 2012. 56-70.

364. International Standard ISO 11137-2. Sterilization of health care products -Radiation - Part 2: Establishing the sterilization dose. Geneva; 2013.

365. Rogers W. Ethylene Oxide Sterilisation - Ubiquitous for Most Non Liquid Heat Sensitive Material. In: Sterilisation of Polymer Healthcare Products. 1st Editio. Shrewsbury: Rapra Technology; 2005.

366. Mendes GC, Brandão TRS, Silva CLM. Ethylene oxide (EO) sterilization of healthcare products. In: Lerouge S, Simmons A, editors. Sterilisation of biomaterials and medical devices. Philadelphia: Woodhead Publishing; 2012. 71–96.

367. International Standard ISO 11135. Sterilization of health-care products - Ethylene oxide - Requirements for the development, validation and routine control of a sterilization process for medical devices. Geneva; 2014.

368. Sousa CS, Torres LM, Azevedo MPF, Camargo TC, Graziano KU, Lacerda RA, Turrini RNT. Sterilization with ozone in health care: an integrative literature review. Revista da Escola de Enfermagem da USP. 2011,45(5),1238–44.

369. Lerouge S. Non-traditional sterilization techniques for biomaterials and medical devices. In: Lerouge S, Simmons A, editors. Sterilisation of biomaterials and medical devices. Philadelphia: Woodhead Publishing; 2012. 97–116.

370. Guzel-Seydim ZB, Greene AK, Seydim AC. Use of ozone in the food industry. Lebensmittel-Wissenschaft & Technologie. 2004,37(4),453–60.

371. Victorin K. Review of the genotoxicity of ozone. Mutation Research. 1992,277(3),221–38.

372. Nagaraja PA. Ozone Sterilization. In: Hospital Sterilization. New Dehli: Jaypee; 2011. 161–3.

373. International Standard ISO 14937. Sterilization of health care products - General requirements for characterization of a sterilizing agent and the development, validation and routine control of a sterilization process for medical devices. Vol. 2009. Geneva;

374. Sionkowska A. Current research on the blends of natural and synthetic polymers as new biomaterials : Review. Progress in Polymer Science. 2011,36(9),1254–76.

375. Kumar HMPN, Prabhakar MN, Prasad CV, Rao KM, Kumar TVA, Rao KC, Subha MCS. Compatibility studies of chitosan/PVA blend in 2 % aqueous acetic acid solution at 30 ◦ C. Carbohydrate Polymers. 2010,82(2),251–5.

376. Wu Y, Yu S, Mi F, Wu C, Shyu S. Preparation and characterization on mechanical and antibacterial properties of chitosan/cellulose blends. Carbohydrate Polymers. 2004,57(4),435–40.

377. Neto CGT, Giacometti JA, Job AE, Ferreira FC, Fonseca JLC, Pereira MR. Thermal Analysis of Chitosan Based Networks. Carbohydrate Polymers. 2005,62(2),97–103.

378. Rinaudo M, Pavlov G, Desbrie J. Influence of acetic acid concentration on the solubilization of chitosan. Polymer. 1999,40(25),7029–32.

379. Hitomi K, Tsukagoshi N. Role of Ascorbic Acid in Modulation of Gene Expression. In: Harris R, editor. Subcellular Biochemistry Volume 25 Ascorbic Acid: Biochemistry and Biomedical Cell Biology. New York: Plenum Press; 1996. 41–56.

380. Chen P-H, Hwang Y-H, Kuo T-Y, Liu F-H, Lai J-Y, Hsieh H-J. Improvement in the Properties of Chitosan Membranes Using Natural Organic Acid Solutions as Solvents. Journal of Medical and Biological Engineering. 2007,27(1),23–8.

381. Montembault A, Viton C, Domard A. Rheometric Study of the Gelation of Chitosan in Aqueous Solution without Cross-Linking Agent. Biomacromolecules. 2005,6(2),653–62.

382. Chen JL, Zhao Y. Effect of Molecular Weight, Acid, and Plasticizer on the Physicochemical and Antibacterial Properties of β -Chitosan Based Films. Journal of Food Science. 2012,77(5),127–36.

383. Lavorgna M, Piscitelli F, Mangiacapra P, Buonocore GG. Study of the combined effect of both clay and glycerol plasticizer on the properties of chitosan films. Carbohydrate Polymers. 2010,82(2),291–8.

384. Srinivasa PC, Ramesh MN, Tharanathan RN. Effect of plasticizers and fatty acids on mechanical and permeability characteristics of chitosan films. Food Hydrocolloids. 2007,21(7),1113–22.

385. Gartner C, L BL, Sierra L, Graf R, Spiess HW, Gaborieau M. Interplay between Structure and Dynamics in Chitosan Films Investigated with Solid-State NMR , Dynamic Mechanical Analysis, and X-ray Diffraction. BioMacromolecules. 2011,12(4),1380–6.

386. Sanyang ML, Sapuan SM, Jawaid M, Ishak MR, Sahari J. Effect of Plasticizer Type and Concentration on Tensile, Thermal and Barrier Properties of Biodegradable Films Based on Sugar Palm (Arenga pinnata) Starch. Polymers. 2015,7(6),1106–24.

387. Matet M, Heuzey M, Pollet E, Ajji A, Avérous L. Innovative thermoplastic chitosan obtained by thermo-mechanical mixing with polyol plasticizers. Carbohydrate Polymers. 2013,95(1),241–51.

388. Oma ÄRC. Effects of Hydrophilic Plasticizers on Mechanical , Thermal , and Surface Properties of Chitosan Films. Journal of Agricultural and Food Chemistry. 2005,53(12),3950–7.

389. Schut J, Bolikal D, Khan I, Pesnell A, Rege A, Rojas R, Sheihet L, Murthy N, Kohn J. Glass transition temperature prediction of polymers through the mass-per-flexible-bond principle. Polymer (Guildf). 2008,48(20),6115–24.

390. Meng Q, Heuzey M, Carreau PJ. Hierarchical Structure and Physicochemical Properties of Plasticized Chitosan. BioMacromolecules. 2014,15(4),1216−1224.

391. Dhawade PP, Jagtap RN. Characterization of the glass transition temperature of chitosan and its oligomers by temperature modulated differential scanning calorimetry. Advances in Applied Science Research. 2012,3(3),1372–82.

392. Quijada-Garridoa I, Iglesias-Gonzáleza V, Mazón-Arechederrab JM, Barrales-Riendaa JM. The role played by the interactions of small molecules with chitosan and their transition temperatures . Glass-forming liquids: 1,2,3-Propantriol (glycerol). Carbohydrate Polymers. 2007,68(1),173–86.

393. Lazaridou A, Biliaderis CG. Thermophysical properties of chitosan, chitosan-starch and chitosan-pullulan films near the glass transition. Carbohydrate Polymers. 2002,48(2),179–90.

394. Pereira FS, Agostini DL da S, Job AE, González ERP. Thermal studies of chitin-chitosan derivatives. Journal of Thermal Analysis and Calorimetry. 2013,114(1),321–7.

395. Gabriela M, Campos N, Helena L, Mei I, Rodrigues A, Jr S. Sorbitol-Plasticized and Neutralized Chitosan Membranes as Skin Substitutes. Materials Research. 2015,18(4),781–90.

396. Nor NAM, Halim AS, Shamsuddin S, Hussin CMC, Ujang Z, Rashid AHA. The effect of chitosan derivatives film on the proliferation of human skin fibroblast: an-in vitro study. Journal of Sustainability Science and Management. 2013,8(2),212–9.

397. 100 types of chitosan - this is a global peak [Internet]. Invest in Saxony-Anhalt. 2011 [cited October 1, 2017]. Available at: http://www.invest-in-saxony-anhalt.com/report-invest/newsletter-iisa/2011/11/100-types-of-chitosan-this-is-a-global

398. Thakhiew W, Devahastin S, Soponronnarit S. Effects of drying methods and plasticizer concentration on some physical and mechanical properties of edible chitosan films. Journal of Food Engineering. 2010,99(2),216–24.

399. Ziani K, Oses J, Coma V, Mate JI. Effect of the presence of glycerol and Tween 20 on the chemical and physical properties of films based on chitosan with different degree of deacetylation. LWT - Food Science and Technology. 2008,41(10),2159–65.

400. Cifuentes SC, Frutos E, Benavente R, González-carrasco JL, Lorenzo V. Strain rate effect on semi-crystalline PLLA mechanical properties measured by instrumented indentation tests. European Polymer Journal. 2014,59,239–46.

401. Hardiman MF, Vaughan TJ, Mccarthy CT. The Effects of Pile-Up, Viscoelasticity and Hydrostatic Stress on Polymer Matrix Nanoindentation. Polymer Testing. 2016,52,157–66.

402. Beyaoui M, Mazeran P-E, Arvieu M-F, Bigerelle M, Guigon M. Analysis of nanoindentation curves in the case of bulk amorphous polymers. International Journal of Materials Research. 2009,100(7),943–9.

403. Fischer-Cripps AC. Factors Affecting Nanoindentation Test Data. In: Ling FF, editor. Nanoindentation. Third Edit. New York: Springer; 2011. 77–104.

404. Díez-Pascual AM, Gómez-Fatou MA, Ania F, Flores A. Nanoindentation in polymer nanocomposites. Progress in Materials Science. 2015,67,1–94.

405. Mishra SK, Kannan S. Development, mechanical evaluation and surface characteristics of chitosan/

polyvinyl alcohol based polymer composite coatings on titanium metal. Journal of the Mechanical Behavior of Biomedical Materials. 2014,40,314–24.

406. Vanlandingham MR, Villarrubia JS, Guthrie WF, Meyers GF. Nanoindentation of Polymers: An Overview. Macromolecular Symposia. 2001,167(1),15–43.

407. Hu Q, Li B, Wang M, Shen J. Preparation and characterization of biodegradable chitosan/hydroxyapatite nanocomposite rods via in situ hybridization: a potential material as internal fixation of bone fracture. Biomaterials. 2004,25(5),779–85.

408. Hasirci V, Lewandrowski KU, Bondre SP, Gresser JD, Trantolo DJ, Wise DL. High strength bioresorbable bone plates: preparation , mechanical properties and in vitro analysis. Bio-Medical Materials and Engineering. 2000,10(1),19–29.

409. Danilchenko SN, Kalinkevich O V, Pogorelov M V, Kalinkevich AN, Sklyar AM, Kalinichenko TG, Ilyashenko VY, Starikov V V, Bumeyster VI, Sikora VZ, Sukhodub LF. Characterization and in vivo evaluation of chitosan-hydroxyapatite bone scaffolds made by one step coprecipitation method. Journal of Biomedical Materials Research Part A. 2011,96(4),639–47.

410. Katti KS, Katti DR, Dash R. Synthesis and characterization of a novel chitosan/montmorillonite/ hydroxyapatite nanocomposite for bone tissue engineering. Biomedical Materials. 2008,3(3),1–12.

411. Pu X, Yao Q, Yang Y, Sun Z, Zhang Q. In vitro degradation of three-dimensional chitosan/apatite composite rods prepared via in situ precipitation. International Journal of Biological Macromolecules. 2012,51(5),868–73.

412. Savioli Lopes M, Jardini AL, Maciel Filho R. Poly (lactic acid) production for tissue engineering applications. Procedia Engineering. 2012,42,1402–13.

413. Kean T, Thanou M. Biodegradation, biodistribution and toxicity of chitosan. Advanced Drug Delivery Reviews. 2010,62(1),3–11.

414. Costa-Pinto AR, Martins AM, Castelhano-Carlos MJ, Correlo VM, Sol PC, Longatto-Filho A, Battacharya M, Reis RL, Neves NM. In vitro degradation and in vivo biocompatibility of chitosan - poly (butylene succinate) fiber mesh scaffolds. Journal of Bioactive and Compatible Polymers. 2014,29(2),137–51.

415. González-Campos JB, Prokhorov E, Luna-Bárcenas G, Fonseca-García A, Sanchez IC. Dielectric Relaxations of Chitosan: The Effect of Water on the a-Relaxation and the Glass Transition Temperature. Journal of Polymer Science. 2009,47(22),2259–71.

416. Fundo JF, Carvalho A, Feio G, Silva CLM, Quintas MAC. Relationship between molecular mobility, microstructure and functional properties in chitosan/glycerol films. Innovative Food Science and Emerging Technologies. 2015,28,81–5.

417. Rokkanen PU. Bioabsorbable Polymers for Medical Applications with an Emphasis on Orthopedic Surgery. In: Dumitriu S, editor. Polymeric Biomaterials, Revised and Expanded. 2nd editio. New York: Marcel Dekker, Inc.; 2001.

418. Zachari MA, Chondrou PS, Pouliliou SE, Mitrakas AG, Abatzoglou I, Zois CE, Koukourakis MI. Evaluation of the alamarblue assay for adherent cell irradiation experiments. Dose-Response. 2014,12(2),246–58.

419. Imhoff BR, Hansen JM. Differential redox potential profiles during adipogenesis and osteogenesis. Cellular & Molecular Biology Letters. 2011,16(1),149–61.

420. Eble JA, Rezende FF. Redox-Relevant Aspects of the Extracellular Matrix and Its Cellular Contacts via Integrins. Antioxidants & Redox Signaling. 2014,20(13),1977–93.

421. Frohbergh ME, Katsman A, Mondrinos MJ, Stabler CT, Hankenson KD, Oristaglio JT, Lelkes PI. Osseointegrative Properties of Electrospun Hydroxyapatite-Containing Nanofibrous Chitosan Scaffolds. Tissue Engineering Part A. 2015,21(5-6),970–81.

422. Yeatts AB, Choquette DT, Fisher JP. Bioreactors to influence Stem Cell Fate: Augmentation of Mesenchymal Stem Cell Signaling Pathways via Dynamic Culture. Biochimica et Biophysica Acta. 2014,1830(2),2470–80.

423. García-Gareta E, Coathup MJ, Blunn GW. Osteoinduction of bone grafting materials for bone repair and regeneration. Bone. 2015,81,112–21.

424. Wang L, Rao RR, Stegemann JP. Delivery of mesenchymal stem cells in Chitosan/collagen microbeads for orthopedic tissue repair. Cells Tissues Organs. 2013,197(5),333–43.

425. Barrère F, van Blitterswijk CA, de Groot K. Bone regeneration: Molecular and cellular interactions with calcium phosphate ceramics. International Journal of Nanomedicine. 2006,1(3),317–32.

426. Yuan H, Fernandes H, Habibovic P, de Boer J, Barradas AMC, de Ruiter A, Walsh WR, van Blitterswijk CA, de Bruijn JD. Osteoinductive ceramics as a synthetic alternative to autologous bone grafting. Proceedings of the National Academy of Sciences. 2010,107(31),13614–9.

427. Barradas A, Yuan H, van Blitterswijk C, Habibovic P. Osteoinductive biomaterials: current knowledge of properties, experimental models and biological mechanisms. European Cells and Materials. 2011,21,407–29.

428. Yuan H, Yang Z, Li Y, Zhang X, De Bruijn JD, De Groot K. Osteoinduction by calcium phosphate biomaterials. Journal of Materials Science: Materials in Medicine. 1998,9(12),723–6.

429. Puvaneswary S, Raghavendran HB, Talebian S, Murali MR, A Mahmod S, Singh S, Kamarul T. Incorporation of Fucoidan in β-Tricalcium phosphate-Chitosan scaffold prompts the differentiation of human bone marrow stromal cells into osteogenic lineage. Scientific Reports. 2016,6(April),24202.

430. Weir MD, Xu HHK. Culture human mesenchymal stem cells with calcium phosphate cement scaffolds for bone repair. Journal of Biomedical Material Research Part B: Applied Biomaterials. 2011,93(1),93–105.

431. Leceta I, Guerrero P, Ibarburu I, Dueñas MT, Caba K de La. Characterization and antimicrobial analysis of chitosan-based films. Journal of Food Engineering. 2013,116(4),889–99.

432. Shen K, Hu Q, Wang Z, Qu J. Effect of 60Co irradiation on the properties of chitosan rod. Materials Science & Engineering C. 2011,31(5),866–72.

433. Lim L-Y, Khor E, Ling C-E. Effects of Dry Heat and Saturated Steam on the Physical Properties of Chitosan. Journal of Biomedical Materials Research Part A. 1999,48(2),111–6.

434. Yamaguchi I, Tokuchi K, Fukuzaki H, Koyama Y, Takakuda K, Monma H, Tanaka J. Preparation and microstructure analysis of chitosan/hydroxyapatite nanocomposites. Journal of Biomedical Materials Research Part A. 2000,55(1),20–7.

435. Lim L-Y, Khor E, Koo O. y Irradiation of Chitosan. Journal of Biomedical Materials Research. 1998,43(3),282–90.

436. Dowling DP, Miller IS, Ardhaoui M, Gallagher WM. Effect of Surface Wettability and Topography on the Adhesion of Osteosarcoma Cells on Plasma-modified Polystyrene. Journal of Biomaterials Applications. 2011,26(3),327–47.

437. Berzina-Cimdina L, Borodajenko N. Research of Calcium Phosphates Using Fourier Transform Infrared Spectroscopy. In: Theophanides T, editor. Infrared Spectroscopy – Materials Science, Engineering and Technology. InTech; 2012. 123–48.

438. Galante R, Rediguieri CF, Kikuchi IS, Vasquez PAS, Colaço R, Serro AP, Pinto TJA. About the Sterilization of Chitosan Hydrogel Nanoparticles. Plos One. 2016,1–18.

439. Thakur AJ. Bone screws. In: The Elements of Fracture Fixation. Third edit. Elsevier; 2015. p. 81–123.

440. Tencer AF, Asnis SE, Harrington RM, Chapman JR. Biomechanics of Cannulated and Noncannulated Screws. In: Asnis SE, Kyle RF, editors. Cannulated Screw Fixation Principles and Operative Techniques. First edit. New York: Springer; 1996. 15–40.

441. ASTM International. F2502 – 05 Standard Specification and Test Methods for Bioabsorbable Plates and Screws for Internal Fixation Implants. West Conshohocken, PA. United States.; 2009.

442. Antoniac I, Laptoiu D, Popescu D, Cotrut C, Parpala R. Development of Bioabsorbable Interference Screws: How Biomaterials Composition and Clinical and Retrieval Studies Influence the Innovative Screw Design and Manufacturing Processes. In: Antoniac I, editor. Biologically Responsive Biomaterials for Tissue Engineering. New York: Springer; 2013. 107–36.

443. Mall NA, Heard WMR, Verma NN, Jr. BRB. Fixation in Revision ACL Reconstruction. In: Marx RG, editor. Revision ACL Reconstruction: Indications and Technique. New York: Springer; 2014. p. 105–17.

444. Purcell DB, Rudzki JR, Wright RW. Bioabsorbable interference screws in ACL reconstruction. Operative Techniques in Sports Medicine. 2004,12(3),180–7.

445. Crowley L V. The Musculoskeletal System. In: An Introduction to Human Disease Pathology and Pathophysiology correlations. 7th Ed. Sudbury: Jones and Bartlett Publishers; 2007. 753–83.

446. AAOS. OrthoInfo [Internet]. American Academy of Orthopaedic Surgeons. [cited June 20, 2016]. Available at: http://orthoinfo.aaos.org/

447. FDA - U.S. Food and Drug Administration. Guidance Document for Testing Biodegradable Polymer Implant Devices [Internet]. 2015.

Available at: http://www.fda.gov/RegulatoryInformation/Guidances/ucm080265.htm

448. Knetsch MLW. Evolution of Current and Future Concepts of Biocompatibility Testing. In: Dumitriu S, Popa V, editors. Polymeric Biomaterials: Structure and Function, Volume 1. CRC Press; 2013. 377–413.

449. ISO(2009). ISO 10993-1 Biological evaluation of medical devices -- Part 1: Evaluation and testing within a risk management process. Geneva, Switzerland; 2009.

450. ASTM International. F1980 - 07 Standard Guide for Accelerated Aging of Sterile Barrier Systems for Medical Devices. 0, West Conshohocken, PA, United States; 2011.

451. ISO(2006). ISO 11607-2 Packaging for terminally sterilized medical devices -- Part 2: Validation requirements for forming, sealing and assembly processes. Geneva, Switzerland; 2006.

452. Huang SJ. Poly(Lactic Acid) and Copolyesters. In: Bastioli C, editor. Handbook of Biodegradable Polymers. 2nd Ed. Shropshire, Eng: iSmithers Rapra Publishing; 2005. 287–302.

453. Avérous L, Pollet E. Biodegradable Polymers. In: Avérous L, Pollet E, editors. Environmental Silicate Nano-Biocomposites. 1st Ed. London: Springer; 2012. 13–39.

454. Huang SJ, Ho L-H, Huang MF, Koening MF, Cameron JA. Similarities and Differences Between Biodegradation and Non Enzymatic Degradation. In: Doi Y, Fukuda K, editors. Biodegradable Plastics and Polymers: Proceedings of the Third InternationaL Scientific Workshop, Osaka, Japan, November 9-11. Amsterdam: Elsevier; 1993. 3–10.

APPENDIX A.1. – Diseases affecting the musculoskeletal system

Diseases and treatments associated with the musculoskeletal system [445,446].

Disease	Part of the musculoskeletal system affected	Description	Treatment
Rheumatoid Arthritis	**Joint and articular cartilage**	Affects the small joints of the hands and feet, producing a chronic inflammation and thickening of the synovial membrane. The inflammation extends over the surface of the articular cartilage, destroying it.	(Nonsurgical) Medication; Exercise; Therapy. (Surgical) Joint replacement surgery.
Osteoarthritis	**Articular Cartilage**	Result of wear and tear degeneration of the major weight bearing joints. It leads to the degeneration of the articular cartilage, leading to roughening of the articular surfaces of the bones	(Nonsurgical) Lifestyle modifications; Medication; Physical therapy. (Surgical) Arthroscopy; Osteotomy; Joint fusion; Joint replacement.
Fracture	**Bone**	Breaking of the bone. It can be evaluated as simple, comminuted or compound.	(Nonsurgical or Surgical) Internal or external fixation.
Osteoporosis	**Bone**	Occurs whenever bone resorption exceeds bone production. The osteoporotic bones are fragile and susceptible to fracture.	(Nonsurgical) Focuses on the prevention of further bone loss – estrogen replacement therapy; calcitonin; bisphosphonates.
Intervertebral disk disease	**Spine disks**	Progressive wear and tear degeneration of both the nucleus (becomes denser) and the annulus (becomes weakened and thinned) of the intervertebral disks. The nucleus may be forced into the spinal canal causing acute back pain and pain along the course of the compressed nerve.	(Nonsurgical) Medication; Physical medicine. (Surgical) Spinal fusion; Disk replacement.
Rotator Cuff Tears	**Shoulder tendons**	When one or more of the rotator cuff tendons is torn, the tendon no longer fully attaches to the head of the humerus. Most tears occur in the supraspinatus muscle and tendon, but other parts of the rotator cuff may also be involved.	(Nonsurgical) Activity modification; Medication; Physical therapy. (Surgical) Open repair; All-arthroscopic repair.
Sprained Thumb	**Ligament**	Occurs when the main ligament in the thumb is injured. Symptoms include bruising, tenderness, and swelling.	(Nonsurgical) Immobilization. (Surgical) Reconnecting the ligament.
Meniscal Tears	**Knee cartilage**	Often happens during sports: players may squat and twist the knee, causing a tear. Older people are more likely to have degenerative meniscal tears since cartilage weakens and wears thin over time.	(Nonsurgical) RICE protocol; Medication. (Surgical) Meniscus repair; Meniscectomy.
Cruciate Ligaments or Collateral Ligaments Injuries	**Knee Ligaments**	The knee joint relies just on these ligaments and surrounding muscles for stability. Any direct contact to the knee or hard muscle contraction (e.g. changing direction rapidly while running) can injure a knee ligament.	(Nonsurgical) RICE protocol; Physical therapy. (Surgical) Rebuilding the ligament.

APPENDIX A.2. – Testing bioabsorbable implants for FDA approval

In order to commercialize medical devices in the U.S., there are two possible ways of obtaining FDA approval. One of them is the premarket notification or 510(k) process, which requires the demonstration of the equivalence of the new implant to another device already in the U.S. market, in terms of effectiveness and safety. The other way is the premarket approval (PMA) process for a device that is completely new or has a new intended use. The 510(k) process may or may not require clinical data whereas the PMA process always requires clinical data concerning the safety and efficacy of the new implant [44].

Biological and Mechanical Evaluation

Contrary to what happens with metallic implants, bioabsorbable polymers are more dependent on testing conditions such as temperature and humidity, which change over time during the healing period as a consequence of material degradation [447]. For these reasons, testing bioabsorbable polymer fixation implants requires special product considerations, as explained below.

The testing of bioabsorbable fixation implants takes place according to the stage of product development. For example, preliminary *in vitro* and *in vivo* biocompatibility tests are normally required during the early phase of product development as a screening set of trials (preliminary go *vs* no-go result-based analysis) [5].

Biocompatibility assessment comprehends several hierarchical stages, aiming to evaluate the effect of different characteristics/properties of newly developed biomaterials on a biological system [320]. The main goal of the *in vitro* testing phase is to assess the safety of the implant in an attempt to minimize the risk for the patient. Several biocompatibility aspects of the material can be determined in an *in vitro* test, namely the cytotoxicity effect, cell growth and functionality effect of the material [448]. The *in vivo* testing using an animal model is also indicated for the assessment of biocompatibility of the polymeric fixation implant. The biocompatibility issues that will be observed *in vivo* are [448,449] :

a) Local toxicity, sensitization and irritation;

b) Acute (systemic) and subacute toxicity;

c) Genotoxicity;

d) Local effects of solid implants in 3-D tissue;

e) Degradation or wear of the device in a living body and the effect of the resultant degradation and wear particles;

f) Functionality of the medical device in a living body.

Standardized experimentation procedures are described in the International Standard ISO-10993 series [449].

The mechanical properties of the new fixation implant are also determined. The *in vitro* testing consists of immersing the implant specimen in a physiological solution at 37°C, mimicking the *in vivo* conditions as closely as possible. Samples are removed from the media after pre-determined elapsed times (typically t = 1, 3, 6, 12, 26, 52 and 104 weeks) and mechanically

tested until the strength of the tested specimen (at a given *t*) drops below 20% of the initial strength. The loss of mass and M_W should also be determined [447].

To assess the pure mechanical properties of a bone fixation implant several mechanical tests can be used such as tensile, compression, bending, shear and torsion tests. The choice of the mechanical test is made in accordance with the final intended application of the new bioabsorbable polymeric implant [5,447]. Although the testing of mechanical properties provide valuable information, biomechanical testing is usually considered more relevant. In biomechanical testing, a complete simulated fixation specimen is tested allowing for the gathering of data for simulating actual fixation properties and behavior of the bone fixation implants [5,447]. Standard testing of the mechanical properties of bioabsorbable implants includes ASTM F2502 [441].

The *in vitro* mechanical degradation profile should also be validated by comparing the *in vivo* degradation rates. Samples should be implanted in an animal model and mechanically tested to determine if there are differences between the outcomes of test samples degraded *in vitro* and *in vivo*. The devices are implanted either at the site of use or at a nearby site, in order to closely simulate the intended clinical application. Therefore, the *in vivo* environment, which includes the effects of enzymes, cells and other variables, allows for the identification of the polymer mass loss and strength profile loss in a clinically relevant way as well as indicating the time required for complete resorption of the implant [5,447,448].

Additionally, FDA also recommends performing the following analysis of the materials comprising the bioabsorbable implant. It is important to note that this evaluation must be performed using sterilized materials [447].

a) Composition and molecular structure (e.g. polydispersity, M_W distribution, intrinsic viscosity and crosslinking agents);

b) Morphology (e.g. % crystallinity, orientation, types and amounts of phases);

c) Composite structure (e.g. laminate structure, reinforcement structure and coating);

d) Physical properties (e.g. roughness, dimensional changes of the material as a function of time and surface areas);

e) Thermal properties (e.g. melting and glass transition temperature).

Shelf-life

The shelf life, or lifespan, of the final product can be assessed following the ASTM F1980 Standard [450]. Accelerated aging tests are used to establish the shelf life of a sterile product over a determined period of time. Data obtained from the study is based on conditions of temperature or, in a more complete version of the test, on conditions of temperature and humidity cycles that simulate the effects of aging on the materials. The time period in which the aging of the materials is simulated will be chosen in accordance with the period claimed (expected) for the product expiration date (1 year, 2 years, etc.). After this study period, tests focusing on the package functionality and product sterilization will be executed according to the International Standard ISO 11607-2 and ISO 11737-2 [355,451]. However, to ensure that accelerated aging studies truly represent real time effects, real time aging studies must be conducted in parallel to optimize the overall study timeframe. Real time studies must be carried out on the claimed shelf life of the product and be performed to their completion. It is important to stress that if the real time aging studies outcome is different when compared

with the outcome of the accelerated aging studies, the first are the most relevant and enforceable.

Having a longer shelf life may alter the initial properties of bioabsorbable implants. For this reason, manufacturers prefer to discard bioabsorbable implants after their expiration date. Currently, the management of polymer waste requires a complementary combination of recycling and incineration for energy production and biodegradation [452]. Since incineration presents environmental issues and recycling a negative eco-balance, mainly due to the energy consumption during the recycling process phases (waste grinding and plastic processing), there is a growing interest in replacing synthetic polymers with other lines of polymers that can be prepared easily from renewable and sustainable sources and that can be also disposed of by biodegradable-bioconversion [453,454]. Hydrolysis and oxidations are the primary processes of polymer degradation. In addition, enzymatic and non-enzymatic processes can also occur simultaneously [454]. PLA is an example of a polymer that can be disposed by biodegradation.

APPENDIX A.3. – Statistical evaluations of chapter 10

- **Chapter 10.1**

Flexural Modulus			
Plasticizers	Concentrations (%)		p-value
Glycerol	5	10	0,28445
	5	15	0,16420
	10	15	0,55196
Sorbitol	5	10	0,13837
	5	15	**0,03658 ***
	10	15	0,14512

Flexural Strength			
Plasticizers	Concentrations (%)		p-value
Glycerol	5	10	0,45391
	5	15	0,13528
	10	15	**0,03827 ***
Sorbitol	5	10	0,15550
	5	15	0,92470
	10	15	0,11102

Flexural Strain			
Plasticizers	Concentrations (%)		p-value
Glycerol	5	10	0,85406
	5	15	0,36440
	10	15	0,20860
Sorbitol	5	10	0,05760
	5	15	0,27949
	10	15	0,13414

Indentation Hardness			
Plasticizers	Compositions (%)		p-value
Glycerol	5	10	**0,00009 ***
	5	15	**0,00001 ***
	10	15	**0,00977 ***
Sorbitol	5	10	0,05624
	5	15	**0,02018 ***
	10	15	0,84845

Indentation Modulus			
Plasticizers	Concentrations (%)		p-value
Glycerol	5	10	**0,00547 ***
	5	15	0,82741
	10	15	**0,01575 ***
Sorbitol	5	10	**0,04908 ***
	5	15	**0,02746 ***
	10	15	**0,00279 ***

- **Chapter 10.2**

Flexural Modulus			
Ceramics	Concentrations (%)		p-value
HA	5	10	0,28881
	5	15	**0,04800 ***
	10	15	**0,01932 ***
HA-TCP	5	10	0,05934
	5	15	**0,00997 ***
	10	15	**0,01115 ***
Granules	5	10	0,24467
	5	15	0,57970
	10	15	0,32434

Flexural Strength			
Ceramics	Concentrations (%)		p-value
HA	5	10	0,52826
	5	15	**0,01967 ***
	10	15	0,29649
HA-TCP	5	10	0,09726
	5	15	0,80462
	10	15	0,09014
Granules	5	10	0,09409
	5	15	0,68411
	10	15	0,33318

Flexural Strain			
Ceramics	Concentrations (%)		p-value
HA	5	10	0,34512
	5	15	**0,03666 ***
	10	15	0,20136
HA-TCP	5	10	0,38361
	5	15	0,06946
	10	15	0,23807
Granules	5	10	0,26147
	5	15	0,21270
	10	15	0,70821

Indentation Hardness			
Ceramics	Concentrations (%)		p-value
HA	5	10	**0,02212 ***
	5	15	**0,00004 ***
	10	15	**0,00341 ***
HA-TCP	5	10	**0,03634 ***
	5	15	**0,03820 ***
	10	15	0,87421
Granules	5	10	**0,000001 ***
	5	15	0,59860
	10	15	**0,00041 ***

Indentation Modulus			
Ceramics	Concentrations (%)		p-value
HA	5	10	0,65274
	5	15	**0,00325 ***
	10	15	**0,04042 ***
HA-TCP	5	10	0,08462
	5	15	**0,00119 ***
	10	15	**0,04384 ***
Granules	5	10	**0,00217 ***
	5	15	**0,00018 ***
	10	15	0,23498

APPENDIX A.4. – Statistical evaluations of chapter 11

- **Chapter 11.2**

Swelling Ratio			
Material	Conditions		p-value
Ch+Gly	PBS 12 weeks	Lysozyme 12 weeks	0,11214
	PBS 12 weeks	PBS 24 weeks	**0,00056 ***
	PBS 24 weeks	Lysozyme 24 weeks	0,18258
	Lysozyme 12 weeks	Lysozyme 24 weeks	0,08746
Ch+Gly+HA-TCP	PBS 12 weeks	Lysozyme 12 weeks	0,97066
	PBS 12 weeks	PBS 24 weeks	0,18406
	PBS 24 weeks	Lysozyme 24 weeks	0,47501
	Lysozyme 12 weeks	Lysozyme 24 weeks	0,13177
PLA	PBS 12 weeks	Lysozyme 12 weeks	0,41888
	PBS 12 weeks	PBS 24 weeks	0,57022
	PBS 24 weeks	Lysozyme 24 weeks	**0,00116 ***
	Lysozyme 12 weeks	Lysozyme 24 weeks	0,54146

Weight Loss			
Material	Conditions		p-value
Ch+Gly	PBS 12 weeks	Lysozyme 12 weeks	0,45406
	PBS 12 weeks	PBS 24 weeks	**0,000003***
	PBS 24 weeks	Lysozyme 24 weeks	0,40208
	Lysozyme 12 weeks	Lysozyme 24 weeks	**0,00069 ***
Ch+Gly+HA-TCP	PBS 12 weeks	Lysozyme 12 weeks	0,28631
	PBS 12 weeks	PBS 24 weeks	**0,00819 ***
	PBS 24 weeks	Lysozyme 24 weeks	0,88467
	Lysozyme 12 weeks	Lysozyme 24 weeks	**0,04002 ***
PLA	PBS 12 weeks	Lysozyme 12 weeks	0,37258
	PBS 12 weeks	PBS 24 weeks	**0,03295 ***
	PBS 24 weeks	Lysozyme 24 weeks	0,43738
	Lysozyme 12 weeks	Lysozyme 24 weeks	**0,00596 ***

Flexural Modulus			
Material	Conditions		p-value
Ch+Gly	Control	PBS 12 weeks	0,31820
	Control	Lysozyme 12 weeks	0,36105
	PBS 12 weeks	Lysozyme 12 weeks	0,78230
	PBS 12 weeks	PBS 24 weeks	0,42351
	Control	PBS 24 weeks	0,46770
	Control	Lysozyme 24 weeks	**0,00001***
	PBS 24 weeks	Lysozyme 24 weeks	0,13588
	Lysozyme 12 weeks	Lysozyme 24 weeks	0,43012
Ch+Gly+HA-TCP	Control	PBS 12 weeks	0,32351
	Control	Lysozyme 12 weeks	0,18963
	PBS 12 weeks	Lysozyme 12 weeks	0,58684
	PBS 12 weeks	PBS 24 weeks	0,95174
	Control	PBS 24 weeks	0,49023
	Control	Lysozyme 24 weeks	0,32894
	PBS 24 weeks	Lysozyme 24 weeks	0,95372
	Lysozyme 12 weeks	Lysozyme 24 weeks	0,71502
PLA	Control	PBS 12 weeks	0,08095
	Control	Lysozyme 12 weeks	**0,01734 ***
	PBS 12 weeks	Lysozyme 12 weeks	0,38526
	PBS 12 weeks	PBS 24 weeks	0,05246
	Control	PBS 24 weeks	0,37938
	Control	Lysozyme 24 weeks	0,10343
	PBS 24 weeks	Lysozyme 24 weeks	0,15829
	Lysozyme 12 weeks	Lysozyme 24 weeks	**0,00307 ***

Flexural Strength			
Material	Conditions		p-value
Ch+Gly	Control	PBS 12 weeks	**0,00011 ***
	Control	Lysozyme 12 weeks	**0,01010 ***
	PBS 12 weeks	Lysozyme 12 weeks	**0,02253 ***
	PBS 12 weeks	PBS 24 weeks	0,05488
	Control	PBS 24 weeks	**0,000007***
	Control	Lysozyme 24 weeks	0,10343
	PBS 24 weeks	Lysozyme 24 weeks	0,24047
	Lysozyme 12 weeks	Lysozyme 24 weeks	0,53436
Ch+Gly+HA-TCP	Control	PBS 12 weeks	**0,00001 ***
	Control	Lysozyme 12 weeks	**0,00082 ***
	PBS 12 weeks	Lysozyme 12 weeks	0,10652
	PBS 12 weeks	PBS 24 weeks	0,26406
	Control	PBS 24 weeks	**0,00011***
	Control	Lysozyme 24 weeks	**0,00054***
	PBS 24 weeks	Lysozyme 24 weeks	0,24998
	Lysozyme 12 weeks	Lysozyme 24 weeks	0,10905
PLA	Control	PBS 12 weeks	**0,00597 ***
	Control	Lysozyme 12 weeks	0,07583
	PBS 12 weeks	Lysozyme 12 weeks	0,28141
	PBS 12 weeks	PBS 24 weeks	0,20031
	Control	PBS 24 weeks	**0,000002***
	Control	Lysozyme 24 weeks	**0,00224 ***
	PBS 24 weeks	Lysozyme 24 weeks	0,11744
	Lysozyme 12 weeks	Lysozyme 24 weeks	**0,00307 ***

Flexural Strain			
Material	Conditions		p-value
Ch+Gly	Control	PBS 12 weeks	**0,00393 ***
	Control	Lysozyme 12 weeks	**0,01818 ***
	PBS 12 weeks	Lysozyme 12 weeks	**0,02249 ***
	PBS 12 weeks	PBS 24 weeks	0,30184
	Control	PBS 24 weeks	**0,00015***
	Control	Lysozyme 24 weeks	**0,04276***
	PBS 24 weeks	Lysozyme 24 weeks	0,28986
	Lysozyme 12 weeks	Lysozyme 24 weeks	0,15394
Ch+Gly+HA-TCP	Control	PBS 12 weeks	**0,01178 ***
	Control	Lysozyme 12 weeks	**0,03810 ***
	PBS 12 weeks	Lysozyme 12 weeks	0,96321
	PBS 12 weeks	PBS 24 weeks	0,93164
	Control	PBS 24 weeks	**0,02651***
	Control	Lysozyme 24 weeks	0,05734
	PBS 24 weeks	Lysozyme 24 weeks	0,97753
	Lysozyme 12 weeks	Lysozyme 24 weeks	0,90120
PLA	Control	PBS 12 weeks	**0,00629 ***
	Control	Lysozyme 12 weeks	**0,00148 ***
	PBS 12 weeks	Lysozyme 12 weeks	0,42184
	PBS 12 weeks	PBS 24 weeks	0,47917
	Control	PBS 24 weeks	**0,00017***
	Control	Lysozyme 24 weeks	**0,00081***
	PBS 24 weeks	Lysozyme 24 weeks	0,55908
	Lysozyme 12 weeks	Lysozyme 24 weeks	**0,04978 ***

- **Chapter 11.3**

Alamar Blue			
Material	Conditions		p-value
Ch+Gly	Day 1	Day 7	**0,0000043 ***
	Day 7	Day 14	**0,0000687 ***
	Day 14	Day 21	**0,0030804 ***
Ch+Gly+HA-TCP	Day 1	Day 7	**0,0000561 ***
	Day 7	Day 14	**0,0000003 ***
	Day 14	Day 21	**0,0000008 ***

APPENDIX A.5. – Statistical evaluations of chapter 12

- **Chapter 12.2.1**

Flexural Modulus			
Material	Sterilization methods		p-value
Ch+Gly	Non-sterilized	Steam	0,11885
	Non-sterilized	EtO	0,93779
	Non-sterilized	Ozone	**0,02875 ***
	Non-sterilized	Gamma	**0,01031 ***
Ch+Gly+HA-TCP	Non-sterilized	Steam	**0,00652 ***
	Non-sterilized	EtO	0,12577
	Non-sterilized	Ozone	0,10169
	Non-sterilized	Gamma	**0,03852 ***

Flexural Strength			
Material	Sterilization methods		p-value
Ch+Gly	Non-sterilized	Steam	0,07655
	Non-sterilized	EtO	0,28698
	Non-sterilized	Ozone	**0,02235 ***
	Non-sterilized	Gamma	**0,04148 ***
Ch+Gly+HA-TCP	Non-sterilized	Steam	**0,00094 ***
	Non-sterilized	EtO	0,88448
	Non-sterilized	Ozone	0,21794
	Non-sterilized	Gamma	**0,01175 ***

Flexural Strain			
Material	Sterilization methods		p-value
Ch+Gly	Non-sterilized	Steam	0,10590
	Non-sterilized	EtO	0,96644
	Non-sterilized	Ozone	0,05011
	Non-sterilized	Gamma	0,17312
Ch+Gly+HA-TCP	Non-sterilized	Steam	**0,00002 ***
	Non-sterilized	EtO	0,75046
	Non-sterilized	Ozone	**0,01157 ***
	Non-sterilized	Gamma	**0,03060 ***

Indentation Hardness			
Material	Sterilization methods		p-value
Ch+Gly	Non-sterilized	Steam	**0,00041 ***
	Non-sterilized	EtO	0,34651
	Non-sterilized	Ozone	0,84429
	Non-sterilized	Gamma	0,75423
Ch+Gly+HA-TCP	Non-sterilized	Steam	0,60510
	Non-sterilized	EtO	**0,00033 ***
	Non-sterilized	Ozone	**0,00539 ***
	Non-sterilized	Gamma	**0,00029 ***

Indentation Modulus			
Material	Sterilization methods		p-value
Ch+Gly	Non-sterilized	Steam	0,30967
	Non-sterilized	EtO	0,13303
	Non-sterilized	Ozone	0,85183
	Non-sterilized	Gamma	**0,01908 ***
Ch+Gly+HA-TCP	Non-sterilized	Steam	**0,00295 ***
	Non-sterilized	EtO	0,56545
	Non-sterilized	Ozone	**0,00023 ***
	Non-sterilized	Gamma	**0,04108 ***

Contact angle			
Material	Sterilization methods		p-value
Ch+Gly	Non-sterilized	Steam	0,88128
	Non-sterilized	EtO	0,05369
	Non-sterilized	Ozone	**0,00115 ***
	Non-sterilized	Gamma	0,08505
Ch+Gly+HA-TCP	Non-sterilized	Steam	**1,90E-14 ***
	Non-sterilized	EtO	**0,00018 ***
	Non-sterilized	Ozone	**0,00027 ***
	Non-sterilized	Gamma	0,18875

Cytotoxicity			
Material	Control	Sterilization methiod	p-value
Ch+Gly	Non-sterilized	Steam	0,46495
	Non-sterilized	EtO	**0,03421 ***
	Non-sterilized	Ozone	0,58143
	Non-sterilized	Gamma	0,14671
Ch+Gly+HA-TCP	Non-sterilized	Steam	0,71492
	Non-sterilized	EtO	0,38355
	Non-sterilized	Ozone	0,12744
	Non-sterilized	Gamma	0,57541
Material	Control	Sterilization method	p-value
Ch+Gly	Negative	Non-sterile	0,64093
	Negative	Steam	**0,04489 ***
	Negative	EtO	0,12397
	Negative	Ozone	**0,00769 ***
	Negative	Gamma	**0,04466 ***
Ch+Gly+HA-TCP	Negative	Non-sterile	0,16449
	Negative	Steam	**0,03969 ***
	Negative	EtO	**0,00589 ***
	Negative	Ozone	**0,00322 ***
	Negative	Gamma	**0,00494 ***

APPENDIX A.6. – 2D model of the ComposiTCP60® (Biomet) bioabsobable screw